Structural and functional characterization of the intracellular kinase domain of vascular endothelial growth factor receptor-2

Inauguraldissertation

zur

Erlangung der Würde eines Doktors der Philosophie

vorgelegt der

Philosophisch-Naturwissenschaftlichen Fakultät

der Universität Basel

von Sandro Manni

aus Italien

Basel, 2013

Genehmigt von der Philosophisch-Naturwissenschaftlichen Fakultät auf Antrag von:

Prof. Dr. Kurt Ballmer-Hofer

(Fakultätsverantwortlicher & Dissertationsleiter)

Prof. Dr. Britta Engelhardt

(Korreferentin)

Basel, 21.05.2013

Prof. Dr. Jörg Schibler

(Dekan)

1. Table of content

2. Abbreviations

AMD	Age-related macular degeneration
Ang-1/-2	Angiopoietin-1/-2
ATP	Adenosine triphosphate
AUC	Analytical ultracentrifugation
BSA	Bovine serum albumin
CD	Carboxy-terminal domain
c-Kit	Stem cell factor receptor
CSF1	Colony stimulating factor-1
CSF1R	Colony stimulating factor-1 receptor
Da, kDa	Dalton, kilo-Dalton
DAG	1, 2-diacylglycerol
DMEM	Dulbecco's modified eagle's medium
DNA	Deoxyribonucleic acid
DTT	Dithiothreitol
E.coli	Escherichia coli
ECD	Extracellular domain
ECM	Extracellular matrix
EDG	Endothelial differentiation sphingolipid G-protein coupled receptor
EDTA	Ethylenediamine tetraacetic acid
EGF	Epidermal growth factor
EGFR	Epidermal growth factor receptor
EM	Electron microscopy
eNOS	Endothelial nitric oxide synthase
Eph	Ephrin receptor
ER	Endoplasmic reticulum
ERK	Extracellular signal-regulated kinase
FAK	Focal adhesion kinase
FBS	Fetal bovine serum
FGF	Fibroblast growth factor
FGFR	Fibroblast growth factor receptor
Flt1	Fms-related tyrosine kinase 1
Flk-1	Fetal liver kinase-1 = VEGFR-2
Flt-4	Fetal liver kinase-4 = VEGFR-3
HEK 293	Human embryonic kidney cells 293
HIF-1	Hypoxia inducible factor-1
HSPG	Heparan sulfate proteoglycan
ICD	Intracellular domain
Ig	Immunoglobulin
IMAC	Immobilized metal affinity chromatography
ITC	Isothermal titration calorimetry
KID	Kinase insert domain

MALS	Multi Angle Light Scattering
MAPK	Mitogen-activated protein kinase
MEK	MAPK kinase
MW	Molecular weight
N-terminus	Amino-terminus or NH2-terminus
Ni-NTA	Nickel-nitrilotriacetic acid
NO	Nitric oxide
Nrp-1/-2	Neuropilin-1/-2
PAE	Porcine aortic endothelial cells
PAO	Phenyl arsine oxide
PBS	Phosphate buffered saline
PCR	Polymerase chain reaction
PDGF	Platelet derived growth factor
PDGFR	Platelet derived growth factor receptor
PI3-K	Phosphoinositol-3 kinase
PIP2	Phosphatidylinositol 4, 5-bisphosphate
PKB	Protein kinase B
PKC	Protein kinase C
PLC-γ	Phospholipase C gamma
PlGF	Placenta growth factor
PMSF	Phenylmethylsulfonyl fluoride
PTB	Phosphotyrosine binding domain
PVDF	Polyvinylidene fluoride
rpm	Rounds per minute
RTK	Receptor tyrosine kinase
SAXS	Small angle X-ray scattering
SCF	Stem cell factor
SDS-PAGE	Sodium dodecylsulfate polyacryl gel electrophoresis
SEC	Size exclusion chromatography
Sf21	Spodoptera frugiperda cells
Sf9	Spodoptera frugiperda cells
SH2	Src homology-2 domain
Shb	Src homology-2 protein in beta-cells
sVEGFR	Soluble VEGFR
TEV	Tobacco etch virus
Tie-1/-2	Angiopoietin receptor-1/-2
TGF	Transforming growth factor
TK	Tyrosine kinase
TMD	Transmembrane domain
TSAd	T-cell-specific adaptor
VE-cadherin	Vascular endothelial cadherin
VEGF	Vascular endothelial growth factor
VEGFR	Vascular endothelial growth factor receptor
WT	Wild type

3. Summary

Vascular Endothelial Growth Factors (VEGFs) are key players in blood and lymphatic vessel development and homeostasis. The family consists of five members, VEGF-A, -B, -C, -D and placenta growth factor (PLGF). They bind to three type V receptor tyrosine kinases (RTKs): VEGF-receptor-1 (VEGFR)-1 (Flt1), VEGFR-2 (KDR/Flk1), and VEGFR-3 (Flt4). VEGFR-2 is the major receptor responsible for angiogenic and vasculogenic signaling by VEGFs involving cell survival, migration and mitogenesis. VEGFRs consist of an extracellular domain (ECD) with seven immunoglobulin-homology domains (Ig-homology domains). The ECD is responsible for ligand binding and contributes to the dimerization process of the receptors by forming homotypic receptor contacts. A single transmembrane helix connects the ECD to the intracellular kinase domain. Ligand binding to VEGFR ectodomains induces dimerization of receptor monomers followed by autophosphorylation of specific tyrosine residues in the intracellular kinase domains. The phosphotyrosine containing activated kinase subsequently recruits signaling proteins thereby activating distinct cellular pathways. Here we show that the introduction of glutamic acid residues into the transmembrane domain (TMD) of VEGFR-2 leads to dimerization and induces conformational changes in the TMD. A subsequent rearrangement of the intracellular kinase domains gives rise to either active or inactive receptor dimers. We also show that the ECD of VEGFR-2 plays an essential autoinhibitory role in the absence of ligand. Furthermore, high-resolution structural analysis of isolated wild type (wt) and mutant TMD by NMR spectroscopy reveal TMD conformations presumably essential for receptor activation.

In a second project, we analysed the function of the kinase insert domain (KID) and the C-terminal domain (CD) in VEGFR-2 activation. We show that these domains regulate VEGFR-2 activity. The KID, and particularly a canonical tyrosine residue located at position 951 are highly relevant for kinase activation. Deletion of the CD renders VEGFR-2 constitutively active and we thus think that the CD of VEGFR-2 maintains the receptor in the inactive state in the absence of ligand. Low resolution structural data derived from small angle X-ray scattering (SAXS) and MALS (Multi Angle Light Scattering) give evidence that the kinase domain of VEGFR-2 undergoes significant conformational changes when switching from the inactive to the active state. The activated kinase domain adopts an elongated, open conformation whereas

the inactivated kinase domain remains in a globular compact conformation with the CD presumably blocking the catalytic site of the kinase similar to the autoinhibited conformation previously demonstrated for the Tie-2 kinase domain. Additional sedimentation equilibrium analytical ultracentrifugation (AUC) experiments of kinase domain mutants demonstrated that the KID and the CD are necessary to sustain an intrinsic dimerization propensity that potentially supports the dimerization process induced by ligand binding to the ECD. Deletion mutants showed lower affinity forming dimers only at higher concentration. In experiments aiming to investigate phosphorylation kinetics of the VEGFR-2 kinase domain we finally showed that VEGFR-2 follows a well-ordered sequence of residue-by-residue phosphorylation.

In a third project we were interested in characterizing the *in vitro* interaction between TSAd and activated VEGFR-2. Y951 mediated complex formation of TSAd with VEGFR-2 was found to be critical for VEGF-induced actin reorganization and migration but did not affect mitogenicity in endothelial and tumour cells. We were interested to gain insights on the binding mode by means of high and low-resolution structural biology methods. Initial size exclusion chromatography (SEC) and MALS analysis verified TSAd-VEGFR-2 interaction *in vitro.* SAXS analysis of the isolated binding partners and the complex revealed that pY951 mediated binding of TSAd resulted in an elongated multiprotein complex in which the binding partners orient in a presumably parallel orientation.

4. Zusammenfassung

Die Familie der vaskulären endothelialen Wachstumsfaktoren (VEGFs) spielt eine entscheidende Rolle bei der Entwicklung und Aufrechterhaltung des Blut- und Lymphgefässsystems. Die Familie besteht aus VEGF-A, -B, -C, -D und PLGF. Die Wachstumshormone binden an drei Typ V Rezeptor-Tyrosin-Kinasen: VEGFR-1 (Flt1), VEGFR-2 (Flk1) und VEGFR-3 (Flt4). VEGFR-2 ist mehrheitlich für die VEGF induzierte Aktivierung von angiogenen und vaskulogenen Signalwegen und den daraus resultierenden biologischen Effekten verantwortlich. Die VEGF-Rezeptoren besitzen eine extrazelluläre Domäne bestehend aus sieben immunoglobulin-ähnlichen Proteindomänen, die nebst der Rekrutierung von Liganden auch der Dimerisierung des Rezeptors durch Ausbildung von homotypischen Kontakten dient. Eine einzelne Transmembranhelix verbindet die extrazelluläre Domäne mit der intrazellulär geteilten Kinasedomäne. Die Ligandenbindung an den Rezeptor führt zu Dimerisierung und der darauf folgenden Aktivierung durch Autophosphorylierung an spezifischen Tyrosinen in der Kinasedomäne. Die Phosphotyrosine rekrutieren daraufhin Signalmoleküle, die in der Lage sind spezifische Signalwege zu aktivieren.

Wir konnten zeigen, dass Glutaminsäure-Mutationen in der Transmembrandomäne von VEGFR-2 zu Konformationsänderungen in der Helix führen. Die daraus folgende Neuausrichtung der Kinasedomänen resultierte in aktiven und inaktiven Rezeptorkonformationen. Es gelang uns auch aufzuzeigen, dass die extrazelluläre Domäne von VEGFR-2 eine wichtige Rolle bei der Blockierung des Rezeptors im inaktiven Zustand in Abwesenheit des Liganden spielt. Hochaufgelöste Strukturanalysen von isolierten Wildtyp und mutierten Transmembrandomänen ergaben Strukturen, die höchstwahrscheinlich bei der Aktivierung des Rezeptors eine essentielle Rolle spielen.

Ein zweites Projekt hatte zum Ziel, die Rolle der Kinase-Insertions-Domäne (KID) und der C-terminalen Domäne (CD) bei der VEGFR-2 Aktivierung zu entschlüsseln. Wir konnten zeigen, dass die KID und die CD die VEGFR-2 Aktivierung regulieren. Die KID und ein spezifisches Tyrosin in Position 951 innerhalb der KID waren essentiell für die Kinaseaktivierung. Deletion der CD führte zu konstitutiver Aktivierung von VEGFR-2. Wir denken, dass die CD den Rezeptor in Abwesenheit des Liganden im inaktiven Zustand behält. Mittels Small Angle X-ray Scattering (SAXS) und Multi Angle Light Scattering (MALS) erhaltene Strukturdaten beweisen,

dass die Aktivierung der Kinasedomäne von VEGFR-2 mit einer signifikanten Änderungen in der Konformation einhergeht. Die aktive Kinasedomäne nimmt eine längliche, offene Konformation ein, wohingegen die Inaktive in einer globulären, geschlossenen Konformation verbleibt. Sehr wahrscheinlich blockiert die CD dabei das katalytische Zentrum des Enzyms, vergleichbar mit dem Mechanismus der von der Tie-2 Kinasedomäne verwendet wird. Sedimentation Equillibrium Analytical Ultracentrifugation (AUC) Experimente haben gezeigt, dass die KID und die CD wichtig sind, um die intrinsische Dimerisierungskapazität der Kinasedomäne zu erhalten. Diese intrinsische Tendenz unterstützt vermutlich die ligandeninduzierte Dimerisierung bei der Rezeptoraktivierung. Deletionsmutanten zeigen eine niedrigere Tendenz zur Dimerisierung mit steigender Proteinkonzentration. Experimente, die zum Ziel hatten die Phosphorylierungskinetik der Kinasedomäne zu untersuchen, ergaben eine zeitlich geordnete sequentielle Aktivierungssequenz.

In einem dritten Projekt untersuchten wir die *in vitro* Interaktion von T-Zell spezifischem Adapterprotein (TSAd) mit der aktiven Kinasedomäne von VEGFR-2. Es wurde gezeigt, dass die Y951 vermittelte Komplexbildung von TSAd mit VEGFR-2 zu VEGF induzierter Aktinreorganisation in den Zellen führt. Die Endothel- und Tumorzellen wurden dadurch zur Migration gebracht, wobei die Mitogenität unverändert blieb. Unser Ziel war es, mittels hoch- und niedrigauflösenden strukturbiologischen Methoden spezifische Informationen zur Interaktion von TSAd und VEGFR-2 abzuleiten. Erste chromatographische Analysen und Experimente mittels Multi Angle Light Scattering (MALS) bewiesen die Interaktion der beiden Proteine *in vitro*. SAXS Analysen der isolierten Bindungspartner und des Komplexes ergaben einen länglichen Signalkomplex, in dem sich die Bindungspartner parallel ausrichten.

5. Introduction

5.1. Vasculogenesis and angiogenesis

The mammalian circulatory systems consist of the cardiovascular and the Lymphatic system. The cardiovascular system is responsible for the delivery of oxygen and nutrients to every cell and organ and at the same time the removal of catabolic products such as carbon dioxide. The lymphatic system, on the other hand, is responsible for draining interstitial fluids from tissues and returning them back into the blood circulation. Furthermore, the lymphatic system filters the blood and the lymph. The lymph is a colourless liquid containing a remarkable number of lymphocytes that are able to fight infections. Vasculogenesis and angiogenesis are the essential processes required for the formation and maintenance of the vascular system. Vasculogenesis describes the *de novo* process of vessel formation from endothelial precursor cells, known as angioblasts, in early development of the embryo. Angioblasts that are differentiated endothelial cells originating from the mesoderm build up an early network of vascular tubes known as the primary vascular plexus (Risau, 1997; Yancopoulos *et al.*, 2000). Pericytes and smooth muscle cells that are recruited towards the vasculature stabilize and support this early network. This primary vascular plexus is then further developed by angiogenic processes. Angiogenesis is defined as the formation of new vessels from the pre-existing vasculature. Angiogenic processes are crucial for the maturation of the new vasculature during embryonic development. Wound healing or e.g. the female reproductive cycle are dependent on angiogenesis in the adult individual (Hyder and Stancel, 1999; Li *et al.*, 2003a). Angiogenesis can be subdivided into two types denoted as sprouting and non-sprouting angiogenesis (intussusception). During sprouting angiogenesis vascular endothelial cells migrate (sprout) into the initially proteolytically degraded extracellular matrix (ECM) guided by the angiogenic signal. During intussusception the vessel proliferates and extends into the lumen and splits into new vessels.

5.2. Molecular basis of vessel formation

Vessel formation and organization relies on complex processes that are not yet fully understood. These mechanisms are orchestrated by a plethora of growth hormones and their receptors. Fibrobalst growth factor (FGF) and later Vascular endothelial growth factor (VEGF) signaling plays a key role during embryonic development of the vascular network. The primary vascular plexus that already contains important vessel structures such as the dorsal aorta or the cardinal vein is formed by VEGFR positive angioblasts. Maturation and sprouting of the vessels is then further directed by VEGF-A. VEGF is the driving force in the formation of the immature vasculature by vasculogenesis and angiogenesis. The importance of VEGF signaling in embryonic development was demonstrated in mice that carried mutations in the VEGF-A alleles. Mice deficient for VEGF-A expression die at embryonic day 9.5-10.5 whereas mice carrying a mutation in one single allele die at embryonic day 11-12 (Carmeliet *et al.*, 1996; Ferrara *et al.*, 1996). VEGF levels must therefore be tightly regulated. The secretion of platelet-derived growth factor-B (PDGF-B) by vascular endothelial cells in response to VEGF-A recruits mural cells such as vascular smooth muscle cells and pericytes to stabilize the immature vasculature. PDGF-B is an important mediator of mural cell proliferation and migration. PDGF-B knockout mice die during embryonic development due to lack of pericyte-associated vessels, microvascular aneurysms and abnormal vascular morphogenesis (Hellstrom *et al.*, 2001). A very similar phenotype can be found in endothelial differentiation sphingolipid G-protein coupled receptor-1 (EDG-1) knockout mice. The EDG1 pathway is therefore also important for mural cell recruitment. Mural cell differentiation from mesenchymal progenitors is induced by transforming growth factor-β1 (TGF-β1) that is mainly produced by endothelial and preexisting mural cells. Studies in mice with targeted disruption of Smad genes, the intracellular mediators of TGF-β signaling, revealed a crucial role of TGF-β1 in embryonic development and initiating angiogenesis (Pepper, 1997). During blood vessel formation Notch signaling is known to inhibit mural cells adjacent to tip cells (Siekmann *et al.*, 2008). Vessel remodelling and stabilization are also guided by the Tie receptors consisting of Tie1 and Tie2 and two ligands, angiopoietin 1 (Ang1) and angiopoietin 2 (Ang2). The angiopoietins act together with VEGF. Ang1 is able to stabilize nascent vessels while Angiopietin-2 (Ang2) prepares the extracellular matrix (ECM) for the invading angiogenic sprouts (Maisonpierre *et al.*, 1997). In the presence of VEGF, Ang2 is able to support

angiogenic sprouting of vessels whereas in its absence Ang2 acts as an antagonist of ang1 and therefore destabilizes nascent vessels. Mice lacking Ang1 show a normal primary vasculature but this vasculature fails to undergo further remodelling due to lack of association with surrounding cells such as pericytes (Sato *et al.*, 1995; Suri *et al.*, 1996). These mice show mainly heart failures caused by problems in association of the endocardium and myocardium. A phenotype similar to Ang1/Tie2-deficient mice is known for mice lacking ephrin-B2 and EphB4 (Wang *et al.*, 1998). Eph receptor tyrosine kinases represent the largest family of receptor tyrosine kinases (RTKs). EphrinB2 was found to regulate angiogenic sprouting by regulating VEGFR-2 and VEGFR-3 internalization through its PDZ domain (Sawamiphak *et al.*, 2010; Wang *et al.*, 2010). Ephrins play therefore a significant role in early angiogenic remodelling. Moreover, ephrin signaling establishes the arterial-venous vessel fate in late stage vascular development. EphrinB2 is expressed in primordial arterial vessels whereas EphB4, its receptor, is expressed in the endothelium of primordial venous vessels (Wang *et al.*, 1998). This expression pattern is suggested to accomplish arterial and venous identity. Along with ephrin signaling, notch signaling besides being involved in vessel sprouting was found to favour arterial vs. venous cell differentiation in zebrafish (Lawson and Weinstein, 2002).

A

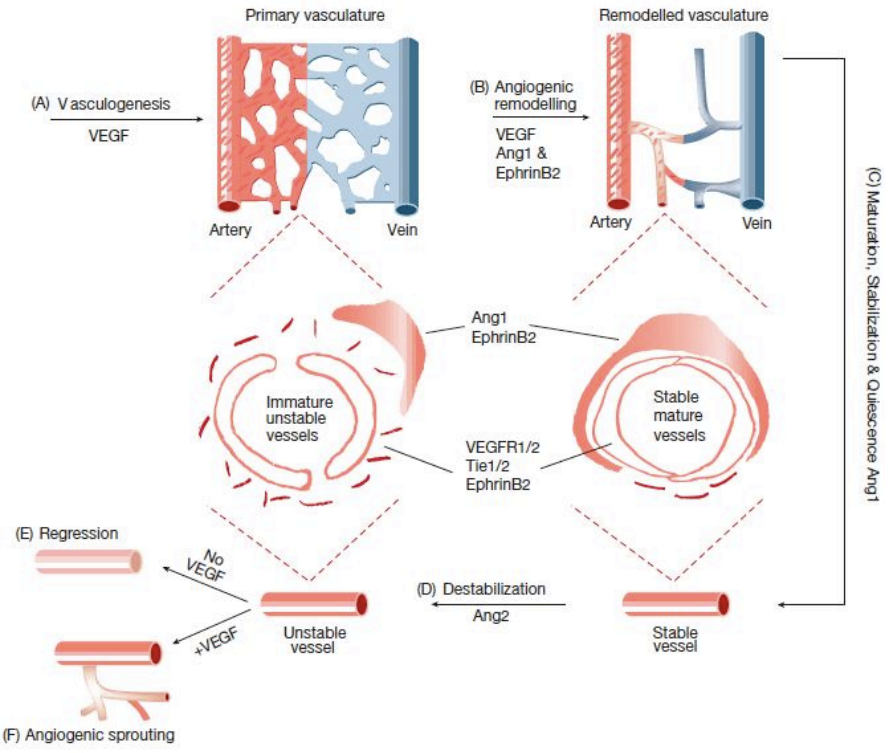

B

Ligand/receptor (cell type)	Putative roles
VEGF/VEGFR1, 2 (EC)	Upregulates proteases for matrix organization
	Generates provisional matrix by increasing permeability
	Upregulates PDGF-β to recruit mural cells to stabilize vessels
	Suppresses apoptosis to stabilize vessels
	Induces EC specialization (such as VVOs and fenestration)
$VEGF_{164}$/VEGFR2 and NRP1 (EC)	Promotes arterial growth (?)
VEGFC/VEGFR3 and NRP2	Guides lymphatic development
EG-VEGF/PKR1, 2 (EC)	Induces EC specialization in endocrine organs (such as fenestration)
Notch pathway (EC, mural cell)	Determines fate of the common progenitor cell (EC versus mural cell?)
	Establishes vessel fate (artery versus vein, upstream of ephrin signaling (in zebrafish?)
EphrinB2/EphB4 (EC)	Determines arterial and venous endothelial cell specialization
	Guides vessel branching
PDGFB/PDGFR-β (EC, mural cell)	Promotes proliferation, migration and recruitment of mural cells
S1P1/EDG1 (EC, mural cell)	Promotes recruitment of mural cells (downstream of PDGFB signaling?)
Ang1/Tie2 (EC)	Stabilizes vessels by facilitating interaction (EC–mural cell and EC–matrix)
	Suppresses apoptosis of ECs
	Induces hierarchical arrangement of vascular branching in the absence of mural cells
Ang2/Tie2 (EC)	Induces apoptosis of ECs in the absence of VEGF
	Determines lymphatic patterning
Ang1/Tie1, 2 (EC)	Coordinates vascular polarity
TGF-β1/TGF-βRII (EC, mural cell)	Promotes the production of ECM and proteases
	Promotes differentiation of fibroblast to myofibroblast to mural cell (through serum response factor)
TGF-β1/ALK1 (EC)	Regulates EC proliferation and migration (activation phase)
TGF-β1/ALK5 (EC)	Regulates vessel maturation (resolution phase)
TGF-β1/ALK1 and endoglin (EC)	Promotes arterio-venous specialization (through Notch/ephrin signaling?)
Syk/SLP76 pathway	Separates lymphatic from blood vessels

Figure 1: Illustration of vasculogenic and angiogenic processes
A) Schematic representation of vascular formation with involved growth factors and receptors (Yancopoulos et al., 2000). B) Ligands and receptors involved in vasculogenesis and angiogenesis (Jain et al., 2003).

In addition to the mentioned signaling pathways such as ephrin or notch signaling the extracellular matrix (ECM) influences branching, remodelling, and pruning of vessels and therefore guides patterning of the mature vasculature. The ECM is able to store several growth factors such as VEGF or FGF. During vascular formation matrix metallo proteases (MMPs) can release these factors by degrading the basement membranes to create spaces for invading vessel sprouts. Hence, further studies are necessary to understand the complex interplay between signaling pathways and the patterning role of extracellular space in vessel formation and maturation.

5.3. Pathological angiogenesis in cancer

Various human diseases are characterized by abnormal or excessive vessel growth. The most famous one is cancer. Solid tumors show poorly organized vasculature impaired to physiological vascular networks. Abnormal angiogenesis can also be found in other diseases such as psoriasis, arthritis or retinopathies induced by age (age-related macular degeneration, AMD) or diabetes. Degenerative diseases like osteoporosis are characterized by a regression of blood vessels (Ferrara and Kerbel,

2005). The growth of quiescent tumors that are modulated by pro- and anti-angiogenic factors (angiogenic switch) can be initiated by various effectors such as engagement of an immune response due to an inflammation or the mutation of oncogenes (Carmeliet and Jain, 2000). Many tumors initially start to grow as avascular cellular masses and subsequently induce angiogenic vessel sprouting towards the tumor site to allow further growth (figure 2a) (Folkman, 1971; Hanahan and Folkman, 1996). If tumors grow to a certain size of approximately 2 mm they become hypoxic. Hypoxia induces the upregulation of the transcription factor hypoxia-inducible factor 1 (HIF-1) that is responsible for the transcription of pro-angiogenic factors such as VEGF or FGF (Carmeliet *et al.*, 1998). The tumor vasculature is organized in a chaotic fashion and vessel walls show abnormal features. Vascular endothelial cells associate in an inhomogeneous way containing wide junctions or forming stacks. Cells undergo spontaneous apoptosis rendering vessel integrity weak and opening space for tumor cells. So called mosaic vessels are thought to have implications in metastasis. Furthermore, endothelial cells show fenestration and some lack expression of endothelial markers such as CD31. Adhesion molecules are not expressed homogeneously. Vessel diameters can vary due to compression of the vessels by the proliferating tumor (Helmlinger *et al.*, 2000). The tumor vasculature also lacks proper assocation with perivascular cells. Moreover, tumor associated pericytes show an abnormal morphology. These features often render vessels leaky. Characteristic for cancerous tissue is an imbalance of pro- and anti-angiogenic factors (Jain and Munn, 2000). VEGF family members are known to induce vessel-leakage (Fukumura *et al.*, 1998) whereas growth factors such as Ang1 do the opposite. Vessel co-option, the use of pre-existing vessels to support tumor growth, represents another way for tumor cells to progress as an initially well-vascularized tumor (Holash *et al.*, 1999a; Holash *et al.*, 1999b). Co-option results in a response of the host vessels since upon tumor growth vessels start to regress due to expression of Ang2 (figure 2b, left). Ang2 therefore represents a biomarker for co-opted vessels. The vessel regression causes the tumor environment to become hypoxic. The hypoxic environment leads to significant tumor cell death but surviving cancerous tissue induces novel angiogenesis by expression of VEGF (figure 2b, middle) (Holash *et al.*, 1999a; Holash *et al.*, 1999b).

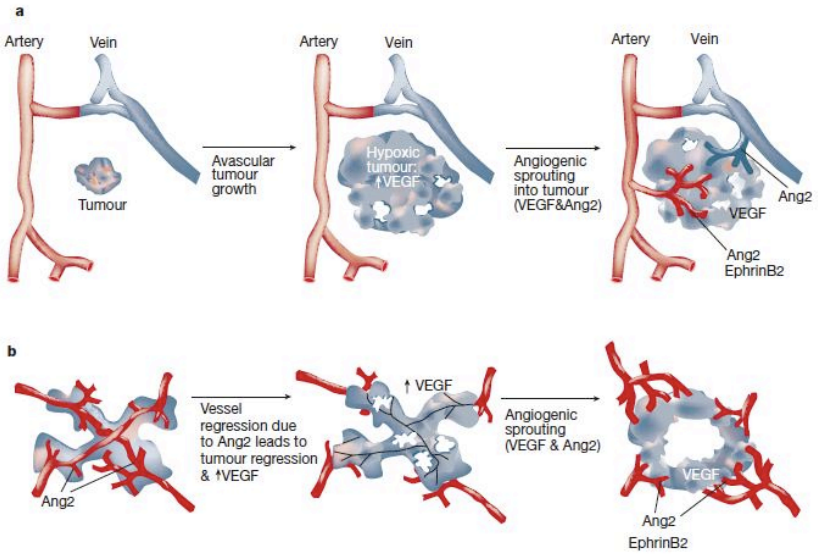

Figure 2: Mechanisms of pathological tumor angiogenesis
A) Induction of angiogenesis by an avascular tumor. B) Tumor growth involving host vessel co-option (Yancopoulos et al., 2000).

5.4. The VEGF/VEGFR signaling system

Vascular Endothelial Growth Factors (VEGFs) and their receptors are the key players in blood and lymphatic vessel development and homeostasis. Three type V receptor tyrosine kinases (RTKs): VEGF-receptor-1 (VEGFR)-1 (Flt1), VEGFR-2 (KDR/Flk1), and VEGFR-3 (Flt4) recruit five ligands: VEGF-A,-B,-C,-D and placenta growth factor (PLGF) in an overlapping receptor binding pattern (figure 3A). VEGF-E, found in orf family parapox viruses, and VEGF-F, found in snake venoms, are structurally highly related to mammalian VEGFs (Shibuya, 2003; Yamazaki *et al.*, 2009). VEGF-A, -B, -C, and PLGF are required for both blood and lymphatic vessel formation and development while VEGF-C and -D were sufficient for lymphatic vessel formation.

A

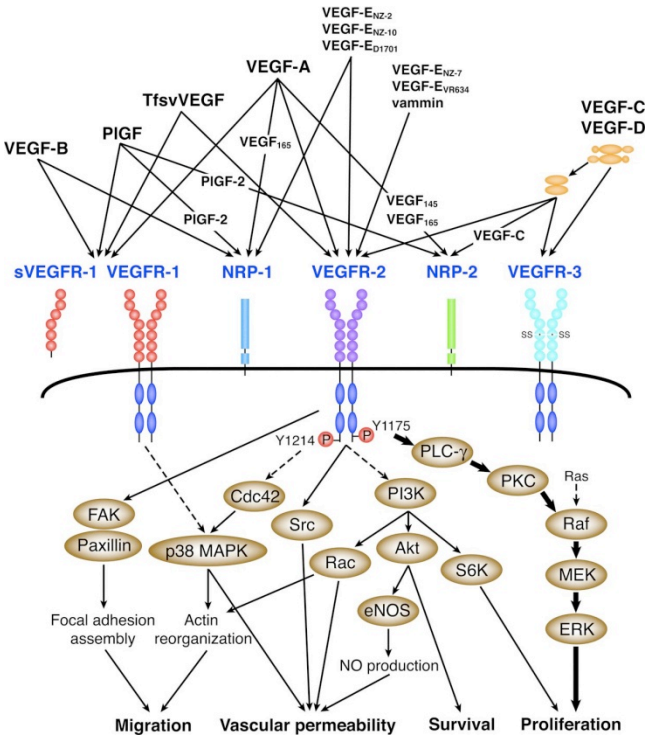

B

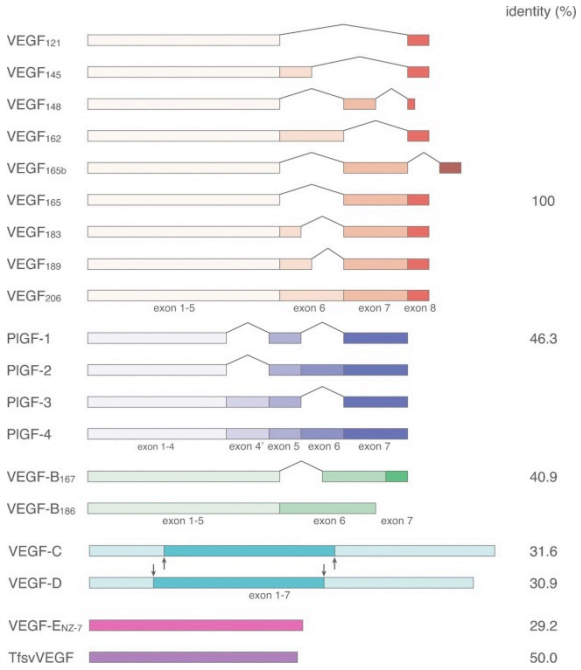

Figure 3: Signaling pathways of VEGFRs
(A) Binding of VEGFs to VEGFRs and neuropilins and signaling pathways of VEGFR-2. (B) Splice variants of the VEGF family. Red: VEGF-A, blue: PLGF, green: VEGF-B, turquoise: VEGF-C and –D, magenta: VEGF-E. Numbers depicted on the right indicate the amino acid sequence identity with VEGF-A$_{165}$. Arrows show sites of proteolytic processing for the generation of VEGF-C and -D with VEGFR-2 specificity (Takahashi and Shibuya, 2005).

VEGF binding to the VEGFR extracellular domains induces dimerization of receptor monomers followed by autophosphorylation of specific tyrosine residues in the receptor kinase domain within the cell. The phosphotyrosine containing activated kinase domains subsequently recruits signaling proteins that are able to activate specific cellular pathways (figure 3A). Alternative splicing or proteolytic processing of VEGFs results in various isoforms (figure 3B), which modulate biological signal transduction. (Takahashi and Shibuya, 2005). Furthermore, known co-receptors such as neuropilin-1 (Nrp-1), neuropilin-2 (Nrp-2) or heparan sulfate proteoglycans (HSPG) influence endothelial cell signaling (Grünewald *et al.*, 2010).

5.4.1. Structure and function of VEGFs and VEGFRs

The VEGF family growth factors represent secreted, dimeric cysteine-linked glycoproteins with a Mr of ~40 kDa. VEGFRs consist of an extracellular domain (ECD) with seven immunoglobulin-homology domains (Ig-homology domains). The fifth Ig-like domain of VEGFR-3 is split in disulfide-linked subunits The ECD is responsible for ligand binding and contributes to receptor dimerization by forming homotypic receptor contacts (Ruch *et al.*, 2007). A single transmembrane helix connects the ECD to the intracellular kinase domain with a regulatory JMD.

VEGF-A

VEGF-A plays pivotal role in vascular development in the embryo but also in adults. The deletion of one single allele in mice causes early lethality at embryonic day 11-12 (Carmeliet *et al.*, 1996;Ferrara *et al.*, 1996). VEGF-A exists in up to nine isoforms due to alternative splicing: VEGF-A_{121}, VEGF-A_{145}, VEGF-A_{148}, VEGF-A_{162}, VEGF-A_{165}, VEGF-A_{165B}, VEGF-A_{183}, VEGF-A_{189}, and VEGF-A_{206} (Figure 3B). All VEGF-A isoforms bind to VEGFR-1 and VEGFR-2 with high affinity. The VEGFR sites of interaction lie on opposite sides of the dimeric VEGF molecule. VEGF-A is expressed in vascular endothelial and immune cells (Ferrara and Davis-Smyth, 1997). The VEGF-A gene consists of eight exons and seven introns (Tischer *et al.*, 1991). All isoforms contain exon 1-5 and in addition exons 8a or 8b. Further combinations of exon 6-7/8 enable binding of heparan sulphate (HS) by basic amino acids. Exon 6a is part of VEGF-A_{145}, VEGF-A_{162}, VEGF-A_{189}, VEGF-A_{183} and VEGF-A_{206} whereas exon

6b is part of VEGF-A_{162} and VEGF-A_{206}. Furthermore, a basic sequence encoded by exon 7 can be found in VEGF-A_{189} and VEGF-A_{206} (Keyt *et al.*, 1996;Poltorak *et al.*, 2000;Poltorak *et al.*, 1997). The importance of HS binding becomes clear when studying VEGF-A_{164}, VEGF-A_{188} knockout mice. Knockout of VEGF-A_{164} or VEGF-A_{188} causes lethality immediately after birth. The reason are organ bleedings or cardiac dysfunction (Carmeliet *et al.*, 1999). Mice expressing only VEGF-A_{120} suffer from impaired angiogenesis in the myocardium, the retina and developmental problems of the skeleton (Maes *et al.*, 2002; Zelzer *et al.*, 2002). VEGF-A_{165b}, a splice variant that lacks the last amino acids compared to VEGF-A_{165} and its family members VEGF-A_{121b}, VEGF-A_{145b} and VEGF-A_{169b} are not expressed in tumors, but are part of the normal VEGF-A pool in normal tissue (Bates *et al.*, 2002; Perrin *et al.*, 2005; Nowak *et al.*, 2008; Woolard *et al.*, 2004; Pritchard-Jones *et al.*, 2007). The aforementioned exon 8b exerts this inhibitory effect by acting as partial agonists of VEGFR-2 (Woolard *et al.*, 2004) due to a lack of binding to Nrp-1 (Cébe-Suarez *et al.*, 2006).

VEGF-B

VEGF-B exists in two alternative isoforms: VEGF-B_{167} and VEGF-B_{186}. Both isoforms have different C-termini compared to VEGF-A. VEGF-B_{167} and VEGF-B_{186} are expressed in muscle tissue, heart, brain or skin and both bind to VEGFR-1 and Nrp-1 (Makinen *et al.*, 1999). VEGF-B_{167} and VEGF-B_{186} differ in their ability to bind to HSPGs. VEGF-B167 binds to HSPGs and is located on the cell surface and the ECM whereas VEGF-B_{186} is not able to bind to HSPSGs and is therefore freely diffusable upon secretion (Olofsson *et al.*, 1996a; Olofsson *et al.*, 1996b). Mice lacking VEGF-B showed no severe defects. VEGF-A could possibly take over the role of VEGF-B and prevent major biological failure (Mould *et al.*, 2003; Sun *et al.*, 2006). Nevertheless, mice demonstrate reduced recovery form brain and heart ischemia. Furthermore they show an impaired heart vasculature and abnormal heart morphology (Aase *et al.*, 2001). VEGF-B has been found in several cancer types but its role in cancer progression has not been attributed at the moment (Salven *et al.*, 1998). It is possible that synergistic effects of VEGF-B with other growth factors can play a role.

VEGF-C

After translation VEGF-C undergoes proteolytic maturation where its carboxy- and amino-terminal ends are cleaved giving rise to the final product being able to bind to VEGFR-3 and with lower affinity to VEGFR-2 (Joukov *et al.*, 1996). VEGF-C plays an important role in lymphangiogenesis and is mainly expressed in the lung or heart but the expression is also enhanced in various solid tumors (Kukk *et al.*, 1996; Pepper, 2001). VEGF-C knockout mice die as embryos due to impaired lymphatic vasculature and severe oedemas (Karkkainen *et al.*, 2003).

VEGF-D

VEGF-D does also undergo proteolytic maturation, similar to VEGF-C by cleavage of its carboxy- and amino-terminal ends to bind to VEGFR-3 and with lower affinity to VEGFR-2. VEGF-D is involved in growth and development of the lymphatic and the blood vasculature. Remarkably VEGF-D knockout mice are viable with negligible defects (Baldwin *et al.*, 2005). The lack of VEGF-D could possibly be compensated by VEGF-C. The exact role of VEGF-D remains to be determined. However, VEGF-D was found to influence metastasis of cancer cells (Stacker *et al.*, 2001).

PlGF

Alternative splicing of PlGF, that was initially isolated from human placenta, (Maglione *et al.*, 1991), gives rise to four different isoforms: PlGF-1 ($PlGF_{131}$), PlGF-2 ($PlGF_{152}$), PlGF-3 ($PlGF_{203}$), and PlGF-4 ($PlGF_{224}$). PlGFs bind to VEGFR-1 but not to VEGFR-2 and -3 (Park *et al.*, 1994). Furthermore, PlGF-2 recognizes Nrp-1 and 2. PlGFs show distinct heparin binding properties. PlGF-2 and -4 bind heparin whereas PLGF-1 and -3 do not (Maglione *et al.*, 1993; Yang *et al.*, 2003). PlGF is expressed in the placenta during human gestation and in the lung, heart or thyroid gland (Persico *et al.*, 1999). PlGF knockout mice did not develop an abnormal vasculature in the embryo but deletion of PlGF had an impact on cancer angiogenesis and pathology such as ischemia (Carmeliet *et al.*, 2001). Cancer progression could be stopped by blocking PlGF and ischemic tissue recovered upon revascularisation.

VEGFR-1

In 1990 VEGFR-1 was isolated from a placental cDNA-library (Shibuya *et al.*, 1990). VEGF-A, VEGF-B, PlGF and some VEGFs in snake venoms bind to VEGFR-1 with high affinity. VEGF-A binding affinity to VEGFR-1 was found to be more than 10 fold higher binding to VEGFR-2 and Ig-homology domain 2 was identified as the ligand-binding site of VEGF-A to VEGFR-1 (Wiesmann *et al.*, 1997). VEGFR-1 expression can be found in vascular endothelial cells, dendritic cells, perycytes, macrophages, monocytes or hematopoietic stem cells (Barleon *et al.*, 1996; Hattori *et al.*, 2002; Sawano *et al.*, 2001). VEGFR-1 knockout mice die at embryonic day 8.5-9. It was shown that death occurs due to increased proliferation of endothelial progenitor cells resulting in a disorganized vasculature (Fong *et al.*, 1995; Fong *et al.*, 1999). Mice expressing a kinase domain-deleted version of VEGFR-1 in contrary developed a normal vasculature and were viable (Hiratsuka *et al.*, 1998). It was suggested that VEGFR-1 acts as decoy receptor modulating embryonic development by sequestering VEGF-A and preventing overstimulation via VEGFR-2. Furthermore, the localization of VEGFR-1 in the membrane seems to be important. 50% of the mice expressing a soluble form of VEGFR-1 ECD die prenatally due to defective vasculogenesis (Hiratsuka *et al.*, 2005). Moreover, Shibuya et al. found a soluble VEGFR-1 isoform (sVEGFR-1) consisting of the first six Ig-homology domains that supports the hypothesis that VEGFR-1 acts as a scavenger (Shibuya *et al.*, 1990). The kinase domain of VEGFR-1 exhibits only weak tyrosine autophosphorylation and signal transduction although VEGF-A shows higher affinity for VEGFR-1 than for VEGFR-2 (Seetharam *et al.*, 1995; Waltenberger *et al.*, 1994). Gille et al. found a repressor sequence in the juxtamembrane domain (JMD) that constitutively inhibits receptor kinase and phosphatidylinositol 3`-kinase (PI3K) activation and endothelial cell migration (Gille et al., 2000). Moreover, mutation of N1050D in the activation loop of VEGFR-1 leads to an increase in activity (Meyer *et al.*, 2006). Depending on ligand-binding VEGFR-1 is able to change its tyrosine phosphorylation pattern and the resulting signaling output (Cunningham *et al.*, 1995; Sawano *et al.*, 1997). VEGF-A binding to VEGFR-1 leads to Y1213 phosphorylation whereas PlGF binding resulted in phosphorylation of Y1309 (Autiero *et al.*, 2003). Both ligands may induce distinct conformational changes in the receptor ECD giving rise to different signal transduction. To date the downstream signaling network of VEGFR-1 is still not well characterized. Various regulatory molecules such as p85/PI3K, PLC-γ1, growth-

factor-receptor-bound-2 protein (Grb2), Src-homology phosphatase-2 (SHP2) or Nck are known to interact with phosphotyrosine residues in the intracellular kinase domain of VEGFR-1 (Matsumoto and Claesson-Welsh, 2001). VEGFR-1 could regulate VEGFR-2 not only by its ability to sequester VEGF-A. It was shown that VEGFR-1 is able to suppress VEGFR-2-induced proliferation of endothelial cells (Zeng *et al.*, 2001). Embryonic stem cells lacking VEGFR-1 show increased VEGFR-2 phosphorylation (Autiero *et al.*, 2003; Olsson *et al.*, 2006) on the other hand earlier studies show that VEGFR-1 is able to amplify VEGFR-2 activity (Autiero *et al.*, 2003; Hiratsuka *et al.*, 2001). The exact mechanism by which VEGFR-1 and VEGFR-2 regulate each other remains to be discovered.

VEGFR-2

VEGFR-2, also known as KDR (kinase insert domain-containing receptor) or Flk-1 (fetal liver kinase-1), is the major receptor responsible for angiogenic and vasculogenic processes by VEGFs involving cell survival, migration, mitogenesis and permeability. The gene was initially isolated in 1991. VEGF-A, VEGF-C, VEGF-E, and proteolitically processed VEGF-D bind to VEGFR-2. Ligand binding of VEGFR-2 involves Ig-homology domains 2 and 3 (Fuh *et al.*, 1998; Leppänen *et al.*, 2010) (Brozzo *et al.*, 2012a). VEGFR-2 is expressed in vascular endothelial cells, hematopoietic cells but was also found in neurons or retinal cells (Kabrun *et al.*, 1997; Shiote *et al.*, 2005; Yang and Cepko, 1996). VEGFR-2 knockout mice die at embryonic day 8 to 9 due to lack of a functional vasculature similar to the deletion of VEGF-A reflecting the importance of the receptor in vasculogenesis (Shalaby *et al.*, 1995). Interestingly VEGF-A has a lower affinity for VEGFR-2 than for VEGFR-1. Nevertheless, VEGFR-2 exhibits strong kinase activity upon ligand binding. VEGFR-2 dimerization and activation leads to autophosphorylation of intracellular tyrosine residues. Of the 19 tyrosine residues in the intracellular domain Y801 in the JMD, Y1054 and Y1059 in the activation loop, Y951 in in the KID and Y1175 and Y1214 in the C-terminus have been mapped as important autophosphorylation sites serving as docking sites for regulatory proteins. These proteins interact with these phosphotyrosines via their Src-homology (SH) or phospho-tyrosine binding (PTB) domains. Phosphorylation of Y1054 and Y1059 is critical for kinase activation and catalytic potentiation (Kendall *et al.*, 1999; Takahashi *et al.*, 2001a). TSAd (T-cell specific adapter protein), an adapter protein lacking intrinsic catalytic activity, was

found to interact with phosphorylated Y951 in the KID of VEGFR-2 via its SH2 domain. Binding of TSAd to Y951 and the subsequent SH3-domain mediated binding of Src to TSAd leads to actin stress fibre formation and cell migration but does not induce mitogenesis (Matsumoto *et al.*, 2005; Wu *et al.*, 2000). Tyrosine 1175 represents the most important autophosphorylation site that initiates multiple signaling pathways. PLC-γ interacts with phosphorylated Y1175 in the CD of the kinase of VEGFR-2 via its SH2-domain. The PLC-γ mediated signaling pathway is a key regulator of vasculogenesis and angiogenesis. In mice the Y1173F mutation (corresponding to Y11775 in humans) induces embryonic death (Sakurai *et al.*, 2005). Binding of PLC-γ to pY1175 results in 1, 2-diacylglycerol (DAG) release following phosphatidylinositol 4, 5-bisphosphate (PIP2) hydrolysis. DAG is able to activate protein kinase C (PKC) and to trigger the release of intracellular calcium. PKC activates the Ras-independent MAPK pathway (Raf-MEK-ERK) that leads to gene transcription and finally endothelial cell proliferation (Cébe-Suarez *et al.*, 2006; Cunningham *et al.*, 1997; Koch and Claesson-Welsh, 2012; Takahashi *et al.*, 1999; Takahashi *et al.*, 2001b). Another adaptor protein, Shb (Src homology 2 protein in beta cells) binds to phosphorylated Y1175 and directly interacts with PI3-K (phosphoinositol-3-kinase) that provokes PKB/Akt (protein kinase B) activation. This pathway leads to an increase of nitric oxide (NO) that results in vascular permeability and in the survival of endothelial cells (Fujio and Walsh, 1999;Holmqvist *et al.*, 2004). Furthermore, Shb is able to bind to FAK (focal adhesion kinase), which modulates focal adhesion complexes and leads to migration of cells (Abedi and Zachary, 1997) (figure 4). Phosphorylated Y1214 recruits Nck that activates a pathway through p38 and induces migration of endothelial cells (Lamalice *et al.*, 2006).

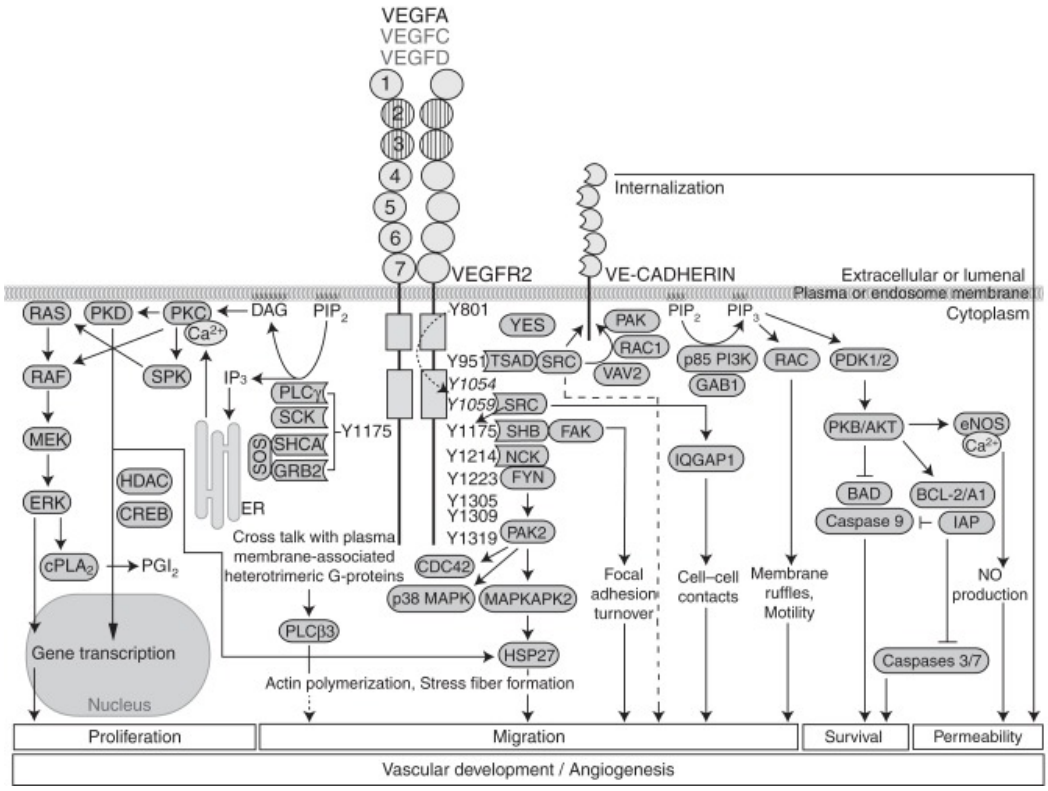

Figure 4: VEGF-A_{165} mediated signal transduction of VEGFR-2
(Koch and Claesson-Welsh, 2012)

VEGFR-2 does also exist in a soluble form similar to VEGFR-1. Soluble VEGFR-2 could be found in mouse and human plasma and consists of only the first six Ig-homology domains. Its function is still not clear. Some studies show that it acts as a scavenger for VEGF-C and negatively regulates lymphangiogenesis (Albuquerque *et al.*, 2009; Ebos *et al.*, 2004).

VEGFR-3

VEGFR-3 (Flt-4) binds to VEGF-C and VEGF-D. It is the main receptor for the development, regulation and survival of lymphatic vessels and plays also a role in the remodelling of the immature blood vasculature. VEGFR-3 is present in endothelial cells during embryogenesis (Kaipainen *et al.*, 1995). VEGFR-3 is synthesized as a precursor molecule and proteolytically processed in the fifth Ig-homology domain of the ECD. The split ECD is held together by a disulfide bridge. As mentioned, during embryonic development VEGFR-3 is expressed in all endothelial cells. In adults expression is restricted to lymphatic vessels (Oliver and Detmar, 2002). VEGFR-3 knockout mice die at embryonic day 9.5 due to defective vascular development

(Dumont *et al.*, 1998). Interestingly, this phenotype differs from VEGF-C knockout mice that die from impaired lymphatic vessels but show normal blood vessels. This indicates the important role of VEGFR-3 in early angiogenesis. Another explanation for such a phenotype is the modulation of VEGFR-2 during embryogenesis. It was shown that VEGFR-3 is able to form heterodimers with VEGFR-2 (Dixelius *et al.*, 2003; Nilsson *et al.*, 2010).

5.4.2. The role of the transmembrane domain of VEGFR-2

RTKs contain a single helical transmembrane segment that for a long time has been considered to play a passive role in dimerization and activation of the receptor. Disease related mutations within the transmembrane domain (TMD) of some receptors demonstrated that the TMD of RTKs is able to contribute to receptor dimerization and activation. Bargmann et al. identified a single V664E mutation in the TMD of the oncogene that gives rise to constitutive dimerization and activation of the receptor leading to tumor formation (Bargmann *et al.*, 1986; Bargmann and Weinberg, 1988). The substitution of the single G380R in the TMD of FGFR-3 leads to achondroplasia, that is a form of dwarfism (Li *et al.*, 1997) and the substitution of A392E has been associated with a human disease called Crouzon syndrome. Two single substitutions of M701N and G708N in the TMD helix of integrin αIIbβ3 are able to activate the integrin such that it constitutively binds fibrinogen (Li *et al.*, 2003b). These examples of induced receptor activations were thought to be driven by interhelical hydrogen bonding of the glutamic acid residues or residues that are capable to act simultaneously as hydrogen bond donor and acceptor (Smith *et al.*, 1996; Sternberg and Gullick, 1989; Zhou *et al.*, 2000). Biochemical studies of receptor mutants carrying polar amino acids such as Asn, Glu, Gln or Asp in micelles and cell membranes proved this assumption (Choma *et al.*, 2000; Gratkowski *et al.*, 2001; Zhou *et al.*, 2000). Moreover, specific dimerization motifs could be identified that presumably drive the dimerization process of the two TMD helices. Sequence motifs such as the heptat repeat (XxxxxxxX, X=G, A or S) the GG4-like repeat (XxxxX X=G, A, S or T, P0 requires a small amino acid, P1 and P2 are hydrophobic residues, P3 an aliphatic side chain and P4 again a small amino acid) or Leucine zippers (Kubatzky *et al.*, 2001; Ruan *et al.*, 2004) are present in several RTKs. The GxxxG motif as an example is present in c-Kit, PDGFR-A, -B or ErbB (Gerber *et al.*,

2004; Mendrola *et al.*, 2002; Sternberg and Gullick, 1990) or Glycophorin A (Lemmon *et al.*, 1992; MacKenzie *et al.*, 1997). Remarkably, the TMD helices of all human RTKs are enriched in small amino acids and thus indicate the importance of these residues in mediating and stabilizing helix-helix contacts in the lipid bilayer. Structural evidence comes from NMR-studies of dimerized TMD-helices. The TMD-helices of ErbB2 associate through a tandem variant of the GG4-motif Thr^{652}-X_3-Ser^{656}-X_3-Gly^{660} that is located in the N-terminal part of the helix (Bocharov *et al.*, 2008). A global analysis of the TMD of the existing 58 RTKs showed that the TMD helices encode an intrinsic propensity to form dimeric structures within the cell membrane and that specific interactions are generally involved in signaling by RTKs (Finger *et al.*, 2009a). Nevertheless, the various RTKs show remarkable differences in the interaction propensity relative to the interaction of the human GpA wt-TMD that reflects the strongest interaction. In this study the TMD-helices of VEGFR-2 showed a moderate intrinsic propensity to form dimers and indeed none of the known dimerization motifs are present. However, the role of the TMD of VEGFR-2 remains unclear so far. It has previously been shown that RTKs can be artificially activated by mutating the TMD. Bell *et al.* (Bell *et al.*, 2000) designed a dimerization interface in an valine TMD of the neu receptor carrying two sequentially positioned glutamic acid residues seven amino acids apart that gave rise to activating and inactivating receptor constructs. However, other results showed that the TMDs of RTK are more likely to interact in an X-shaped conformation (Bocharov *et al.*, 2008; Gullick *et al.*, 1992; Mineev *et al.*, 2010; Smith *et al.*, 1996). Introduction of the dimerization interface used by Bell *et al.* into the TMD of VEGFR-2 resulted in an activation pattern of VEGFR-2 similar to neu. Sequentially arranged glutamic acid residues in an otherwise all valine TMD helix in VEGFR-2 gave rise to either active or inactive dimers. Dimerization is therefore required but not sufficient for activation of VEGFR-2 (Dell'Era Dosch and Ballmer-Hofer, 2009a).

5.4.3. The intracellular kinase domain of VEGFR-2

Tyrosine phosphorylation plays an essential role in signal transduction of cells. This posttranslational modification of proteins must be tightly controlled in order to avoid deregulation of cells. Protein tyrosine kinases are the enzymes that catalyse the phosphoryl transfer from ATP (γ-phosphate) onto the hydroxyl group of specific

protein substrate side chains. VEGFRs belong to the platelet-derived growth factor receptor (PDGFR) family. Other members of this family are PDGFRα and -β, colony stimulating factor-1 receptor (CSF-1R) or stem cell growth factor receptor (c-Kit). Compared to other kinases, these family members contain a kinase insertion domain (KID). The only structural information available for the intracellular domain of VEGFR-2 derives from a partial structure lacking parts of the JMD, 50 of the 68 residues of the KID and the entire ~200 residues carboxy-terminal domain (CD) (McTigue *et al.*, 1999a). Several crystal structures of the same protein in complex with various inhibitors are available at present. A crystal structure of the kinase domain of VEGFR-1 in complex with an inhibitor has been solved in 2009 and is available in the PDB database (3HNG). The intracellular kinase domain of VEGFR-1 and VEGFR-2 adopts a typical bilobal structure that is split by the KID. The N-lobe of the kinase domain consists predominantly of antiparallel β-sheets and one single α-helix denoted as the αC-helix. The αC-helix is an important element that is used to switch the kinase on or off. The C-lobe of the kinase domain is of mainly α-helical nature. The active site of the enzyme is located in the cleft between the N- and the C-lobe. VEGFR-2 is activated according to the general mechanism accounting for RTKs activation. RTKs are activated through ligand-induced dimerization, which rearranges the cytoplasmic tyrosine kinase domains. Dimerization facilitates autophosphorylation of specific tyrosine residues in the kinase domain that serve as recruitment sites for regulatory proteins. Activation of tyrosine kinases usually requires the phosphorylation of tyrosine residues on the JMD and in the activation loop. Substantial reorientation of the αC-helix is necessary to activate the kinase domain. In the open conformation ATP and substrate bind to specific sites between the N- and the C-lobe of the enzyme. Detachment of the γ-phosphate of ATP and its transfer to the substrate occurs in the closed conformation. Finally release of ADP and phosphorylated substrate take place in the transition from the closed to the open conformation (Kornev *et al.*, 2006). Coordinated movements between the open and the closed conformation of both lobes are thought to be stabilized by hydrophobic contacts referred to as flexible hydrophobic “spine” (figure 5).

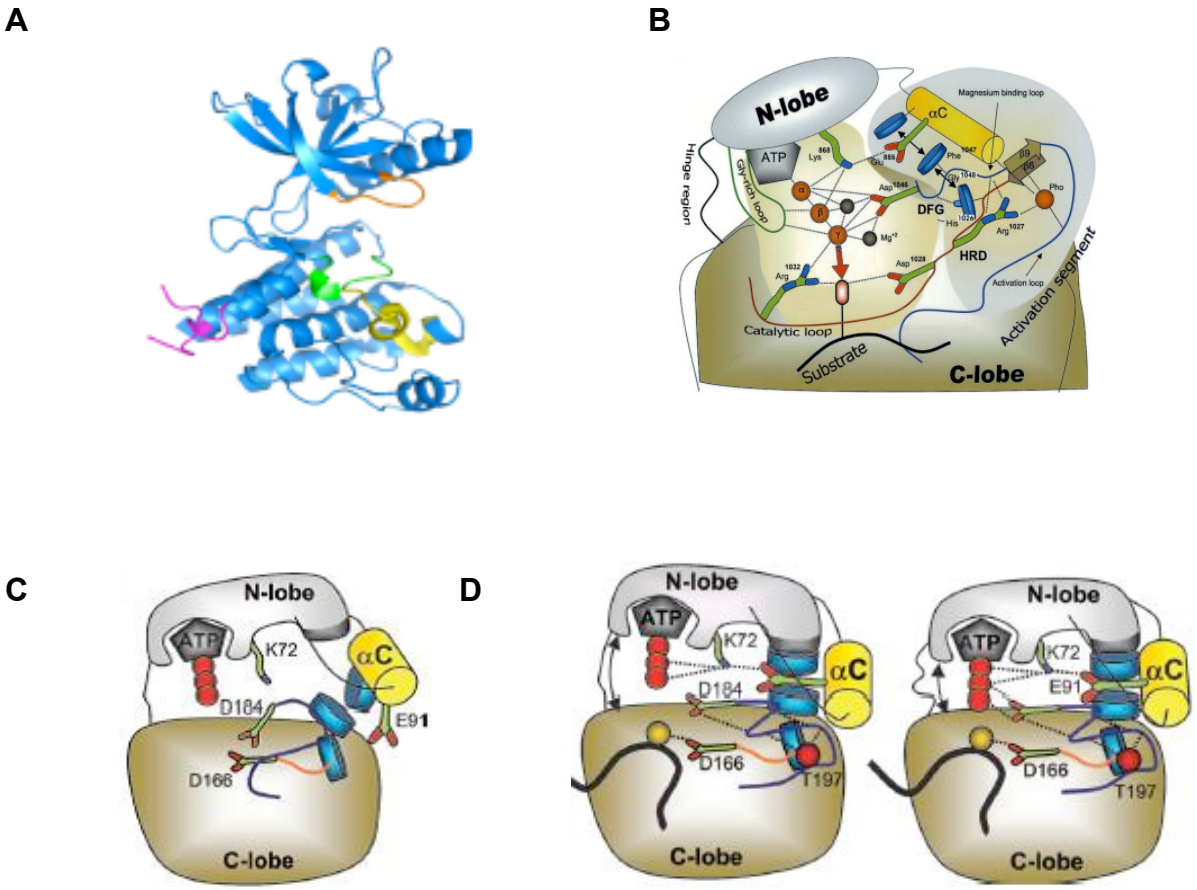

Figure 5: The intracellular kinase domain
(A) Overall structure of VEGFR-2 kinase domain (McTigue et. al, 1999, 1VR2). Orange: Glycine-rich loop. Green: Activation loop. Yellow: Catalytic loop. Magenta: Boundaries of the KID. (B) Diagram with interaction between the human VEGFR-2 protein tyrosine kinase catalytic core residues, ATP and the substrate. Important residues in contact with ATP or the substrate are depicted in the light khaki background. Secondary structures and residues important for regulation of the catalytic activity can be found in the grey background. Hydrophobic interactions between the HRD motif, the DFG motif and the αC-helix are indicated by black arrows. Polar contacts are indicated by dashed lines. Pho: phosphotyrosine (Roskoski et al., 2008). (C) General model of protein kinase activation in PKA: Inactive kinase conformation. The activation loop and the "spine" are distorted. The molecule is destabilized and the lobes can move independently. (D) General model of protein kinase activation in PKA: Active kinase conformation. T^{197} orients the DFG aspartate to interact with ATP and the DFG phenylalanine for building up a hydrophobic "spine" that is completed by the movement of the αC-helix. The hydrophobic spine stabilizes the kinase domain for catalysis. This conformation is stabilized by the K^{72}-E^{91} interaction. Spine residues are indicated as blue disks and the shaded grey portion of the N-lobe (Kornev et al., 2006).

It was shown that activation of certain RTKs such as the FGFR or the EGFR family are additionally controlled by an allosteric interaction between the two kinase domains in an asymmetric dimer (Stamos *et al.*, 2002; Zhang *et al.*, 2006). The mechanism resembles that of a cyclin and its cyclin dependent protein kinase. One kinase domain (the activator) acts as the "cyclin" by activating the second kinase

domain that plays the role of a cyclin dependent protein kinase (the receiver). In later studies it was shown that the JMD of EGFR is actively involved in the formation of the asymmetric dimer (Endres *et al.*, 2013). Disruption of the asymmetric dimer interface in EGFR leads to drastic reduction of autophosphorylation and enzymatic activity (Jura *et al.*, 2009). The same mechanism was found in FGFR1 and FGFR2. The structures of FGFR1 and FGFR2 show an asymmetric dimer in the process of autophosphorylation at their canonical tyrosine sites (Bae *et al.*, 2010; Bae and Schlessinger, 2010; Chen *et al.*, 2008) (figure 6).

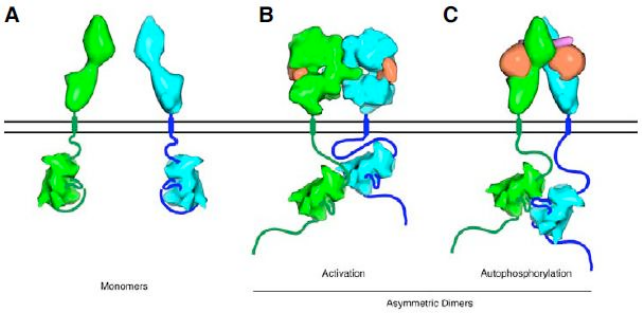

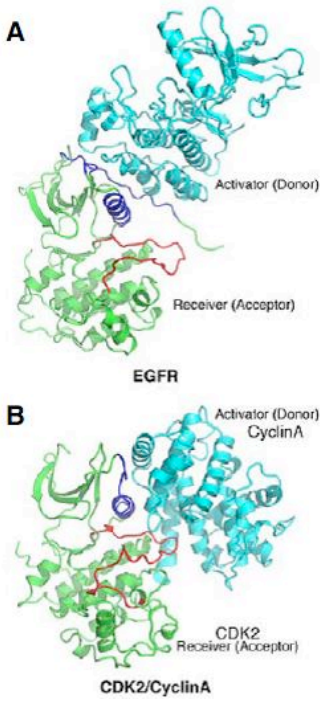

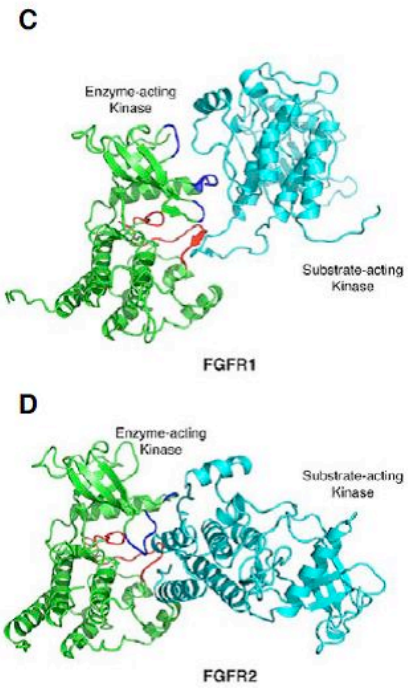

Figure 6: Asymmetric dimer formation in RTKs
Top panel: Schematic representation of (A) monomeric forms of EGFR. (B) Asymmetric dimer formation upon ligand binding. The JMD stabilizes the asymmetric dimer. (C) Asymmetric EGFR dimers in the event of trans autophosphorylation. The green kinase is the enzyme-acting kinase while the blue kinase is the substrate-acting one. Middle panel: (A) Asymmetric dimer formation in the event of initial activation of EGFR. Activator kinase: Cyan. Receiver kinase: Green. The activation loop in the receiver (red) adopts an open conformation. The interface of the asymmetric region (blue) is mainly formed by the α-C helix, and the JMD of the receiver kinase. (B) Complex structure of CDK2 and Cyclin A (1FIN). Bottom panel: (C) Asymmetric dimer formation of FGFR1 in the event of trans phosphorylation (3GQI). Y583 in the KID of the kinase domain is bound to the catalytic site of the other kinase. (D) Asymmetric dimer formation of FGFR2in the event of trans autophosphorylation (3CLY). C-terminal Y769 is bound to the catalytic site of the other kinase. The Glycine-rich loop participates in asymmetric homodimer formation in both FGFR1 and FGFR2 (Bae and Schlessinger, 2010)

5.4.4. The active site of VEGFR-2

Protein tyrosine kinases catalyse the phosphotransfer reaction of the γ-phosphate from ATP onto a protein substrate. This important posttranslational modification is evolutionarily conserved from prokaryotes to humans. As a result, also the catalytic subunits of protein kinases are highly conserved. The active site between the N- and the C-lobe of the kinase domain consists of a nucleotide binding site, the catalytic loop that is essential for the transfer reaction and the large and flexible activation loop that regulates the activity of the kinase domain. In VEGFR-2 the residues

forming the ATP binding site are E917-N923 that connect the N- and the C-lobe and residues L840-I849. Among these residues is the glycine-rich (G-loop) or often also referred to as the nucleotide binding loop (G841-G846). In the crystal structure of the truncated VEGFR-2 kinase domain The G-loop adopts a well-ordered conformation resembling the unliganded FGFR1 structure (Mohammadi *et al.*, 1997). The G-loop is able to alter its position depending on the activation and ligand-bound state of a kinase. The position of the G-loop in FGFR1 and VEGFR-2 is comparable although the VEGFR-2 structure contains no bound ATP (McTigue *et al.*, 1999b). The adenine ring of ATP is known to form two conserved hydrogen bonds with the protein backbone. In the crystal structure of FGFR1 that contains the ATP analog adenylyl methylenediphosphate (AMP-PCP) these two hydrogen bonds are formed between the adenine amino group and the backbone carbonyl of E562 that corresponds to E917 in the G-loop of VEGFR-2. Efficient catalysis depends on a protein stretch denoted as the catalytic loop. In kinases the catalytic loop connects helix αE with β-sheet β7. The sequence of the catalytic loop contains a highly conserved stretch of residues: HRD-LAARN that in VEGFR-2 corresponds to H1026-N1033. Moreover, a conserved aspartate (D1028) within this stretch that acts as a “catalytic base” is highly important for the phosphotransfer reaction (Johnson *et al.*, 1996). The position of the loop backbone and its residues in VEGFR-2 show similarities with the catalytic loop in the unliganded FGFR1 and in the activated insulin receptor tyrosine kinase (IRK) in complex with a peptide substrate and an ATP analogue (Hubbard, 1997). The side chain carboxylate of the catalytic aspartate D1028 is hydrogen-bonded to the conserved side chains arginine R1032 and asparagine N1033. The activation loop, a large flexible loop in the active site of kinases, is known to regulate kinase activity by changing its conformation and is characterized by conserved residues DFG at the beginning and APE at the end of the loop (Johnson *et al.*, 1996). Conformational change is often induced by phosphorylation of specific tyrosine residues in this loop. The structure of the insulin receptor kinase domain was first to demonstrate autoinhibition of RTKs by its own activation loop (Hubbard, 2004). Tyrosine Y1162 in the activation loop blocks the active site from being accessed by ATP and the substrate. Upon *trans*-phosphorylation of the residue the *cis*-autoinhibitory conformation of the activation loop is disrupted and the kinase is activated. The αC-helix subsequently stabilizes ATP binding by reorienting itself. In FGFR1 the tyrosines in the activation loop stabilize the inactive state of the kinase

and do not directly block the substrate binding site. The ATP binding site remains still accessible (Bae and Schlessinger, 2010; Chen *et al.*, 2007). In VEGFR-2 the activation loop involves residues D1046-E1075. Two tyrosines being part of the activation loop are known to be phosphorylated upon activation of the kinase: Y1054 and Y1059 (Dougher Vermazen *et al.*, 1994). The VEGFR-2 protein used to determine the 3D structure was *in* vitro phosphorylated prior to crystallization and phosphorylation at Y1059 was detected (McTigue *et al.*, 1999a). Surprisingly, the activation loop adopted an inhibited conformation. Electron densities for the central segment of the activation loop (G1048-G1063) could not be assigned due to the high flexible nature of the loop also observed in other kinases (Huse and Kuriyan, 2002). Residues 1064-E1075 adopted a conformation comparable to the unliganded FGFR1 structure. The crystal-packing environment possibly induces this conformation inhibitory to substrate binding.

5.4.5. The JMD of VEGFR-2

It has previously been shown that subdomains outside the active site of RTKs are important for recruitment of regulatory proteins, stabilization of the active conformation and the triggering of autoinhibition of the kinase domain. As demonstrated in several crystal structures, the JMD is such a regulatory element. The JMD is involved in formation of the activated asymmetric dimer in EGFR. Models and recently NMR structures proved that parts of the JMD form an antiparallel helical dimer (Endres *et al.*, 2013). Phosphorylation of the JMD in c-Kit is required for activation (Ma et al., 1999). In the insulin receptor, phosphorylation of tyrosine residues in the JMD creates binding sites for signaling molecules. Here the JMD does not regulate kinase activity. In muscle-specific kinase (MuSK), Eph family (figure 7a, 7b) or TGF-β family RTks the JMD binds to an autoinhibitory cleft in the N-lobe. The JMD forms an alpha-helical structure and reorients the the catalytically important alpha C-helix (Hubbard, 2004; Wybenga-Groot *et al.*, 2001). The JMD of type III receptor kinases Flt3, c-Kit or CSF-1 (figure 7c) binds in an interface between the N- and the C-lobe of the kinase domain and sterically prevents the activation loop and the C-α helix from adopting an active conformation (Griffith *et al.*, 2004; Mol *et al.*, 2004; Mol *et al.*, 2003; Schubert *et al.*, 2006).

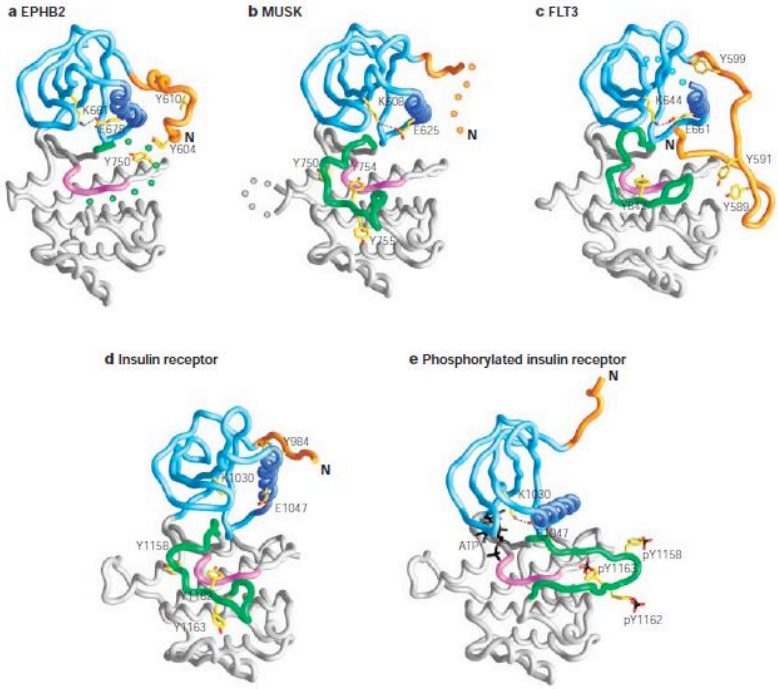

Figure 7: Autoinhibitory mechanisms of the JMD in RTKs
Crystal structures of (A) unphosphorylated EPHB2 (B) unphosphorylated MuSK (C) unphosphorylated FLT3 (D) unphosphorylated insulin receptor and (E) phosphorylated insulin receptor. Figures are shown as backbone representations. The side chains and ATP in part are shown in stick representation. Juxtamembrane regions: Orange. N-terminal kinase lobes: Light blue with α-helix C in dark blue. C-terminal kinase lobes: Grey with catalytic loop in pink and the activation segments in green. Disordered regions are represented in spheres (Hubbard, 2004).

The JMD of VEGFR-2 may follow a similar mechanism previously found in type III RTKs. It was shown that the kinase domain of VEGFR-2 carrying the JMD exhibits higher thermostability than the JMD-deleted kinase domain (Solowiej *et al.*, 2009). Furthermore, it was shown that *in vitro* activation of the isolated kinase domain of VEGFR-2 by ATP leads to phosphorylation at Y801 as a first event followed by phosphorylation of Y1054 and Y1059 in the activation loop that finally leads to activation of the kinase (Dougher Vermazen *et al.*, 1994;Kendall *et al.*, 1999; Solowiej *et al.*, 2009). The initial phosphorylation of Y801 occurs via an intramolecular mechanism and the kinase domain may therefore initiate the release of the autoinhibitory JMD from the catalytic cleft as a first step in the activation process. Further structural studies will be required to explain the exact autoinhibitory mechanism of the JMD in VEGFR-2.

5.4.6. The KID of VEGFR-2

The KID or the region between helices αD and αE does not show any conservation among kinase domains. Length, amino acid composition and structure of the insertion domains seem not to follow strict rules. In earlier studies it was shown that deletion or mutation of the KID did not alter the kinetic properties of the enzyme but rather that the KID was important for recruitment of signaling molecules through phosphorylated tyrosine residues residing on the KID (Heidaran *et al.*, 1991; Kazlauskas and Cooper, 1989; Lev *et al.*, 1992). The deletion of 58 of the 64 residues of the CSF-1R KID decreased substrate phosphorylation by 10% and the complete deletion of 98 residues of the KID in PDGFR-β decreased the kinase activity by 80%. The crystal structure of the kinase domain of Tie-2 revealed an important role for the KID as a regulatory element for kinase activation. In the inactive state the phenyl ring of Y1112 of the CD of Tie-2 is packed between hydrophobic side chains of L696, L579, F1114 and R577 inside the KID. As a result the CD folds back onto the kinase domain and blocks the active site. The KID of VEGFR-2 comprises 68 residues (N933 to L1000). These residues connecting helices αD and αE are highly charged and hydrophilic. The KID contains six lysine, five arginine, eight glutamic acid and five aspartic acid residues. Furthermore it contains a canonical tyrosine residue denoted Y951 is a target for autophosphorylation (Matsumoto *et al.*, 2005).

5.4.7. The C-terminal domain of VEGFR-2

Not much is known about the role of the C-terminal domain in VEGFR-2 activation. Chimeric receptor constructs that contained the ECD of colony stimulating factor receptor (CSF) receptor fused to the C-terminus-deleted kinase domain of VEGFR-2 showed no activation of the kinase domain upon CSF stimulation (Meyer *et al.*, 2003). Based on that Meyer *et al.* proposed that the kinase domains of VEGFR-2 adopt an inactive dimeric conformation in the absence of the CD. The same effects could be found in CD-deleted EGFR. The deletion of the 164 amino acid CD of EGFR inactivates the receptor (Wedegaertner *et al*, 1992). Peptides derived from the C-terminus of Met were able to inhibit kinase domain activation *in vitro*. Furthermore, cell delivery of such peptides abolished HGF-dependent Met phosphorylation and

downstream signaling (Bardelli *et al.*, 1999). The only structural evidence for an active contribution of the CD in receptor activation comes from the Tie-2 receptor (figure 9). The C-terminus inhibits the monomeric kinase domain of Tie-2 in the inactive state (Shewchuk *et al.*, 2000a). Tyrosine Y1112, a major C-terminal phosphorylation site, is packed in a hydrophobic pocket inside the KID of the kinase domain. This enables the C-terminal strand to block substrate access to the active site of the kinase.

A **B**

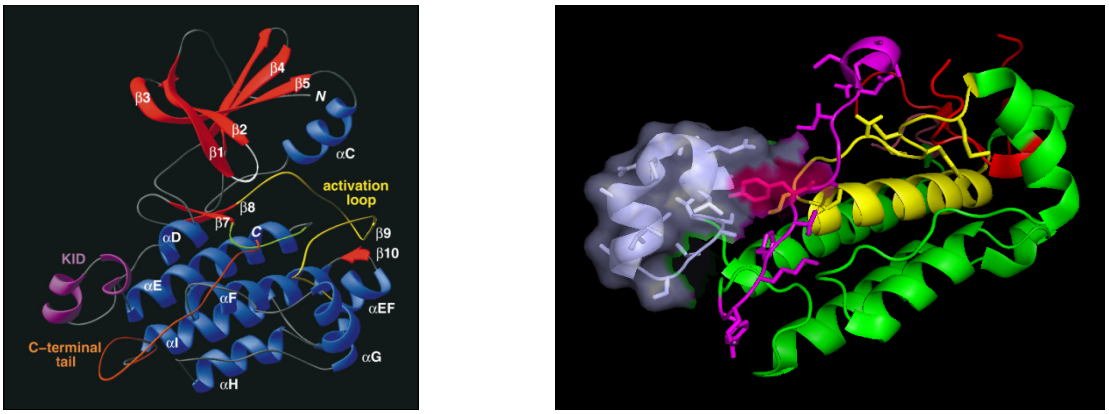

Figure 9: Crystal structure of Tie-2
(A) Ribbon representation of the inactive Tie-2 kinase domain structure. α-helices: Blue. β-sheets: Red. Nucleotide-binding loop: White. Catalytic loop: Green. Activation loop: Yellow. KID: pink. The inhibitory C-terminal tail is depicted in orange (Shewchuck et al., 2000). (B) PyMOL model of Y1112-KID interaction. The C-terminal tail is shown in magenta. Tyrosine Y1112 is depicted in red. The KID is colored in white.

Interestingly, the activation loop of Tie-2 adopts an active conformation in the crystal structure. Cell biological follow-up studies verified these structural data (Niu *et al.*, 2002; Sturk *et al.*, 2009). A similar mechanism may also exist in PDGFR but to date structural studies have not been described. The crystal structures of the kinase domain of VEGFR-2 does not reveal valuable insights on the role of specific kinase subdomains in VEGFR-2 activation (McTigue *et al.*, 1999a). This is due to the fact that dramatic protein truncations were necessary to crystallize the protein.

5.5. Aim of the thesis

The VEGF/VEGFR signaling system is a critical regulator of angiogenesis and vasculogenesis during normal development but also in several pathological conditions such as cancer. The five VEGF ligands bind to three receptors with overlapping specificity. Additional VEGF co-receptors such as neuropilins or HSPGs further modulate the final biological output. VEGF binding to its receptor induces dimerization of receptor monomers, followed by rearrangement of the intracellular kinase domains. The proper alignment of the kinase domains leads to autophosphorylation on distinct tyrosine residues and recruitment of intracellular signaling molecules. The subsequent activation of specific cellular pathways leads to the biological output. Although there is an increasing amount of data describing angiogenic processes, the exact mechanism of activation, modulation and inhibition of the intracellular kinase domain of VEGFRs still needs more profound insights.

One of the aims of this thesis was to study the role of the TMD during VEGFR-2 activation. At the beginning we knew that many RTKs are artificially dimerized and activated by manipulating the TMD. Furthermore, we had the knowledge from studies of our own lab showing that the use of an artificial all valine TMD carrying two sequentially arranged glutamic acid residues promotes the formation of either active or inactive VEGFR-2 dimers. From these experiments using such artificial TMDs we knew that dimerization of VEGFR-2 is necessary, but not sufficient for receptor activation. We wanted to confirm the previous findings in the context of the wt-TMD and therefore gain additional insights using a more physiological system. In order to shed light on conformational changes within the TMD helices during the activation process of VEGFR-2 we also used high-resolution structural biology methods.

Another aim was to analyse the function of individual kinase subdomains such as the KID and the CD in VEGFR-2 activation using cell biological and structural biology methods. We knew from other VEGFR-2 related RTKs that these subdomains have the ability to regulate the activity of the intracellular receptor kinase domains. In this project we also performed experiments aiming to investigate the phosphorylation and dimerization kinetics of the VEGFR-2 kinase domain to obtain deeper insights into the mechanism of kinase activation.

As a third aim, we characterized the *in vitro* interaction between TSAd and activated VEGFR-2. From cell biological studies it was known that pY951 mediated complex

formation of TSAd with VEGFR-2 is required for VEGF-induced actin reorganization and migration of endothelial and tumor cells. Our goal was to understand the mode of binding of the non-canonical SH2-domain of TSAd interacting with pY951 of VEGFR-2. Furthermore, we aimed to analyse the overall structure of the complex using low- and high-resolution structural biology methods.

6. Materials and Methods

6.1. Functional analysis of transmembrane and kinase domain mutants of VEGFR-2

In order to investigate the role of the TMD and define contributions of the ECD in the activation process of VEGFR-2 we designed several TMD mutants. Further we designed VEGFR-2 mutants containing deletions in distinct domains within the catalytic kinase. TMD mutants were cloned by introducing a single or double glutamic acid mutation into the wt-TMD helix. The two glutamic acid residues in the double mutants were spaced seven amino acids apart. Glutamic acid residues were then sequentially moved across the TMD helix for both types of mutants. For the TMD and the catalytic domain mutants we designed both ligand-independent, ECD truncated constructs (deletion of amino acids 25–755, accession number P35968) and full-length constructs including the complete ECD of VEGFR-2. Constructs were cloned into mammalian expression vectors. The ECD truncated constructs were cloned into the mammalian expression vector pCDNA3 (Invitrogen) whereas the full-length VEGFR-2 mutant constructs were cloned into the eGFP expression vector pBE. All constructs contained a HA tag.

6.1.1. Cloning of transmembrane and kinase domain mutants of VEGFR-2

ΔECD-VEGFR-2 TMD mutant constructs

The HA-tagged wt-TMD ΔECD-VEGFR-2 construct was cloned by Debora Dell'Era-Dosch. In order to generate mutations within the TMD we applied site-directed mutagenesis on the wt-construct. To introduce a second point mutation we used the mutated constructs as a template for site-directed mutagenesis. We used the following primers (mutated bases in red):

5'-3' primer sequence	TMD Mutation
For 5'-GAACTTGGAAATCATTGAACTAGTAGGCA-3' Rev 5'-GAAGTAGCCAGAAGAACATGGCAATC-3'	I767E
For 5'-TGGAAATCATTATTGAAGTAGGCACG-3' Rev 5'-GAAGTAGCCAGAAGAACATGGCAATC-3'	L768E
For 5'-CATTATTCTAGAAGGCACGGCGGTG-3' Rev 5'-GTAGCCAGAAGAACATGGCAATCACC-3'	V769E
For 5'-CATTATTCTAGTAGAAACGGCGGTGATTG-3' Rev 5'-GAAGTAGCCAGAAGAACATGGCAATC-3'	G770E
For 5'-CTAGTAGGCGAAGCGGTGATTGC-3' Rev 5'-CAAGAAGTAGCCAGAAGAACATGGC-3'	T771E
For 5'-CTAGTAGGCACGGAAGTGATTGCC-3' Rev 5'-CAAGAAGTAGCCAGAAGAACATGGC-3'	A772E
For 5'-GCACGGCGGAAGTGATTGCC-3' Rev 5'-CAAGAAGTAGCCAGAAGAACATGGC-3'	V773E
For 5'-CGGCGGTGGAAGCCATGTTCT-3' Rev 5'-CAAGAAGTAGCCAGAAGAACATGGC -3'	I774E
For 5'-GGCGGTGATTGAAATGTTCTTCT-3' Rev 5'-CAAGAAGTAGCCAGAAGAACATGGC-3'	A775E
For 5'-GGTGATTGCCGAATTCTTCTGGCTAC3' Rev 5'-GTAGCCAGAAGAATTCGGCAATCACC-3'	M776E

For 5‘-GTGATTGCCATGGAATTCTGGCTACTTCT-3‘ Rev 5‘-GAAGTAGCCAGAAGAACATGGCAATC -3‘	F777E
For 5‘-CATTATTCTAGAAGGCACGGCGGTG-3‘ Rev 5‘-GTAGCCAGAAGAATTCGGCAATCACC-3‘	V769E M776E
For 5‘-CATTATTCTAGTAGAAACGGCGGTGATTG-3‘ Rev 5‘-GAAGTAGCCATTCGAACATGGCAATC-3‘	G770E F777E
For 5‘-CTAGTAGGCGAAGCGGTGATTGC-3‘ Rev 5‘-CAAGAAGTAGCCATTCGAACATGGC-3‘	T771E F778E

Table 1: Primers used for TMD mutagenesis of VEGFR-2 in pCDNA3
Glutamic acid mutations are colored in red.

The constructs were amplified by PCR using Phusion High-Fidelity DNA polymerase (Finnzymes). Template DNA was digested by adding 1 µL of DpnI (Fermentas) to the PCR mixture and incubating 6h at 37°C. To select for the mutated constructs 0.5 µL of the PCR reaction mixture was transformed into electrocompetent E.Coli DH10β and plated on LB-Amp agar plates. After 16 h incubation at 37°C colonies were picked from the plate to set up 5 mL overnight cultures. Plasmid-DNAs were extracted with a Miniprep Kit (Qiagen). The introduced mutations were verified by sequencing the plasmid-DNAs (Microsynth AG).

Full-length VEGR-2 TMD mutant constructs

The HA-tagged full-length wt-TMD-VEGFR-2 construct was cloned by Debora Dell'Era-Dosch. In order to generate single glutamic acid mutations within the TMD we applied site-directed mutagenesis on the wt construct. To introduce a second point mutation we used the initially mutated constructs as a template for site-directed mutagenesis. We used the following primers (mutated bases in red):

5‘-3‘ primer sequence	TMD Mutation
For 5‘-GAACTTGGAAATCATTGAACTAGTAGGCA-3‘ Rev 5‘-GAAGTAGCCAGAAGAACATGGCAATC-3‘	I767E
For 5‘-TGGAAATCATTATTGAAGTAGGCACG-3‘ Rev 5‘-GAAGTAGCCAGAAGAACATGGCAATC-3‘	L768E
For 5‘-CATTATTCTAGAAGGCACGGCGGTG-3‘ Rev 5‘-GTAGCCAGAAGAACATGGCAATCACC-3‘	V769E
For 5‘-CATTATTCTAGAAGGCACGGCGGTG-3‘ Rev 5‘-GTAGCCAGAAGAATTCGGCAATCACC-3‘	V769E M776E
For 5‘-CATTATTCTAGTAGAAACGGCGGTGATTG-3‘ Rev 5‘-GAAGTAGCCATTCGAACATGGCAATC-3‘	G770E F777E
For 5‘-CTAGTAGGCGAAGCGGTGATTGC-3‘ Rev 5‘-CAAGAAGTAGCCATTCGAACATGGC-3‘	T771E F778E
For 5‘-CTAGTAGGCACGGAAGTGATTGCC-3‘ Rev 5‘-GACAAGAAGTAGTTCGAAGAACATGGC-3‘	A272E W779E
For 5‘-GCACGGCGGGAAATTGCC-3‘ Rev 5‘-ATGACAAGAAGTTCCCAGAAGAACATG-3‘	V773E L780E
For 5‘-CGGCGGTGGAAGCCATGTTCT-3‘ Rev 5‘-GGATGATGACAAGTTCTAGCCAGAAGAACA-3‘	I774E L781E

Table 2: Primers used for TMD mutagenesis of VEGFR-2 in pCDNA3 and pBE
Glutamic acid mutation is colored in red.

ΔECD-VEGFR-2 KD and full-length VEGFR-2 KD deletion constructs

The HA-tagged ΔECD-VEGFR-2 and the HA-tagged full-length VEGFR-2 kinase domain deletion mutants were cloned with two separate PCR reactions. In order to generate the final constructs we designed hybrid primers with sections coding for the donor and the acceptor vector. The first section of the primer was used for a first PCR reaction with the purpose to amplify the sequence of interest. The second part of the primers with overhangs complementary to the destination vectors served as primer for a second PCR reaction with the aim to insert the initially amplified sequence into the acceptor vector. Fragments resulting from the first PCR reaction were gel purified by using a gel-purification Kit (Qiagen) and used for the second

PCR reaction. For the PCR reactions we used Phusion High-Fidelity DNA polymerase (Finnzymes). Template DNA in the second PCR reaction was digested by adding 1 µL of DpnI (Fermentas) to the PCR mixture and incubating 6h at 37°C. To select for the correct constructs 0.5 µL of the PCR reaction mixture was transformed into electrocompetent *E.Coli* DH10β and plated on LB-Amp agar plates. After 16 h incubation at 37°C colonies were picked from the plate to set up 5 mL overnight cultures. Plasmid-DNAs were extracted with a Miniprep Kit (Qiagen). The constructs were verified by sequencing the plasmid-DNAs (Microsynth AG). We used the following primer:

5‘-3‘ primer sequence	Construct
For 5‘-CAGGAAAAGACGAACTTGGAAATCATTATTCTAGTAGGCACG-3‘ Rev 5‘-TTCCATGCTCAAAGTCTCTGATATCGGAAGAACAATGTAGTCTT-3‘	Wt-TMD ΔKID
For 5‘-CAGGAAAAGACGAACTTGGAAATCATTATTCTAGTAGGCACG -3‘ Rev 5‘-ATAGAATAGGGCCCTCTAGTTTATCACGGAAGAACAATGTAGTCTT-3‘	Wt-TMD ΔC
For 5‘-CAGGAAAAGACGAACTTGGAAATCATTATTCTAGTAGGCACG-3‘ Rev 5‘-GAATAGGGCCCTCTAGTTTATCACGGAAGAACAATGTAGTCTT TGCCATCCTGCTGAGCATTAGC-3‘	Wt-TMD ΔKIDΔC

Table 3: Primers used for cloning of VEGFR-2 kinase domain deletion mutants

6.2. Cell culture and activity screening of transmembrane and kinase domain mutants of VEGFR-2

HEK293 cells were cultured at 37°C, 5% CO2 in DMEM (BioConcept, #1-26F03-I) containing 10% fetal bovine serum (FBS), 100 units/mL penicillin and 100 µg/mL streptomycin. In order to monitor receptor activity of the various TMD constructs, HEK293 cells were transiently transfected with the appropriate plasmid and their lysates were analysed via immunoblotting 24 h post transfection. For transfection HEK293 cells were seeded in 6-well plates to reach a confluency of 60%. After 24 h the cells were transiently transfected using Fugene® (Roche Diagnostics) according to the suppliers manual. To prevent overexpression and therefore spontaneous activation of the receptor on the membrane the 2 µg of DNA were diluted 1:5 with the

empty vector. Cells transfected with constructs that were ECD-deleted were incubated 24 h before lysis. Cells transfected with the full-length VEGFR-2 mutants were cultured for 24 h and then starved (DMEM + 0.1% BSA) for 4 h. Full-length VEGFR-2 constructs were stimulated for 10 min with 50 ng/mL VEGF-A_{165} (produced by Thomas Schleier) prior to lysis. Immediately after incubation or stimulation cells were washed twice with ice cold PBS. After washing cells were incubated 15 min with 150 µL of Lysis buffer (50 mM Tris-HCl pH 7.5, 100 mM NaCl, 0.1% Triton X-100, Roche protease inhibitor cocktail and 1 mM Na_3VO_4) on ice. After lysis the cell suspensions were flash frozen in liquid nitrogen and stored at –20°C. Prior to analysis of cell lysates, debris were removed by centrifugation (10'000 x *g*, 25 min, 4°C) and total amount of protein in the supernatant was measured with the DC assay (modified Lowry assay) of Biorad. The cell lysates were then subjected to western blot analysis. Secondary antibodies were alkaline phosphatase (AP) coupled. Lumi-Phos™ WB (Thermo Scientific) was used as an AP substrate. We used the following primary and secondary antibodies:

Antibody	Primary	Secondary	Dilution
pY1054/59, mouse, Calbiochem	X		1:1000
pY951 (15D2), rabbit, Cell Signaling	X		1:1000
pY1175 (19A10), rabbit, Cell Signaling	X		1:1000
PLC-γ1 (D9H10), rabbit, Cell Signaling	X		1:1000
pPLC-γ (Y783), rabbit, Cell Signaling	X		1:1000
β-actin (clone AC-74), mouse, Sigma	X		1:1000
HA (clone 3F10), rat, Roche Diagnostics	X		1:1000
Goat anti-mouse AP, Southern Biotech		X	1:10'000
Goat anti-rabbit AP, Southern Biotech		X	1:10'000
Goat anti-rat AP, Southern Biotech		X	1:10`000

Table 4: Primary and secondary antibodies used for activity screening of TMD and KD mutants of VEGFR-2

6.3. Structural analysis of the transmembrane domain of VEGFR2 by NMR

In collaboration with Alexander S. Arseniev we determined the spatial structure of wt and mutant TMD homodimers of VEGFR-2 (residues 759-795) in membrane mimicking DPC micelles by conventional ^{13}C, ^{15}N-heteronuclear NMR techniques. The sequence for the modified TMD-helices were PCR amplified out of an artificially synthesized sequence (Genewiz) coding for the TMD of VEGFR-2 and digested with NdeI, HindIII prior to ligation into an *E.Coli* expression vector. The helical proteins were subsequently expressed in a cell free expression system. We used the following coding sequences:

PCR fragment: wt-TMD

TAC CAG *CAT ATG* GAA AAA ACC AAC CTG GAG ATC ATT ATT CTA GTA GGC ACG GCG GTG ATT GCC ATG TTC TTC TGG CTA CTT CTT GTC ATC ATC CTA CGG ACC GTT AAG CGT GCT AAC GGT GGC TAA TAG *AAG CTT* GCT TAC CAG

Amino acid sequence: wt-TMD

IIILVGTAVIAMFFWLLLVIILRTV

EKTNLEIIILVGTAVIAMFFWLLLVIILRTVKRANGG

PCR fragment: V769E-TMD

TAC CAG *CAT ATG* GAA AAA ACC AAC CTG GAG ATC ATT ATT CTA GAA GGC ACG GCG GTG ATT GCC ATG TTC TTC TGG CTA CTT CTT GTC ATC ATC CTA CGG ACC GTT AAG CGT GCT AAC GGT GGC TAA TAG *AAG CTT* GCT TAC CAG

Amino acid sequence: V769E-TMD (activated)

IIILEGTAVIAMFFWLLLVIILRTV

EKTNLEIIILEGTAVIAMFFWLLLVIILRTVKRANGG

Figure 10: PCR fragments and corresponding amino acid sequences of VEGFR-2-TMDs used for preparation of expression vectors for cell free expression.
The sequences depicted in green are flanking TMD residues to minimize terminal effects on water-membrane interfaces. In order to improve expression with the cell free expression system we exchanged the rare codons (cyan) coding for Leu and Arg (CTA->CTG/CGG->CGT). DNA and amino acid sequence coding for the activating glutamic acid is colored in red. Restriction sites for *NdeI* and *HindIII* endonucleases are underlined.

Expression, labelling, purification and lipid/detergent reconstitution of the proteins as well as data acquisition and data processing was performed according to (Bocharov *et al.*, 2008; Mineev *et al.*, 2010).

6.4. Cloning of VEGFR-2 kinase domain mutants for protein expression

In order to biophysically investigate the role of distinct regulatory domains in the kinase domain of VEGFR-2 we designed mutant constructs for insect cell expression. All constructs were TMD-deleted. The constructs were cloned into the previously described MultiBac vector pfl (Fitzgerald *et al.*, 2006). All constructs contained a C-terminal 10xHis tag with a preceding tobacco etch virus (TEV) cleavage site. The soluble ΔTMD-VEGFR-2 KD constructs were cloned with two separate PCR reactions described in 6.1.1. We used the following primers:

5‘-3‘ primer sequence	Construct
For 5‘-CGGAATTCAAAGGCCTACGTCGACCACCATGCTACGGACCGTTA AGCGGGC -3‘ Rev 5‘-CTTTTATCAGTGATGGTGATGGTGATGGTGATGGTGATGCTGGA AGTAGAGGTTCTCAACAGGAGGAGAGAGCTCAGTGTGGTC-3‘	VEGFR-2 KD
For 5‘-CGGAATTCAAAGGCCTACGTCGACCACCATGCTACGGACCGTTAA GCGGGC-3‘ Rev 5‘-CTTTTATCAGTGATGGTGATGGTGATGGTGATGGTGATGCTGGAAGT AGAGGTTCTCAACAGGAGGAGAGAGCTCAGTGTGGTC-3‘	K868M VEGFR-2 KD
For 5‘-GGAGGGGAACTGAAGACAGGCTACTTGTCCATCGTCATGGATCCAGA TGAACTCCCATTG-3‘ Rev 5‘-CAAAGTCTCTGATATCGGAAGAACAATGTAGTCTTTGCCATCCTGCTG AGCATTAGCTTGCA-3‘	ΔKID VEGFR-2 KD
For 5‘-TGGAGAACTCTCTGTGGATCTGAAACGGCACTTAG-3‘ Rev 5‘-ACAGAGAGTTCTCCAACGTAGTCTTTCCCTTGACGGAATCG-3‘	mKID VEGFR-2 KD (mutated out of VEGFR-2 KD)
For 5‘-CGGAATTCAAAGGCCTACGTCGACCACCATGCTACGGACCGTTAAGC GGGC-3‘ Rev 5‘-CTTTTATCAGTGATGGTGATGGTGATGGTGATGGTGATGCTGGAAGT AGAGGTTCTCATCCTGCTGAGCATTAGCTTGCA-3‘	ΔC VEGFR-2 KD
For 5‘-CGGAATTCAAAGGCCTACGTCGACCACCATGATGGATCCAGATGAACT CCCATTG-3‘ Rev 5‘-CTTTTATCAGTGATGGTGATGGTGATGGTGATGGTGATGCTGGAAGTA GAGGTTCTCATCCTGCTGAGCATTAGCTTGCA -3‘	ΔJMDΔKIDΔC VEGFR-2 (Y1175) KD

Table 5: Primers used for cloning of VEGFR-2 kinase domain mutants in pfl used for protein expression in insect cells

6.5. Expression, purification and determination of phosphorylation state of VEGFR-2 kinase domain proteins

Expression of kinase domain constructs was performed in Sf21 insect cells. Baculovirus production, infection and expression procedures were applied according to (Fitzgerald et al, 2006). Insect cells were cultured at 27°C in serum-free Insect-XPRESS™ medium with L-glutamine (Lonza, #BE12-730Q). In order to maintain a suitable oxygen level within the culture vessel, cells were grown in such a way that they did not exceed a density of 1.5 x 10^6 cells/mL during protein expression. All constructs were monitored for their protein expression levels over a period of 5 days after initial infection. Protein expression-levels in the cells were analysed by taking aliquots of 0.2 x 10^6 cells every day (5 Aliquots). Cell pellets were lysed with lysis

buffer (50 mM Tris-HCl pH 7.5, 100 mM NaCl, 0.1% Triton X-100, Roche protease inhibitor cocktail) and subjected to western blot analysis. Blots were decorated with a primary anti 5xHis (Sigma) and with a secondary goat anti-mouse AP (Bioconcept) antibody using dilutions of 1:1000 and 1:10'000, respectively. Cells were harvested at their highest protein expression-levels 3 days post infection. After a centrifugation step of 30 min at 900 x *g* and 4°C the cell pellets were flash frozen in liquid nitrogen and stored at -80°C. Harvested cell pellets were thawed on ice and resuspended in hypotonic buffer (50mM Hepes pH 8, 10 mM NaCl, 10 mM imidazole, 5% glycerol, Roche inhibitor cocktail). After incubation of 1h at 4°C the solution was vortexed and a centrifugation step of 30 min at 900 x *g* and 4°C was applied to remove the nuclei. The supernatant containing the protein of interest was filtered (45 µm) and then purified with a previously equilibrated nickel charged 1 mL HiTrap™ Chelating HP column (GE Healthcare). The proteins were loaded on the column and washed with wash buffer (50mM Hepes pH 7.5, 500 mM NaCl, 10% glycerol, 1mM DTT). The elution of the proteins was performed by applying an imidazole gradient up to 350 mM. For the second purification step the eluate of the NiNTA column was concentrated up to 2 mL and loaded on a Superdex 200 16/60 column. Proteins were eluted with elution buffer: 50 mM Hepes pH 7.5, 150 mM NaCl, 5% glycerol, 1 mM DTT. The eluates of the NiNTA and the SEC column were analyzed by Coomassie stained SDS-PAGE and Immunoblotting using an antibody of Sigma recognizing the His-tag (anti penta-His, mouse, 1:1000). The phosphorylation state of the purified proteins was determined via Immunoblotting using phospho-specific antibodies described in section 6.2.

6.5.1. *In vitro* phosphorylation / dephosphorylation

In order to achieve phosphorylation of all the tyrosine residues in the purified kinase domain proteins we incubated the proteins with 4 mM ATP and 28 mM $MgCl_2$ immediately after elution from the NiNTA column. ATP and $MgCl_2$ were automatically removed in the SEC purification step. Dephosphorylation of kinase domain proteins was performed with AP (Fermentas). 1 mL purified proteins of 2 mg/mL were incubated with 1000 units of AP for 48 h at 4°C. AP was removed by loading the protein-AP mixture on a 1 mL NiNTA column and applying a wash step with following final elution at 350 mM imidazole with buffers described in section 6.5. The eluted

fractions contained the dephosphorylated kinase domain proteins. Dephosphorylation of proteins was verified by immunoblotting using phospho-specific antibodies described in section 6.2.

6.6. Cloning of murine TSAd for protein expression

The coding sequence of murine TSAd was cloned into the Multibac vector pfl according to section 6.4. TSAd was designed with a C-terminal 10xHis tag with a preceding TEV site. We used the following primers:

5‘-3‘ primer sequence	Construct
For 5‘-CGGAATTCAAAGGCCTACGTCGACCACCATGGAGTTCTGCTTGGCCCAAC-3‘ Rev 5‘ –CTTTTATCAGTGATGGTGATGGTGATGGTGATGGTGATGCTGGAAGTAGAG GTTCTCGGAGGGGCTCCCTCTTTC-3‘	Murine TSAd

Table 6: Primers used for cloning of murine TSAd into pfl vector for protein expression in insect cells

6.7. Expression and purification of murine TSAd and TSAd-VEGFR-2 complex

Expression and purification of murine TSAd and TSAd-VEGFR-2 complex was conducted according to section 6.5 except of the usage of different buffers: Harvested cells were thawed on ice and resuspended in the following hypotonic buffer: 50 mM Tris ph 8.5, 10 mM NaCl, 10 mM imidazole, 5% glycerol, Roche protease inhibitor cocktail. IMAC purification was performed with the following wash and elution buffer: 50 mM Tris pH 8.3, 500 mM NaCl, 10 % glycerol, 1 mM DTT and 50 mM Tris pH 8.3, 350 mM NaCl, 350 mM imidazole, 10 % glycerol, 1 mM DTT, respectively. For the SEC purification step we used the following SEC buffer: 50mM Tris pH 8.3, 150 mM NaCl, 5% glycerol, 1 mM DTT.

6.8. Biophysical characterization of recombinant proteins

6.8.1. Multi Angle Light Scattering analysis

Multi Angle Light Scattering (MALS) analysis was conducted on an Agilent 1100 HPLC-system (Agilent Technologies) coupled to a Superdex 200HR 10/30 column (GE Healthcare) of analytical-grade quality. The column was further connected to the Wyatt miniDAWN Tristar (Wyatt Technologies) unit. The instruments and the attached column were equilibrated with buffer prior to run. 100 µL of concentrated protein was injected into the system for analysis. The elution profiles of the experiments were collected as UV-absorbance (280nm) spectra and intensity of Rayleigh scattering at three different angles. The ASTRA™ software (Wyatt Technologies) was applied to assign the molecular mass averages.

6.8.2. Small-Angle X-ray Scattering

Small-angle X-ray scattering (SAXS) data was collected at the cSAXS beamline X12SA at the Swiss Light Source (SLS) in Villigen, Switzerland. The scattered intensities were recorded on a Pilatus 2M detector. The intensities were collected in the scattering vector interval between 0.008 [1/Å] – 0.400 [1/Å]. The length of the scattering vector is defined as $q = 4\pi\sin\theta/\lambda$, where 2θ is the scattering angle and the wavelength λ=1 Å. A Silver Behenate sample was used to calibrate the length of the scattering vector q (Huang *et al.*, 1993). Protein samples and the corresponding buffer solutions were measured in quartz capillaries of 1mm in diameter (Hilgenberg GmbH, Germany). The data of each protein sample was measured at three different concentrations. The background scattering was recorded by measuring the empty capillaries and the corresponding protein buffers prior to protein sample measurements. For data collection 10 different spots along the capillary were scanned with an exposure time of 0.5 s. The collected frames were analyzed for radiation damage. Frames showing no signs of damage were averaged using MATLAB with macros programmed by John Missimer and Kaisa Kisko. Background scattering of the buffer was subtracted by using MATLAB. In order to check for complete folding and domain flexibility of all measured proteins we calculated Kratky-plots. The distance distribution function p(r) was calculated using GNOM and

AUTOPOROD out of the ATSAS package (Petoukhov *et al.*, 2007a). The radius of gyration Rg was calculated with the p(r) function and out of the data in the linear Guinier-region. The program DAMMIF (Petoukhov *et al.*, 2007b) was used for *ab initio* shape reconstructions from the p(r) functions. At least 10 and up to 20 independent DAMMIF runs were averaged, aligned and, refined back to the original envelope volume using DAMAVER and DAMFILT (Petoukhov *et al.*, 2007b). SUPCOMB13 was used to overlay calculated DAMMIF structures. Superimpositions of existing crystal structures with the SAXS envelopes was done with the program SITUS (Wriggers and Chacon, 2001). CRYSOL was used to calculate p(r) functions of existing crystal structures. The model-p(r) functions were subsequently compared with experimental data to monitor data consistency. Models were visualised using PyMol (www.schrodinger.org).

6.8.3. Analytical ultracentrifugation

For the analytical ultracentrifugation (AUC) experiments we used a Beckman ProeomLab XL-I centrifuge. The sedimentation equilibrium experiments were performed as duplicates at 4°C for three different concentrations of 10, 30 and 80 µM. The three concentrations were chosen based on previous MALS experiments at high protein concentrations (>20 mg/mL) where dimers could be assigned. Protein sample concentration was adjusted in SEC buffer described in section 6.5. For the AUC experiments we used an An-50 Ti rotor (Beckmann) and charcoal-filled epon six sector cells. The runs were performed at two speeds of 14’000 and 20’000 rpm. For data collection we used the refractive index detection system (Aviv Biomedical) of the analytical ultracentrifuge. Data analysis was performed using Ultraspin software package (MRC, Cambridge).

6.8.4. Mass spectrometry

To identify and validate the recombinant proteins we sent samples for analysis to the Functional Genomics Center in Zürich. Proteins were initially separated via SDS-PAGE. Bands corresponding to the molecular weight of the recombinant proteins were localized with coomassie-blue staining, cut out and sent to Zürich for analysis.

The gel bands were cut in small pieces and washed twice with 100 µL of 100 mM NH_4HCO_3/50% acetonitrile and washed once with 50µL acetonitrile. The supernatants were discarted. 10 µL of trypsin (10 ng/µL in 10 mM Tris/2 mM $CaCl_2$, pH 8.2) and 10 µL of buffer (10 mM Tris/2 mM $CaCl_2$, pH 8.2) were added to the samples. The samples were incubated over night at 37°C. After incubation the supernatants were removed and the gel pieces were extracted twice with 100 µL 0.1% TFA/50% acetonitrile. All supernatants were combined and dried. To dissolve the dried samples 25 µL of 0.1% formic acid was used. The samples were then transferred into auto sampler vials. 0.5 µL of the sample was injected for ESI-MS-MS (Waters Synapt G2)**.** Database searches (of detected peptides) were performed by using the Mascot search programs (NCBI: all species).

7. Results

7.1. Functional analysis of VEGFR-2 mutants carrying an artificial dimerization interface in the transmembrane domain

It has previously been shown that many receptor tyrosine kinases can be artificially dimerized and activated by interactions mediated by their TMD. Previous experiments in our lab focused on the role of dimerization and activation of VEGFR-2 by using artificial dimerization-promoting TMDs. Dimerization and activation was achieved by introducing glutamic acid residues at specific positions to an all valine TMD. Only receptor kinase dimers with specific spatial orientation were activated. Dimerization is therefore required but not sufficient for activation of VEGFR-2 carrying artificial Vx/x + 7E TMD. To further confirm these findings in the human VEGFR-2, we designed constructs that contained the wild-type TMD with glutamic acid residues in distinct positions.

7.1.1. Activity of extracellular domain-deleted VEGFR-2 mutants carrying a single glutamic acid dimerization promoting interface in the transmembrane domain

Initially we used VEGFR-2 constructs that were ECD-deleted (765-1356). It was therefore possible to study the activation mechanism independently from VEGF and compare mutants carrying TMDs containing glutamic acid point mutations with the previously screened Vx/x + 7E TMD-helices, where only distinct dimerization-promoting variants were able to activate the receptor kinase. In the first constructs we mutated one single amino acid to glutamic acid. The receptor constructs were cloned into the mammalian expression vector pcDNA3 and contained a N-terminal HA-tag for immunodetection. Glutamic acid point mutations were introduced into the TMD by site-directed mutagenesis. Mutations of the wt-TMD are shown in table 7.

ΔECD-VEGFR-2 wt	HA	**IIILVGTAVIAMFFWLLLVIILRTV**	VEGFR-2 KD
ΔECD-VEGFR-2 I767E	HA	**IIELVGTAVIAMFFWLLLVIILRTV**	VEGFR-2 KD
ΔECD-VEGFR-2 L768E	HA	**IIIEVGTAVIAMFFWLLLVIILRTV**	VEGFR-2 KD
ΔECD-VEGFR-2 V769E	HA	**IIILEGTAVIAMFFWLLLVIILRTV**	VEGFR-2 KD
ΔECD-VEGFR-2 G770E	HA	**IIILVETAVIAMFFWLLLVIILRTV**	VEGFR-2 KD
ΔECD-VEGFR-2 T771E	HA	**IIILVGEAVIAMFFWLLLVIILRTV**	VEGFR-2 KD
ΔECD-VEGFR-2 A772E	HA	**IIILVGTEVIAMFFWLLLVIILRTV**	VEGFR-2 KD
ΔECD-VEGFR-2 V773E	HA	**IIILVGTAEIAMFFWLLLVIILRTV**	VEGFR-2 KD
ΔECD-VEGFR-2 I774E	HA	**IIILVGTAVEAMFFWLLLVIILRTV**	VEGFR-2 KD
ΔECD-VEGFR-2 A775E	HA	**IIILVGTAVIEMFFWLLLVIILRTV**	VEGFR-2 KD
ΔECD-VEGFR-2 M776E	HA	**IIILVGTAVIAEFFWLLLVIILRTV**	VEGFR-2 KD
ΔECD-VEGFR-2 F777E	HA	**IIILVGTAVIAMEFWLLLVIILRTV**	VEGFR-2 KD

Table 7: Schematic representation of ΔECD-VEGFR-2 mutants carrying a single glutamic acid dimerization interface in the TMD
The wt-TMD sequence of VEGFR-2 is shown on top. HA: Haemaglutinin tag, point mutations are highlighted in red, VEGFR-2 KD: Kinase domain of VEGFR-2.

The TMD-mutants were transiently expressed in HEK293 cells. After lysis we assessed receptor activity by immunoblotting with an antibody specific for pY1175 the major phosphorylation site of VEGFR-2. For the detection of the total amount of receptor protein the same membrane was decorated with an anti-HA antibody. Three constructs carrying glutamic acid point mutations at positions I767, L768 and V769 showed significantly higher activity than the construct with the wt-TMD. Mutant V769E reproducibly showed the highest activity, all the other point mutations showed less dramatic increase compared to the activity of the wt-construct (figure 11) indicating that a distinct orientation of the kinase domain is required to fully activate the receptor kinase reminiscent of earlier mutagenesis using Vx/x + 7E TMD receptors.

A

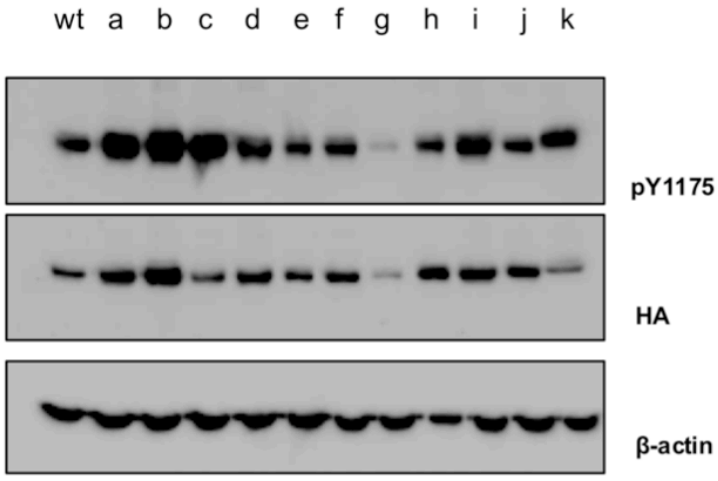

wt	**Wt-TMD**
a	**I767E-TMD**
b	**L768E-TMD**
c	**V769E-TMD**
d	**G770E-TMD**
e	**T771E-TMD**
f	**A772E-TMD**
g	**V773E-TMD**
h	**I774E-TMD**
i	**A775E-TMD**
j	**M776E-TMD**
k	**F777E-TMD**

B

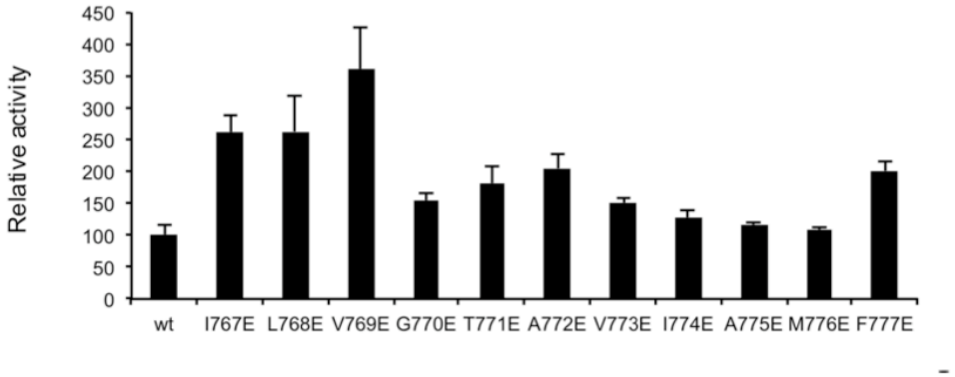

Figure 11: Activity of ΔECD-VEGFR-2 mutants with glutamic acid point mutations in the TMD
(A) Lysates from HEK293 cells were separated by SDS-PAGE and transferred to a PVDF membrane. The membrane was decorated with an antibody specific for pY1175 then stripped and incubated with an antibody recognising the HA-tag of the receptor. Equal loading was confirmed by incubating the membrane with an anti-β-actin antibody. A representative experiment is shown in (A). (B) Quantification using three independent experiments. Receptor phosphorylation is indicated as mean ± S.E. with wt set to 100%.

We observed significant basal receptor activation in the construct carrying the native TMD probably due to the lack of the ECD (figure 11). Moreover, this finding agrees with previous experiments from our lab where the ΔECD-VEGFR-2 mutant carrying the wt-TMD showed constitutive dimer formation in co-immunoprecipitation assays (Dell'Era Dosch and Ballmer-Hofer, 2009b). In order to prevent spontaneous trans-activation of the receptor kinase as a result of overexpression within the cell membrane we used carrier DNA in the transfection assays to dilute the expression plasmid and to attenuate protein expression.

In the next experiments we compared ECD-deleted wt-TMD VEGFR-2 with full-length wt-TMD VEGFR-2 in VEGF-stimulated and unstimulated cells. The ΔECD construct was cloned into the mammalian expression vector pcDNA3 and contained a HA-tag for immunodetection at the N-terminus. The full-length VEGFR-2 construct was cloned into the mammalian eGFP expression vector pBE and contained a HA-tag for immunodetection at the N-terminus. Both constructs were transiently transfected in HEK293 cells. After lysis we assessed receptor activity by immunoblotting with an antibody specific for pY1175 and anti-HA for total amount of receptor, respectively. The data shows that the ΔECD construct has 50% of the activity of full-length VEGFR-2 (figure 12).

A

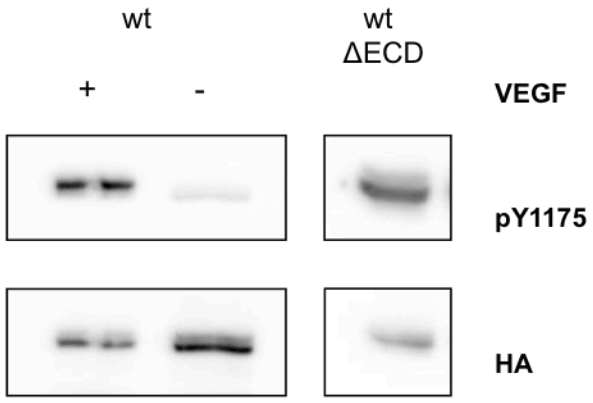

B

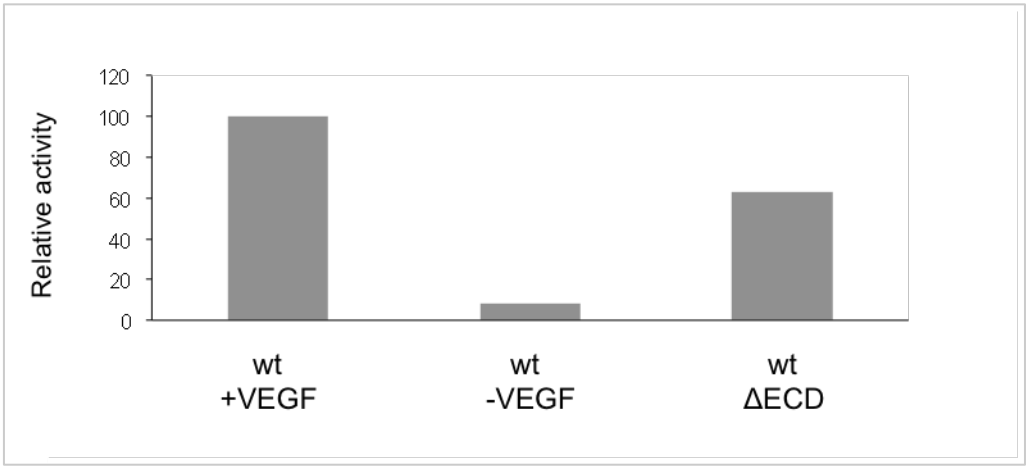

Figure 12: Activity of ΔECD-mutant compared to full length VEGFR-2
Activity of the full-length wt-TMD construct is shown in comparison to the ΔECD wt-TMD mutant. (A) Lysates from HEK293 cells were separated by SDS-PAGE and transferred to a PVDF membrane. The membrane was decorated with an antibody specific for pY1175 then stripped and incubated with an antibody recognising the HA-tag of the receptor. (B) Quantification of Blot shown in (A).

7.1.2. Activity of full-length VEGFR-2 mutants carrying a single glutamic acid dimerization interface in the transmembrane domain

To see whether the constitutively activating mutations L768E and V769E identified in the ECD-truncated VEGFR-2 constructs were able to activate the receptor by compensating for the apparent ECD-mediated inhibition of dimerization in the absence of ligand we introduced these mutations into the TMD of the full-length receptor. Mutant G770E, that showed pY1175 phosphorylation similar to the wt, was introduced as a negative control (table 8).

ΔECD-VEGFR-2 L768E	HA	**IIIEVGTAVIAMFFWLLLVIILRTV**	VEGFR-2 KD
ΔECD-VEGFR-2 V769E	HA	**IIILEGTAVIAMFFWLLLVIILRTV**	VEGFR-2 KD
ΔECD-VEGFR-2 G770E	HA	**IIILVETAVIAMFFWLLLVIILRTV**	VEGFR-2 KD

Table 8: Schematic representation of full-length VEGFR-2 mutants with single glutamic acid mutations in the TMD
The wt-TMD sequence of VEGFR-2 is shown on top. HA: Haemaglutinin tag, point mutations are highlighted in red, VEGFR-2 KD: Kinase domain of VEGFR-2.

The full-length VEGFR-2 mutants with a single glutamic acid point mutation were transiently transfected in HEK293 cells and Y1175 phosphorylation was determined. Mutation L768E and V769E, active in the ΔECD-VEGFR-2 constructs, did not show significantly higher activity than wt-VEGFR-2 neither in VEGF-stimulated nor in unstimulated cells (figure 13). This data indicates that the dimerization promoting energy of a single glutamic acid residue introduced into the wt-TMD does not compensate for the repulsive force induced by the extracellular domain of VEGFR-2.

A

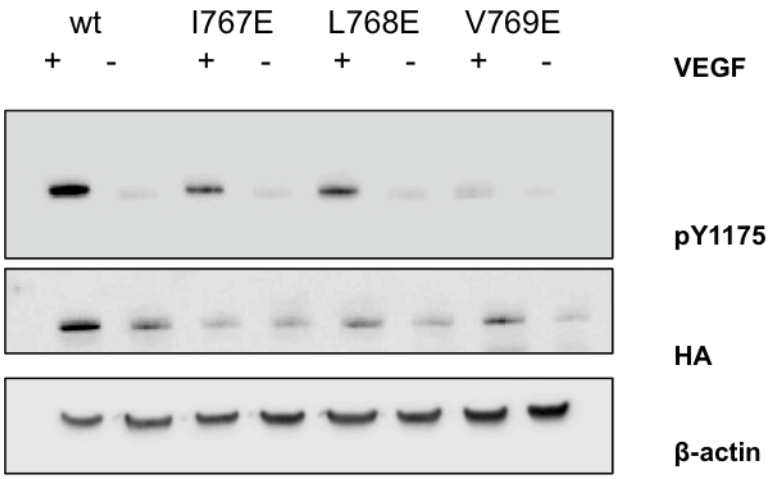

B

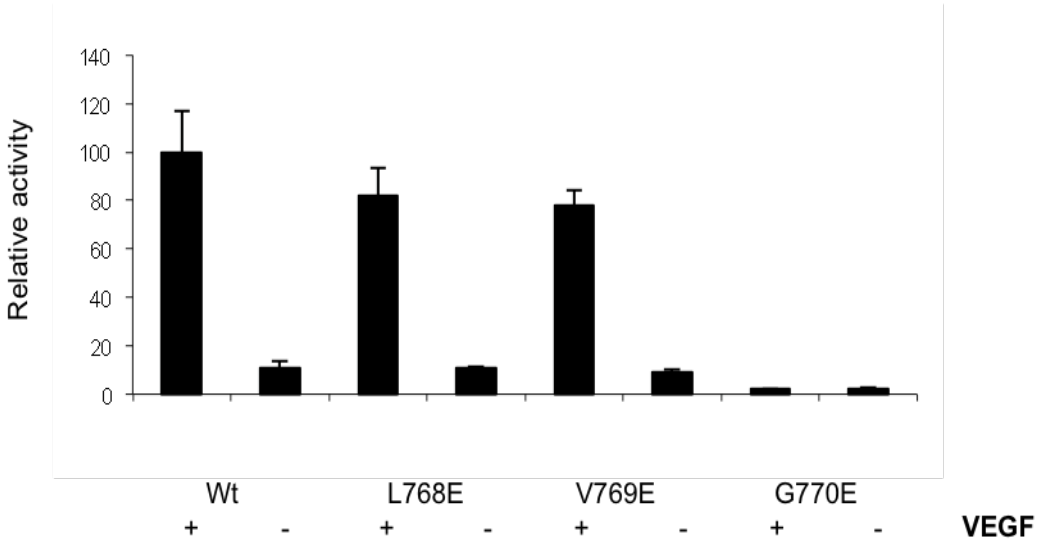

Figure 13: Activity of full-length VEGFR-2 mutants with single glutamic acid mutations in the TMD
(A) Activity of the L768E, V769E and G770E mutants is shown in comparison to wt VEGF stimulated and VEGF unstimulated cells. (B) Quantification using three independent experiments, receptor phosphorylation is given as mean ± S.E. with wt set to 100%.

7.1.3. Activity of extracellular domain-deleted VEGFR-2 mutants carrying a double glutamic acid dimerization interface in the TMD

The TMD of receptor tyrosine kinases consists of a single alpha helix. A full helix turn contains ~ 3.5 amino acids. For the next set of experiments we designed mutants with dimerization motifs consisting of two glutamic acid mutations in the wt-TMD. Our constructs localize the two glutamic acid residues on the same face of the helix, giving rise to a more rigid dimerization interface. The glutamic acids were spaced seven residues apart and thus two helix rotations apart in the TMD-helix. This motif was sequentially shifted along the TMD-helix in order to generate dimers with distinct spatial orientations. We introduced the glutamic acid mutations at position V769E (that was previously found to activate the receptor)/M776E; G770E/F777E and T771E/F778E (table 9).

ΔECD VEGFR-2 wt	**HA**	**IIILVGTAVIAMFFWLLLVIILRTV**	**VEGFR-2 KD**
ΔECD-VEGFR-2 V769E; M776E	**HA**	**IIILEGTAVIAEFFWLLLVIILRTV**	**VEGFR-2 KD**
ΔECD-VEGFR-2 G770E; F777E	**HA**	**IIILVETAVIAMEFWLLLVIILRTV**	**VEGFR-2 KD**
ΔECD-VEGFR-2 T771E; F778E	**HA**	**IIILVGEAVIAMFEWLLLVIILRTV**	**VEGFR-2 KD**

Table 9: Schematic representation of ΔECD-VEGFR-2 mutants with double glutamic acid mutations in the TMD
The wt-sequence of the TMD is shown on top. HA: Haemaglutinin tag, point mutations are highlighted in red, VEGFR-2 KD: Kinase domain of VEGFR-2.

In the absence of ligand the mutants were transiently transfected into HEK293 cells and Y1175 phosphorylation was determined. Mutant V769E/M776E, G770E/F777E and T771E/F778E were all inactive as compared to wt (figure 14). The data therefore reveal the tight regulation of the kinase since this rigidified interface maintains the kinase dimers in an inactive conformation.

A

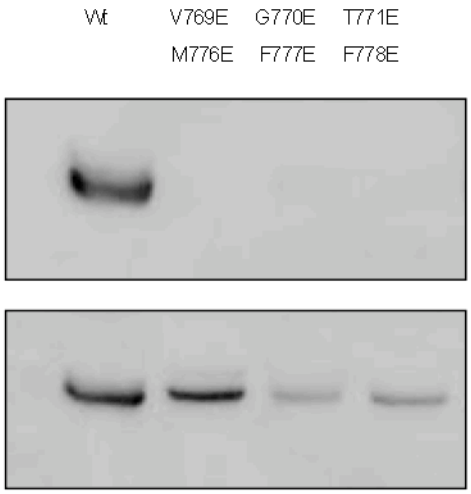

B

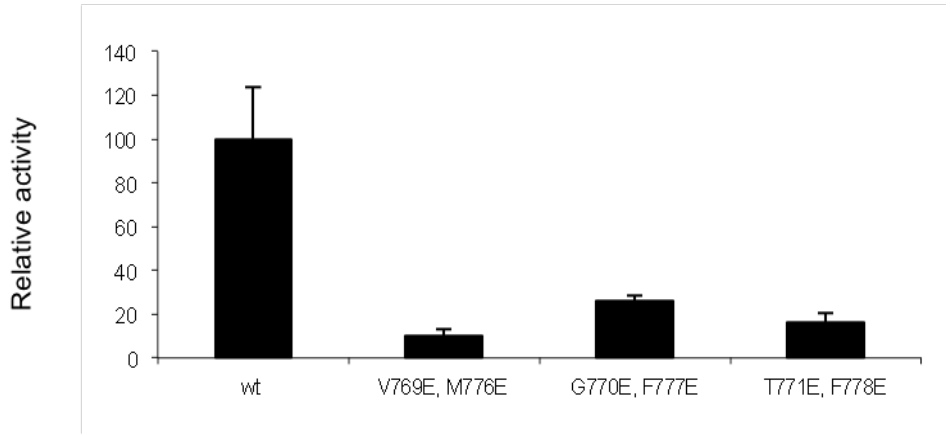

Figure 14: Activity of ΔECD-VEGFR-2 mutants with double glutamic acid dimerization interface in the TMD
(A) Activity of V769E/M776E, G770E/F777E and T771E/F778E mutants is shown in comparison to wt. (B) Quantification using three independent experiments, receptor phosphorylation is indicated as mean ± S.E. with wt set to 100%.

7.1.4. Activity of full-length VEGFR-2 mutants carrying a double glutamic acid dimerization interface in the transmembrane domain

We next evaluated whether it was possible to generate a dimerization interface that was strong enough to compensate for the repulsive force exerted by the extracellular domain in the absence of ligand that might thus be able to activate the receptor. We were also interested whether in the context of the full-length receptor distinct activating and inactivating dimeric conformations similar to those in the ΔECD-VEGFR-2 constructs could be identified. Mutated positions within the wt-TMD are shown in table 10.

ECD-VEGFR-2 wt	HA	**IIILVGTAVIAMFFWLLLVIILRTV**	VEGFR-2 KD
ECD-VEGFR-2 V769E; M776E	HA	**IIILEGTAVIAEFFWLLLVIILRTV**	VEGFR-2 KD
ECD-VEGFR-2 G770E; F777E	HA	**IIILVETAVIAMEFWLLLVIILRTV**	VEGFR-2 KD

ECD-VEGFR-2 T771E; F778E	HA	**IIILVGEAVIAMFEWLLLVIILRTV**	VEGFR-2 KD
ECD-VEGFR-2 A772E; W779E	HA	**IIILVGTEVIAMFFELLLVIILRTV**	VEGFR-2 KD
ECD-VEGFR-2 V773E; L780E	HA	**IIILVGTAEIAMFFWELLVIILRTV**	VEGFR-2 KD
ECD-VEGFR-2 I774E; L781E	HA	**IIILVGTAVEAMFFWLELVIILRTV**	VEGFR-2 KD

Table 10: Schematic representation of full-length VEGFR-2 mutants with double glutamic acid point mutations in the TMD
The wt-sequence of the TMD is shown on top. HA: Haemaglutinin tag, point mutations are highlighted in red, VEGFR-2 KD: Kinase domain of VEGFR-2.

Full-length VEGFR-2 TMD mutants carrying two glutamic acid mutations were transiently transfected into HEK293 cells and Y1175 phosphorylation was determined. Mutant G770E/F777E and T771E/F778E showed constitutive activity in VEGF-stimulated and in unstimulated cells (figure 15). All the other mutants were constitutively inactive. The data again indicates that only distinct orientations of the kinase domain are able to fully activate the receptor kinase. This clearly shows that the TMD of VEGFR-2 carrying a double glutamic acid dimerization interface is able to compensate for the repulsive force exerted by the receptor ECD. The constitutively active G770E/F777E and the inactive mutant I774E/L781E were previously found to have the same effect in the all valine TMD. This demonstrates a common spatial arrangement of the two TMD-helices in the cell membrane, which is independent of the amino acid composition of the TMD.

A

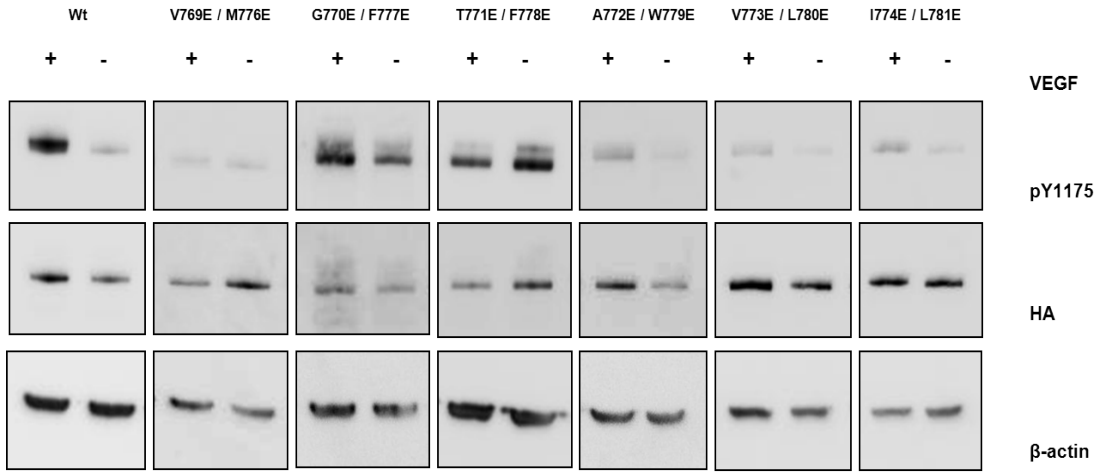

B

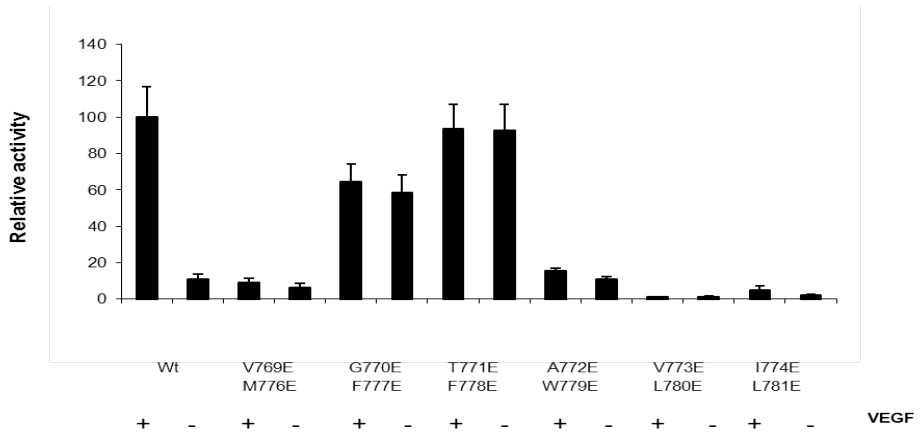

Figure 15: Activity of full-length VEGFR-2 mutants with double glutamic acid dimerization interface in the TMD
(A) Activity of the double mutants is shown in comparison to wt in VEGF stimulated and VEGF unstimulated cells. (B) Quantification using three independent experiments. Receptor phosphorylation is indicated by mean ± S.E. with wt set to 100%.

7.2. 3D-structure of the transmembrane domain of VEGFR-2 determined by NMR spectroscopy

It was shown earlier that several TMD-helices present in membrane proteins interact with each other via distinct dimerization motifs like the heptad- (XxxxxxxX, where X is G, A or S) or the GG4-like-repeat (XxxxX, where X is G, A, S or T). Helices containing such dimerization motifs have thus a strong propensity to interact with each other. The small amino acid residues in these motifs are important to bring the TMD-helices in close proximity. As a consequence helix-helix interactions are mediated and stabilized by van der Waals interactions and/or hydrogen bonding. The

VEGFR-2 TMD helix does not contain such a dimerization motif. Nevertheless, it was shown that the VEGFR-2 TMD helix has a low propensity to dimerize relative to the strong interaction of the wt-TMD of for instance human glycophorin A (GpA) (Finger *et al.*, 2009b). Our goal was to determine the structural basis of helix-helix interaction in the wt and in the TMDs containing our previously introduced artificial glutamic acid residue dimerization motif. In collaboration with an NMR research group we determined the interaction of two wt and mutant TMD-helices of VEGFR-2 (residues 759-795) in membrane mimicking DPC micelles using conventional ^{13}C, ^{15}N-heteronuclear NMR spectroscopy. At the conclusion of this thesis we obtained preliminary unrefined data.

7.2.1. 3D-structure of the wild type transmembrane domain of VEGFR-2

The NMR chemical shifts, connectivities and NMR relaxation data show that the peptides form long α-helical structures between amino acid 761-794 (figure 16).

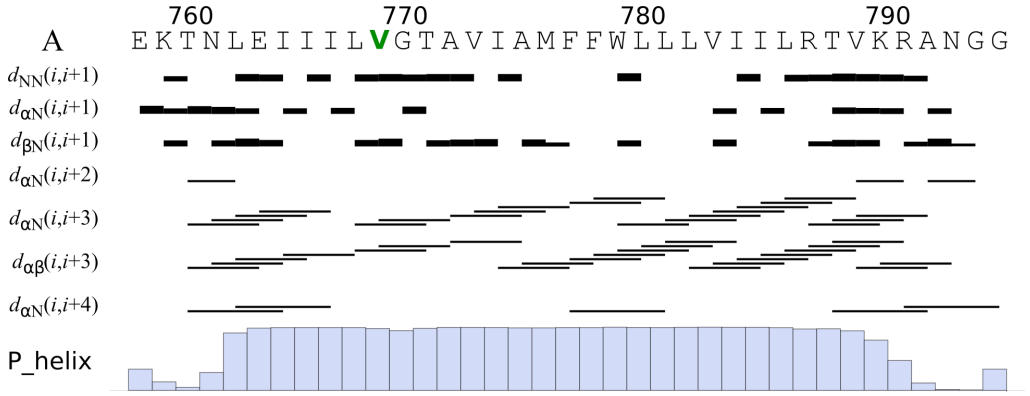

Figure 16: NMR data of wt-TMD peptides of VEGFR-2
Sequential and medium range characteristic NOE-based distances (dxx(i1,i2) are shown by horizontal lines. Line thickness is proportional to the intensity of the corresponding peak in the NOESY spectrum. Contacts not imposing restraints on the spatial structure were removed by the built-in algorithm of the CYANA software (Guentert, 2003). P_helix indicates the α-helical propensity predicted by the TALOS+ software on the basis of NMR chemical shifts (Shen *et al.*, 2009). Figure by Alexander S. Arseniev.

In order to monitor the dimerization process we recorded NMR spectra at various protein/DPC concentrations. In the experimental conditions used (figure 17) we found two different forms with population states that were dependent on detergent/protein

ratio. The dilution of the sample with detergent revealed that these two states corresponded to the monomeric wt-TMD helix and the wt-TMD dimer (figure 17A). At protein/DPC ratio of 1:150 the population of the monomeric state was ~70%. Additionally, the dilution of the sample with detergent showed a very slow transition. The free energy of dimerization (ΔG_0) was found to be -2.1±0.2 kcal/mol (figure 17B).

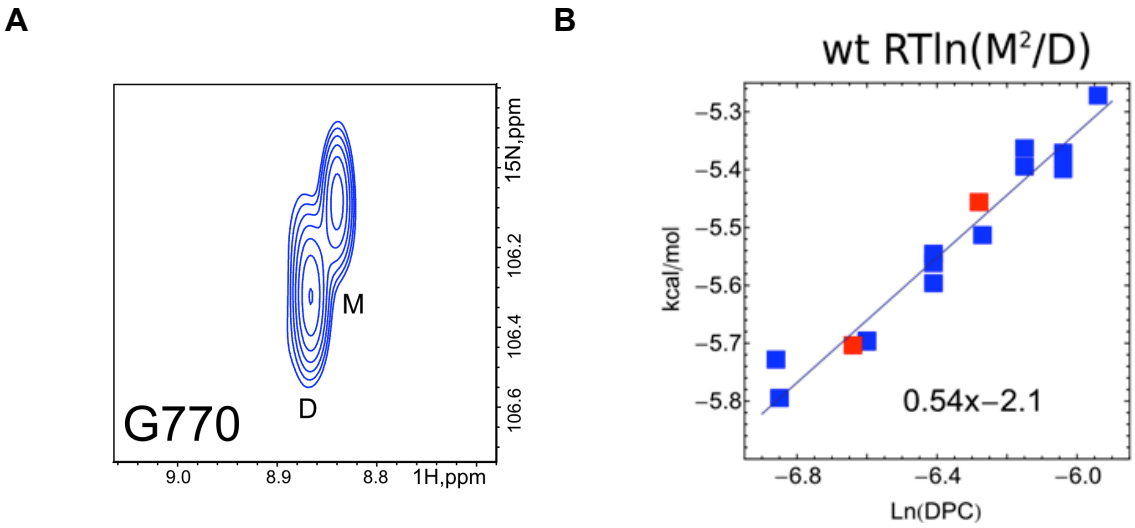

Figure 17: Spectra of cross-peaks of different oligomeric states and corresponding oligomerization constant of wt-TMD
(A) Signals of amide group residue G^{770} in ^{1}H, ^{15}N-TROSY-HSQC spectrum of VEGFR-2 wt TMD (see Appendix for full spectra). Cross peaks originating from monomeric (M) and dimeric (D) species are assigned Spectra was acquired with the following conditions: Lipid/protein ratio = 300 : 1, 318K and pH 4.5. (B) Oligomerization constants of VEGFR-2 wt-TMD. Apparent free energies of dimerization are plotted against the logarithm of concentration of empty micelles. Red points indicate a two-fold dilution of the sample with water. Significant points have a linear dependence of the form $y = ax+b$ where a equals γRT and b represents the standard free energy (ΔG_0). Standard conditions are 1M of empty DPC micells and 318K. Figure by Alexander S. Arseniev.

The VEGFR-2 wt-TMD helices appeared as symmetrical dimer with a left-handed orientation. The angle between the axes of helices was 25±1°C. Heteronuclei-filtered NOESY experiments revealed nine intermolecular contacts which were used for the calculation of the 3D-structure. The dimerization surface is long and apolar and spans across the entire helix. The dimer interface consists of a hydrophobic “heptad-repeat”-like cluster stabilized by intermonomeric van der Waals interactions of side chains: $T^{761}xxE^{764}xxI^{767}L^{768}xxT^{771}A^{772}xxA^{775}xxF^{778}W^{779}xL^{781}L^{782}xxI^{785}xxxV^{789}$. The polar and flexible N- and C-termini are solvent exposed. The interface is further

stabilized by a symmetric edge to face stacking interaction of F778 and W779 (figure 18).

A

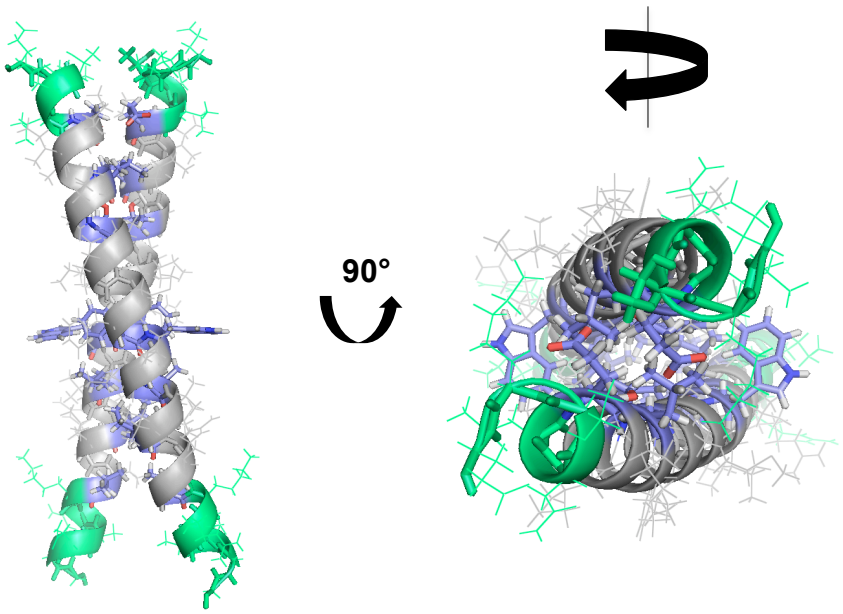

B

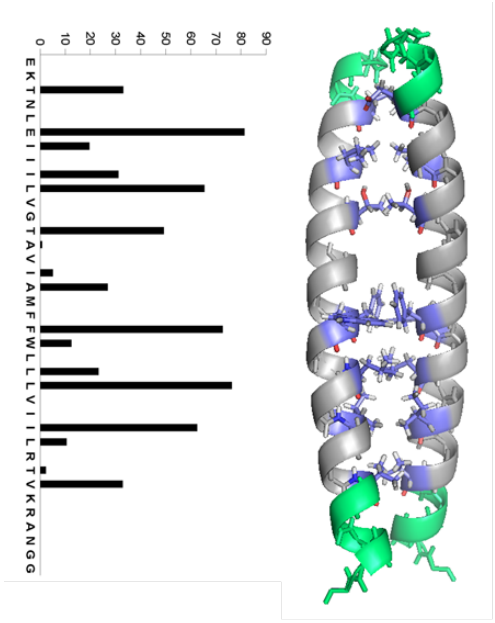

Figure 18: 3D-structure of the wt-TMD of VEGFR-2
(A) Overall structure of the TMD of VEGFR-2 side and top-view. Axis and orientation is indicated on top. (B) Intermonomeric contact surface area of VEGFR-2 TMD residues shown as percentage of the total solvent accessible area. N- and C-termini are colored in green. Helix backbone exposed to hydrophobic environment is depicted in grey. Dimerization interface is colored in blue. Models were made with PyMOL. Figures by Sandro Manni and Alexander S. Arseniev.

7.3. 3D-structure of the V769E transmembrane domain of VEGFR-2

The NMR chemical shifts, connectivities and NMR relaxation data show that the V769E-TMD-peptides synthesized and inserted into DPC micelles at pH 4.5 form long α-helical structures between amino acids 761-794 similar to the wt-TMD helices (figure 18A). Contacts of I, V and L- methyl groups of the TMD-section to residual protons of DPC methyl groups could be found in C^{13}-filtered NOESY experiments indicating a "true" TMD-helix but not a surface-bound helix.

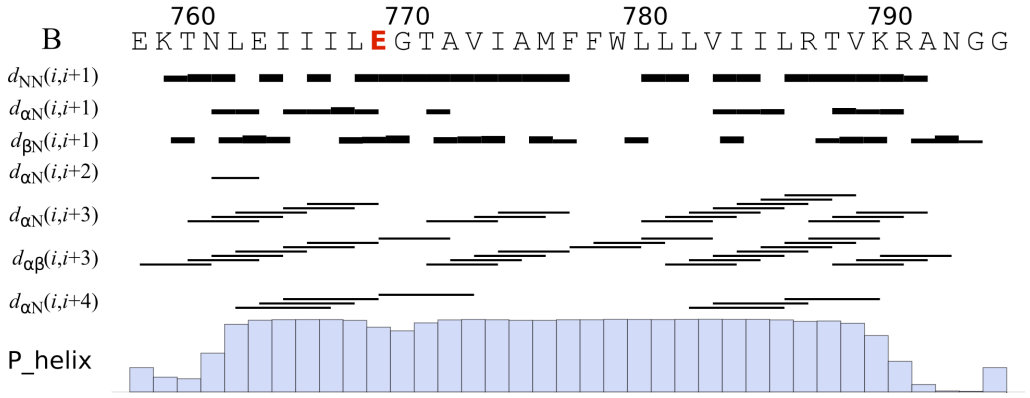

Figure 18: NMR data of V769E-TMD peptides of VEGFR-2
Sequential and medium range characteristic NOE-based distances (dxx(i1,i2) are shown by horizontal lines. Line thickness is proportional to the intensity of the corresponding peak in the NOESY spectrum. Contacts not imposing restraints on the spatial structure were removed by the built-in algorithm of the CYANA software (Guentert, 2003). P_helix indicates the α-helical propensity predicted by the TALOS+ software on the basis of NMR chemical shifts (Shen *et al.*, 2009). Figure by Alexander S. Arseniev.

For the V769E-TMD we found three oligomeric states as characterized by correlation times for rotational diffusion (figure 19A and Appendix). In order to find the exact model for the oligomerization process we tested three equilibrium models by diluting the sample with water and concentrated DPC solution: "monomer-dimer1-dimer2", "monomer-dimer-trimer" and "monomer-dimer-tetramer". When calculating the free energies of oligomerization from the signals derived from ^{1}H, ^{15}N-TROSY-HSQC spectra we found that only the "monomer-dimer-trimer" model fitted the obtained data with the following ΔG_0 values: ΔG_{dimer} = -2.4 ± 0.2 kcal/mol, ΔG_{trimer} = -2.9 ± 0.2 kcal/mol (figure 19B). The energetic contribution to dimerization caused by the V769E mutation is -0.3 kcal/mol. The contribution is therefore not significant and lies in the range of experimental error.

A

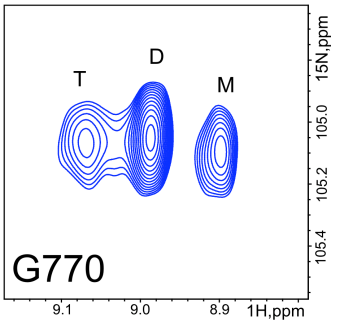

B

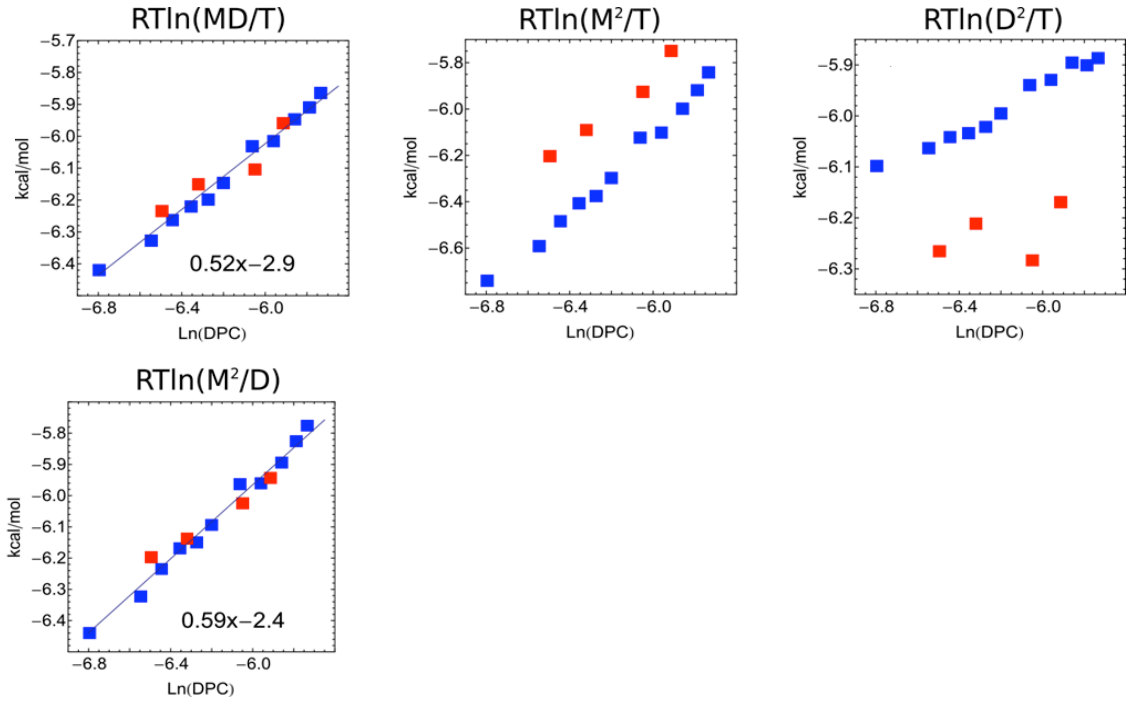

Figure 19: Cross-peaks of different oligomeric states and calculated oligomerization energies of tested models
(A) Signals of amide group residue G^{770} in ^{1}H, ^{15}N-TROSY-HSQC spectrum of VEGFR-2 V769E-TMD (see Appendix for full spectra). Cross peaks originating from monomeric (M), dimeric (D) and trimeric (T) species are indicated. Spectra was acquired with the following conditions: Lipid/protein ratio = 300 : 1, 318K and pH 4.5. (B) Oligomerization constants of VEGFR-2 V769E-TMD. Free energies of oligomerization are calculated out of intensities of signals derived from ^{1}H, ^{15}N-TROSY-HSQC spectra according to different equilibrium models: "trimerization: MD/T; two dimers: M^2/T; tetramerization: D^2/T; dimerization: M^2/D. Free energies are plotted against the logarithm of concentration of empty micelles. Red points indicate a two-fold dilution of the sample with water. Significant points have a linear dependence of the form $y = ax+b$ where a equals γRT and b represents the standard free energy (ΔG_0). Standard conditions are 1M of empty DPC micelles and 318K. Figure by Alexander S. Arseniev.

The determination of the dimeric spatial structure of V769E TMD of VEFR-2 was significantly affected by the presence of the highly stable trimeric state (stable up to

200:1 DPC/protein ratio). In order to investigate the 3D-structure we applied the analysis of covariance of N-H chemical shifts upon dimerization of wt and mutant V769E-TMD. To perform the analysis the chemical shift of the backbone N-H group derived from the ^{15}N-TROSY spectrum (cosine of angles between vectors) that arises from dimerization of the helices was plotted against the ratio of their modules (figure 20). Chemical shifts were measured in Hz to balance contributions of shift-changes for protons and nitrogen.

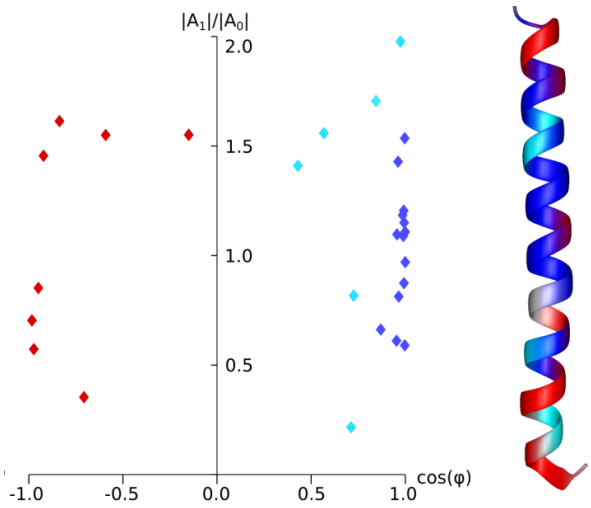

Figure 20: Analysis of covariance in amide chemical shift changes during dimerization of wt- and V769E-TMD
The cosine of angle between the vectors of each residue in the 2D ^{1}H, ^{15}N-TROSY-HSQC NMR signal (cos(θ)) was plotted against the ratio of their modules ($|A_1|$ / $|A_0|$). Good correlations are shown in blue. Points having “some” correlation are shown in cyan and points with no correlation are shown in red. The spatial structure of a TMD monomer of VEGFR-2 colored according to the correlation in the graph is depicted on the right. Figures by Alexander S. Arseniev.

During the dimerization process most of the residues showed a good correlation for chemical shift-changes of the nitrogen and the amide-proton. This means that with high probability the spatial structure of the wt-TMD and the one of the mutant V769E-TMD adopt the same dimeric conformation. Introdution of the mutation V769E in the TMD of VEGFR-2 does therefore not induce a conformation different from the wt-dimer.

To analyse the trimeric form we prepared a concentrated sample (90% trimer) with a detergent / protein ratio of 60 to perform a X-filtered NOESY experiment. The quality of the spectrum was poor due to line broadening and allowed only the detection of

seven interhelical contacts. These seven contacts were used to generate a symmetrical trimer with 21 distance restraints. The resulting spatial structure is shown in figure 21. The trimerization interface consists of the following residues: T761, E764, I765, L768, E769, A772, V773, M776, F777, W779, and L780. Due to the quality of the structure it is not possible to derive binding determinants such as H-bonding interactions. The interaction between the helices may be supported by H-bonds formed by the side chain of E769. Furthermore, stacking of aromatic rings may further stabilize the structure.

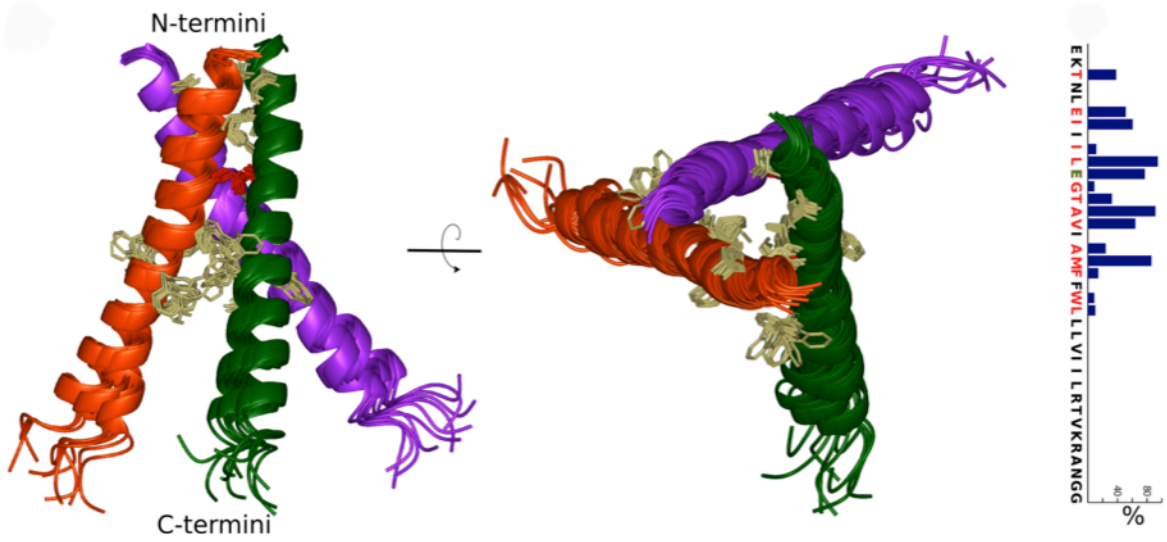

Figure 21: Model of trimeric V769E-TMD of VEGFR-2 represented by the 10 best spatial structures
Backbone atoms are shown in ribbon representation. Residues in the interface are shown in yellow. The intermonomeric contact surface area of V769E-TMD residues is indicated on the right in percentage of the total solvent accessible area. Figures by Alexander S. Arseniev.

Based on the overall structure of the trimer it is feasible that side chain E769 interacts with the carbonyl group of L768 and the amide group of A772. Interestingly, the asymmetric dimeric unit shares similar geometrical parameters previously found in TMD structures corresponding to the active state of other RTKs such as the TMD of ErbB2 (angle between the axes of helices of -50 ± 5° and C-termini pointing away from each other). Taken together the introduction of a glutamic acid residue at position 769 in the TMD of VEGFR-2 does not thermodynamically promote dimerization but allows for additional surface area and therefore novel helix-helix

interaction sites that may be used by the ECD-deleted VEGFR-2 construct to form the active state.

7.3.1. Functional analysis of kinase domain mutants of VEGFR-2

The only structural information describing the kinase domain of VEGFR-2 is available in a crystal structure representing the monomeric catalytic core of the cytoplasmic domain of VEGFR-2. In this structure one finds the highest sequence homology among all receptor tyrosine kinases. In order to achieve crystallization of the protein, dramatic truncations were necessary and it is therefore not possible to derive any information on the regulation of the monomeric kinase by the domains missing in this structure such as the kinase insert domain (KID) or the C-terminal domain of the receptor. It could be shown earlier that these domains have an impact on the regulation of receptor tyrosine kinases. The C-terminus of the Tie-2 receptor for example auto-inhibits the activity of the kinase domain in the absence of the ligand. This inhibitory mechanism is clearly dependent on the KID. In chimeric receptor constructs consisting of the extracellular domain of the CSF receptor and the kinase domain of VEGFR-2 carrying a truncated C-terminus it was shown that the catalytic domain of VEGFR-2 could not be activated by ligand (CSF) binding. Here we studied the role of the KID and the C-terminal tail in the regulation of VEGFR-2. We studied the native VEGFR-2 and not chimeric constructs since we assumed that the ECD of VEGFR-2 plays an essential role in receptor dimerization and is required to exactly position the intracellular domains relative to each other in active dimers.

7.3.2. Activity of extracellular domain deleted-kinase domain mutants

We performed our initial experiments with constructs that were all ECD-deleted. We investigated whether the domain truncations had an effect on kinase activity independently from VEGF. Besides the wild type construct (aa 765-1356), we designed a VEGFR-2 mutant according to the construct used for crystallization that lacked the 50 central residues of the 68 residues of the KID (aa 765-939 and aa 990-1356). Another construct was truncated at the C-terminus (aa 765-1180). To monitor phosphorylation we maintained the phosphorylation site Y1175 including its

consensus recognition motif. Finally we created the double deleted constructs that lacked the KID and the C-terminus. The catalytic domain mutants were transiently transfected into HEK293 cells and Y1054/59 and Y1175 phosphorylation was determined (figure 22).

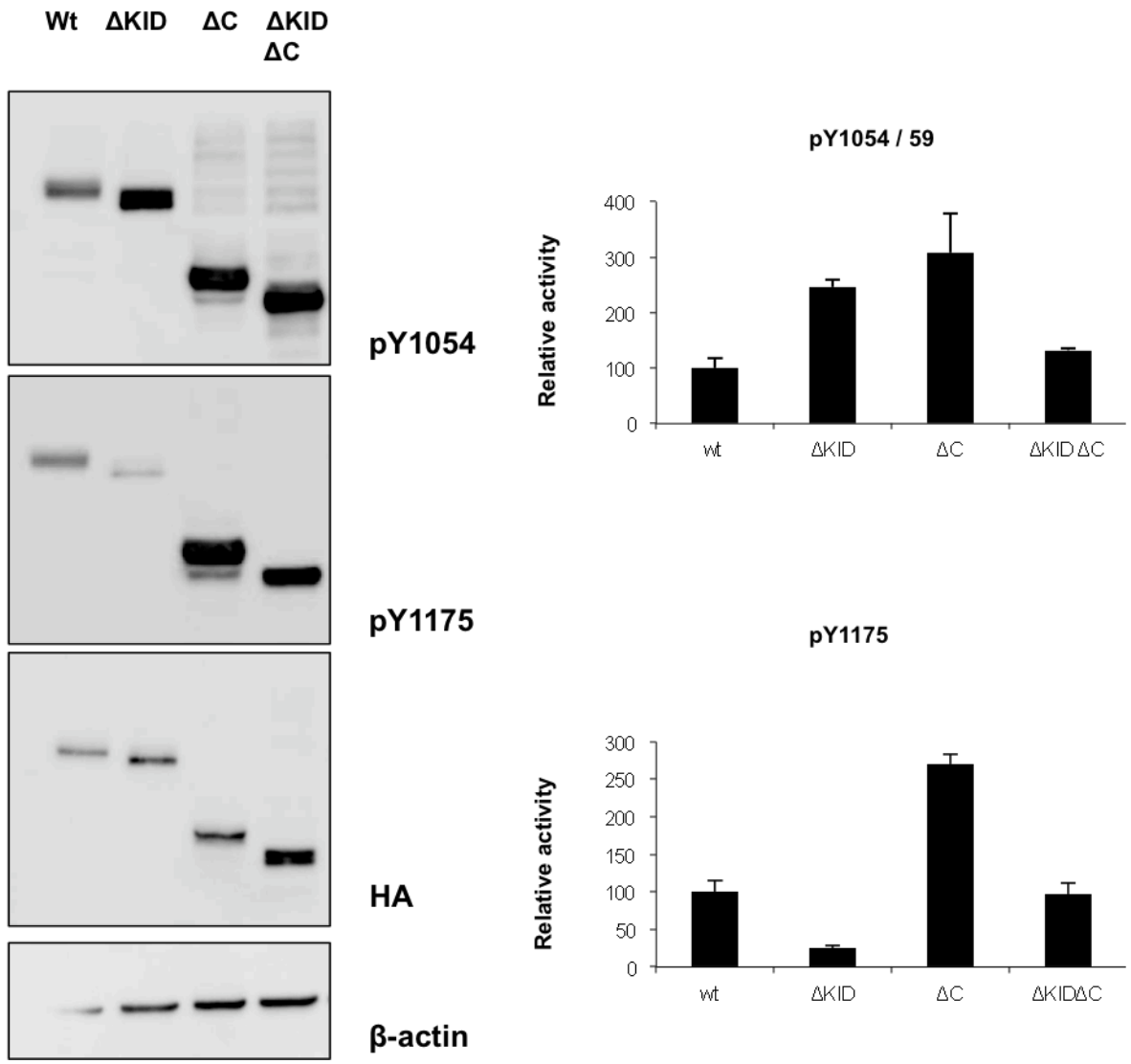

Figure 22: Activity of ΔECD-VEGFR-2 kinase domain mutants
Y1054/59 and Y1175 phosphorylation of kinase domain mutants is shown in comparison to the wt. pY1054/59 and pY1175 quantification using three independent experiments, receptor phosphorylation is indicated as mean ± S.E. with wt set to 100%.

VEGFR-2 constructs with KID-deletion showed drastically reduced phosphorylation at Y1175 while the activation loop sites Y1054/59 were still phosphorylated. The VEGFR-2 construct with C-terminal deletion showed a significantly higher activity (3 fold increase) than wt when determined by phosphorylation of Y1175 or Y1054/59.

7.3.3. Activity of full-length VEGFR-2 kinase domain mutants

In a next set of experiments we introduced the kinase domain mutations of the ECD-deleted VEGFR-2 constructs into the full-length receptor and studied receptor phosphorylation in transfected HEK293 cells. Y1054/59 and Y1175 phosphorylation was determined (figure 23).

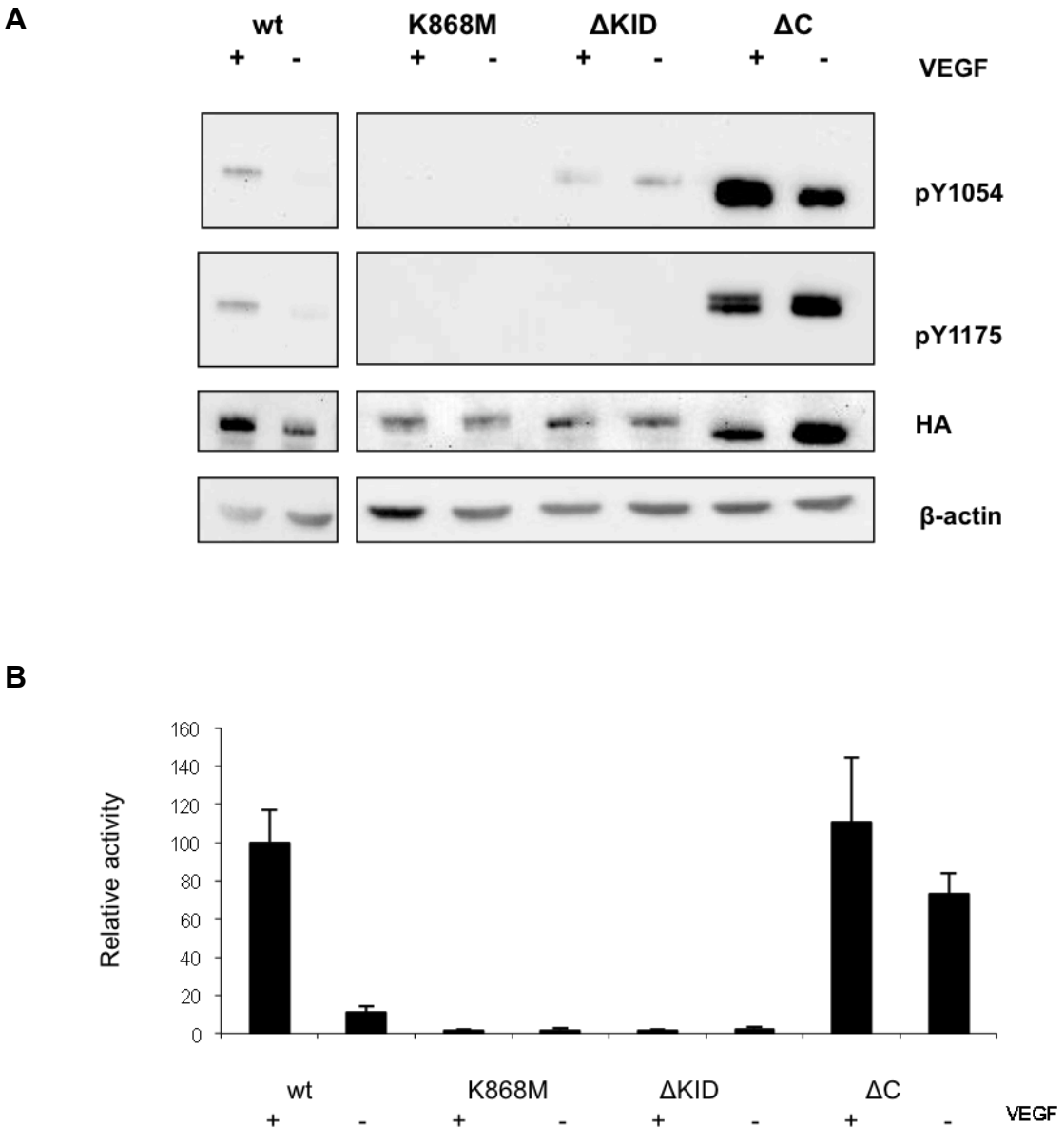

Figure 23: Activity of full-length-VEGFR-2 kinase domain mutants
(A) Y1054/59 and Y1175 phosphorylation of kinase domain mutants is shown in comparison to wt in VEGF stimulated control. (B) pY1054/59 and pY1175 quantification using three independent experiments, receptor phosphorylation is indicated as mean ± S.E. with wt set to 100%.

The results show that our previous data obtained with the ΔECD-VEGFR-2 kinase domain mutant constructs were reproducible in the context of the full-length receptors (figure 23). The VEGFR-2 construct with the KID deletion showed reduced phosphorylation at Y1175 while the activation loop sites Y1054/Y1059 were phosphorylated. The full-length VEGFR-2 constructs carrying the C-terminal deletion showed receptor activation independent of VEGF stimulation at levels of the stimulated wt construct. As a negative control we used a mutant construct (K868M) that is deficient for binding ATP and therefore unable to catalyse autophosphorylation reactions.

7.3.4. Downstream signaling by kinase domain mutants

Phosphorylation of Y1175 at the C-terminus of the intracellular kinase domain of VEGFR-2 leads to recruitment of PLC-γ. The activation of PLC-γ promotes 1, 2-diacylglycerol (DAG) release resulting from phosphatidylinositol 4,5-bisphosphate (PIP2) hydrolysis. DAG activates protein kinase C (PKC) that further activates members of the MAP kinase family, which results in upregulation of immediate early genes. We determined phospholipase C-γ activation using the above analysed cell lysates (figure 24). PLC-γ activity was monitored by immunoblotting using an antibody specific for pPLC-γ. For the detection of total PLC-γ the same membrane was decorated with an anti PLC-γ antibody.

A

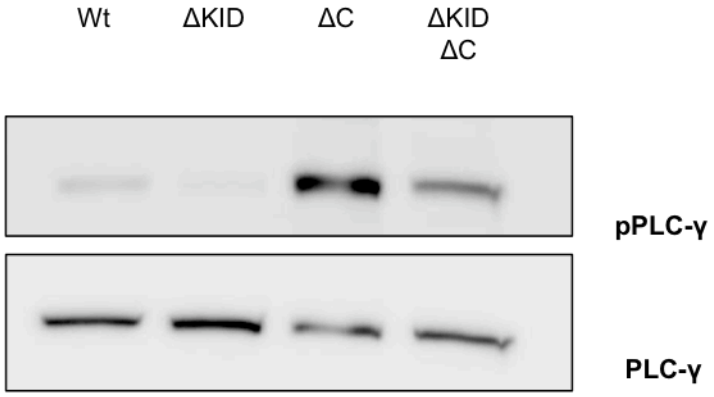

B

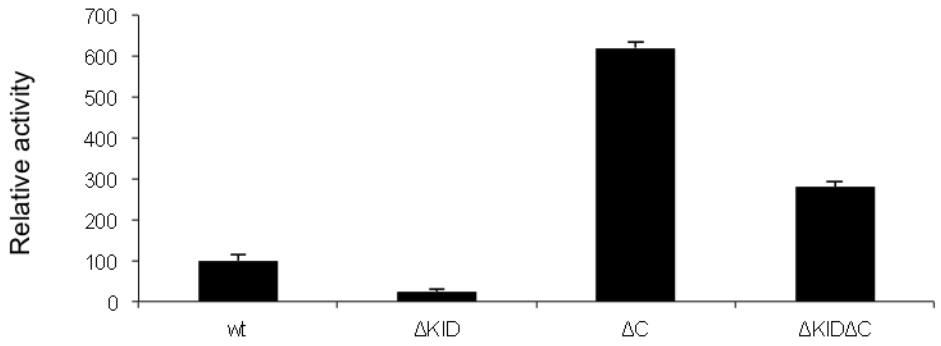

Figure 24: PLC-γ activity of ΔECD-VEGFR-2 kinase domain mutants
(A) PLC-γ activity of kinase domain mutants is shown in comparison to wt. (B) Quantification using three independent experiments. Relative activity is indicated as mean ± S.E. with wt set to 100%.

Activation of PLC-γ was consistent with the phosphorylation pattern of the ΔECD-VEGFR-2 constructs and was not dependent on VEGF. The VEGFR-2 construct with the KID deletion showed no PLC-γ activation while a construct with C-terminal deletion showed significantly higher PLC-γ activity (7 fold increase) compared to wild type.

We next determined PLC-γ activity in full-length VEGFR-2 kinase domain mutant constructs (figure 25).

A

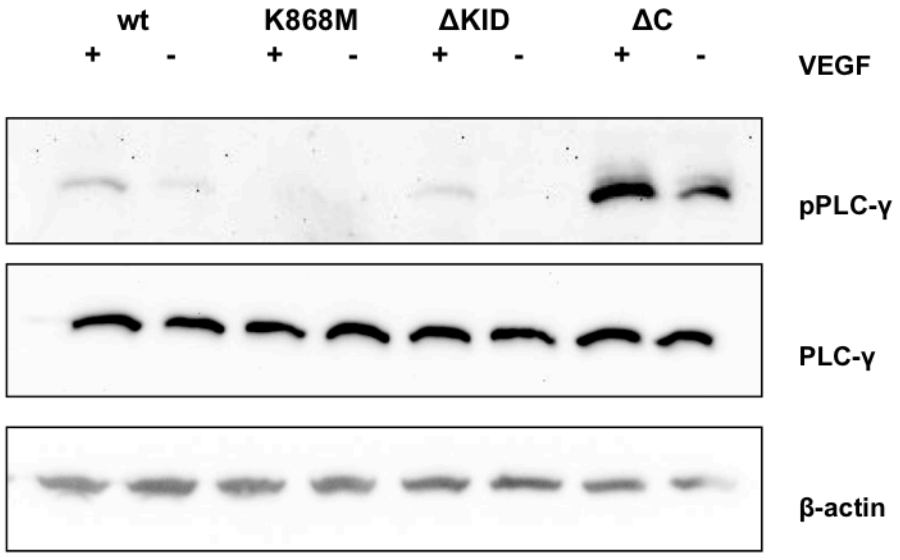

B

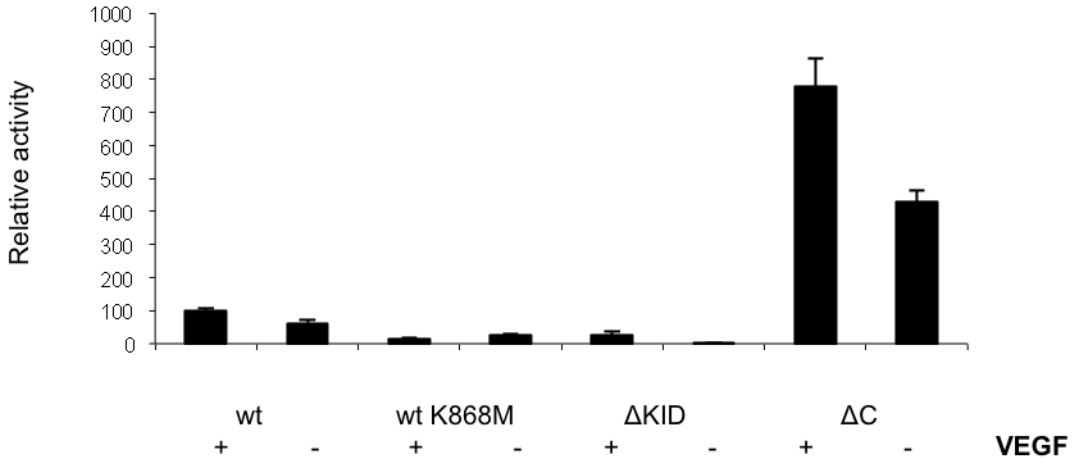

Figure 25: PLC-γ activity of full-length VEGFR-2 kinase domain mutants
(A) PLC-γ activity is shown in comparison to VEGF stimulated wt-control (B) Quantification using three independent experiments, Relative activity is indicated by mean ± S.E. with wt set to 100%.

PLC-γ activation in these constructs was comparable to the ΔECD-VEGFR-2 constructs. The VEGFR-2 construct with the KID deletion showed no signaling through PLC-γ while the construct with the C-terminal deletion showed constitutive activation (8 fold increase) as compared to VEGF stimulated wt receptor. The activation was independent of VEGF. As a negative control we used a mutant construct (K868M) that was deficient in ATP binding and therefore not able to autophosphorylate to activate downstream effectors.

7.3.5. Activity of full-length VEGFR-2 Y951F mutant

The results of the VEGFR-2 constructs with the KID deletion showed reduced phosphorylation at Y1175 and therefore no downstream signaling through PLC-γ. These findings let us speculate about a more complex mechanism for VEGFR-2 activation that involved also the KID. Our working hypothesis was that prior to Y1175 phosphorylation Y951, situated in the KID, has to be phosphorylated first. We mutated Y951 to F and determined the phosphorylation pattern of VEGFR-2 in VEGF stimulated and unstimulated cells (figure 26).

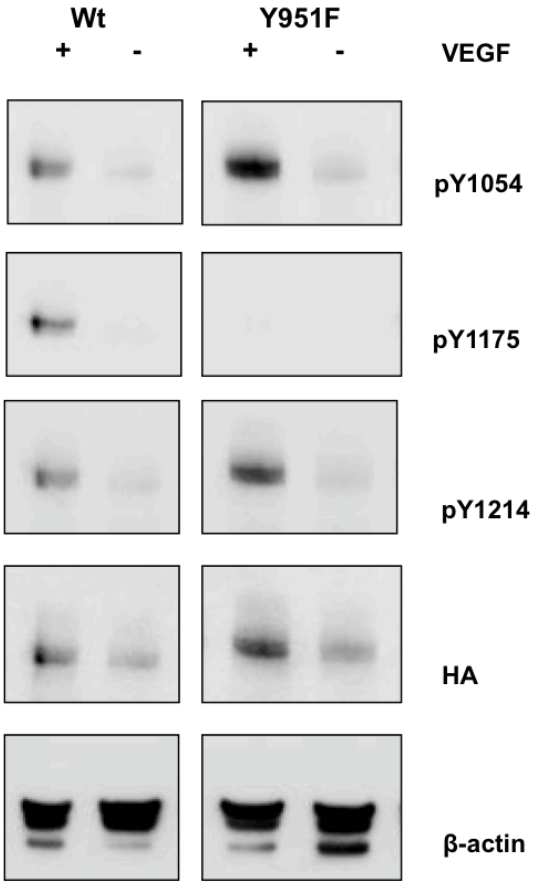

Figure 26: Phosphorylation pattern of VEGFR-2 Y951F mutant compared to wt
Phosporylation of Y1054/59, Y1175 and Y1214 of the mutants is shown in comparison to wt in VEGF stimulated and control cells.

The VEGFR-2 mutant Y951F showed no phosphorylation at Y1175 neither in VEGF stimulated nor in VEGF unstimulated cells whereas Y1054/59 in the activation loop and Y1214 in the C-terminal tail were phosphorylated. The data shows that phosphorylation at Y951 is mandatory for downstream signaling to Y1175.

7.4. Expression, purification and biophysical characterization of VEGFR-2 kinase domain proteins

At the beginning of this project there was only limited structural and functional information on the kinase domain of VEGFR-2 available. The only structural information available to date is based on crystal structures of the catalytic core of VEGFR-2 (1VR2) and VEGFR-1 (3HNG). To achieve crystallization all the regulatory domains such as the JMD, KID or the C-terminal tail had been removed in the used constructs. Biophysical and biochemical information is required to understand the role of these domains and therefore we engineered several mutant constructs for high level expression in insect cells (table 11).

Construct	JMD	KID (Y_{951}VGAIP)	Murine KID (Y_{951}VGELS)	C-terminus	K868M
VEGFR-2 KD	+	+	-	+	-
K868M VEGFR-2 KD	+	+	-	+	+
ΔJMD VEGFR-2 KD	-	+	-	+	-
ΔKID VEGFR-2 KD	+	-	-	+	-
mKID VEGFR-2 KD	+	-	+	+	-
ΔC VEGFR-2 KD (+Y1175)	+	+	-	- (+Y1175)	-
ΔJMDΔC VEGFR-2 KD (+Y1214)	-	+	-	+ (+Y1214)	-
ΔJMDΔKIDΔC VEGFR-2 KD (+Y1175)	-	-	-	- (+Y1175)	-

Table 11: Schematic representation of VEGFR-2 kinase domain constructs used for high level expression
VEGFR-2 KD: Full-length kinase domain (786-1356). **K868M VEGFR-2 KD**: Full-length kinase domain with K868M mutation in the ATP binding site of the kinase. **ΔJMD VEGFR-2 KD**: Kinase domain with JMD deletion (807-1356). **ΔKID VEGFR-2 KD**: Kinase domain with KID deletion (786-939 / 991-1356). **mKID VEGFR-2 KD**: Human kinase domain carrying murine KID. **ΔC VEGFR-2 KD (+Y1175)**: Kinase domain with C-terminal deletion (786-1179, including Y1175 and consensus recognition motif). **ΔJMDΔC VEGFR-2 KD (+Y1214):** Kinase domain with JMD deletion and C-terminal truncation (807-1228, including Y1214 and consensus recognition motif). **ΔJMDΔKIDΔC VEGFR-2 KD**: Kinase domain with JMD deletion, KID deletion and C-terminal deletion (807-939, 991-1179) including Y1175 and consensus recognition motif).

Besides kinase constructs with domain mutations we also created a kinase mutant that was deficient in ATP binding (K868M) and a mutant carrying the murine KID for further binding studies with TSAd (see next chapters). All the constructs were cloned into one of the two multiple cloning sites of the Multibac baculovirus expression vector pFL (Berger *et al.*, 2004). The pFL plasmid contains two bidirectionally oriented expression cassettes for the production of multiprotein complexes. Our intention was to use this vector for future expression of complexes between the kinase domain and TSAd which binds to Y951 of VEGFR-2. All the constructs carried a C-terminal 10xHis-tag with a preceding TEV protease cleavage site allowing tag removal. The pfL vectors were then used to generate baculovirus for insect cell infection. Recombinant protein expression was performed in baculovirus infected Sf21 insect cells. Sf21 cells are ovarian cells originating from Spodoptera frugiperdia. The infected cells were harvested 72-96 h post infection. Expression of the recombinant protein was verified by immunoblotting using an 5xHis-tag specific antibody. Expression of proteins with a Mr ranging from 37.5-65.9 kDa (theoretical) could be verified (figure 27).

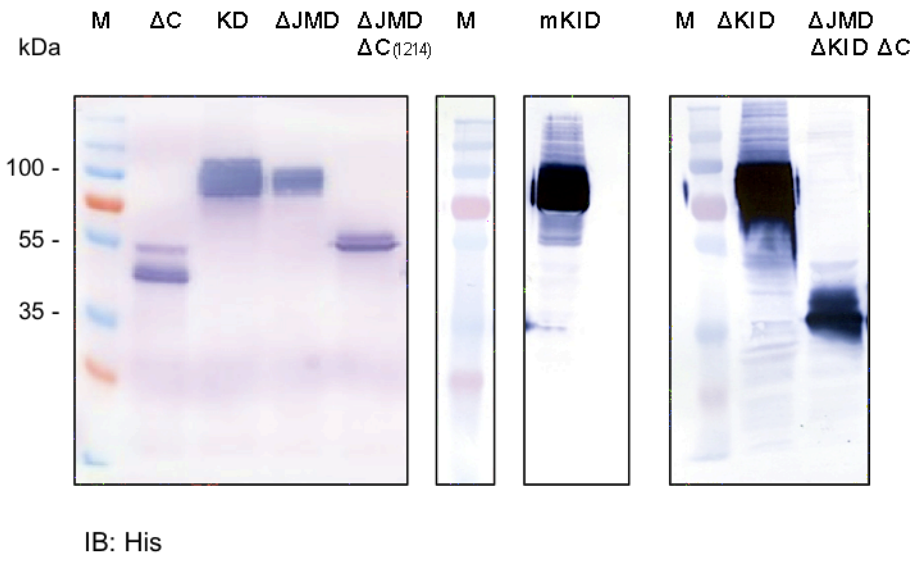

Figure 27: Expression of VEGFR-2 kinase domain proteins in Sf21 insect cells
Baculovirus infected cell lysates were analyzed for their recombinant proteins on immunoblots using an antibody recognising the His-tag.

In a first step the proteins were purified by immobilized metal ion affinity chromatography (IMAC) to remove most of the impurities. Proteins were eluted using an imidazole gradient. SDS-PAGE was used to monitor the quality of the eluate. In a second step we purified the proteins via size exclusion chromatography (SEC). After this step the proteins showed a purity of 95% as judged from SDS-PAGE. The protein yields ranged from 1-4 mg per litre of cultured cells. In order to achieve homogenous phosphorylation of the kinase domains we phosphorylated the proteins *in vitro* after the first IMAC purification step by addition of ATP and $MgCl_2$. The phosphorylation state of the purified protein was then determined using specific anti phospho-tyrosine antibodies (figure 28).

A

IMAC purification

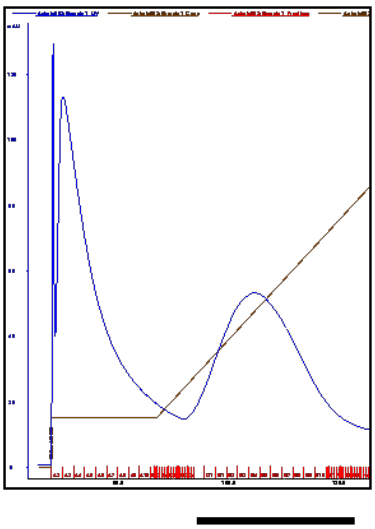

SEC purification

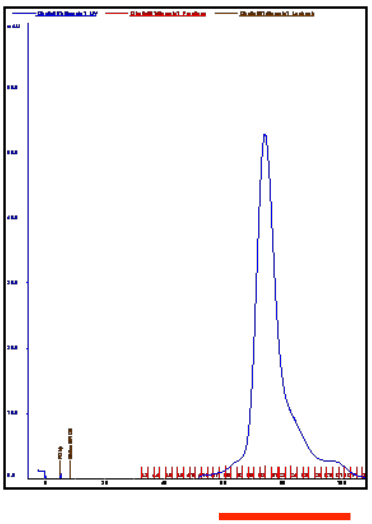

elution volume: 73.86 mL

eluate

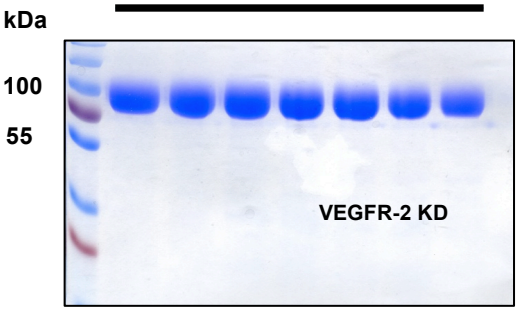

eluate

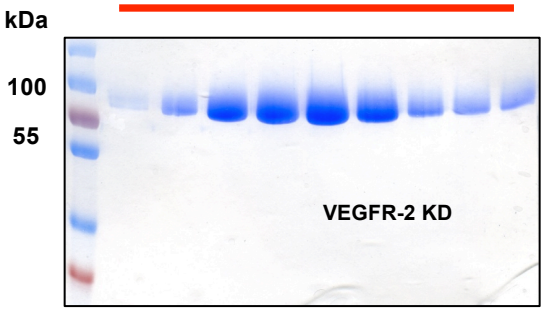

eluate

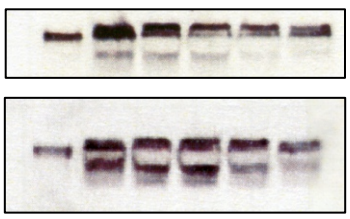

eluate

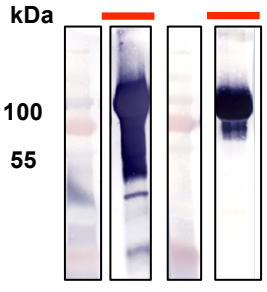

B

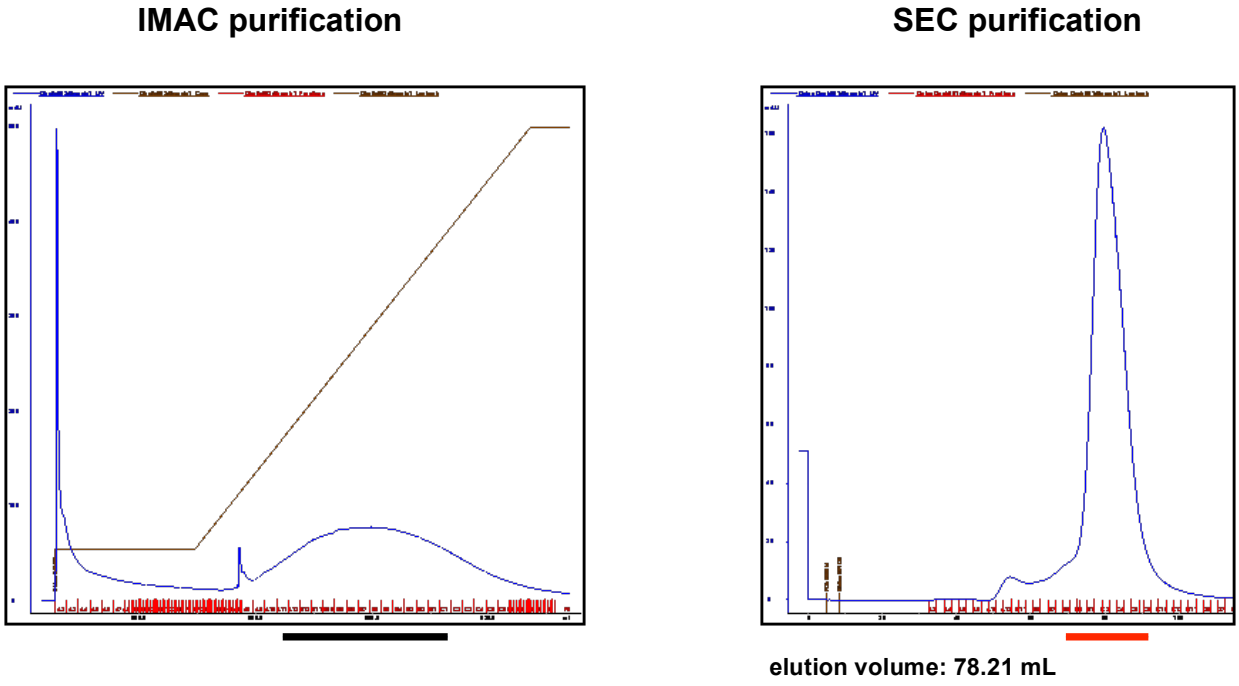
IMAC purification
SEC purification
elution volume: 78.21 mL
eluate
kDa
75
50
K868M VEGFR-2 KD
eluate
kDa
75
50
K868M VEGFR-2 KD
KD KD+I M
KD KD+I M
KD KD+I M kDa
100
55
IB: pY1175
pY951
pY1054/59

C

IMAC purification

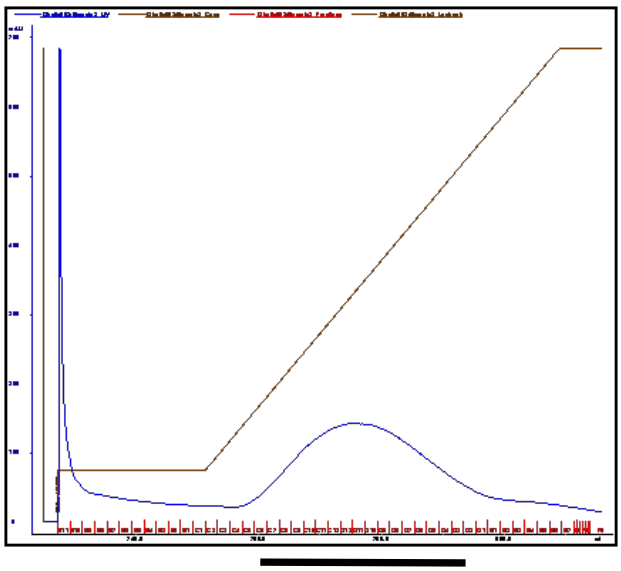

SEC purification

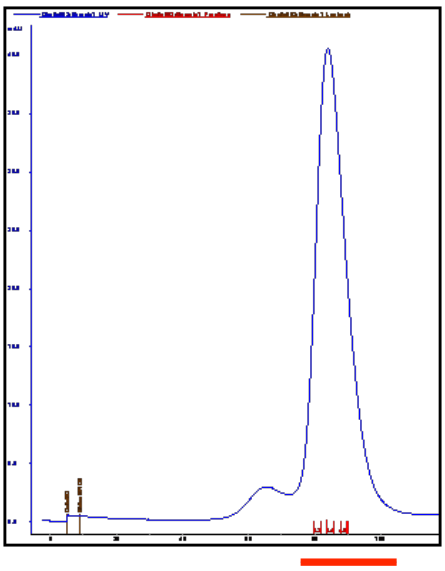

elution volume: 76.45

eluate

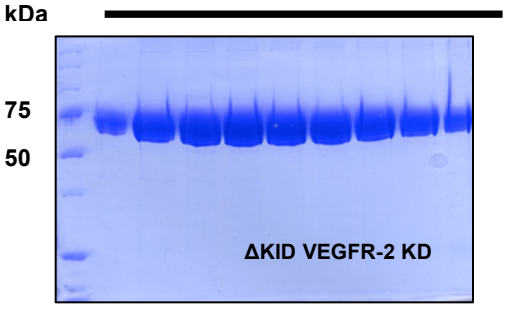

eluate

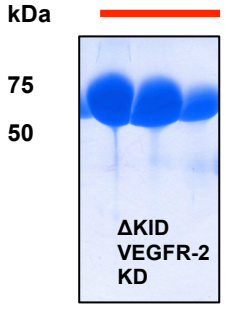

eluate **eluate**

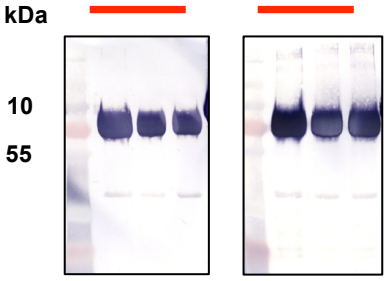

IB: pY1175 **His**

D

IMAC purification

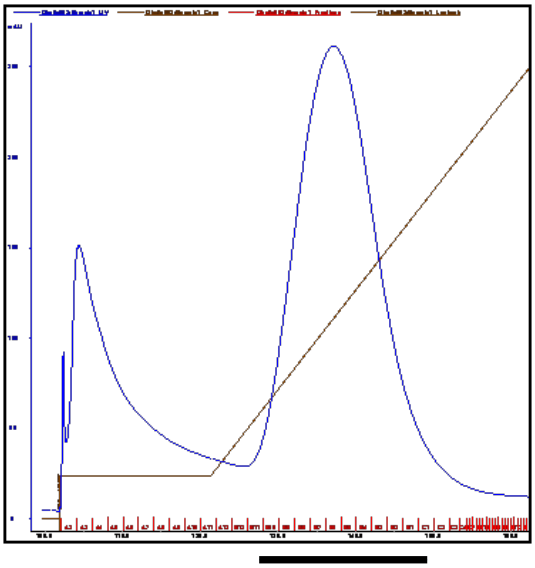

SEC purification

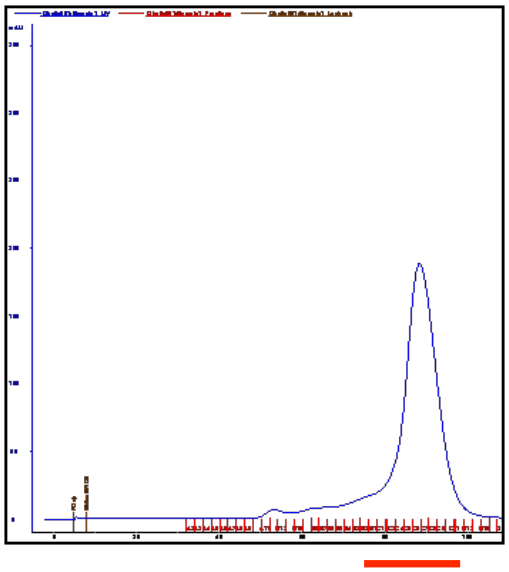

elution volume: 88.18 mL

eluate

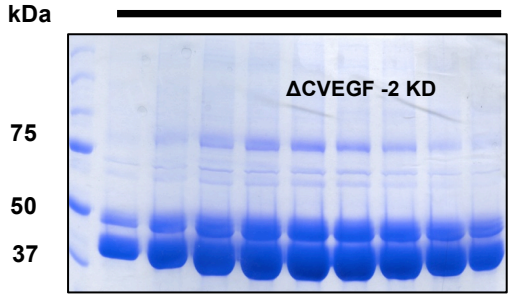

eluate

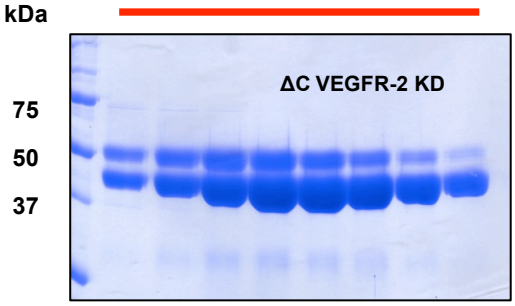

eluate

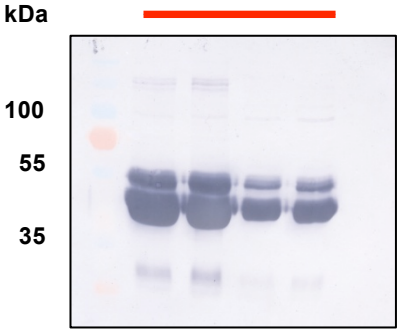

IB: His

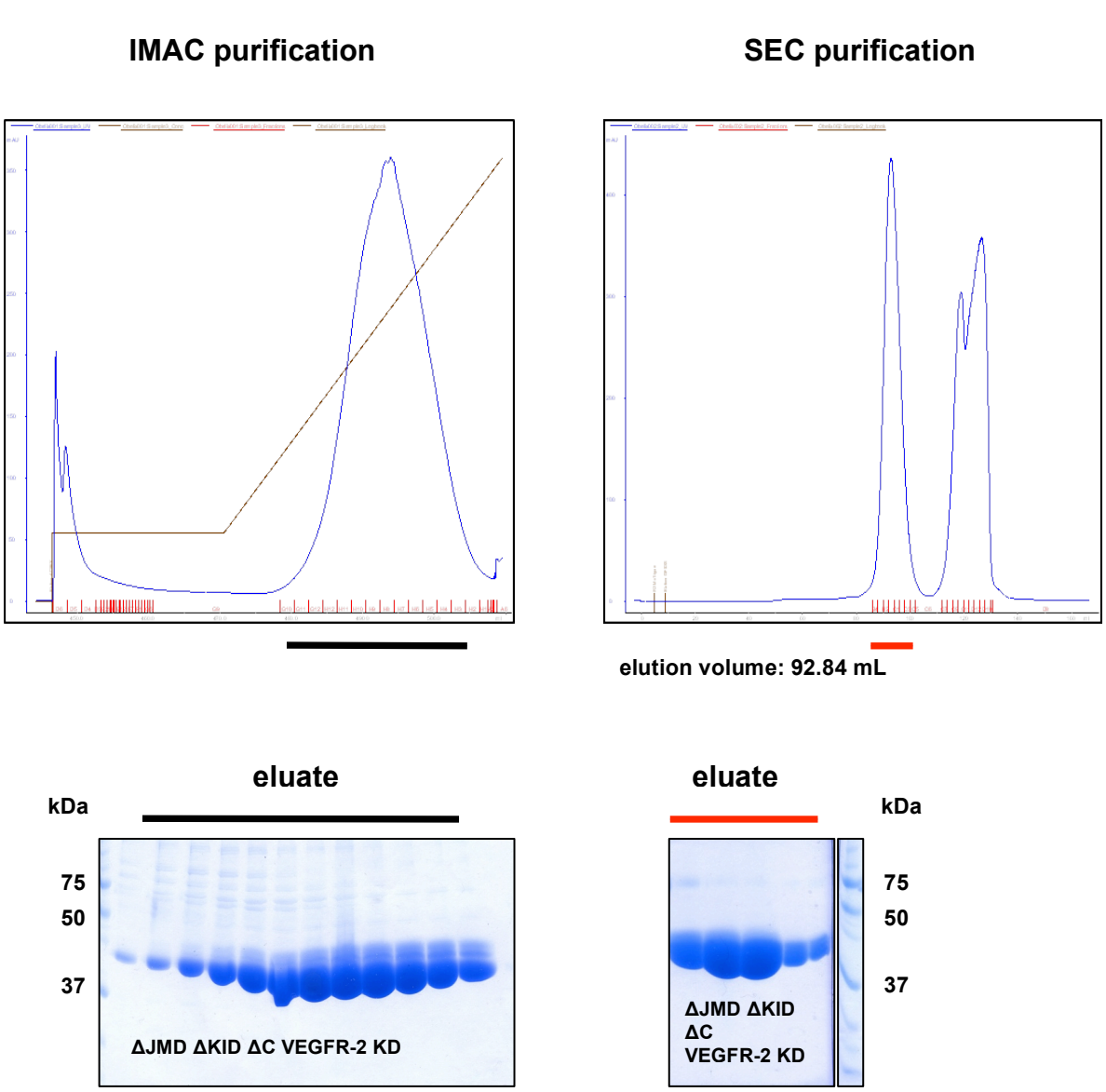

Figure 28: Purification of VEGFR-2 kinase domain constructs
(A) VEGFR-2 KD and its inactive counterpart (B) K868M VEGFR-2 KD. To monitor phosphorylation state of K868M VEGFR-2 KD we used inhibitor treated VEGFR-2 KD that mimicks the K868M mutation. (C) ΔKID VEGFR-2 KD (D) ΔC VEGFR-2 KD (E) ΔJMDΔKID ΔC VEGFR-2 KD. Purified proteins were analyzed on immunoblots using an antibody against the His-tag. Phosphorylation state of the proteins was analysed using phosphosite-specific antibodies described in section 6.2.

All VEGFR-2 kinase domain proteins were expressed in an upscaled format. Purification of VEGFR-2 KD, K868M VEGFR-2 KD, ΔKID VEGFR-2 and mKID VEGFR-2 (analogous to VEGFR-2 KD, not shown) appeared as one single homogeneous band on SDS-gels and were fully phosphorylated at their critical phospho-sites (shown for the full-length VEGFR-2 KD) after treatment with ATP and $MgCl_2$. ΔC VEGFR-2 KD showed an additional weaker band of slightly higher

molecular weight (close to 50 kDa). The His-tag antibody recognized both bands therefore it was probably the result of an exposed cleavage site in this C-terminally deleted construct. The retention time and the resulting elution volume was consistent with the Mr of each kinase domain construct: VEGFR-2 KD: 73.86 mL < ΔKID VEGFR-2 KD: 76.45 mL < ΔC VEGFR-2 KD: 88.18 mL < ΔJMDΔKIDΔC VEGFR-2 KD. VEGFR-2 KD and K868M VEGFR-2 KD with the same Mr of 65.9 kDa differed slightly in their retention time: VEGFR-2 KD: 73.86 mL and K868M VEGFR-2 KD: 78.21 mL. The shift can be explained with the different phosphorylation pattern of each protein and the resulting alteration in the shape (hydrodynamic radius) of these proteins. K868M VEGFR-2 KD adopts a more compact inactive conformation that results in a retention time different from VEGFR-2 KD (78.21mL vs 73.86 mL). While VEGFR-2 KD shows phosphorylation at all the critical Y-residues, K868M VEGFR-2 KD shows only partial phosphorylation at Y1175. Y1054/59 and Y951 were not phosphorylated when the cells were treated with a VEGFR-2 specific inhibitor during protein production. Inhibitor binding mimicks K868M mutation that prevents ATP from binding to VEGFR-2 KD.

7.4.1. Multi Angle Light Scattering (MALS) analysis of purified VEGFR-2 kinase domain proteins

Besides visualizing purity and homogeneity of the recombinant proteins by SDS-PAGE we analysed proteins by MALS to determine protein quality and Mr. MALS allows to determine the Mr of a protein independent of its shape. Shape information of the analysed proteins can be extracted from the elution volume of the coupled SEC column in the same way as in normal SEC and is standardised with an appropriate standard protein. All the purified kinase domain proteins were analysed separately (figure 29).

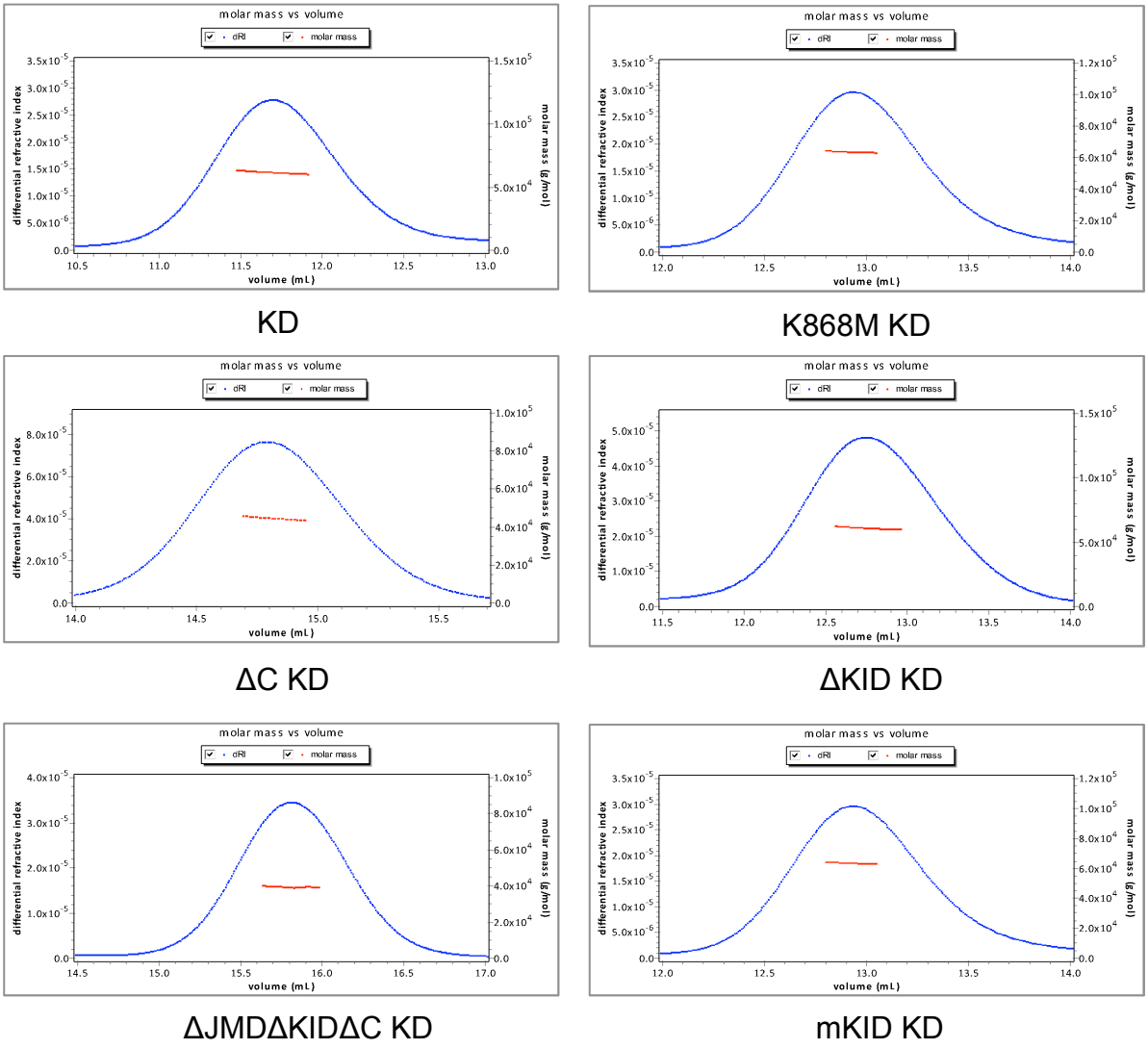

Figure 29: MALS analysis of VEGFR-2 kinase domain constructs

The theoretical Mw of the kinase domain proteins could be verified with a small percentage error (table 12). The proteins were injected at concentrations of 2 mg/mL. Taken into account a 1:10 dilution on the coupled SEC column the final concentration of the kinase domains in the system resulted in concentrations in the low µM range (3-5 µM). All proteins were monomeric and showed a homogeneous mass distribution at this concentration.

VEGFR-2 kinase domain construct	**Theoretical Mr** [kDa]	**Experimental Mr** [kDa] **(MALS)**
KD	65.9	61.62 (0.2%)
K868M KD	65.9	64.94 (0.5%)
ΔC KD (+Y1175)	45.9	44.87 (0.4%)
ΔKID KD	60.6	59.52 (0.4%)
ΔJMDΔKIDΔC KD (+Y1175)	37.5	39.37 (0.7%)
mKID KD	65.9	65.91 (0.4%)

Table 12: Comparison of theoretical and experimentally determined Mr of VEGFR-2 kinase domain proteins by MALS

7.4.2. Analytical Ultracentrifugation (AUC) analysis of VEGFR-2 kinase domain proteins

We found that VEGFR-2 constructs carrying specific domain deletions showed different activation profiles. KID deletion and mutation of the KID residue Y951 to F resulted in a defect in phosphorylation at Y1175 whereas deletion of the C-terminus rendered the kinase constitutively active.

With the various kinase domain mutants we performed sedimentation equilibrium AUC, which is able to separate proteins based on their Mr and not on their shape or hydrodynamic properties. We were especially interested in the concentration dependence of the kinase domain. In this way we might detect an intrinsic dimerization propensity of the KD in the absence of the ECD and the TMD. Another focus was to determine the dimerization propensity of the activating and inactivating kinase mutants (ΔC and ΔKID mutants). Three different concentrations of each kinase domain protein were analysed at two different rotor speeds (10, 30 and 80 µM at 14'000 and 20'000 rpm). The concentrations were chosen based on earlier MALS experiments of the kinase domain at high concentrations (>20 mg/mL) where small dimer peaks were observed (data not shown). For data collection we used the refractive index detection (Aviv Biomedical) together with a Beckman ProteomLab XL-I analytical ultracentrifuge. The data was fitted with a double-exponential

monomer-dimer equilibrium model with fixed monomer and dimer Mr. The data yielded a good fit. All the constructs showed dimer formation at increasing concentration (dimer : monomer ratio). Kd values were subsequently determined using the monomer-dimer amplitudes (see table in figure 30) of the 14’000 rpm run for at least two concentrations. Kd values calculated with amplitudes of the 20’000 rpm were not significant due to early sedimentation of the dimer (amplitudes of the dimer around 0, see tables). All the figures show representative graphs from the global analysis of each kinase construct for the highest concentration at 14’000 rpm and 20’000 rpm with the experimental and calculated values given in the table below. A good alignment of the residuals for the two speeds at 14’000 and 20’000 rpm was only achieved for VEGFR-2 ΔJMDΔKIDΔC KD that has the smallest Mr of 37.5 kDa. The good fit results from the incomplete sedimentation of the protein at 20’000 rpm due to its lower Mr compared to the other constructs.

AUC of VEGFR-2 KD in fully phosphorylated state

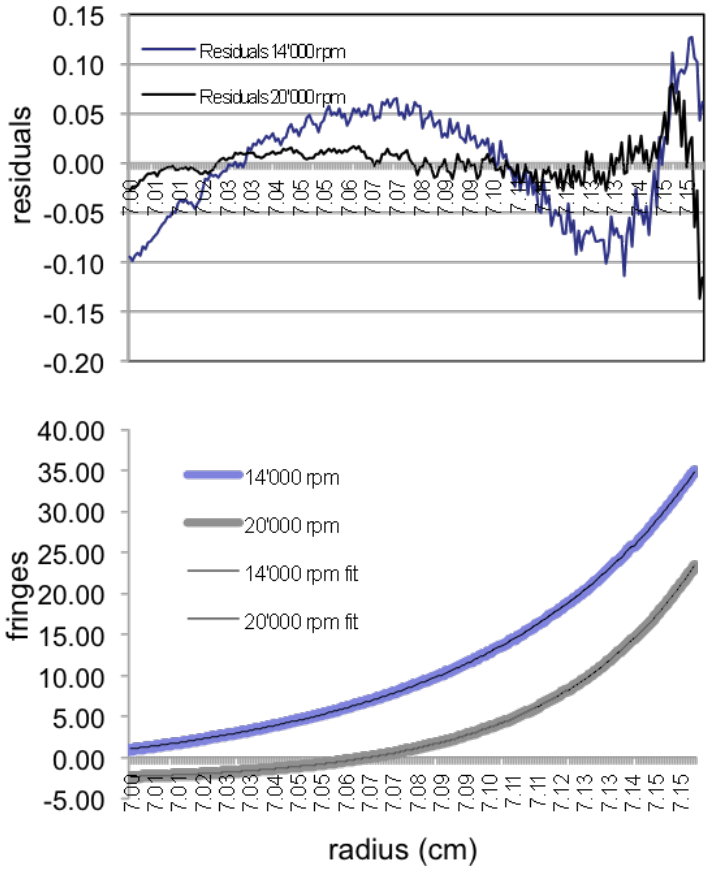

Conc [µM]	M 14'000rpm	D 14'000rpm	D/M	M 20'000rpm	D 20'000rpm	Kd [M] (14'000rpm)
10	2.296	0.432	0.18	1.782	0.110	-
30	7.879	2.798	0.35	6.011	0.171	$0.12E^{-3}$
80	15.415	5.630	0.36	10.330	0.050	$0.2E^{-3}$

AUC of VEGFR-2 KD lacking the KID in fully phosphorylated state

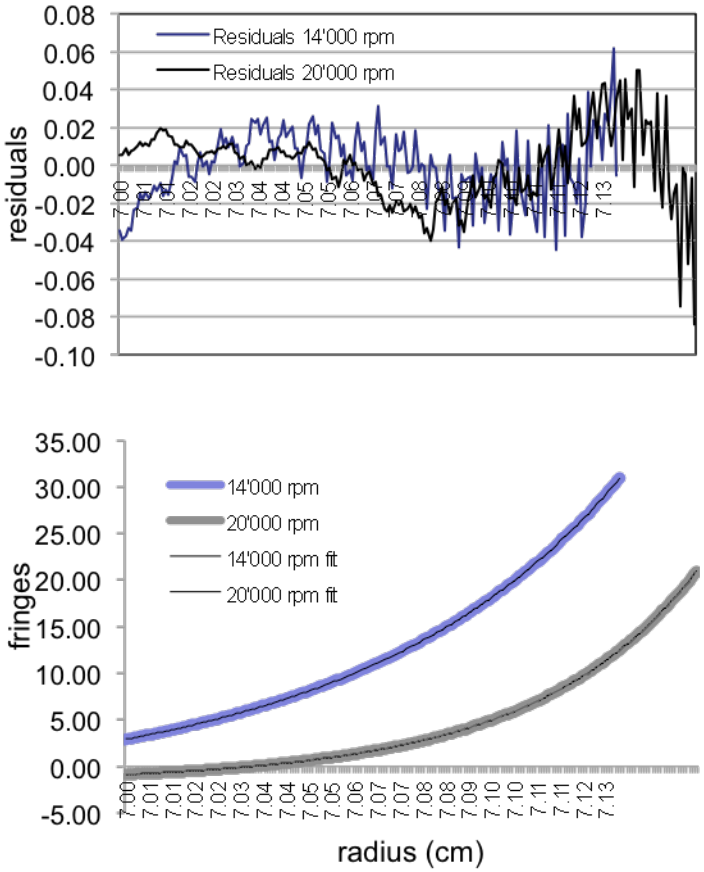

Conc [µM]	M 14'000rpm	D 14'000rpm	D/M	M 20'000rpm	D 20'000rpm	Kd [M] (14'000rpm)
10	3.752	0.373	0.09	3.594	0.178	$0.22E^{-3}$
30	9.104	2.488	0.27	8.690	0.529	$0.19E^{-3}$
80	20.858	9.657	0.46	16.871	1.415	$0.26E^{-3}$

AUC of VEGFR-2 KD lacking the C-terminus in fully phosphorylated state

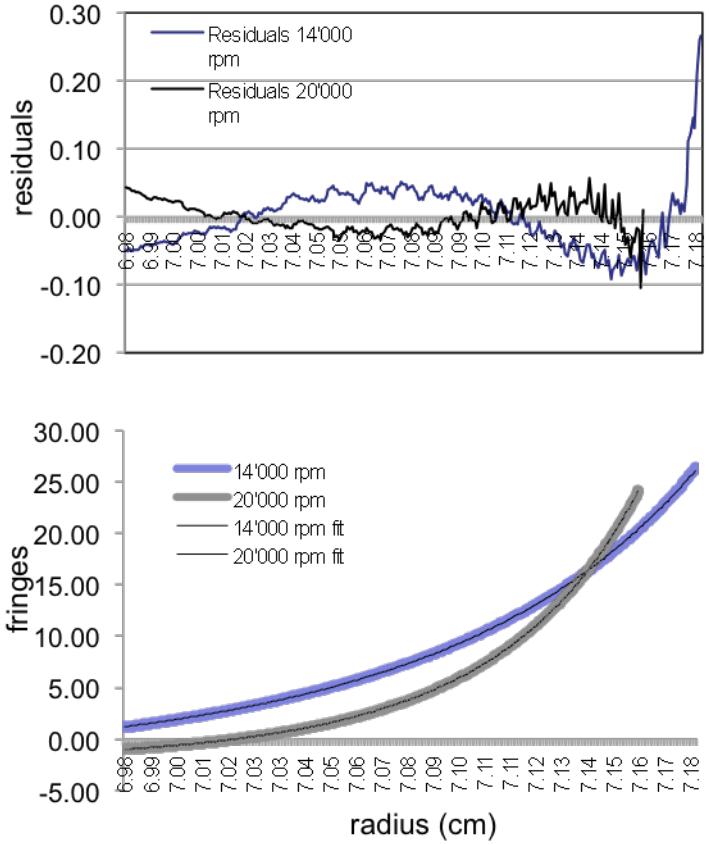

Conc [µM]	M 14'000rpm	D 14'000rpm	D/M	M 20'000rpm	D 20'000rpm	Kd [M] (14'000rpm)
10	2.09	0.02	0	2.073	0.024	-
30	5.04	0.59	0.11	4.991	0.335	$0.3E^{-3}$
80	11.84	3.92	0.33	10.640	1.753	$0.28E^{-3}$

AUC of VEGFR-2 KD lacking the JMD, KID and C-terminus in fully phosphorylated state

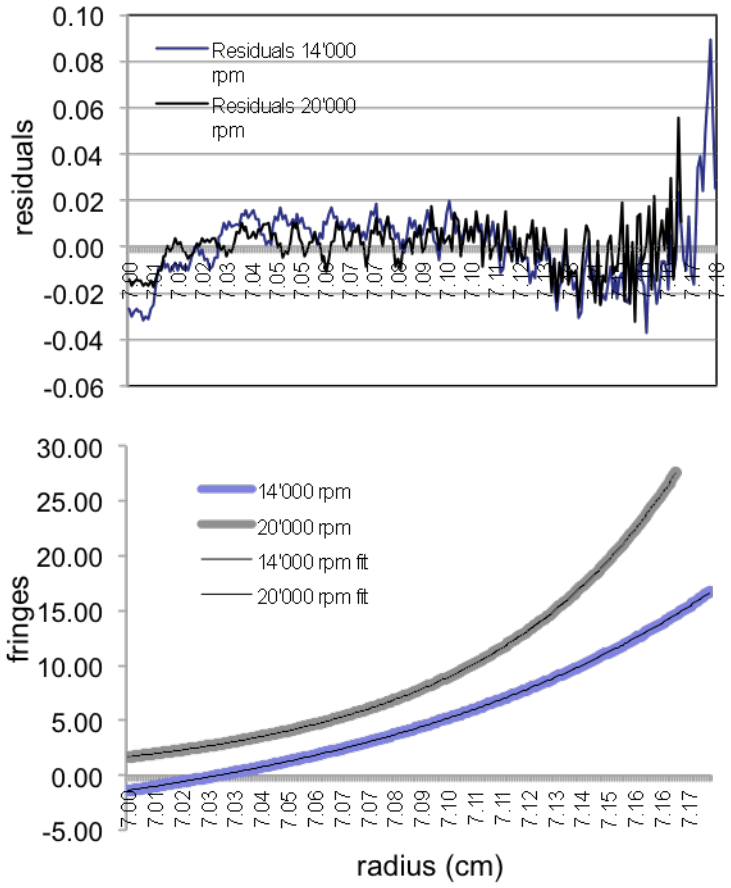

Conc [µM]	M 14'000rpm	D 14'000rpm	D/M	M 20'000rpm	D 20'000rpm	Kd [M] (14'000rpm)
10	1.865	0.052	0.02	1.873	0.029	$0.6E^{-3}$
30	5.531	0.455	0.08	5.451	0.340	$0.6E^{-3}$
80	12.113	3.005	0.24	11.661	1.688	0.46^{E-3}

Figure 30: Sedimentation equilibrium AUC of VEGFR-2 KD constructs
The global analysis of the highest concentration at 14'000 and 20'000 rpm and the corresponding fit of each kinase construct are shown in the upper graph. The lower graph shows the overlay of the two residuals of each speed at 14'000 and 20'000 rpm. All the experimental and calculated values are indicated in the tables below: M: monomer amplitude; D: dimer amplitude; D/M: dimer / monomer ratio; Kd: dissociation constant.

The fully phosphorylated full-length kinase domain of VEGFR-2 (VEGFR-2 KD) showed the highest concentration dependent propensity to dimerize with an apparent Kd of 160 ± 56 µM whereas the truncated construct ΔJMDΔKIDΔC VEGFR-2 KD showed the lowest tendency to dimerize at higher concentrations with a Kd of 553 ± 80 µM. The Kd of kinase constructs carrying KID and C-terminal truncations were 225 ± 35 and 290 ± 14 µM respectively (table 12). The phosphorylated kinase domain itself has therefore a low propensity to dimerize at high concentration. Deletion of the C-terminus does not favour dimerization as one might expect from the fact that this construct showed constitutive activity in the above shown *in vivo* experiments.

Construct	Kd ± S.E. [µM]
VEGFR-2 KD	160 ± 56
ΔKID VEGFR-2 KD	225 ± 35
ΔC VEGFR-2 KD	290 ± 14
ΔJMDΔKIDΔC VEGFR-2 KD	553 ± 80

Table 12: Kd values of VEGFR-2 kinase domain mutant constructs
Kd values were determined as mean ± S.E. from at least two concentrations.

7.4.3. *In vitro* phosphorylation kinetics of purified VEGFR-2 kinase domain

VEGFR-2 kinase tyrosine sites are phosphorylated upon ligand stimulation of the receptor. It has been shown that Y801 in the JMD is phosphorylated as a first event followed by Y1054 and Y1059 in the activation loop. Activation loop phosphorylation leads to a further increase in kinase activity. To date the order of autophosphorylation of the downstream signaling tyrosine residues has not been determined. We previously found that Y951 has to be phosphorylated in order to activate receptor signaling trough phosphorylated Y1175. Our concept was to enzymatically characterize the kinase domain of VEGFR-2 and to determine the order of the phosphorylation events. We performed an *in vitro* phosphorylation assay with the completely dephosphorylated kinase domain of VEGFR-2 (VEGFR-2 KD). The

reaction took place at high ATP and low protein concentration. Aliquots of several time points (sampled over 30min) of the reaction were stopped and monitored by immunoblotting (figure 31A). Phosphorylation intensities over time showed that after 5 min the pY1054/59 signal shows the strongest intensity and reaches saturation at the fastest rate. This finding confirms previously published data where Y1054 and Y1059 phosphorylation immediately followed Y801. The second highest extent of phosphorylation at 5 min was detected for pY1212 and then followed by pY951. The slowest phosphorylation rate was observed for Y1175. All pY-intensity signals reached saturation after 30 min. These findings support our previous results where Y951 was shown to be phosphorylated first in order to allow phosphorylation of Y1175 and promote downstream signaling to PLC-γ (section 7.3.5).

A

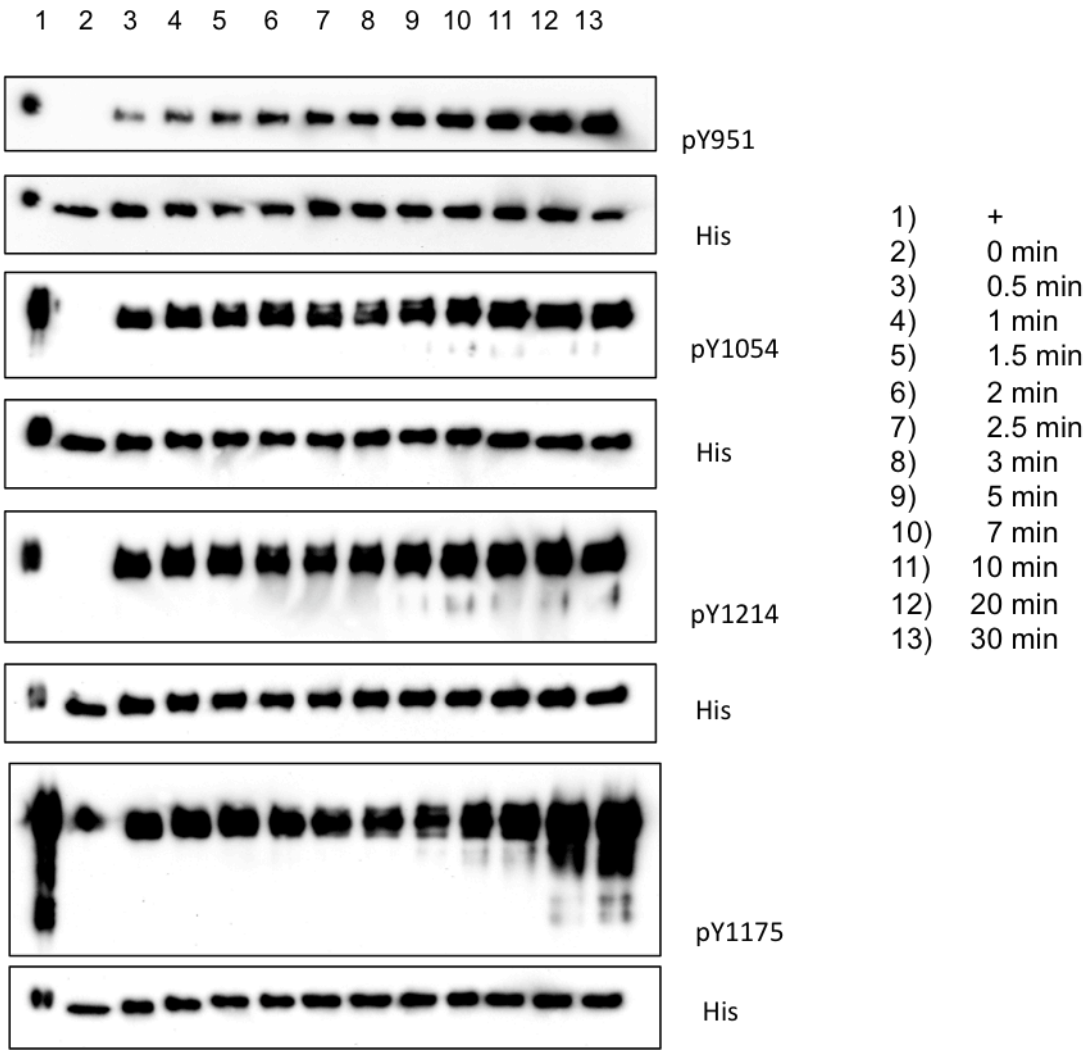

B

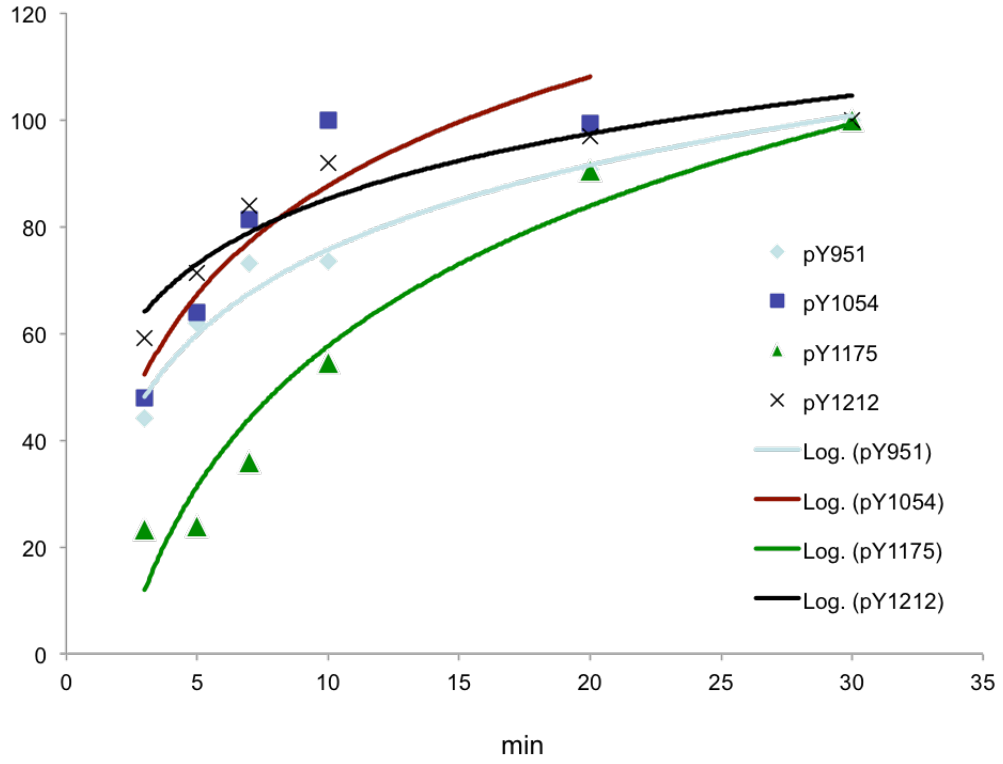

Figure 31: Phosphorylation kinetics of VEGFR-2 KD
(A) The phosphorylation-reaction was stopped at several time points. Samples were analysed by immunoblotting using phospho-specific antibodies described in section 6.2. (B) Quantification of relative phosphorylation intensities over time with highest intensity of each site set to 100% (saturation).

7.4.4. Solution structural analysis of VEGFR-2 kinase domain proteins by Small Angle X-ray Scattering (SAXS) and Multi Angle Light Scattering (MALS)

SAXS is used to retrieve shape and size information from macromolecules in solution. *Ab initio* modelling allows to model low-resolution structures of proteins. From a SAXS experiment it is possible to determine the maximum intramolecular distance of a particle (Dmax), the radius of gyration (Rg) that is defined as the root-mean-squared distance of all elemental scattering volumes from their centre of mass weighted by their scattering densities, the hydrated particle volume or the Mr of a protein. The p(r) function (distance-distribution function) can be calculated by Fourier-transformation from the scattering intensities of the SAXS experiments. It is known from other receptor tyrosine kinases that subdomains like the JMD or the C-terminus tightly regulate the catalytic kinase domain. Our goal was to visualize the various

active and inactive conformations of the VEGFR-2 kinase domain induced by phosphorylation / dephosphorylation or deletion of subdomains. We performed SAXS analysis of the previously biophysically characterized constructs mKID VEGFR-2 KD, K868M VEGFR-2 KD, ΔKID VEGFR-2 and ΔJMDΔKIDΔC KD VEGFR-2 as a control for the published crystal structure. All proteins were measured at various concentrations. mKID VEGFR-2 KD, K868M VEGFR-2 KD and ΔKID VEGFR-2 KD showed a flat intensity curve whereas ΔJMDΔKIDΔC VEGFR-2 KD showed more features. The Guinier-approximation yielded comparable Rg values for the various concentrations measured. Aggregation was visible for ΔKID VEGFR-2 KD at concentration 5 and 1 mg/mL ΔJMDΔKIDΔC VEGFR-2 KD showed signs of aggregation at concentration 1.01 and 5.01 mg/mL. These Rg values were not used for calculation of final Rgs (table 13). The Kratky plots confirmed a general globular fold. The p(r) functions of mKID VEGFR-2 KD, K868M VEGFR-2 KD and ΔKID VEGFR-2 KD had a defined maximum and a tail indicating that the proteins were of elongated shape. ΔJMDΔKIDΔC VEGFR-2 KD showed a p(r) function with defined maximum but no elongated tail, just a small bulge at Dmax that is probably an artefact of the collected data (figure 32A). Nevertheless the p(r) function indicates a globular protein as expected from the corresponding crystal structure of the protein. All Dmax values are summarized in (table 13). The result of the *Ab initio* modelling of mKID VEGFR-2 KD in the fully phosphorylated state was an elongated shape with a Dmax of 167 Å. At one end the SAXS envelope shows a bigger volume that is narrowing down to the other end. *Ab initio* modelling of K868M VEGFR-2 KD yielded a very similar model with a more compact “head”-part and the same elongated “tail”-domain seen in the mKID VEGFR-2 KD model. The bigger volume of the “head”-part in the K868M VEGFR-2 KD model presumably results from partial phosphorylation of the protein. The activation loop adopts an inactive conformation inside the cleft between the N- and the C-lobe of the kinase domain (no phosphorylation at Y1054/59) and the JMD is probably folded back onto the kinase domain as shown before for inactive kinases of the same family (Griffith *et al.*, 2004;Mol *et al.*, 2004;Mol *et al.*, 2003;Schubert *et al.*, 2006). The model of ΔKID VEGFR-2 KD in the fully phosphorylated state showed a similar picture with a smaller Dmax of 124 Å and less volume in the “head”-domain presumably due to the lack of the KID (figure 32B). Superimposition of the crystal structure of VEGFR-2 catalytic domain (1VR2) with the SAXS envelopes resulted in a good fit with the bigger “head”-part of the particles

mKID VEGFR-2 KD, K868M VEGFR-2 KD and ΔKID VEGFR-2. However, the crystal structure represents only a part of the catalytic core of the kinase domain where the JMD, the KID and the C-terminus are missing. Furthermore flexible loops like parts of the activation loop or the JMD are not visible and SAXS models show therefore a bigger volume. In addition, proteins in solution contain a hydration shell that expands the volume of the SAXS envelopes. The overlay of the crystal structures with the SAXS models (ΔJMDΔKIDΔC VEGFR-2 KD) by SITUS yielded several plausible conformations (one representative superimposition is shown in figure 32C). In order to fit the experimental SAXS data of ΔJMDΔKIDΔC VEGFR-2 KD with the calculated solution scattering profile of the crystal structure of VEGFR-2 (1VR2) we used CRYSOL. The fit was good with a Chi value of 0.483 (figure 32D).

Structure of VEGFR-2 KD in fully phosphorylated state

A

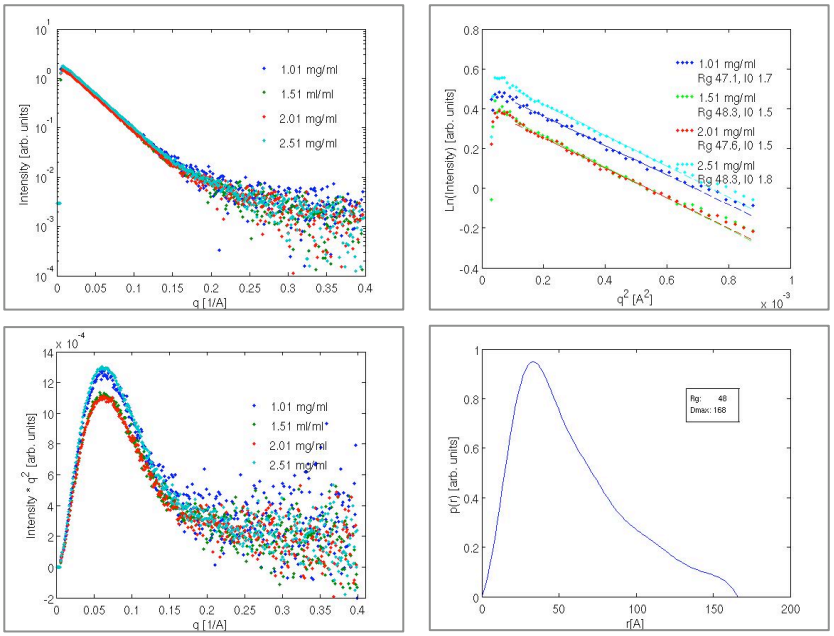

B

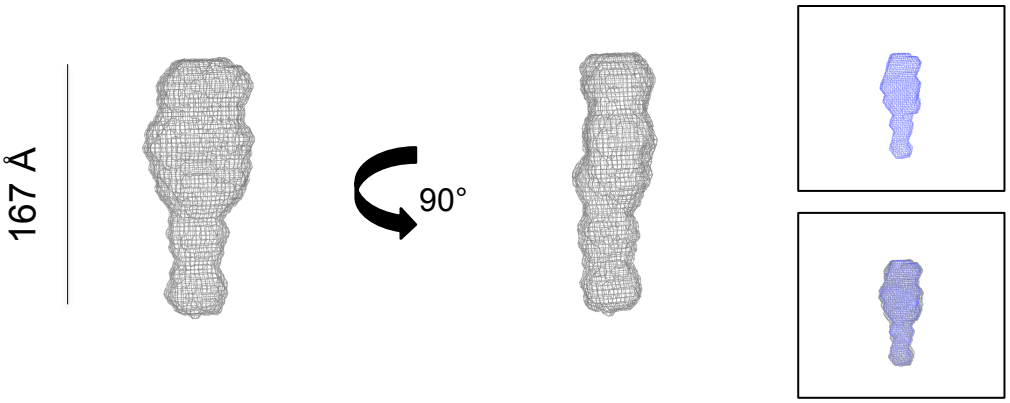

C

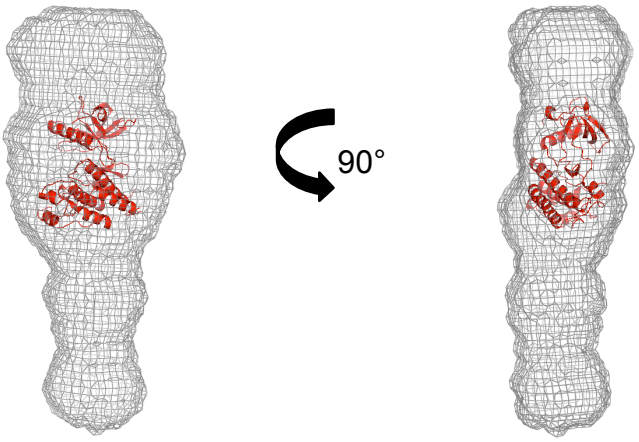

Structure of K868M VEGFR-2 KD in partially phosphorylated state

A

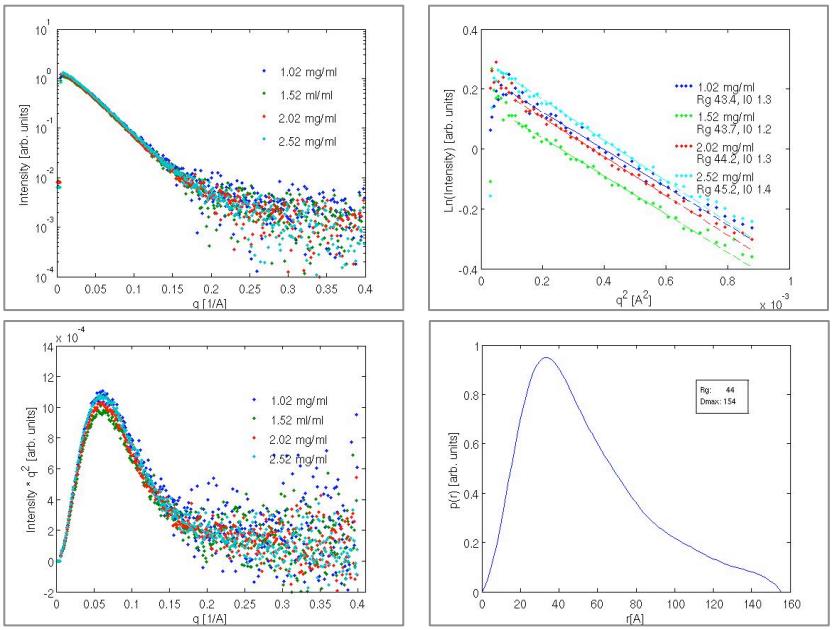

B

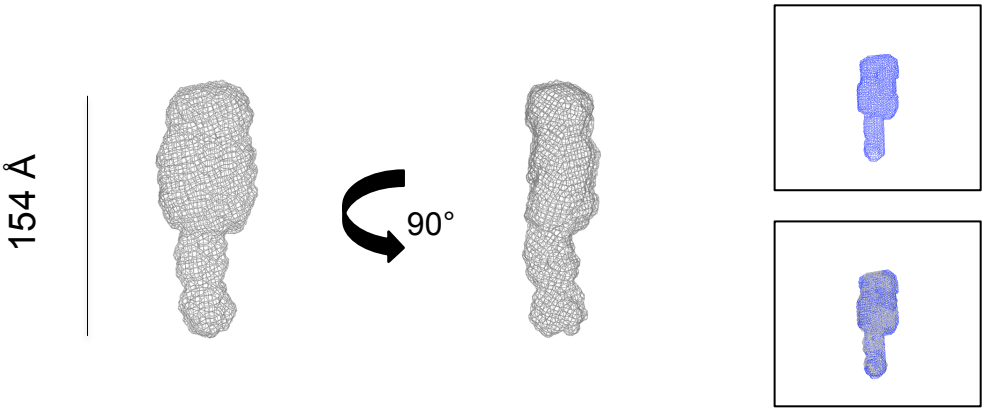

C

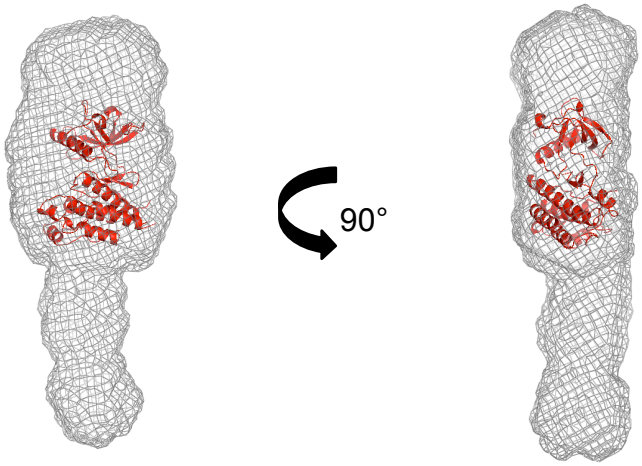

Structure of the phosphorylated VEGFR-2 KD lacking the KID

A

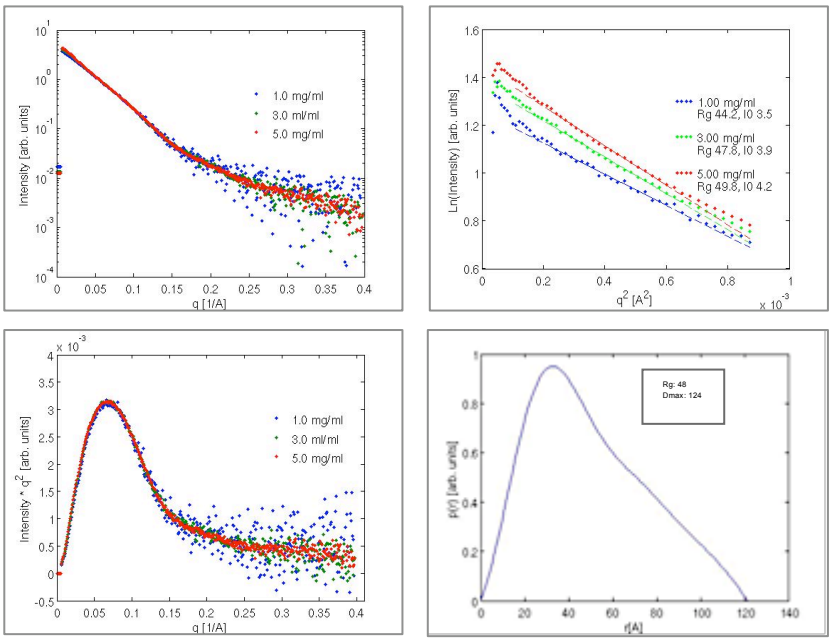

B

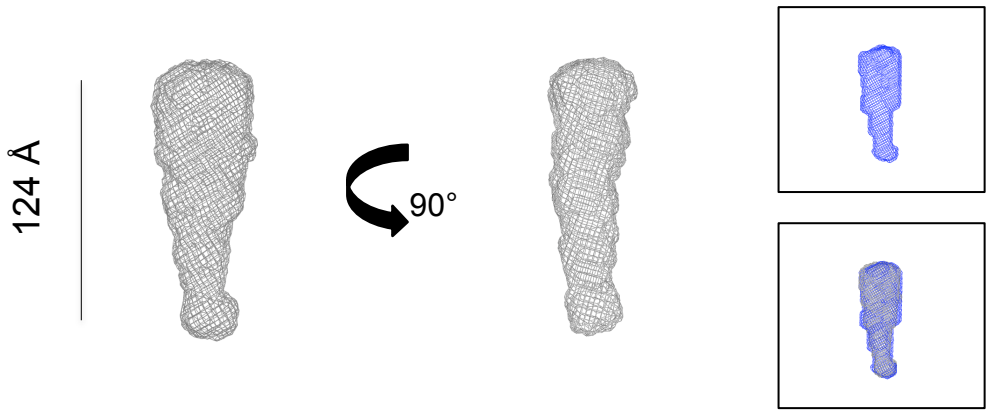

C

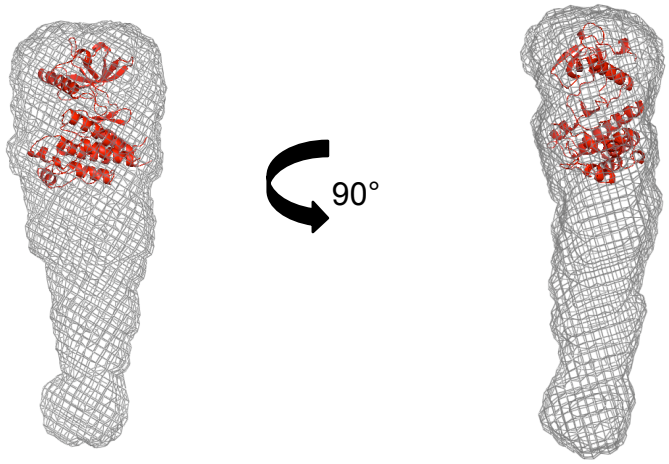

Structure of VEGFR-2 KD lacking the JMD, KID and the CD in fully phosphorylated state

A

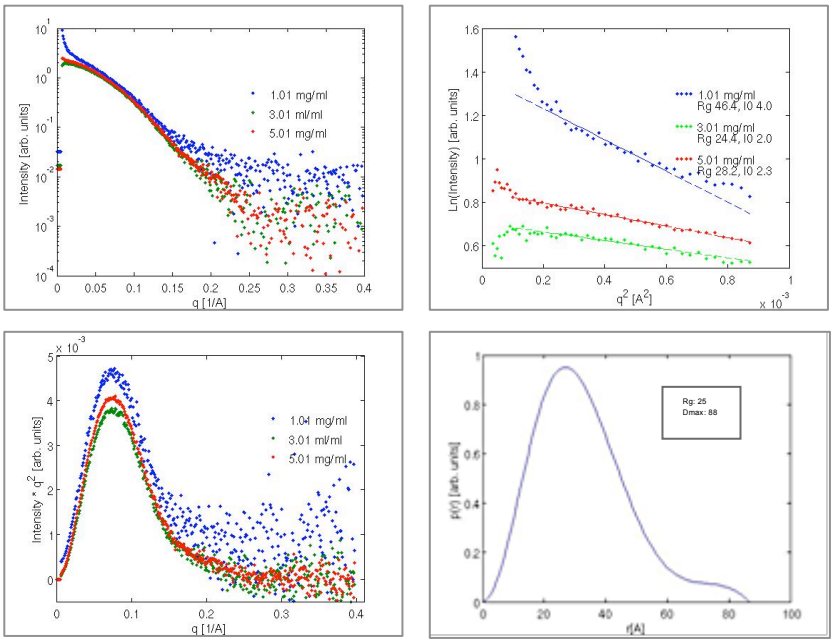

B

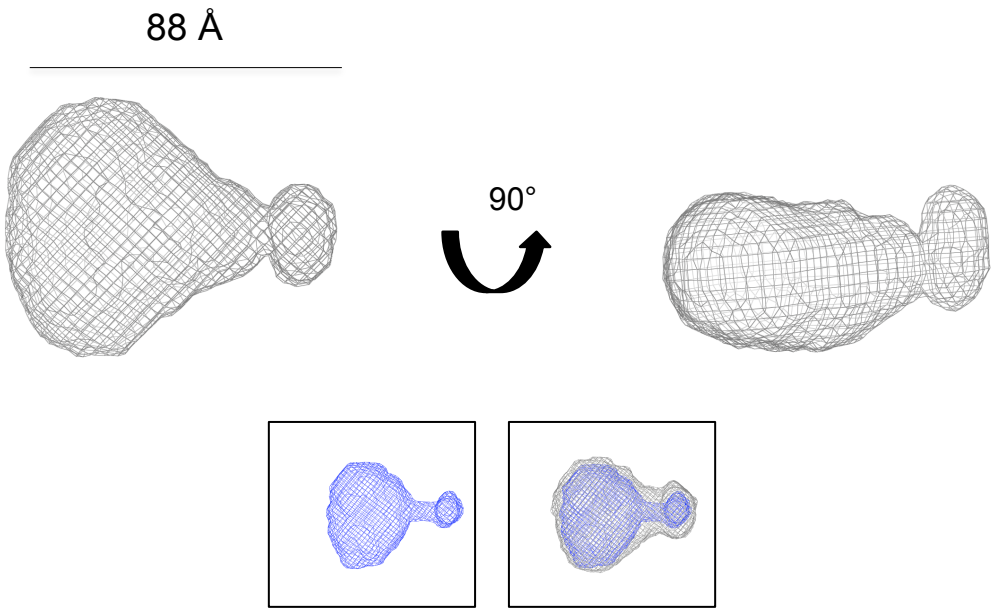
88 Å
90°

C

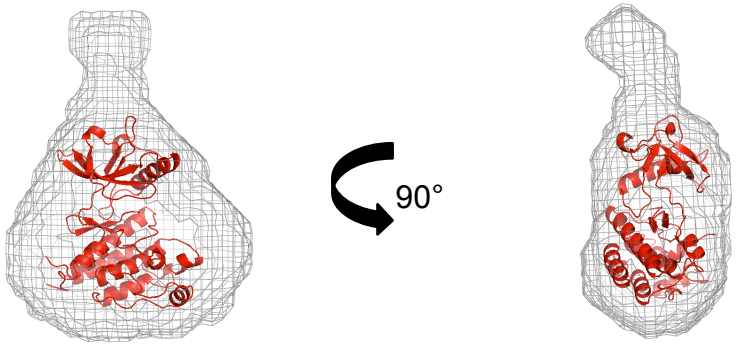
90°

D

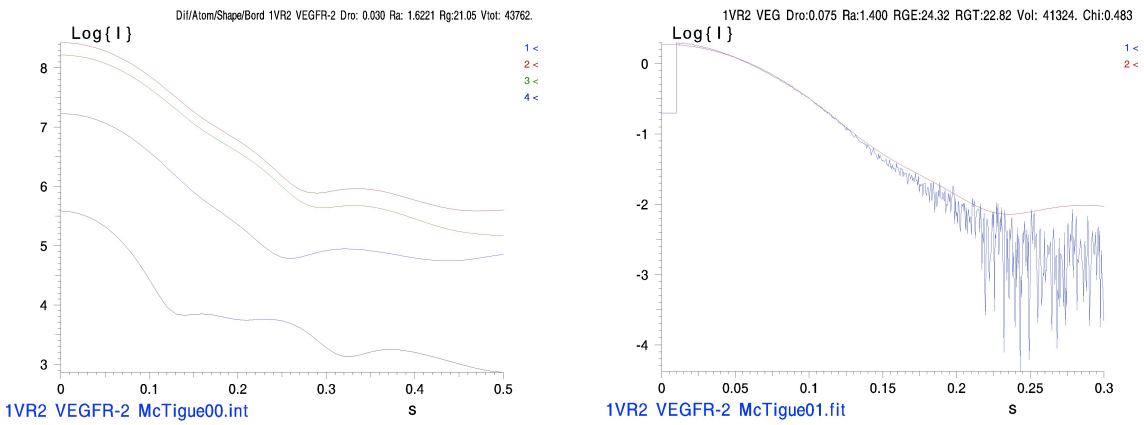
Dif/Atom/Shape/Bord 1VR2 VEGFR-2 Dro: 0.030 Ra: 1.6221 Rg:21.05 Vtot: 43762.
Log{I}
1 <
2 <
3 <
4 <
8
7
6
5
4
3
0
0.1
0.2
0.3
0.4
0.5
s
1VR2 VEGFR-2 McTigue00.int
1VR2 VEG Dro:0.075 Ra:1.400 RGE:24.32 RGT:22.82 Vol: 41324. Chi:0.483
Log{I}
1 <
2 <
0
-1
-2
-3
-4
0
0.05
0.1
0.15
0.2
0.25
0.3
s
1VR2 VEGFR-2 McTigue01.fit

Figure 32: SAXS results of VEGFR-2 kinase domain constructs
(A) Shown for all measured concentrations are: The intensity plotted as a function of s, linear Guinier region with calculated Rg-values, The Kratky-plot and the p(r)-function as calculated from AUTOGNOM for the experiment used for *ab initio* modelling. (B) The averaged *ab initio* model (grey). The most typical particle (blue, small box). (C) SITUS superimposition of the *ab initio* model with the crystal structure of the truncated VEGFR-2 catalytic domain (PDB: 1VR2). For VEGFR-2 ΔJMDΔKIDΔC KD: (D) CRYSOL evaluation of the solution scattering from the crystal structure of the VEGFR-2 catalytic domain (PDB: 1VR2) and the fitting with the experimental SAXS data. 1) Experimental scattering vector. 2) Theoretical intensity in solution 3) theoretical intensity *in-vacuo* 4) Solvent scattering. Figures by Sandro Manni and Kaisa Kisko using PyMOL.

The overlay of the *ab initio* models, the scattering profiles and the p(r) functions of VEGFR-2 KD, K868M VEGFR-2 KD and ΔKID VEGFR-2 are visualized in figure 33. Differences in intensities and the p(r) functions clearly indicate differences in shape.

A

Construct	Concentrations [mg/mL]	Rg [Å] (Guinier-region) ± S.E.	Dmax ± S.E. [Å]
mKID VEGFR-2 KD	1, 1.5, 2	47.9 ± 0.4	167.5 ± 1.5
K868M VEGFR-2 KD	1.5, 2.5	44 ± 0.6	153.9 ± 2.2
ΔKID VEGFR-2 KD	1.5, 2.5	48.1 ± 2.4	123.8 ± 8.1
ΔJMDΔKID ΔC VEGFR-2 KD	3, 5	25.2 ± 0.6	88.3 ± 2.2

Table 13: Summary of SAXS experimental parameters determined by SAXS
Rg and Dmax values were determined as mean ± S.E. for at least two concentrations.

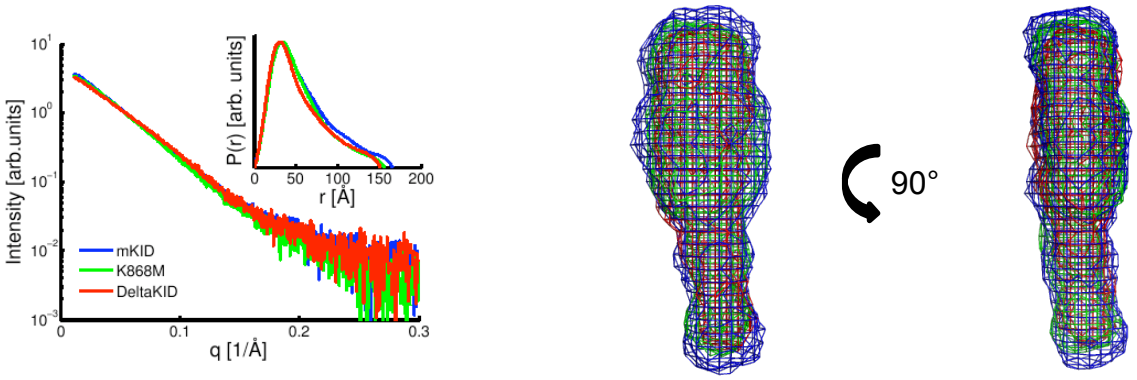

Figure 33: Overlay of scattering-intensity plots, p(r)-functions and *ab initio* models of mKID VEGFR-2 KD, K868M VEGFR-2 KD and ΔKID VEGFR-2 KD
Blue: mKID VEGR-2 KD. *Green:* K868M VEGFR-2 KD. *Red:* ΔKID VEGFR-2 KD. Figures by Sandro Manni and Kaisa Kisko.

At the conclusion of this thesis we had not yet collected a high quality SAXS-dataset of the dephosphorylated (inactive) KD of VEGFR-2. We were therefore not able to generate an *ab initio* structural model. Nevertheless, we monitored conformational changes between the active (phosphorylated) and the inactive (dephosphorylated) KD of VEGFR-2 by MALS. As mentioned above it is possible to derive shape information from MALS data. The information can be derived from the elution volume of the coupled SEC column. The elution volumes of the measured proteins may slightly vary from those of previous runs (section 7.5) since we performed these experiments with a new SEC column and different analytical SEC columns from the same type show slightly different features. Comparison of experimental MALS data was always performed with data of samples obtained from the same column. To directly compare the active with the inactive KD we overlaid the elution profiles of the separately analysed samples (figure 34A). The theoretical Mr of the sample proteins could be verified with a small percentage error (table 14). All proteins were monomeric and showed a homogeneous mass distribution (concentrations of 2 mg/mL). The previously observed shift of the SEC elution peak in SEC purification and MALS experiments of VEGFR-2 KD and K868M VEGFR-2 KD was indeed confirmed in these experiments. Furthermore, the elution peak of the dephosphorylated VEGFR-2 KD was shifted towards a higher volume: VEGFR-2 KD: 13.3 mL < K868M VEGFR-2 KD: 13.41 mL < dephos VEGFR-2 KD: 13.57 mL. The shift clearly arises from the changes in the hydrodynamic properties of the protein

indicating an altered molecular shape. Taken together the dephosphorylated inactive VEGFR-2 KD adopts a more compact conformation than VEGFR-2 KD and K868M VEGFR-2 KD which are partially phosphorylated after purification from cell lysates.

A **B**

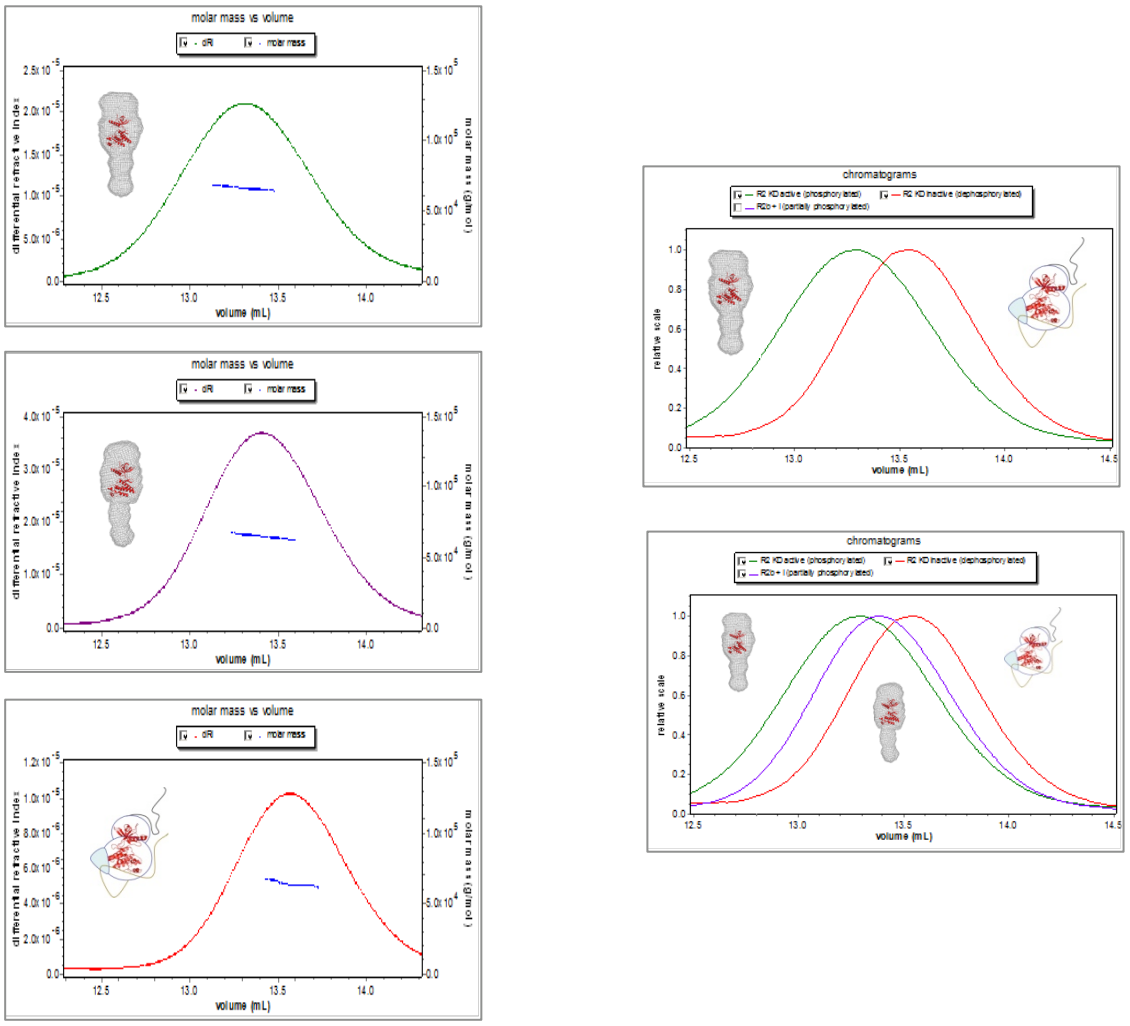

Figure 34: MALS analysis of VEGFR-2 kinase domain constructs
(A) MALS analysis of VEGFR-2 KD (top), K868M VEGFR-2 KD (middle) and dephosphorylated VEGFR-2 KD. Molecular envelope derived from SAXS data is indicated in the corresponding graph. (B) Overlay of MALS data for VEGFR-2 KD with K868M VEGFR-2 KD (top) and VEGFR-2 KD, K868M VEGFR-2 KD and dephosphorylated VEGFR-2 KD (bottom). Molecular envelope is indicated in the graph. Dephosphorylated VEGFR-2 KD envelope is shown as a representative illustration with the crystal structure of VEGFR-2 (1VR2) as the catalytic core of the KD. The CD is depicted as a schematic loop colored in khaki. The JMD is depicted as a schematic black loop.

VEGFR-2 KD constructs	Theoretical Mr [kDa]	Experimental Mr [kDa]
VEGFR-2 KD	65.9	66.4 (0.1%)
VEGFR-2 KD + I	65.9	65.5
VEGFR-2 KD dephos	65.9	63.9 (0.1%)

Table 14: Comparison of theoretical and experimentally determined Mr of VEGFR-2 kinase domain proteins in different phosphorylation states. VEGFR-2 KD: fully phosphorylated, VEGFR-2 KD + I: phosphorylated CD, VEGFR-2 dephos: fully dephosphorylated protein.

7.5. Expression, purification and biophysical characterization of TSAd and of a TSAd-VEGFR-2 KD complex

The adapter protein TSAd initially identified in immune cells was found to interact with VEGFR-2 Y951 via its central SH2-domain. In order to perform biophysical studies with TSAd and with a complex between TSAd and the kinase domain of VEGFR-2 we cloned the murine version of TSAd (366 AA) into one of the two multiple cloning sites of the Multibac vector pFL. The constructs carried a C-terminal 10xHis-tag with a preceding TEV protease cleavage site for tag-removal. Recombinant protein was expressed in baculovirus infected Sf21 insect cells. The infected cells were harvested 72-96 h post infection. Expression of the recombinant protein was verified by immunoblotting using a 5xHis-tag specific antibody. A protein with a Mr of 42 kDa was detected (figure 35). Varying the virus inoculum did not change the expression level. TSAd was also detected in the culture supernatant due to baculovirus induced leakage of insect cells.

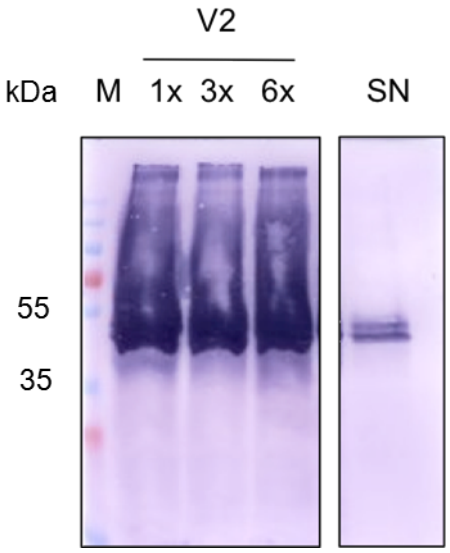

Figure 35: Expression of TSAd in Sf21 insect cells
Sf21 insect cells were infected with various amounts of TSAd baculovirus. (1x-6x). The recombinant protein was detected by immunoblotting using an antibody against the His-tag. SN: Supernatant.

To optimize the solubility of TSAd for further purification we performed a solubility screening by lysing the cells with lysis buffers in the pH range of 6-9. Earlier attempts to purify TSAd with a theoretical Pi of 7.34 at pH of 6 did not succeed. Best solubility of TSAd was achieved in Tris buffer of pH 8-8.5 (figure 36). Hence, all following purification steps were conducted at pH 8.3.

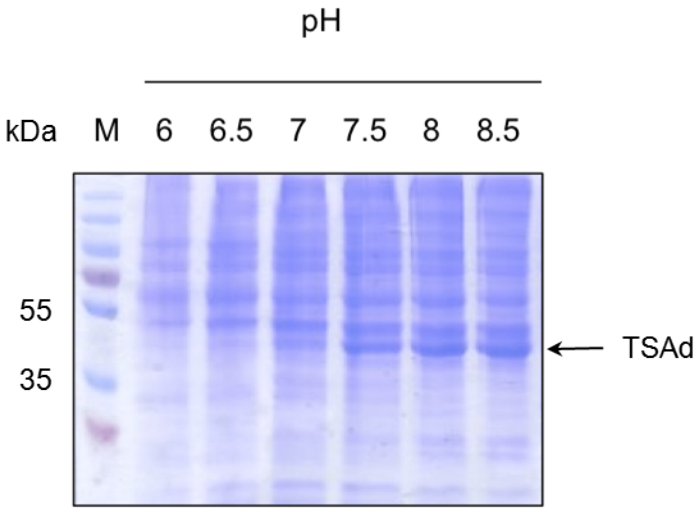

Figure 36: Solubility of TSAd in the pH range of 6-8.5
TSAd could be solubilised with Tris buffer at pH 8-8.5.

The complex of TSAd with the KD of VEGFR-2 was evaluated by co-infecting Sf21 insect cells with baculoviruses of both constructs. TSAd and the TSAd-VEGFR-2 KD complex were purified by IMAC with increasing imidazole concentration to remove most of the impurities. After IMAC the purified complex was *in vitro* phosphorylated to achieve a homogenously phosphorylated protein population and to increase binding of TSAd to pY951 of the VEGFR-2 KD. In a second step we purified the proteins via SEC (figure 37). SEC purification yielded a protein purity of 95% as judged from SDS-PAGE. The protein yield ranged from 0.5-1.5 mg per litre of cultured cells for TSAd and the complex. The SEC fractions of the purified complex contained equal amounts of TSAd and VEGFR-2 KD along the entire elution peak indicating efficient complex formation.

A

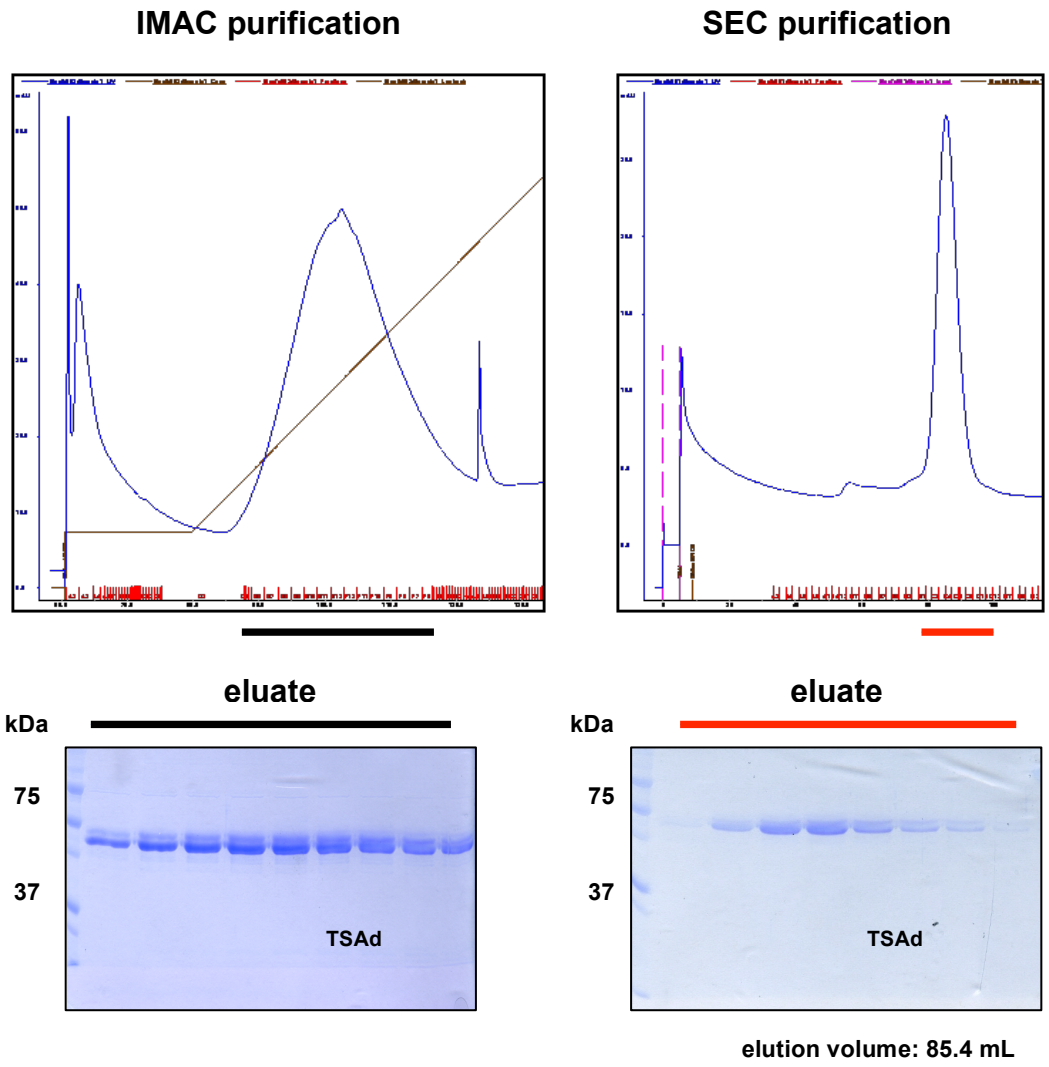

B

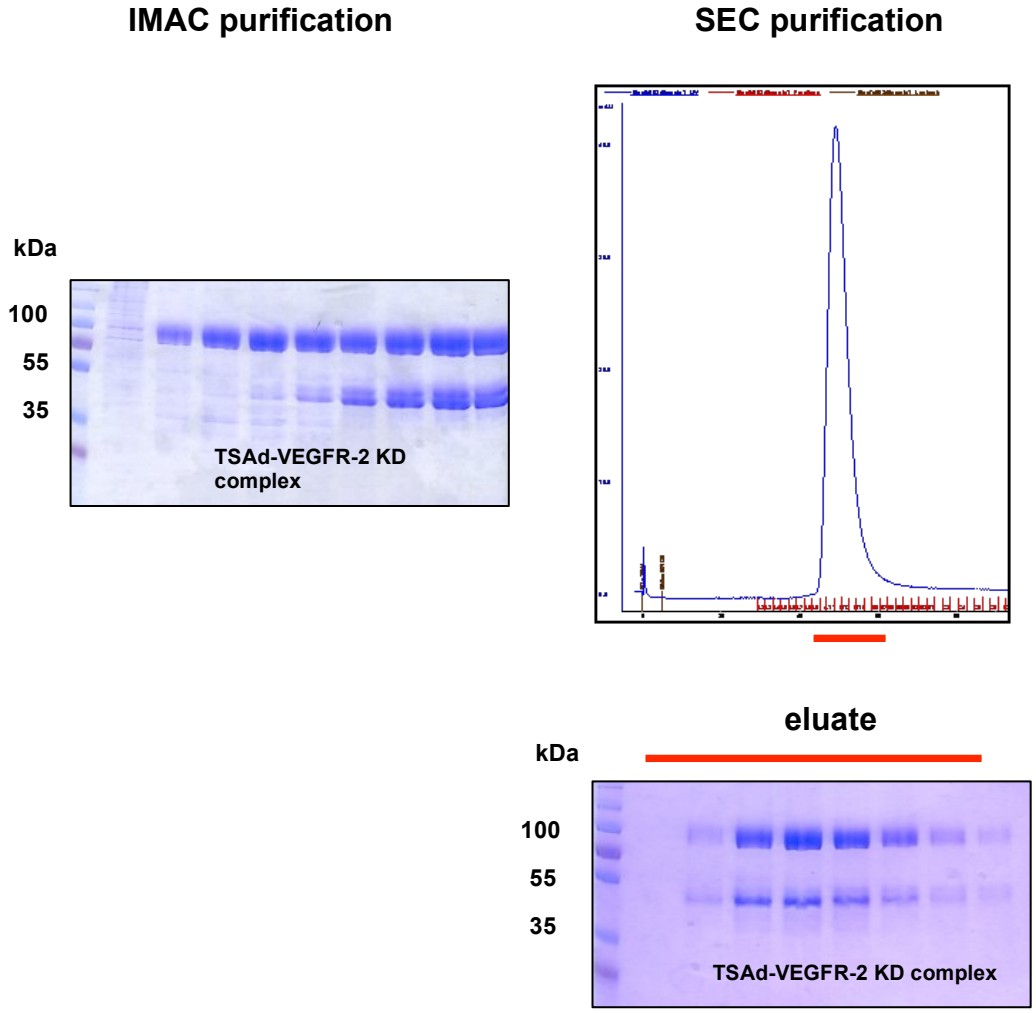

Figure 37: Purification of TSAd and TSAd-VEGFR-2 KD complex
(A) IMAC and SEC purification of TSAd and (B) TSAd-VEGFR-2 KD complex.

7.5.1. SEC analysis of TSAd-VEGFR-2 KD complex

SEC separates proteins on the basis of mass and shape. A gel filtration column that was calibrated with globular proteins was used to determine the mass of a standard globular protein based on the elution volume. A nonglobular protein with identical Mr will elute differently since it has different hydrodynamic radius. We used a calibrated Superdex S-200 16/60 column to monitor TSAd binding to the VEGFR-2 kinase domain. TSAd and TSAd-VEGFR-2 KD complex were purified by IMAC as shown above (figure 38A). IMAC fractions of TSAd and TSAd-VEGFR-2 KD complex were pooled at a ratio of 1:1 and loaded on the gel filtration column (figure 38B). As a result we detected an excess of TSAd on the column. The following elution peaks

were identified: TSAd-VEGFR-2 KD complex at 71.72 mL and TSAd eluted at 83.54 mL. VEGFR-2 KD eluted at 73.86 mL as shown in section 7.4. All protein species eluted with a well-defined retention time. The complex peak was obviously shifted to the left (elution of heavier protein species) compared to the elution peak of VEGFR-2 KD. It was not possible to determine the appropriate Mr of VEGFR-2 KD and therefore the Mr of TSAd-VEGFR-2 complex since VEGFR-2 KD is elongated in the fully phosphorylated state (see *ab initio* models of previous SAXS experiments).

A

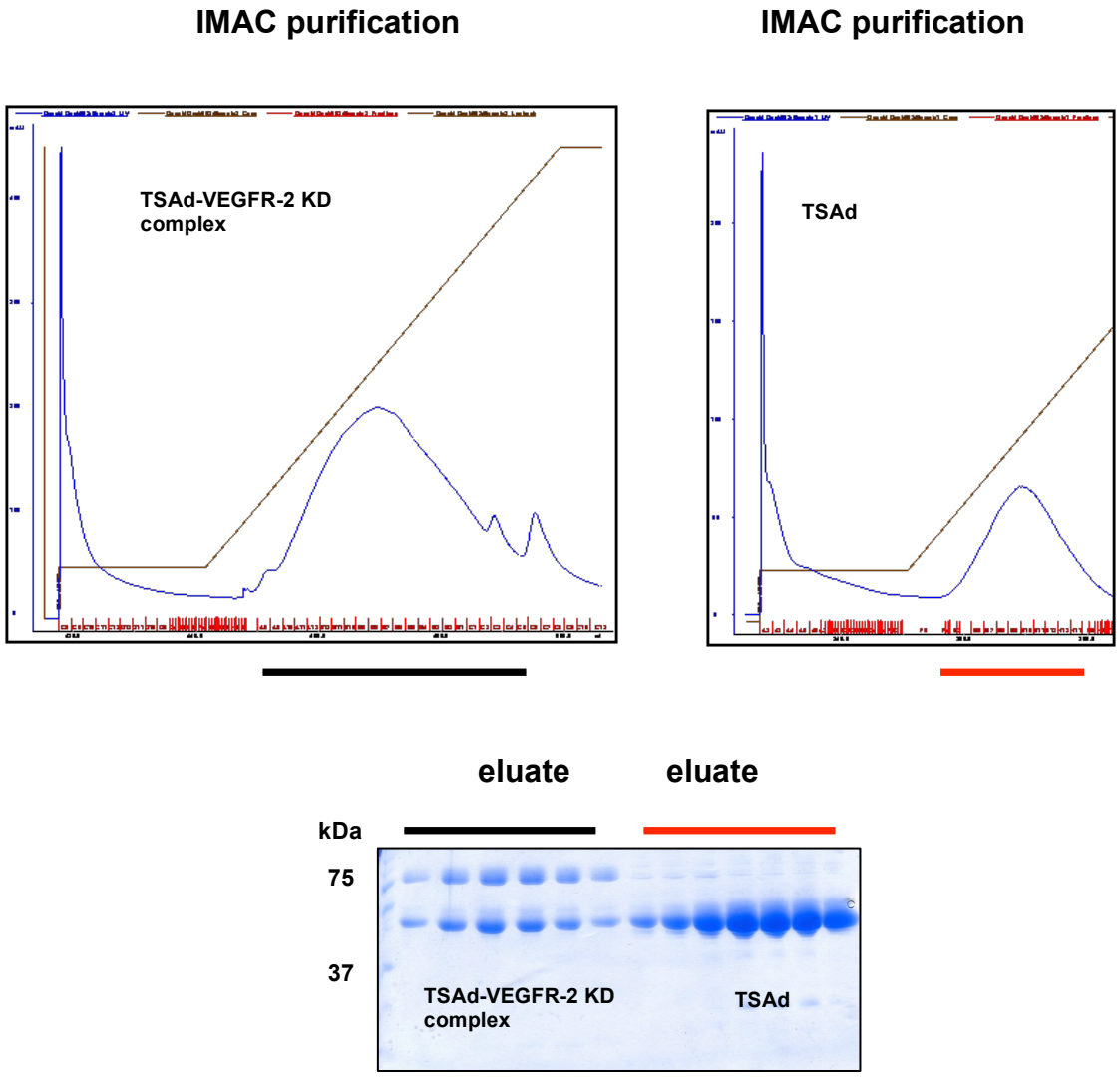

B

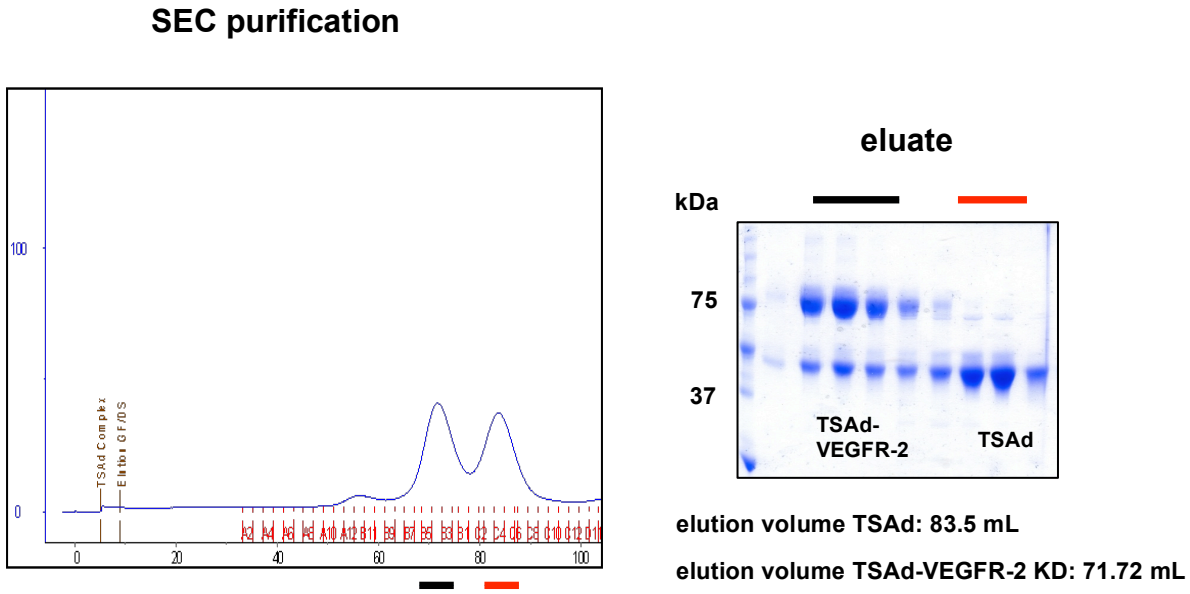

C

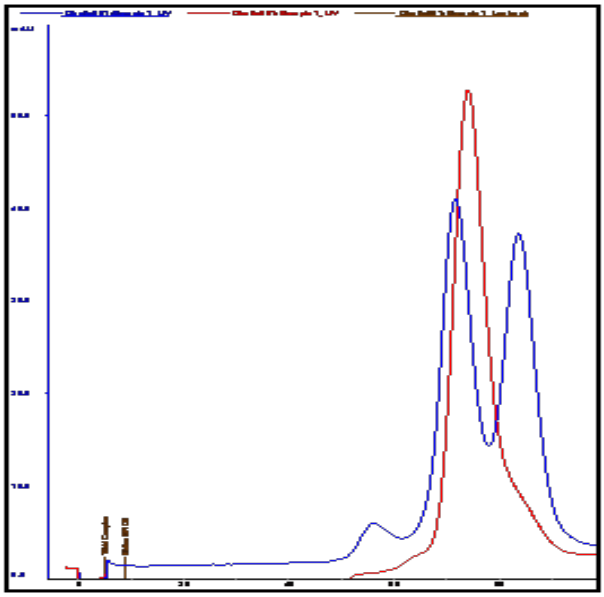

Figure 38: Analysis of TSAd-VEGFR-2 KD complexes
(A) IMAC purification of TSAd and TSAd-VEGFR-2 KD complex. (B) SEC purification of pooled IMAC factions. (C) Overlay of SEC purifications of TSAd, TSAd-VEGFR-2 KD complex (blue) and VEGFR-2 KD (red).

7.5.2. Mass spectrometry of TSAd

In order to confirm protein identity and to verify the expression of the full-length protein we sent a protein sample to the Functional Genomics Center Zürich. The sample was proteolytically digested and the peptides were analysed via LC/ESI/MS/MS. The peptide sequences were used for a database search with the Mascot search program. The most significant hits are marked in yellow (figure 39A). TSAd was identified with good sequence coverage. In the course of TSAd purification we always co-purified an unknown protein with the Mr of 70kDa. We were able to identify the unknown protein as heat shock protein 70 (figure 32B). Hsc70 proteins (in eukaryotes) are ubiquitously expressed proteins that are important for proper protein folding and are upregulated upon cellular stress. Hsc70 recognizes hydrophobic residues on the surface of partially denatured proteins or during release from ribosomes. Interaction with the nascent not yet folded peptide chain prevents aggregation of newly synthesized proteins. Although we obtained reasonable amounts of TSAd protein, production seems to be a challenge for the expressing organism. We further noticed a remarkable loss of protein between IMAC and SEC purification steps that may result from instability of the protein.

A

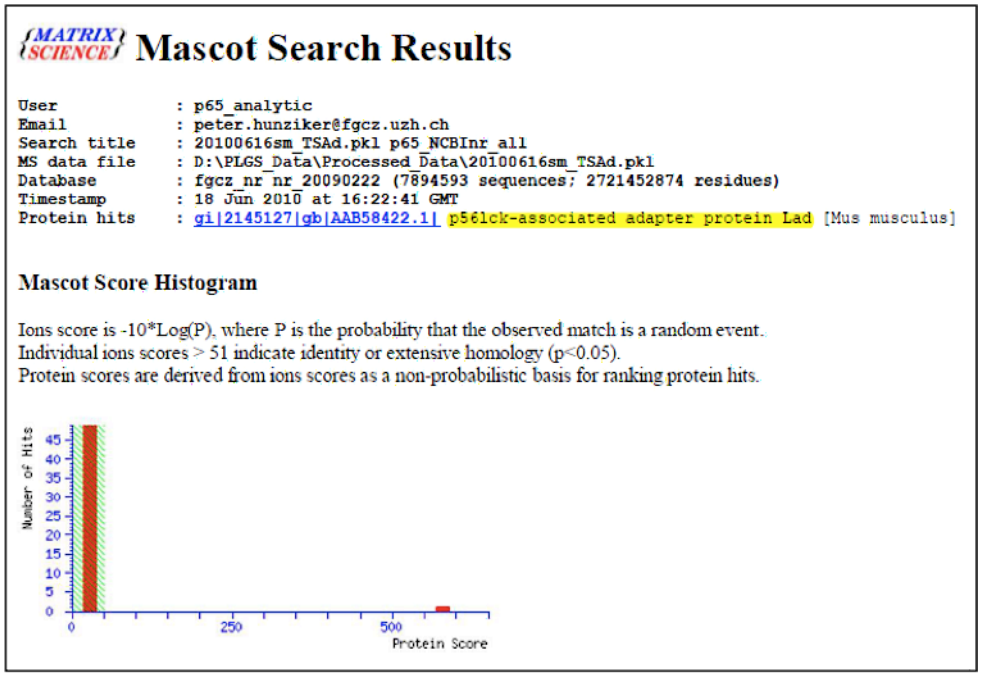

MATRIX SCIENCE **Mascot Search Results**

User : p65_analytic
Email : peter.hunziker@fgcz.uzh.ch
Search title : 20100616sm_TSAd.pkl p65_NCBInr_all
MS data file : D:\PLGS_Data\Processed_Data\20100616sm_TSAd.pkl
Database : fgcz_nr nr_20090222 (7894593 sequences; 2721452874 residues)
Timestamp : 18 Jun 2010 at 16:22:41 GMT
Protein hits : gi|2145127|gb|AAB58422.1| p56lck-associated adapter protein Lad [Mus musculus]

Mascot Score Histogram

Ions score is -10*Log(P), where P is the probability that the observed match is a random event.
Individual ions scores > 51 indicate identity or extensive homology (p<0.05).
Protein scores are derived from ions scores as a non-probabilistic basis for ranking protein hits.

B

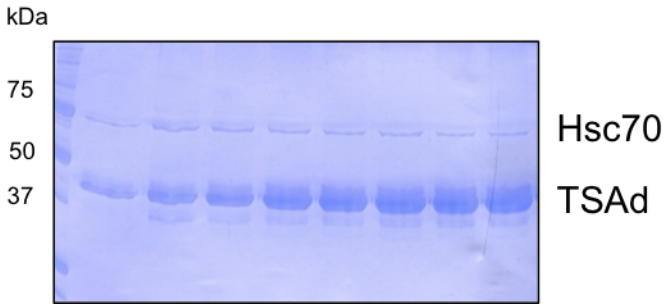

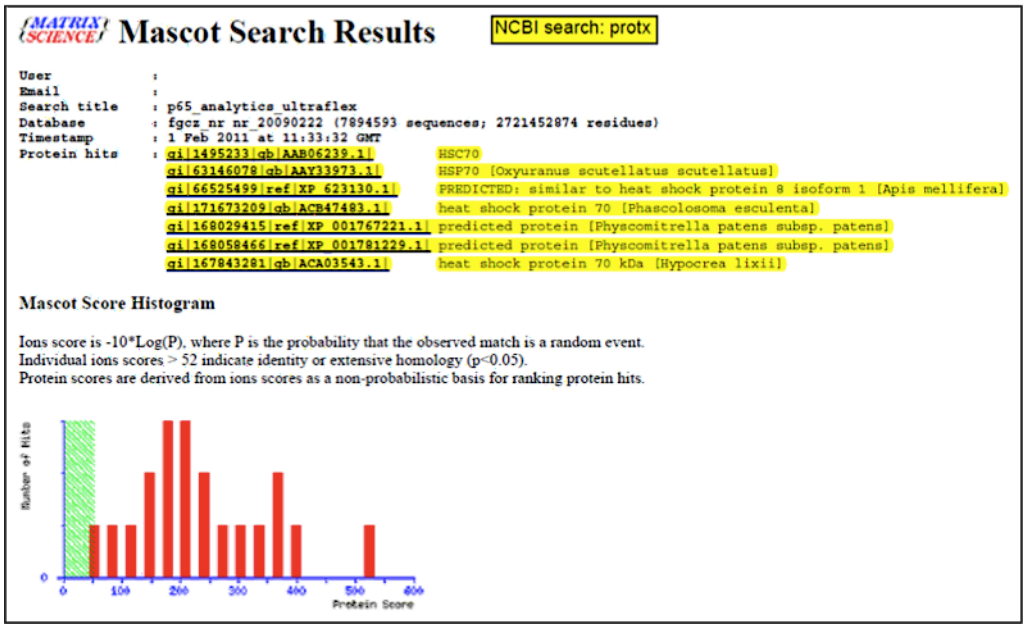

MATRIX SCIENCE **Mascot Search Results** NCBI search: protx

User :
Email :
Search title : p65_analytics_ultraflex
Database : fgcz_nr nr_20090222 (7894593 sequences; 2721452874 residues)
Timestamp : 1 Feb 2011 at 11:33:32 GMT
Protein hits :

gi|1495233|gb|AAB06239.1|	HSC70
gi|63146078|gb|AAY33973.1|	HSP70 [Oxyuranus scutellatus scutellatus]
gi|66525499|ref|XP_623130.1|	PREDICTED: similar to heat shock protein 8 isoform 1 [Apis mellifera]
gi|171673209|gb|ACB47483.1|	heat shock protein 70 [Phascolosoma esculenta]
gi|168029415|ref|XP_001767221.1|	predicted protein [Physcomitrella patens subsp. patens]
gi|168058466|ref|XP_001781229.1|	predicted protein [Physcomitrella patens subsp. patens]
gi|167843281|gb|ACA03543.1|	heat shock protein 70 kDa [Hypocrea lixii]

Mascot Score Histogram

Ions score is -10*Log(P), where P is the probability that the observed match is a random event.
Individual ions scores > 52 indicate identity or extensive homology (p<0.05).
Protein scores are derived from ions scores as a non-probabilistic basis for ranking protein hits.

Figure 39: Mass spectrometry of TSAd and a co-purified Hsc70 protein
A) Mascot search results for TSAd B) Coomassie gel showing TSAd (lower band) together with a co-purified 70 kDa protein (upper band). Lower panel: Mascot search results of 70 kDa protein.

7.5.3. Multi Angle Light Scattering (MALS) analysis of TSAd and a TSAd-VEGFR-2 KD complex

To confirm binding of TSAd to VEGFR-2 KD we performed a MALS analysis. TSAd, VEGFR-2 KD and VEGFR-2 K868M (as a negative control) KD were first analysed without their binding partner. The analysis of VEGFR-2 KD and VEGFR-2 K868M KD is shown in section 7.5 and 7.8. TSAd was injected at a concentration of 2 mg/mL. The TSAd peak was monodisperse and showed a homogeneous mass distribution corresponding to a monomer (figure 40A). The theoretical Mr of TSAd was verified with a small error (table 14). VEGFR-2 KD, VEGFR-2 K868M KD and TSAd eluted at distinct volumes. TSAd-VEGFR-2 KD and TSAd-K868M VEGFR-2 were purified from a co-infected culture as shown in section 7.9 The purified protein fractions were loaded on the SEC column coupled to the MALS instrument. TSAd-VEGFR-2 fractions gave rise to two peaks with Mr of 119 and 46.64 kDa corresponding to the theoretical Mr of the 1:1 TSAd-VEGFR-2 KD complex (108 kDa) and the theoretical Mr of excess monomeric TSAd (42.1 kDa). TSAd-K868M VEGFR-2 KD fractions resulted in two peaks with Mr of 72.65 and 49.9 kDa corresponding to the theoretical values of monomeric VEGFR-2 K868M KD and monomeric TSAd.

We conclude that VEGFR-2 KD (human KID) forms a complex with murine TSAD when Y951 is phosphorylated. The inactive VEGFR-2 K868M does not bind to murine TSAd due to the lack of phosphorylation at Y951 (figure 40B).

A

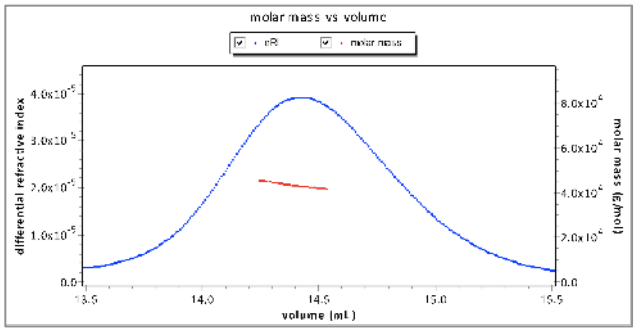

B

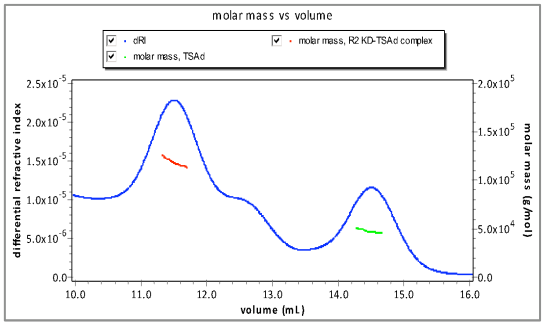

TSAd-VEGFR-2 complex

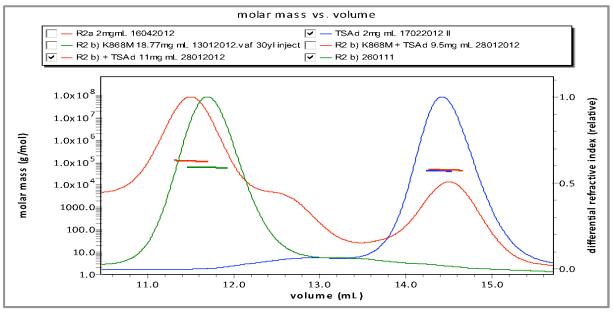

TSAd-VEGFR-2 KD, VEGFR-2 KD, TSAd

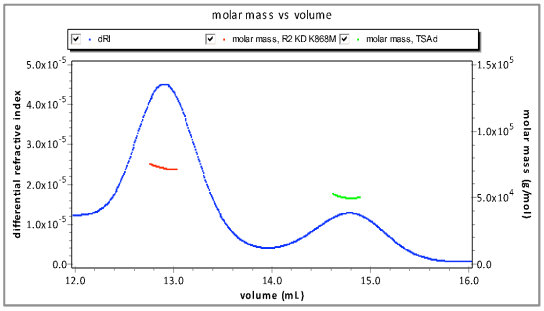

TSAd-K868M VEGFR-2 KD

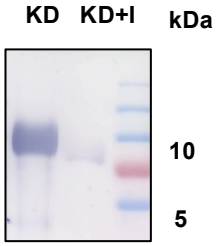

pY951

Figure 40: MALS analysis of TSAd and TSAd-VEGFR-2 KD complex
A) Analysis of TSAd. B) Analysis of TSAd-VEGFR-2 KD and TSAd-K868M VEGFR-2 KD (left panels). Overlay of TSAd-VEGFR-2 KD, VEGFR-2 KD and TSAd is shown in the top right panel. Y951 phosphorylation of VEGFR-2 KD and VEGFR-2 KD shown in a kinase-Inhibitor treated culture of VEGFR-2 KD, KD+I) is shown in the lower right panel.

Construct	**Theoretical Mr** [kDa]	**Experimental Mr** [kDa]
VEGFR-2 KD	65.9	61.62 (0.2%)
K868M VEGFR-2 KD	65.9	64.94 (0.5%)
TSAd	42.1	43.41 (0.3%)
TSAd-VEGFR-2 KD complex	108	119 (5%); 46.64 (14%)
TSAd-K868M VEGFR-2 KD	65.9; 42.1	72,65 (1%); 49.9 (4%)

Table 14: MALS analysis of TSAd and TSAd-VEGFR-2 KD complex
Comparison of theoretical and experimentally determined Mr of VEGFR-2 KD, K868M VEGFR-2 KD, TSAd and the complex of TSAd with VEGFR-2 KD via MALS.

In addition, we propose that the SH2-domain of murine TSAd also binds to VEGFR-2 KD *in vitro* when Y951 is phosphorylated while K868M VEGFR-2 KD does not bind to murine TSAd due to the lack of phosphorylation at Y951. The binding is mediated by the consensus recognition sequence of the SH2-domain of TSAd, which is different for murine and human Y951. The murine sequence differs in two amino acids: Y_{951}VGAI (human) vs. Y_{951}VGEL (murine). Yet both sequences are recognized by the TSAd SH2-domain.

7.5.4. Solution Structure of TSAd and TSAd-VEGFR-2KD complex determined by Small Angle X-ray Scattering (SAXS)

We performed a SAXS analysis of the biophysically characterized constructs TSAd and TSAd-VEGFR-2 KD complex (figure 41). Our goal was to characterize the interaction of the two binding partners and to obtain an overall structure. All proteins were measured at several concentrations. TSAd and TSAd-VEGFR-2 KD complex showed a flat intensity curve. The Guinier-approximation of TSAd showed comparable Rg values for the two concentrations measured. Two of the three measured concentrations (1 and 4.7 mg/mL) of TSAd-VEGFR-2 KD complex showed significant signs of aggregation. Further processing was therefore exclusively conducted with the 2 mg/mL protein sample. Kratky plots of TSAd and TSAd-VEGFR-2 KD complex confirmed a general globular fold. P(r) functions of TSAd and TSAd-VEGFR-2 KD had a defined maximum and a tail indicating that the proteins were elongated. All Rg and Dmax values are summarized in table 15. The *Ab initio* model of TSAd showed an elongated shape with a broad globular central domain and a Dmax of 137 Å. We superimposed the crystal structure of the SH2 domain of src (PDB: 1O4C) with the SAXS envelope of TSAd using SITUS software. The SH2-domain of src is homologous to the SH2-domain of TSAd (figure 41C). The crystal structure of the SH2-domain fitted well into the globular domain of the *ab initio* model of TSAd. The data is also in agreement with the predicted secondary structure of TSAd. *Ab initio* modelling of TSAD-VEGFR-2 KD complex resulted in an elongated protein with a Dmax of 202 Å. The quality of this sample was not satisfying and needs to be verified by additional measurements. Nevertheless it was possible to retrieve a model from the data measured at the concentration of 2 mg/mL. Alignment of TSAd and VEGFR-2 KD with the *ab initio* model of TSAd-VEGFR-2 KD complex

(figure 42) suggests a linear interaction of TSAd with the ”head” part of the kinase domain. The sum of the calculated volumina belonging to VEGFR-2 KD and TSAd corresponds to the total volume of the complex (table 15).

Structure of TSAd

A

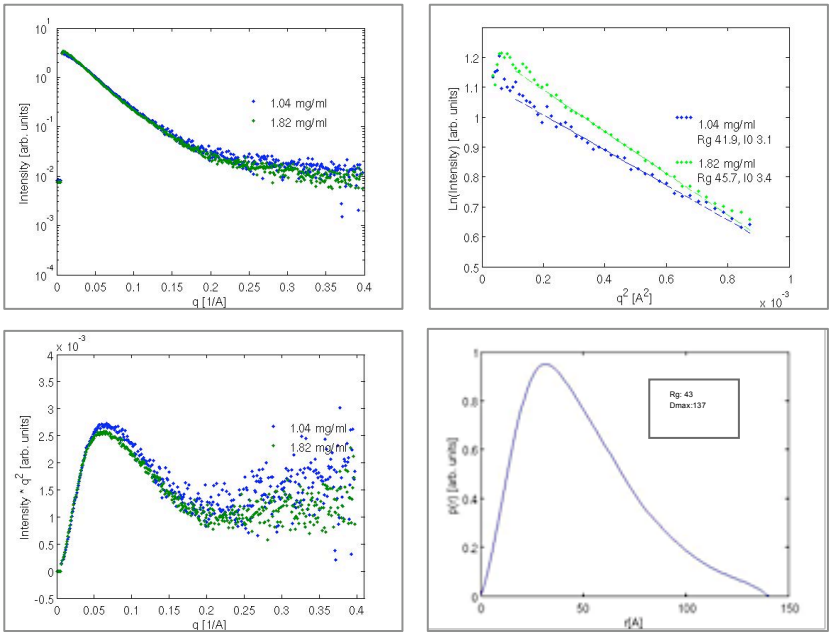

B

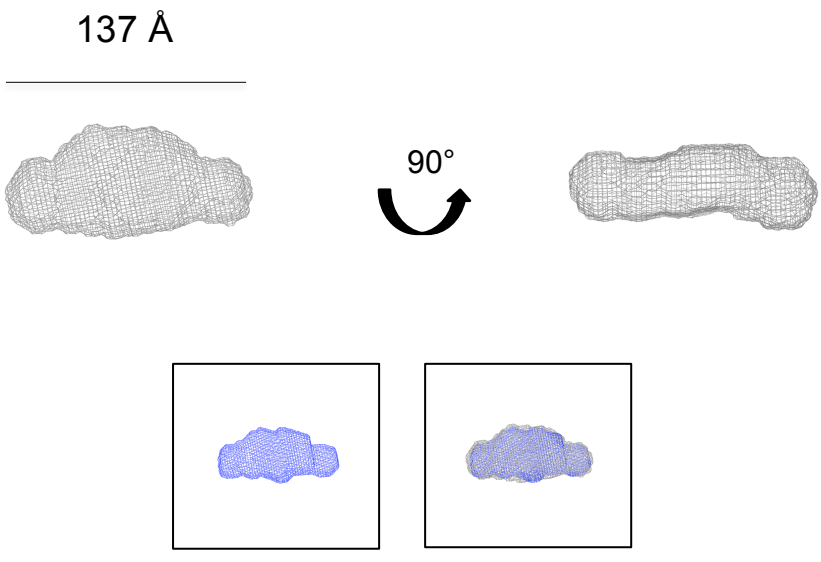

C

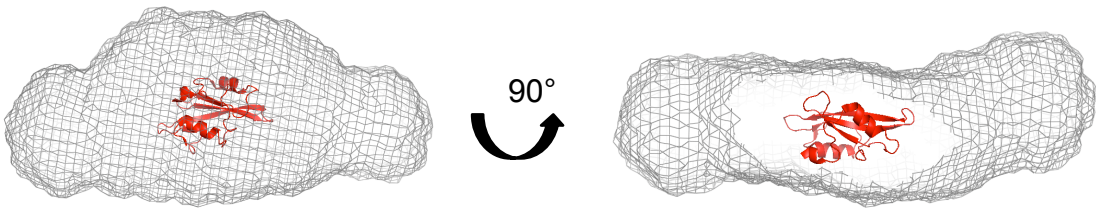


```
HUMAN: VRAP   95 WFHGFITRREAERL-LE---PK-PQ-GCYLVRFSESAV-TFVLT
HUMAN: PLC   646 WYYDSLSRGEAEDM-LM---RI-PRDGAFLIRKREGSD-SYAIT
DROME: CSW   111 WFHGNLSGKEAEKLILE---RG-KN-GSFLVRESQSKPGDFVLS
RAT:   LNK   119 WFHGPISRVRAAQL-VQLQGPD-AH-GVFLVRQSESRRGEYVLT
CHICK: SRC    82 WFHGKITREQAERL-LY---PP-ET-GLFLVRESTNYPGDYTLC


HUMAN: VRAP      YRSRTCCRHFLLAQLRDGRHVVLGEDSAHARLQDLLLHYTAHPL 175
HUMAN: PLC       FRARGKVKHCRIN--RDGRHFVLGTSAYFESLVELVSYYEKHSL 725
DROME: CSW       VRTDDKVTHVMI-RWQDKKYDVGGGES-FGTLSELIDHYKRNPM 191
RAT:   LNK       FNLQGRAKHLRLVLTERGQCRV--QHLHFPSVVDMLRHFQRSPI 201
CHICK: SRC       VSCEGKVEHYRI--IYSSSKLSIDEEVYFENLMQLVEHYT     157
```

Structure of TSAd-VEGFR-2 KD complex

A

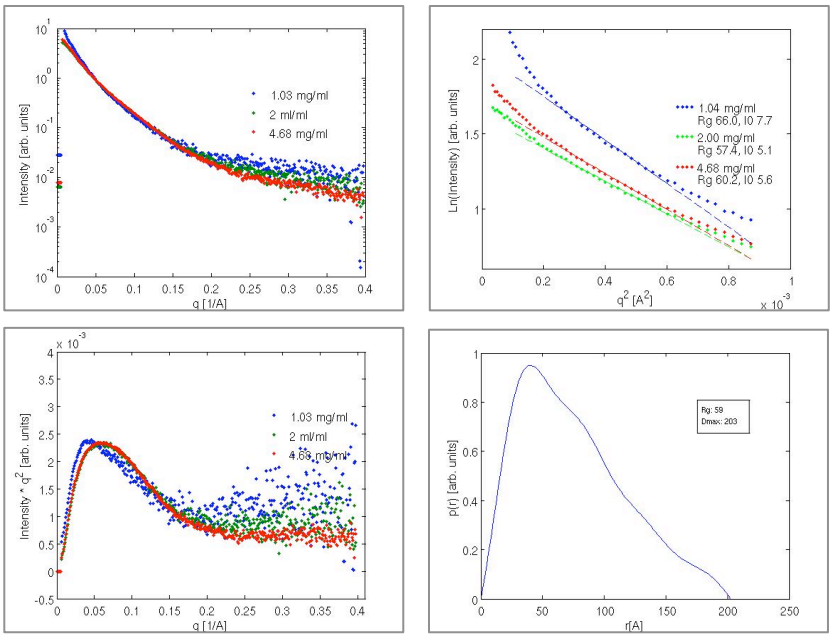

B

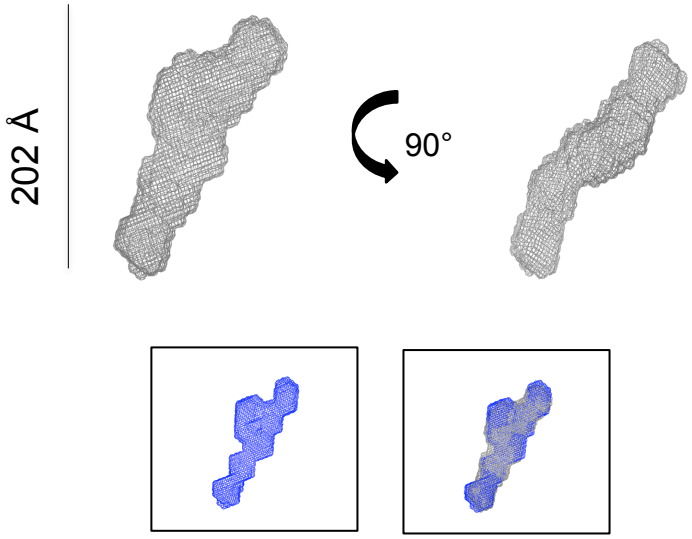

Figure 41: SAXS results of TSAd and TSAd-VEGFR-2 complex
A) Shown for all measured concentrations: The intensity plotted as a function of s, the linear Guinier region with calculated Rg-values, the Kratky-plot and the p(r)-function as calculated from AUTOGNOM for the experiment used for *ab initio* modelling. B) The averaged *ab initio* model (in grey), the most typical particle (blue particle, small left box) and the most typical paricle superimposed with the averaged envelope (small box on the right) C) SITUS superimposition of the *ab initio* model of TSAd with the crystal structure of the SH2-domain of src (PDB: 1O4C). Alignment of TSAd-SH2 domain with those of other cytoplasmic signaling proteins. Boxed, unshaded: identical amino acids. Boxed, shaded: Conserved amino acids (Li-Wha Wu et al., 1999). Figures by Sandro Manni and Kaisa Kisko.

SAXS experimental parameters are summarized in table 15. Overlay of the scattering intensities, p(r) functions and the *Ab initio* models, of VEGFR-2 KD, TSAd and TSAd-VEGFR-2 KD, are visualized in figure 42.

A

Construct	Concentrations [mg/mL]	Rg [Å] (Guinier-region) ± S.E.	Dmax ± S.E. [Å]
TSAd	1, 1.8	42.6 ± 3.4	136.9 ± 4.4
TSAd-VEGFR-2 KD complex	1, 2, 4.7	59.16	202.63

B

Construct	Volume (x10^3) [Å] (*ab initio* model)
mKID VEGFR-2 KD	134.9
TSAd	104.1
TSAd-VEGFR-2 KD complex	234.2

Table 15: SAXS experimental parameters
A) Rg and Dmax values for TSAd were determined as mean ± S.E. for at least two concentrations. Rg and Dmax values for TSAd-VEGFR-2 KD complex were determined from one single concentration. (B) Volumes of VEGFR-2 KD, TSAd and TSAd-VEGFR-2 KD complex determined by SAXS and used for *ab initio* modelling.

A

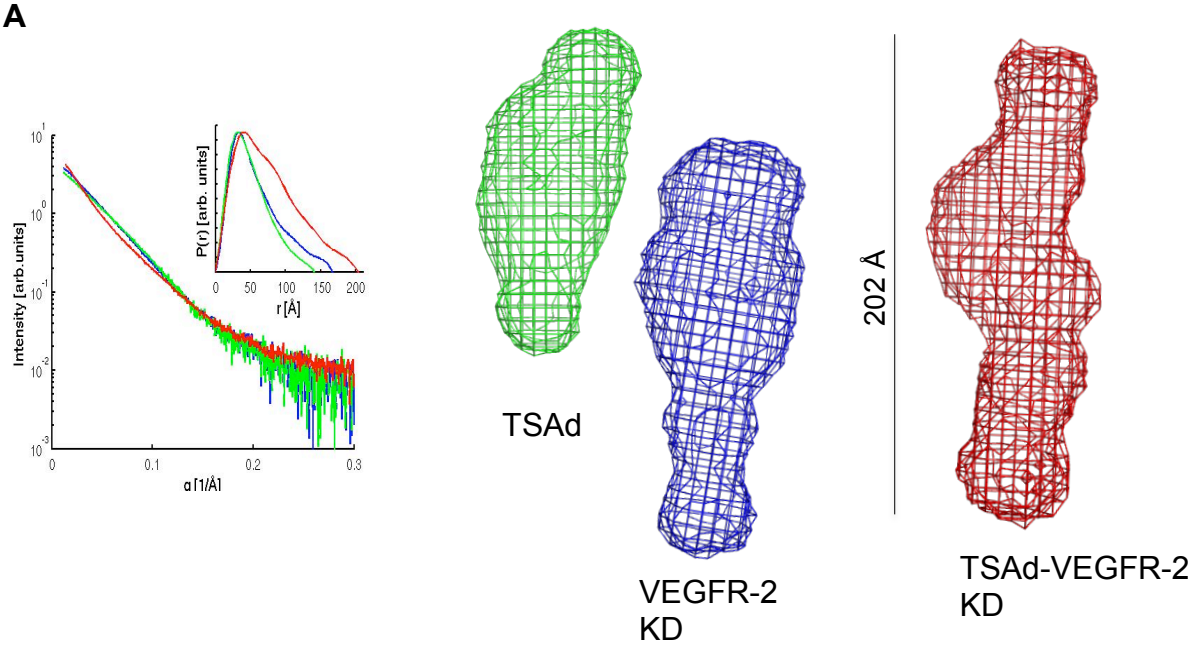

B

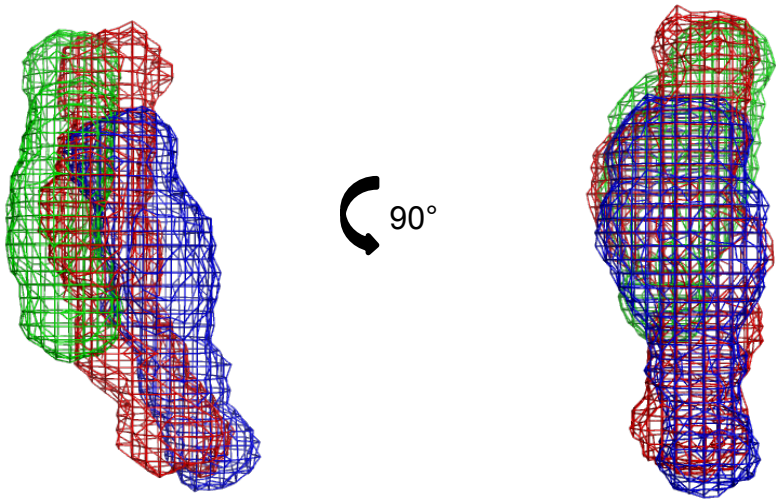

Figure 42: Overlay of intensities, p(r)-functions and *ab initio* models of mKID VEGFR-2 KD, K868M VEGFR-2 KD and ΔKID VEGFR-2 KD
Figures by Sandro Manni and Kaisa Kisko.

8. Discussion and Outlook

8.1. The Role of the transmembrane domain in VEGFR-2 activation

VEGFR-2 is a key regulator of vasculogenesis and angiogenesis. Ligand binding to the ECD of VEGFR-2 induces distinct conformational changes within the receptor resulting in receptor dimerization. It was shown that, besides ligand-receptor contacts, receptor dimers are engaged in homotypic interactions in domains 4 and 7 (Ruch *et al.*, 2007). To activate the receptor, the intracellular kinase domains must be reoriented in a distinct orientation. In the case of the EGFR (Zhang *et al.*, 2006) and the FGFR (Bae *et al.*, 2010) the activated kinase domains form an asymmetric dimer. One of the goals of this project was to shed light on the role of the TMD during VEGFR-2 activation. Earlier studies on Neu (Bell *et al.*, 2000; Lofts *et al.*, 1993) or EGF receptors (Smith *et al.*, 1996) made clear that receptor tyrosine kinases can also be artificially dimerized and activated by interactions mediated by their TMDs. Previous experiments in our lab examined the role of dimerization and activation of VEGFR-2 by using artificial TMDs consisting of sequentially arranged glutamic acid residues in an all valine transmembrane helix (Dell'Era Dosch and Ballmer-Hofer,

2009a). Introduction of glutamic acid residues at specific positions of the TMD gave rise to either active or inactive dimers. Dimerization is therefore required but not sufficient for activation of VEGFR-2. We were able to confirm these findings in the context of the wt-TMD of VEGFR-2. Our ECD-deleted VEGFR-2 constructs carrying glutamic acid point mutations in the TMD gave rise to either active or inactive receptors. I767E, L768E and V796E showed significantly higher receptor activity compared to wt. V769E was the most active (3.5x increase compared to wt) whereas several other point mutations along the TMD showed activities in the range of wt. An interesting finding was that these activating single glutamic acid mutations did not affect the baseline activity of full-length VEGFR-2 and could still be activated by ligand. These data suggest that the ECD of VEGFR-2 plays an important role in the autoinhibition of the kinase domain in the absence of the ligand as discussed earlier (Tao *et al.*, 2001). Furthermore, our lab recently published data demonstrating that binding of VEGF to recombinantly produced ECD protein encompassing Ig-domains 1-7 of VEGFR-2 is 1.0-1.7 kcal/mol less favourable than binding of VEGF to Ig-homology domains 2-3 (Brozzo *et al.*, 2012b). Based on these findings we propose that Ig-domains 4-7 attenuate receptor activity in the absence of ligand. The observed energetic penalty might arise from the reported homotypic interactions in Ig-domains 4 and 7. In agreement with this it was shown for the FGFR3 that the ECD prevents dimerization in the absence of ligand with a ΔG of 1 kcal/mol (Chen *et al.*, 2010). A392E, a mutation in the TMD helix of FGFR3, has been associated with a human disease called Crouzon syndrome. It has been reported that the change in free energy of dimerization of the isolated TMD of FGFR3 in lipid bilayers induced by this mutation is -1.3 kcal/mol (Li *et al.*, 2006). Based on these thermodynamic data it is thus possible that the A392E mutation activates FGFR3 by stabilizing receptor dimers in the absence of ligand giving rise to the observed receptor-mediated pathology. The ΔG change by a single glutamic acid residue in the TMD in a particular position in ECD-deleted receptor constructs therefore reflects the reorientation of the kinase domains and thus activates the receptor. As shown by our data, change in ΔG is not sufficient to compensate for the repulsive force of the ECD in full-length receptor constructs. The ECD might thus reduce the structural flexibility of the TMD in the lipid bilayer and allow only distinct conformations of the TMD-helix. To override steric hindrance induced by the VEGFR-2 ECD and to maintain the receptor in an active conformation sustained by glutamic acid-induced hydrogen

bonding in the lipid bilayer a single glutamic acid residue is thus not sufficient. When comparing ECD-deleted VEGFR-2 with VEGF stimulated full-length VEGFR-2 and unstimulated receptor it becomes apparent that the ECD of VEGFR-2 tightly regulates receptor kinase activity. ECD-deleted VEGFR-2 shows a 50% increase in activity compared to unstimulated full-length VEGFR-2 constructs in agreement with previous experiments from our lab using ECD-deleted VEGFR-2 constructs (Dell'Era Dosch and Ballmer-Hofer, 2009a).

We also studied the mechanism of VEGFR-2 activation by comparing ECD-deleted with full-length constructs carrying two glutamic acid mutations in the TMD. In these artificial TMDs glutamic acids were spaced 7 residues apart thereby positioning them on the same face of the helix. The idea was to rigidify the dimerization interface and to generate dimers with specific spatial orientations of the two monomers that might either activate or inactivate the receptor similar to the all valine TMD constructs studied previously in our lab. The introduction of two glutamic acid mutations is expected to compensate for the repulsive force of the ECD and to facilitate the formation of distinct dimeric TMD conformations. Surprisingly, the introduction of glutamic acid pairs in the TMD of the ECD-deleted VEGFR-2 constructs at positions V769E/M776E, G770E/F777E and T771E/F778E gave rise to inactive receptor variants whereas mutations G770E/F777E and T771E/F778E were able to activate the full-length receptor independent from VEGF stimulation (figure 43B and C). The positions of the activating pair of mutations G770E/F777E and the inactivating I774E/L781E mutations is in agreement with our earlier data obtained with all valine TMDs where V770/777E gave rise to active and V774/781E to inactive receptor constructs. The fact that the V769E mutation activated the ECD-deleted receptor while V769E/M776E gave rise to inactive ECD-deleted receptors documents the tight control of the activation of VEGFR-2. As a matter of fact no disease-related constitutively active or inactive VEGFR-2 variants are known, demonstrating that activation of VEGFR-2 must be tightly regulated presumably to prevent embryonic lethality resulting from vascular defects (Shalaby *et al.*, 1995).
Our data also show that the orientation of the interacting side chains in the dimerized TMDs vary in the presence or absence of the ECD. On the other hand the V770/777E mutations in the all valine TMD gave rise to active receptors both in the ECD-deleted and in full-length receptors presumably as a result of reduced sterical

hindrance in the all valine dimeric helices, which allows for increased side chain flexibility. The introduction of a single glutamic acid residue into the TMD of VEGFR-2 may allow for flexibility so that the kinase domains are able to orient relative to each other in an active conformation. Introduction of a pair of glutamic acid residues further restricts this flexibility by maintaining the TMD helices in either an activating or an inactivating receptor conformation. Based on our findings we speculate that there are possibly two alternative arrangements of the TMD helices in the dimeric and active full-length VEGFR-2 (G770E/F777E and T771E/F778E, see figure 43B). Both conformations are rotated by 100° relative to each other along the helix axis since two adjacent side chain residues span an angle of 100° in a helix while a full turn of 360° involves 3.6 amino acids (figure 43A).

A

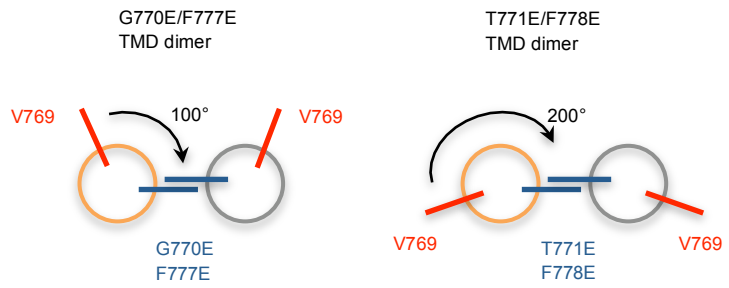

B

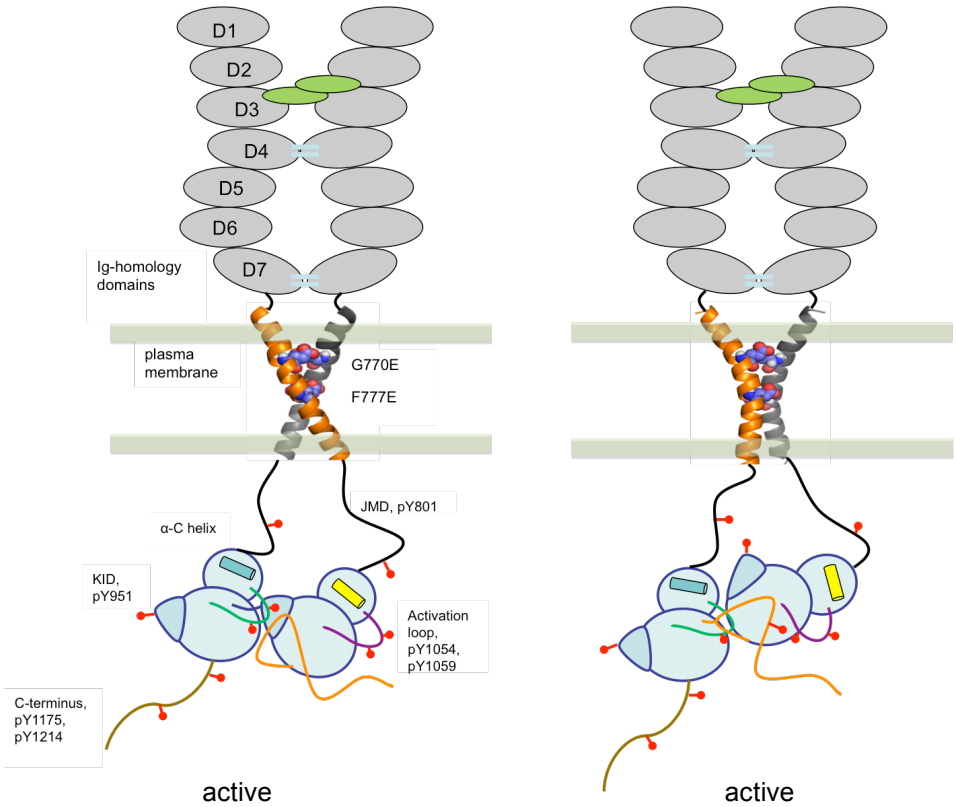

C

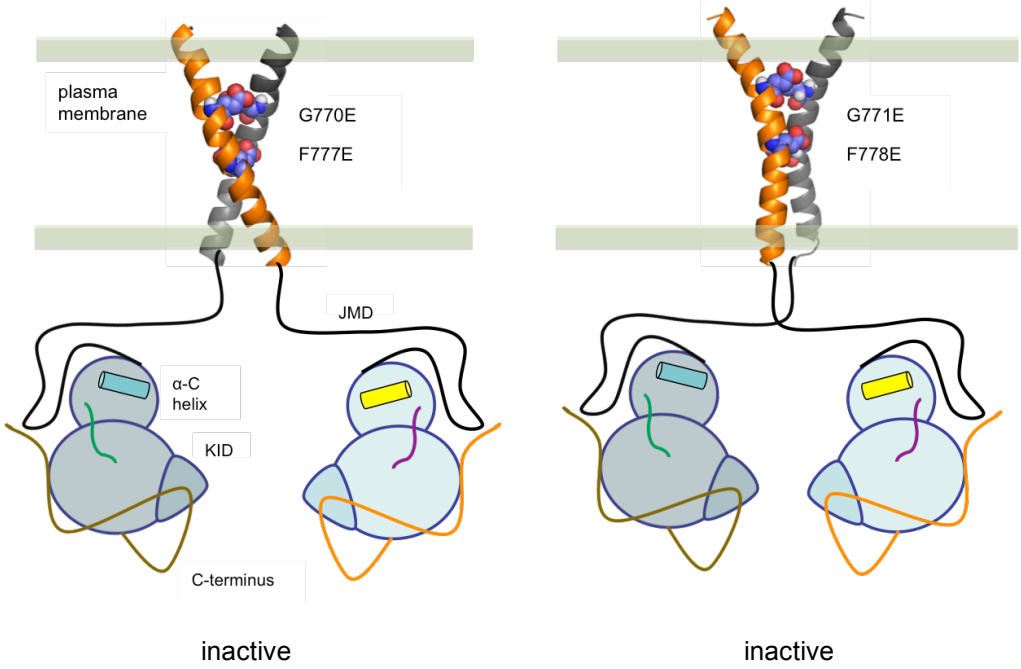

Figure 43: Schematic representation of putative TMD helix orientation by double glutamic acid dimerization TMDs
(A) Schematic top view of helices and rotation angles relative to V769 (B) Introduction of glutamic acid pairs G770E/F777E and T771E/F778E into the TMD of the full-length receptor leads to constitutive activation. Each glutamic acid pair may induces a distinct activated dimeric KD conformation (each TMD corresponds to one asymmetric activated dimer). (C) The same mutations as in (B) render ECD-deleted receptors inactive (KDs are shown as inactive, symmetric dimers). A) B) C) Active and inactive kinase dimers arrangements are shown as possible asymmetric and symmetric dimers, respectively (interaction via KID or C-terminus,). Ig-domains 1-7 of the ECD are indicated. VEGF is depicted in green. Homotypic interactions in domains 4 and 7 in the ECD are indicated as blue parallel lines. JMD: black loop. The αC-helix is shown for each KD in either a blue or a yellow colored cylinder. The activation-loop is shown for each KD as either a green or magenta loop. KID: dark blue colored domain. The C-terminus is shown for each KD as either a brown or orange loop. Phosphorylation sites are depicted as red dots. TMDs are indicated by a schematic dimeric helix arrangement with monomers in orange and grey. Helices were generated with PyMOL.

To further elucidate the exact molecular mechanism of receptor activation it is indispensable to generate high-resolution structural information. Based on our previous cell biological data we therefore solved the structure of TMD helix-dimers in the native and the V769E containing TMD helices in collaboration with Alexander S. Arseniev using NMR spectroscopy. It has previously been shown that the TMD of VEGFR-2 has an intrinsic propensity to dimerize although none of the known dimerization motifs like a distinct heptat (XxxxxxxX, X=G, A or S) or the GG4-like repeat (XxxxX, X=G, A, S or T) motifs is present (Finger *et al.*, 2009a). Bell *et al.* (Bell *et al.*, 2000) proposed a model in which the rotational angle perpendicular to the

plane of the plasma membrane at which the kinase subunits interact with each other is important for receptor activation (in their case the neu receptor). However, several other results show that the TMDs of RTK are more likely to interact in an X-shaped conformation (Bocharov *et al.*, 2008; Gullick *et al.*, 1992; Mineev *et al.*, 2010; Smith *et al.*, 1996). Our NMR data indeed show that the wt-TMD of VEGFR-2 adopts such an X-shaped, symmetrical dimer with a left-handed helix orientation.

The dimerization interface spans across the entire helix and consists mainly of apolar, hydrophobic contacts formed by a "heptad-repeat"-like cluster: $T^{761}xxE^{764}xxI^{767}L^{768}xxT^{771}A^{772}xxA^{775}xxF^{778}W^{779}xL^{781}L^{782}xxI^{785}xxxV^{789}$. The interface is further stabilized by a symmetric edge to face stacking interaction of F778 with W779. NMR analysis of the dimerization process at the lower protein / DPC ratio of 1:150 gave rise to ~70% monomeric TMD-helices. This is in agreement with earlier dimerization studies using Toxcat assays which showed that the wt-TMD of VEGFR-2 is a weak dimerizer (Finger *et al.*, 2009a). The dimeric conformation coexists with the monomeric state and represents the thermodynamically most stable form of the wt-TMD helix in a lipid environment. The dimer may indeed represent a stable conformation activating ECD-deleted VEGFR-2 which would agree with our data showing a 50% increase in activity compared to the unstimulated full-length VEGFR-2 construct (figure 44). Our data also shows that introduction of a glutamic acid residue at position 769 of the TMD of VEGFR-2 did not induce a conformational change of the TMD helix. Furthermore, the energetic contribution to dimer formation by the V769E mutation was insignificant (-0.3 kcal/mol) and the calculated dimer structure was with high probability identical to the previously found wt-TMD dimer (good correlation for chemical shift-changes of the nitrogen and the amide-proton). Mutation of V769 to E769 creates a third trimeric and highly stable oligomeric state generating additional surface area that promotes helix-helix interactions leading to active ECD-deleted VEGFR-2 constructs. The asymmetric dimeric unit in the trimer shares similar geometrical parameters previously found in TMD structures corresponding to the active state of RTKs such as the EGFR (Bocharov *et al.*, 2008). The angle between the axes of helices are -50 ± 5° and C-termini point away from each other. To determine the conformations of the activating TMD in the context of the full-length VEGFR-2 we performed NMR studies on TMD-helices carrying our previously identified activating glutamic acid pairs G770E/F777E and T771E/F778E.

Unfortunately we were not able to finish these experiments at the conclusion of this thesis.

Taken together, our structural data demonstrates that the introduction of a single glutamic acid residue at position 769 in the TMD of VEGFR-2 does not thermodynamically favour dimerization but allows for additional surface area that generates multiple oligomeric states. This might suggest that the activation of the V769E mutant of ECD deleted VEGFR-2 constructs is kinetically rather than thermodynamically driven. E769 might “trap” the dimer in an energetically unfavourable conformation thereby exposing binding sites for additional helix-helix interactions that, depending on the concentration of receptors in the cell membrane, give rise to a stable trimeric form. The wt-TMD dimer may therefore represent an intermediate state that is entropically favoured. Further structural and kinetic studies are now required to shed light on these processes.

A

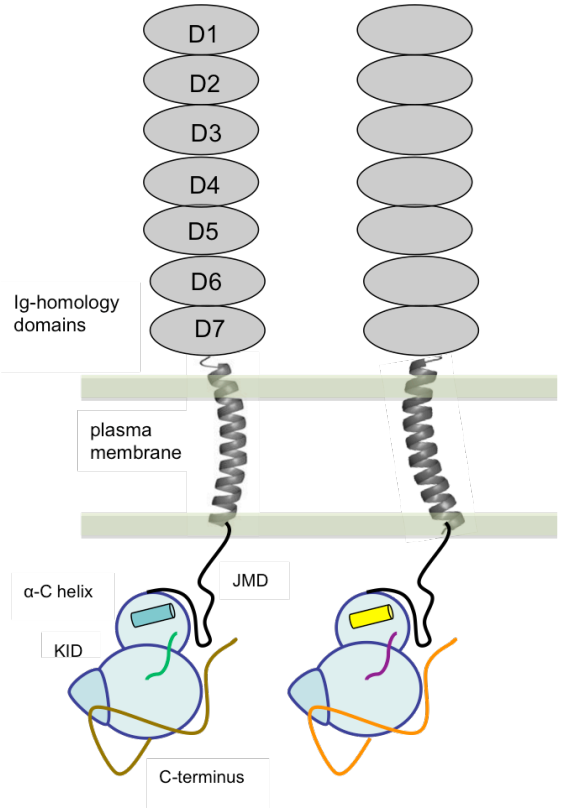

inactive

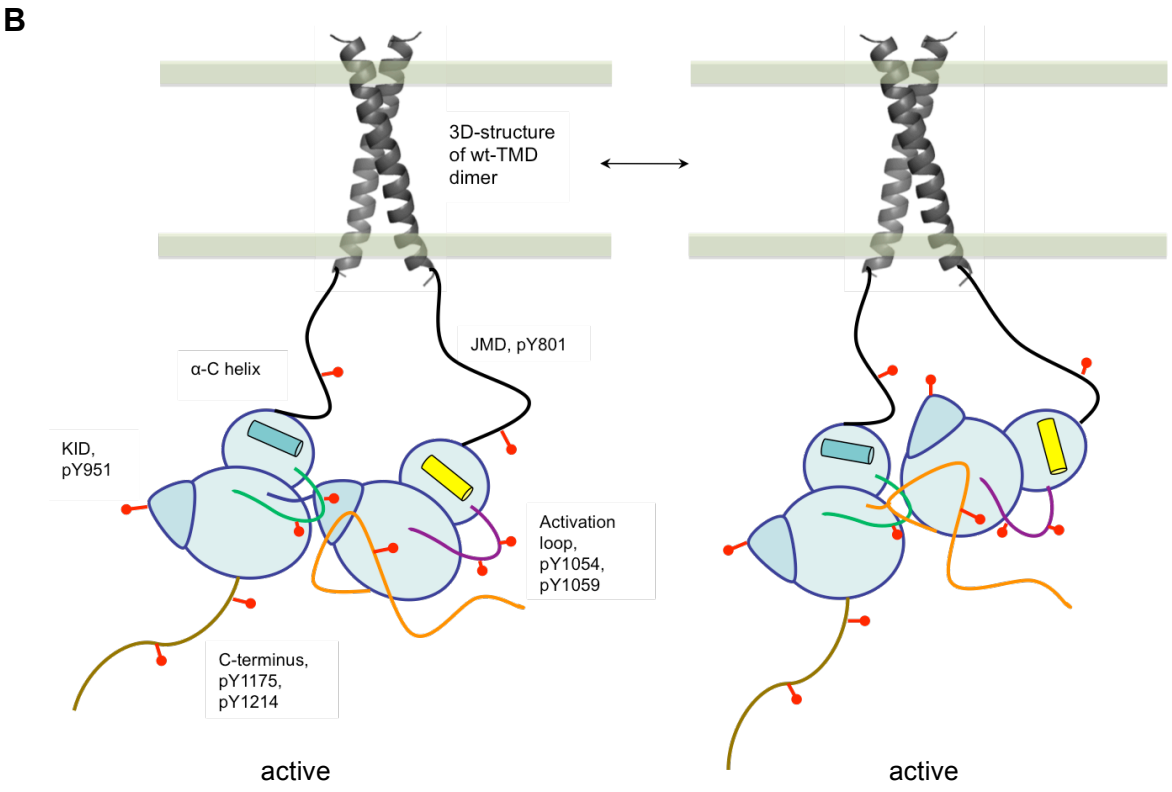

Figure 44: Role of the ECD and the TMD in VEGFR-2 activation
(A) ECD-deleted VEGFR-2 shows spontaneous activation compared to unstimulated full-length VEGFR-2 (50% increase, B). A) B) Active dimeric kinase conformations are shown as asymmetric dimers (interaction via KID or C-terminus). Inactive kinases in the full-length receptor are shown as monomers. JMD: black loop. The αC-helix is shown for each KD in either a blue or a yellow colored cylinder. The activation loop is shown for each KD in either a green or magenta loop. KID: dark blue colored domain. The C-terminus is shown for each KD in either a brown or orange loop. Phosphorylation sites are depicted as red dots. Experimentally determined 3D-structure of the wt-TMD is colored in grey.

8.2. The role of the kinase insert and the C-terminal domain in VEGFR-2 activation

The goal of this project was to identify the function of distinct VEGFR-2 kinase subdomains such as the KID and the CD. Previous data from several research groups suggest that these domains fulfil regulatory functions of receptor tyrosine kinases in general. Deletion of the KID of αPDGFR, for instance, impaired PDGF induced autophosphorylation of tyrosine residues, phosphatidylinositol turnover and receptor-associated PI-3 kinase activity (Heidaran *et al.*, 1991) and deletion of 164 amino acids in the C-terminus of EGFR rendered the receptor inactive. Hence, the C-terminus of EGFR is required for the receptor to adopt a fully active conformation (Wedegaertner *et al*, 1992). Another regulatory contribution of the CD was described

for the Met-receptor. Peptides derived form the CD inhibited the kinase domain *in vitro* and the intracellular delivery of such peptides impaired HGF-dependent Met phosphorylation and downstream signaling (Bardelli *et al.*, 1999). To date the only structural information that is able to explain the role of the KID and the CD in RTK activation derives from the Tie-2 receptor (Shewchuk *et al.*, 2000b). This structure represents an inactivated monomeric kinase domain that is inhibited by its CD. The phenyl ring of Y1112 that represents a major C-terminal phosphorylation site is packed between the hydrophobic side chains of L696, L579, F1114 and R577 in the KID of Tie-2. The KID is therefore an essential structural element enabling inactivation of Tie-2 via the CD. The negative regulatory role of the CD was further verified in later studies where it was shown that mutation of Y1112F or deletion of the CD of Tie-2 leads to receptor activation (Niu *et al.*, 2002; Sturk *et al.*, 2009). Since the mentioned subdomains are missing in the crystal structure of VEGFR-2 (McTigue *et al.*, 1999a) their role in kinase regulation remains unclear. In addition to further structural analysis it was therefore essential to perform functional studies to gain more insight into the regulation of the kinase domain of VEGFR-2. We found that KID-deleted constructs showed reduced phosphorylation at Y1175 in HEK293 cells, but, most remarkably, the activation-loop residues Y1054/59 of VEGFR-2 was still phosphorylated. McTigue *et al.* (McTigue *et al.*, 1999a) demonstrated earlier that the truncated kinase domain of VEGFR-2 used for crystallization did not show a significant decrease in the catalysis of the phosphotransfer reaction *in vitro*. The KID is therefore not necessary for phosphorylation of the activation loop and the subsequent activation of the kinase domain. But, as our data show, the absence of the KID prevents phosphorylation at downstream phosphorylation sites such as Y1175 (figure 44A). To see whether this effect is induced by the complete deletion of the KID or whether it is the dependence of Y1175 phosphorylation on phosphorylation at Y951 we mutated this residue. Our data show that phosphorylation of Y1175 requires prior phosphorylation at Y951. Phosphorylation of Y1212 further downstream of Y1175, on the other hand seems not to be affected by the Y951F mutation. Based on these findings we propose that VEGFR-2 activation depends on the coordinated phosphorylation of specific sites.

The CD-deleted VEGFR-2 constructs were constitutively active with strong phosphorylation signals at Y1175 and Y1054/59 (figure 45B). We verified the data in the full-length and in ECD-deleted receptor constructs with and without VEGF-

stimulation. Downstream signaling via PLC-γ was consistent with the phosphorylation pattern of the constructs.

A

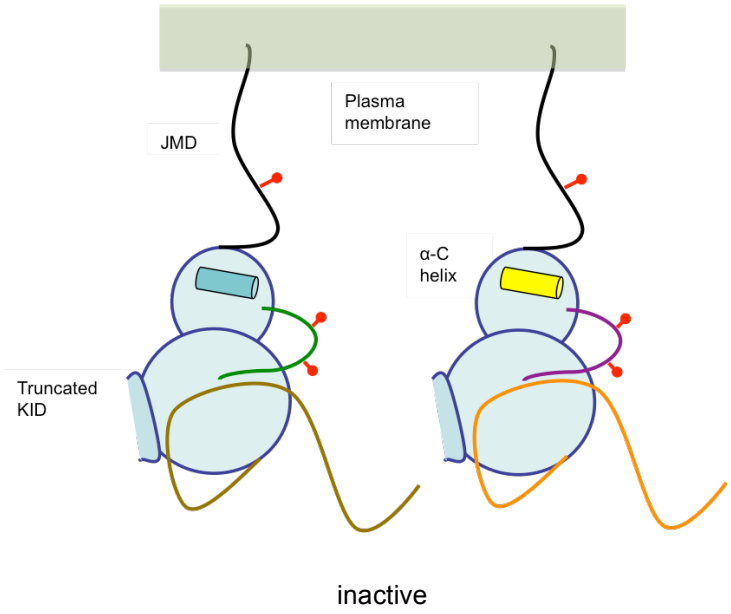

B

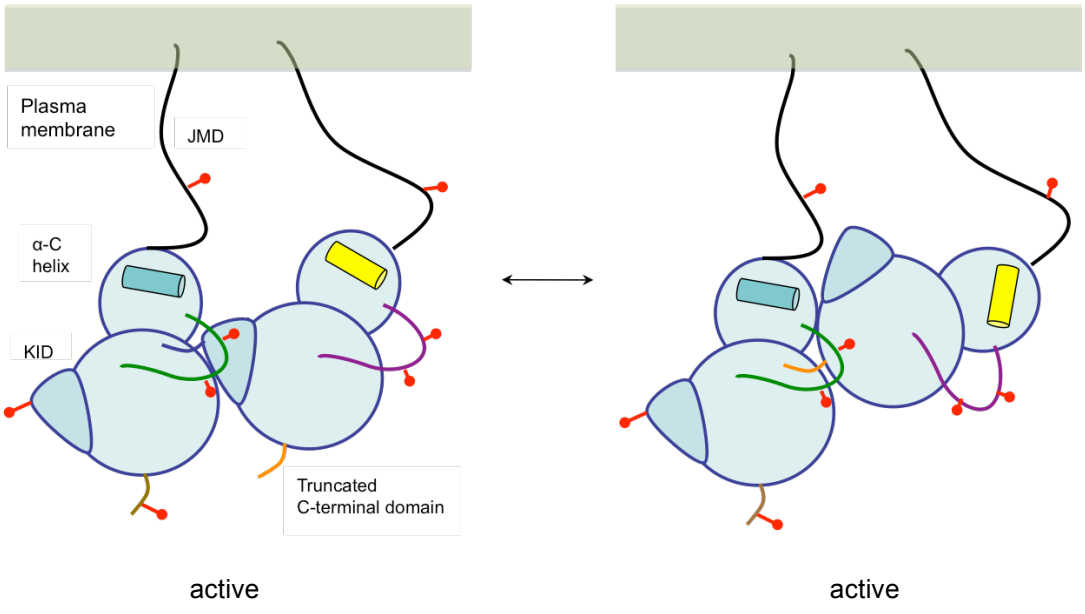

Figure 45: Schematic representation of VEGFR-2 KD mutants
(A) KID-deletion prevents phosphorylation at Y1175 of the KD whereas the activation loop sites Y1054 and Y1059 are phosphorylated. (B) Deletion of the CD renders VEGFR-2 constitutively active independent of VEGF stimulation (shown as two alternative active asymmetric dimers).

This data is not in agreement with earlier reports where chimeric receptor variants carrying the ECD of the CSF receptor fused to the CD-deleted kinase domain of VEGFR-2 were not activated upon CSF stimulation (Meyer *et al.*, 2003). The authors proposed the existence of an inactive dimer of the kinase domain in the absence of the CD. On the basis of previously discussed results concerning our TMD-mutant constructs we think that the ECD of VEGFR-2 plays a crucial role in autoinhibition and activation of the KD of VEGFR-2. To perform these tasks the ECD must be able to orient the kinase domains inside cells based on bioavailability of ligand. Replacement of the native ECD with the ECD from a different RTK impairs the authentic regulatory mechanism. Based on our results, such data acquired with chimeric VEGFR-2 constructs should therefore be considered with caution.
Our data for the KID and the CD of VEGFR-2 let us propose a highly ordered and complex activation mechanism that is initiated upon ligand binding to the ECD.

In order to perform further biophysical experiments and to gain a deeper insight into the regulatory mechanism of the kinase of VEGFR-2 we expressed several mutant constructs in Sf21 insect cells yielding protein of high purity and amounts in the milligram range. MALS analysis of recombinant proteins confirmed their monodispersity. All kinase domain proteins produced in this way were monomeric at the measured protein concentration of 2 mg/mL.
We were further interested whether the kinase shows intrinsic potential to dimerize at increasing concentration and whether activating and inactivating kinase domain modifications were able to alter the intrinsic dimerization propensity. From previous crystal structures we knew that kinase-subdomains could have an impact on dimer formation. It was shown e.g. that the intracellular JMD of EGFR is involved in formation of the activated asymmetric dimer. The C-terminal half of the JMD-segment links the activated kinase domain to the activator kinase while the N-terminal half is thought to potentiate dimerization by adopting an antiparallel helical dimeric conformation (Jura *et al.*, 2009). In the crystal structure of the FGFR1 dimer phosphotyrosine Y583 in the KID of one monomer is bound to the catalytic cleft of the other monomer resulting in asymmetric dimer formation (Bae *et al.*, 2010). Chen *et al.* (Chen *et al.*, 2008) solved the crystal structure of FGFR-2 in the act of trans-phosphorylation of Y769 which represents the most important phosphorylation site in the CD. The asymmetric dimer was formed by residues close to the C-terminus upon

interacting with the active site of the participating kinase monomer.
Our sedimentation equilibrium AUC-data demonstrates that the activated, fully phosphorylated kinase domain of VEGFR-2 has a low, but significant propensity to form dimers when increasing protein concentration (Kd=160 ± 56 µM). Specific subdomains of VEGFR-2 enhance dimerization while deletion of the JMD, KID and the CD results in a reduction of the affinity (Kd=553 ± 80 µM). This data is in agreement with the literature. Notably the deletion of the CD reduces dimer formation (Kd=290 ± 14 µM) *in vitro* although this construct showed constitutive activation of the receptor in HEK293 cells. The same effect was observed with the KID-deletion mutant (Kd=225 ± 35 µM). We assume that in the plasma membrane of cells deletion of the CD leads to receptor dimerization. To prove receptor dimerization also in live cells additional co-immunoprecipitation or crosslinking experiments are required.
McTigue et al. (McTigue *et al.*, 1999a) were not able to see a significant difference in catalytic activity by comparing the truncated kinase domain of VEGFR-2 (ΔJMD, ΔKID and ΔC) used for crystallization with the full-length kinase *in vitro.* To further clarify the role of the CD and the KID in the isolated, monomeric VEGFR-2 kinase protein, kinase assays of the specific deletion mutants would be helpful.

Besides looking at active and inactive mutants it is crucial to acquire also information on the activation process itself. It has previously been demonstrated that autophosphorylation in the kinase domain of RTKs occurs in an ordered and sequential way (Furdui *et al.*, 2006). Upon activation of the isolated kinase domain of VEGFR-2 by ATP, Y801 in the JMD is phosphorylated as a first event, followed by Y1054 and Y1059 phosphorylation in the activation loop that further potentiates kinase activity (Dougher Vermazen *et al.*, 1994; Kendall *et al.*, 1999; Solowiej *et al.*, 2009). From crystal structures of type III receptor tyrosine kinases we know that the JMD binds at an interface between the N- and the C-terminal subunits of the kinase domain and sterically blocks the activation loop and the αC-helix from adopting a catalytically active conformation (Griffith *et al.*, 2004; Mol *et al.*, 2004; Mol *et al.*, 2003; Schubert *et al.*, 2006). Similarly, phosphorylation of Y801 in the JMD domain of VEGFR-2 might initiate the release of the autoinhibitory JMD from the catalytic cleft as the initial step in the activation process. In agreement with this idea phosphorylation of the JMD of the c-Kit receptor was shown to be required for activation (Ma et al., 1999). Another study found that only Y1175 was important for

the activation process, while the mutant Y801F in the JMD and Y1214F in the CD did not affect phosphorylation of Y1175 (Takahashi *et al.*, 2001b). In addition, studies with chimeric VEGFR-2 receptors proposed a role for Y1214 during receptor autophosphorylation and kinase activation (Dayanir *et al.*, 2001;Meyer *et al.*, 2002). However such data obtained with chimeric RTKs must be considered with care because such constructs may not adequately reflect the situation in wt-receptors. Later knock-in studies in mice proved the dispensability of Y1214 in physiological function (Sakurai *et al.*, 2005).

Based on our finding that Y1175 is phosphorylated after phosphorylation of Y951, we performed *in vitro* phosphorylation assays with the completely dephosphorylated and thus inactivated KD of VEGFR-2. After 5 min the pY1054/59 signal showed the strongest intensity reaching saturation at the fastest rate. In agreement with Solowiej *et al.* (Solowiej *et al.*, 2009) who showed hat Y1054/59 immediately follows phosphorylation of the JMD residue Y801 of VEGFR-2. Autophosphorylation of Y801 occurs via an intramolecular mechanism as determined by Solowiej*et al.* who found that autophosphorylation was independent of the enzyme concentration. In our experiments the degree of phosphorylation of Y801 could not be monitored due to the lack of a suitable phospho-specific antibody for analysis. Phosphorylation of Y1214 closely follows activation of Y1054/59. The latest phosphorylation event with the slowest phosphorylation rate takes place at Y1175 immediately following phosphorylation of Y951. Further experiments would be necessary to determine whether autophosphorylation of downstream tyrosines is mediated via an inter- or intramolecular mechanism.

These results support our previous activation data for the Y951F mutant and also show that Y1214 does not act as a bottleneck of receptor activation since it is immediately phosphorylated after activation (figure 46).

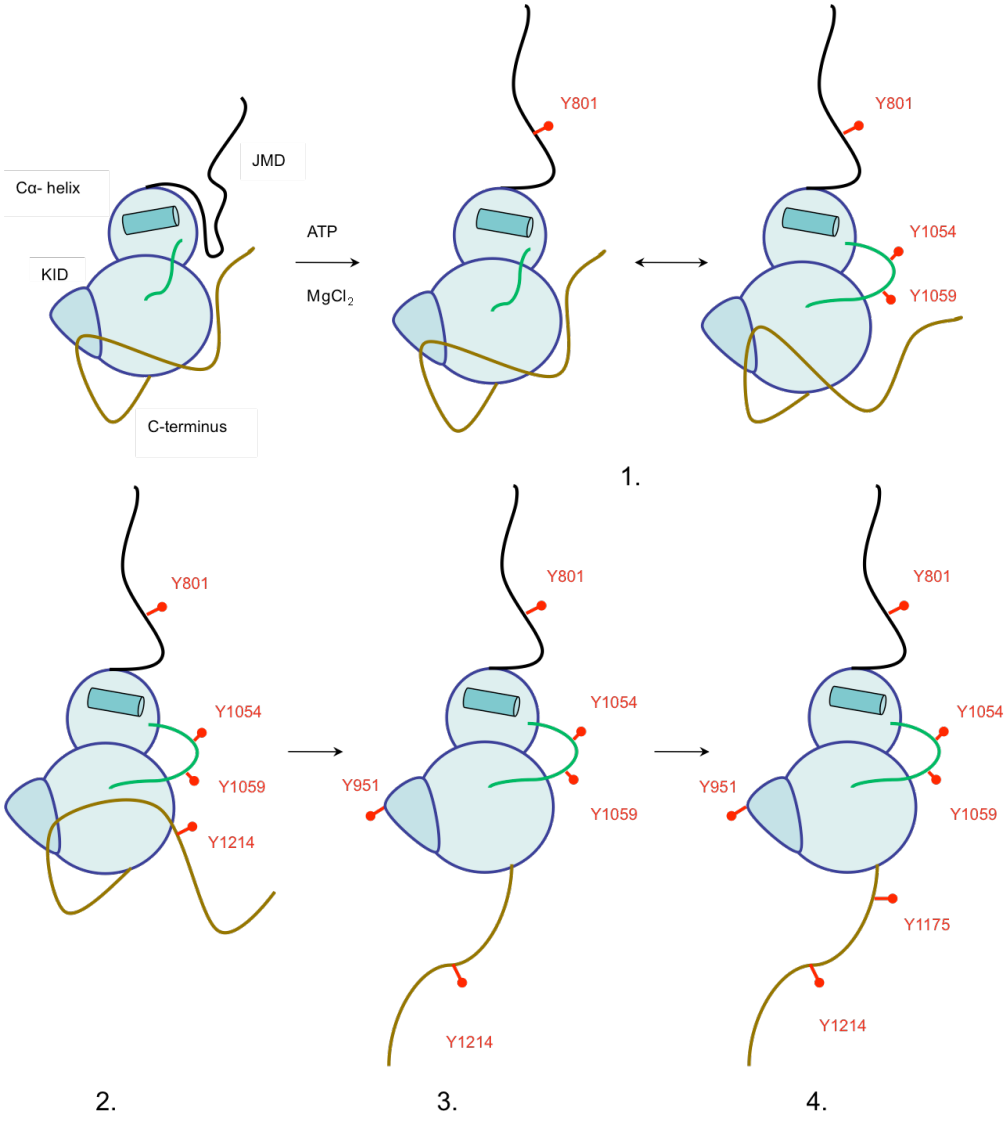

Figure 46: Autophosphorylation of soluble VEGFR-2 kinase domain
Initial phosphorylation of activation loop residues Y1054/59 leads to activation of VEGFR-2 KD and phosphorylation of the C-terminal Y1214 closely follows. The latest phosphorylation event with the slowest phosphorylation rate takes place at Y1175 immediately following phosphorylation of Y951.

VEGFR-2 is activated according to the generally accepted mechanism for activation in RTKs. VEGF binding to the monomeric ECD of VEGFR-2 induces dimerization and subsequent activation of the KD, which leads to downstream signaling. However, less well understood is how these pathways are modulated, amplified and timed in response to environmental changes. It is essential for the cell to maintain receptor signaling within a narrow time window. Suppression and limitation of signal duration is crucial to prevent over-stimulation and deregulation of the cell. Major downstream phosphorylation sites of VEGFR-2 are Y951 in the KID of VEGFR-2 that serves as a

docking site for TSAd (Matsumoto *et al.*, 2005;Wu *et al.*, 2000) and regulates actin reorganization and migration but not mitogenicity upon VEGF-stimulation in endothelial cells. pY1175 is a binding sites for downstream mediators such as PLC-γ1 and is responsible for activation of mitogenic and survival pathways. NCK binds to pY1214 and activates Cdc42 and p38MAPK (Lamalice *et al.*, 2004). It was discussed earlier that phosphorylation of Y951 may be specifically regulated since this site was found to be phosphorylated in some but not all tested endothelial cell lines expressing VEGFR-2 (Matsumoto *et al.*, 2005). Activation of the Y951-mediated signaling pathway might be affected by VEGF splice variants specific for co-receptors such as neuropilin. Furthermore, phosphorylation of Y951 was more pronounced in vessel structures lacking associated pericytes, which are displaced from vessels during angiogenesis. It is therefore possible that Y951 phosphorylation is required for active angiogenesis and might play only a minor role in differentiated vessels.

To visualize the conformational changes arising from activation within the kinase domain of VEGFR-2 we applied structural biological techniques. A prerequisite to solve a high-resolution structure is the generation of high quality diffracting protein crystals. Crystallization trials with activated (phosphorylated) kinase domain mutant constructs did not yield protein crystals so far (Appendix). Hence, we used SAXS to determine structures at low resolution. SAXS studies depend on monodispersity of the measured protein. Since our purification protocol yielded homogeneous protein of high purity we met the requirements for the analysis. Our previous MALS and AUC analysis showed that VEGFR-2 kinase domain proteins in the concentration range of 2 mg/mL are monomeric in solution. SAXS requires protein concentration in this range. Examination of dimeric symmetry of VEGFR-2 kinase domain protein interaction in solution was not possible since we would have required much higher protein concentrations which would prevent proper measurement due to intermolecular van der Waals interactions and perhaps aggregation. Thus, our characterization refers to monomeric VEGFR-2 kinase domains in solution. Several structural studies on monomeric kinase domains have been performed in the past. As mentioned before most studies were conducted with truncated proteins analyzing only the conserved catalytic domain. The role of specific kinase subdomains like the KID and the CD could not be addressed for most of the studies. Shewchuk *et al.* (Shewchuk *et al.*, 2000b) solved the crystal structure of the inactive and monomeric

form of the full-length Tie-2 kinase domain. In the crystal structure the CD adopts an inhibitory conformation by folding back on the catalytic cleft of the KD. The conformation of the CD is stabilized by hydrophobic interactions of Y1112 with the KID of the kinase domain. The negative regulatory role of the CD was then further examined (Niu *et al.*, 2002; Sturk *et al.*, 2009). Our activation data of VEGFR-2 are in perfect agreement with these data. Deletion of the CD of VEGFR-2 leads to constitutive activation similar to Tie-2 suggesting an analogue autoinhibitory mechanism for these RTKs. We anticipate that a completely inactive VEGFR-2 kinase would adopt a compact and globular conformation as compared with the fully activated kinase. To address this we performed a SAXS analysis of the phosphorylated VEGFR-2 kinase mutants. *Ab initio* modelling of the full-length VEGFR-2 kinase in the phosphorylated state gave rise to particles with an overall elongated shape. One end of the protein was globular while the other end was much thinner with a total length of ~167Å. The crystal structure of the catalytic domain of VEGFR-2, which lack the CD (McTigue *et al.*, 1999a) fitted nicely to the globular domain of the particle. The solution structure of the partially phosphorylated kinase domain (K868M VEGFR-2 KD) showed a very similar overall shape with the globular part having a larger diameter. This compact structure may result from the activation loop folded back on the core KD in the inactive kinase conformation and the JMD in the inactive conformation as shown in previous crystal structures of VEGFR-2 related RTKs such as Flt3 (Griffith *et al.*, 2004). The particle in solution was smaller with a total length of ~154 Å reflecting an overall more compact shape. The deletion of the KID in the fully phosphorylated protein did not affect the overall particle shape. However, significant differences were found in the total length of 124 Å and the smaller globular catalytic domain of the kinase.

The KID of VEGFR-2 with a length of 68 amino acids is one of the largest among RTKs. We further investigated the truncated kinase domain protein of VEGFR-2 using the published crystal structure (McTigue *et al.*, 1999a). As expected *ab initio* modelling of the data showed a globular shape and CRYSOL fitting of the solution scattering data retrieved from the published crystal structure with our experimental data gave a good fit. The particle clearly showed a smaller Dmax value of 88 Å and a smaller Rg value of 25 Å due to the missing kinase subdomains including the large ~200 amino acid CD. In order to retrieve an *ab initio* model of the inactive kinase of VEGFR-2 we completely dephosphorylated the protein and subjected the sample to

SAXS analysis. Unfortunately the sample quality was poor and we were not able so far to collect a satisfying dataset for further processing. Data collection is currently repeated with higher quality samples.

To gain structural information we performed also a MALS analysis of the active, partially active and inactive KD proteins (VEGFR-2 KD, K868M VEGFR-2 KD and dephosphorylated VEGFR-2 KD). MALS analysis allows to besides determine the Mr of a protein and to retrieve its Rg with radii >10 nm. Rg is defined as the mass weighted average distance from the centre to each mass element in the molecule. For proteins with radii <10 nm, which accounts for most of the proteins, light scattering is not depending on the incident angle. Therefore light is scattered equally at all angles (such particles are known as Raleigh scatterers). Experimentally determined radii of such proteins are not very accurate. However, as shown before it will be possible to obtain accurate Rg values using SAXS or SANS (small angle neutron scattering). An indication referring to the globularity of a protein could be provided by calculating the ratio of Rg/Rh where Rh represents the hydrodynamic radius. Rh is defined as the equivalent radius of a hard sphere diffusing with the same rate as the protein and can be determined using dynamic light scattering (DLS). The characteristic Rg/Rh ratio for a globular protein is ~0.775 meaning that Rg is smaller than Rh. The Rg/Rh ratio of an elongated protein, like the active KD of VEGFR-2, would deviate upwards from 0.775, i.e. Rg will be larger than Rh. The SEC on the MALS instrument will supply additional important shape information of the analyzed proteins. The partially and completely dephosphorylated kinase domains clearly adopt a more compact conformation compared to the fully phosphorylated and active kinase as shown by their shift in the elution volume on the SEC which is in the order VEGFR-2 KD: 13.3 mL < K868M VEGFR-2 KD: 13.4 mL < dephosphorylated VEGFR-2 KD: 13.6 mL. The progressively more tight packing of the KD can only arise from a conformational change in the CD induced by dephosphorylation of C-terminal tyrosine residues (figure 47).

A

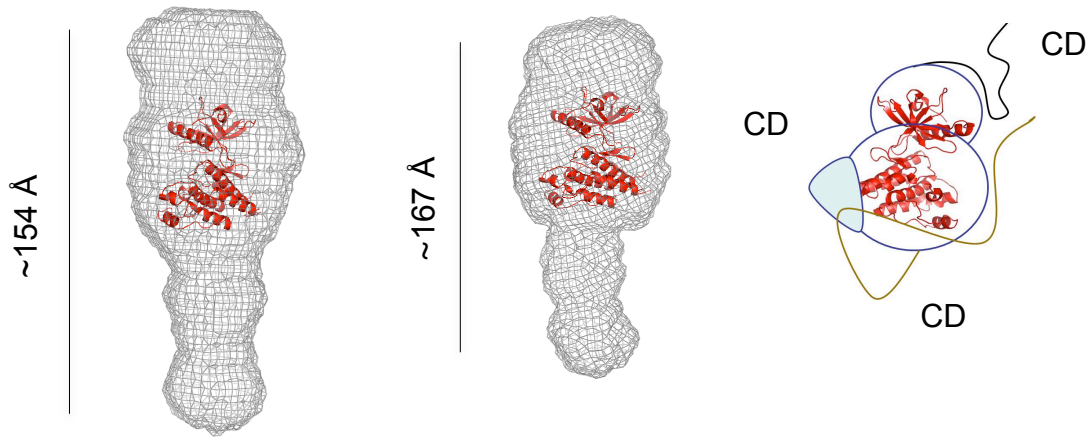

B

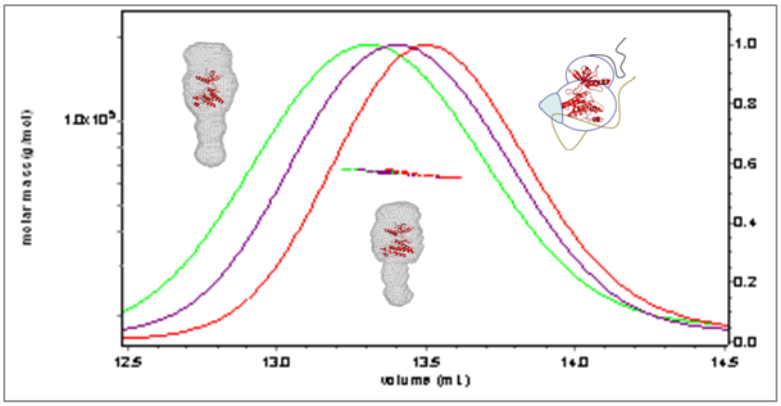

Figure 47: Progressively tight packing of VEGFR-2 KD upon dephosphorylation
(A) Crystal structure of catalytic domain (in red, 1vr2) fitted into the experimentally determined SAXS envelopes of VEGFR-2 KD, K868M VEGFR-2 KD and a schematically drawn envelope of dephosphorylated VEGFR-2 KD where the JMD and the CD are folded back on the catalytic core of the KD. (B) Overlay of coupled SEC-MALS experiments of VEGFR-2 KD, K868M VEGFR-2 KD and dephosphorylated VEGFR-2 KD. JMD: black loop. CD: brown loop.

Taken together, we think that the CD of VEGFR-2 folds back onto the kinase domain to prevent spontaneous activation. Deletion of the CD renders the KD constitutively active as demonstrated by our cell biological data in HEK293 cells. In the fully active state the kinase domain adopts an elongated, open conformation as supported by our preliminary SAXS analysis. We assume that the KD of VEGFR-2 follows a similar autoinhibitory mechanism as previously demonstrated for the Tie-2 kinase domain. In order to determine the precise shape and structure of the different kinase constructs additional SAXS analysis with high quality samples is required and crystallization

trials with dephosphorylated kinase domain mutant constructs should be considered as well. A high-resolution structure of the autoinhibited KD would shed light on the exact activation mechanism.

8.3. Structural analysis of TSAd and TSAd-VEGFR-2 complex

The adapter protein TSAd, initially identified in immune cells, was previously found to interact with VEGFR-2 by binding to Y951 via its central SH2-domain in a yeast-two hybrid screen (Wu *et al.*, 2000). Y951 mediated complex formation of TSAd with VEGFR-2 was found to be essential for VEGF-induced actin reorganization and migration but did not affect VEGF mitogenicity (Matsumoto *et al.*, 2005). In this project we were interested in characterizing the interaction between TSAd and VEGFR-2 *in vitro* to gain insight into the binding mode and the structural requirements using low and high-resolution methods. The human KID sequence differs from the murine sequence in three amino acids and we therefore expected no problems using murine TSAd with the human receptor. Initial expression trials of recombinant murine TSAd performed in *E.Coli* were not successful and resulted in inclusion bodies with aggregated protein. Eukaryotic protein expression in Sf21 insect cells finally yielded amounts in the range of milligrams of murine full-length TSAd. However, expression of TSAd is challenging also in insect cells. The tedious purification procedure of TSAd and co-purified HSC70 heat shock protein hinted at the presence of potentially unfolded protein. Nevertheless, it was possible to purify temporarily stable TSAd protein to perform biophysical measurements. We verified that murine TSAd is able to bind to human VEGFR-2 KD *in vitro* through its central SH2-domain. We further demonstrated that binding is dependent on phosphorylation at Y951 as shown in earlier *in vivo* studies (Matsumoto *et al.*, 2005). As mentioned above the human KID differs from the murine sequence in three amino acids C-terminal to Y951 (human): KDY_{951}VGAIP (human) vs.KDY_{949}VGELS (mouse). Sequence specificity of phosphopeptides was analyzed in a previous study using a library of phosphopeptides that were degenerate at the three positions adjacent to the phosphotyrosine (Songyang *et al.*, 1993). They found that SH2-domains of Src, Fyn, Lck, Fgr, Abl, Crk, and Nck prefered sequences with the general recognition motif pY-hydrophilic-hydrophilic-I/P whereas SH2-domains of p85, PLC-γ, and SHPTP2 prefered pY-hydrophobic-X-hydrophobic. Only very few SH2-domains

recognized unique sequences in this assay. The exceptions are the SH2-domains of Src, Fyn, Lck, and Fgr that belong to the Src subfamily. They all recognized the sequence pY-E-E-I. The KID of VEGFR-2 contains a hydrophobic V at position +1, G at position +2 and A in the +3 position (human) therefore matching the binding mode of the p85 subgroup. It has previously been discussed that the SH2-domain of TSAd may have a unique structure since the amino acid sequence of the domain is quite different from SH2-domains of other proteins and only shares limited homology with SH2-domains of PLC-γ, corkscrew (protein tyrosine phosphatase), LNK (cytosolic protein tyrosine kinase) and c-Src. Using a yeast-two hybrid system Wu et al. demonstrated that the isolated SH2-domain of TSAd by itself was not able to bind VEGFR-2 (Wu *et al.*, 2000). The same applies for the isolated N- and C-terminal domains of TSAd. SH2-domain-mediated binding of TSAd to VEGFR-2 KD may therefore be influenced by N- and C-terminal domains of TSAd. We found that the isolated SH2-domain of TSAd was highly unstable as shown in our expression trials of the isolated SH2-domain constructs, which gave rise to insoluble protein. Purification of SH2-domain proteins was solely possible in the presence of detergents (Appendix). High-resolution structures of TSAd bound to its phosphopeptide substrate or one of its interaction partners may be required to define the exact binding determinants.

To understand how TSAd binds to VEGFR-2 KD from a structural point of view we performed SAXS analysis of the purified complex. The p(r) function of the complex clearly deviated from the p(r) functions of the binding partners suggesting a much longer particle with multiple domains. *Ab initio* modelling of TSAD-VEGFR-2 KD complex resulted in an elongated protein with a Dmax of ~202 Å. Superposition of TSAd and VEGFR-2 KD on to the SAXS derived envelope of TSAd-VEGFR-2 KD complex with PyMOL software matched well when orienting the two binding partners in parallel although binding of TSAd to VEGFR-2 KD seems to distort the CD of VEGFR-2 via a conformational change. The calculated volume of the complex corresponds well to the sum of the individual volumes of TSAd and VEGFR-2 KD. We therefore conclude that pY951 mediated binding of TSAd to VEGFR-2 KD leads to an elongated shape of this signaling complex in which the binding partners orient in a parallel orientation. Up to now, sample quality was not satisfying enough to further study the complex structure. Hence, measurements must be repeated in order

to verify these results. High resolution structural data of the complex will remain the final goal to decipher the binding mode and orientation of the binding partners.

9. Conclusion

VEGFRs and their ligands are key players in both physiological and pathological angiogenesis and vasculogenesis. VEGFR-2 represents the prevailing receptor engaging angiogenic and vasculogenic signaling pathways induced by VEGFs. Hence, VEGFR-2 is a clinically very attractive and validated target for drug development. Mechanistic studies giving new insights into the receptor activation mechanism are therefore important to find new targeting sites for the development of novel pharmaceutical compounds. We were able to verify and expand previous studies made by our own lab (Dell'Era Dosch and Ballmer-Hofer, 2009a). The introduction of glutamic acid residue into the wt-TMD of VEGFR-2 gave rise to either activate or inactive receptor variants. These findings proved that receptor dimerization is necessary but not sufficient for receptor kinase activation. Moreover, we were able to visualize the conformational changes in the TMD of VEGFR-2 induced by activating glutamic acid residues using high-resolution structural biology methods. We identified TMD conformations presumably important for receptor activation. In the course of this project we also showed that the ECD of VEGFR-2 plays an essential role maintaining the receptor in the inactive state in the absence of ligand. Furthermore, the ECD promotes the correct TMD conformation during the activation process, which culminates in the proper orientation of the intracellular kinase domains leading to receptor activation.

In a second project, we aimed at elucidating the role of specific individual kinase subdomains such as the KID and the CD in VEGFR-2 activation based on previously reported data for related RTKs (Niu *et al.*, 2002; Shewchuk *et al.*, 2000b; Sturk *et al.*, 2009). We also studied the role of distinct tyrosine residues as targets of autophosphorylation. In this study we discovered that the KID and a particular tyrosine residue located within the KID at position 951 regulate phosphorylation of another canonical downstream tyrosine residue at position 1175, which regulates the activation of downstream signaling pathways. In addition, we were able to verify these results with biochemical data of the soluble kinase domain. From these findings we conclude that VEGFR-2 follows a well-ordered activation sequence orchestrated by stepwise phosphorylation of a series of tyrosine residues located in the various subdomains of the kinase. Furthermore, we found that the CD of VEGFR-2 is able to autoinhibit the receptor in the absence of ligand since its deletion leads to

constitutive, ligand-independent activation of VEGFR-2. Our structural studies support this finding. Low-resolution structural analysis of the activated compared to the inactivated KD reveals significant conformational rearrangement. We showed that the active kinase adopts an elongated open conformation whereas the inactive state adopts a compact globular conformation with the CD blocking the catalytic site of the KD as previously found for the Tie-2 receptor (Shewchuk *et al.*, 2000b).

In a third project we looked at the *in vitro* interaction between TSAd and active VEGFR-2. We demonstrated that TSAd binds to pY951 of VEGFR-2 *in vitro* via its central SH2-domain as previously proposed by cell biological studies (Matsumoto *et al.*, 2005). Furthermore, we were able to structurally characterize the TSAd-VEGFR-2 KD complex as well as the individual proteins using low-resolution structural analysis. Isolated TSAd adopts a symmetrical conformation with a large central globular domain, presumably corresponding to its SH2-domain as predicted from secondary structure analysis. Structural analysis of the TSAd-VEGFR-2 complex showed an elongated signaling complex in which the binding partners orient in a mostly parallel orientation.

10. Appendix

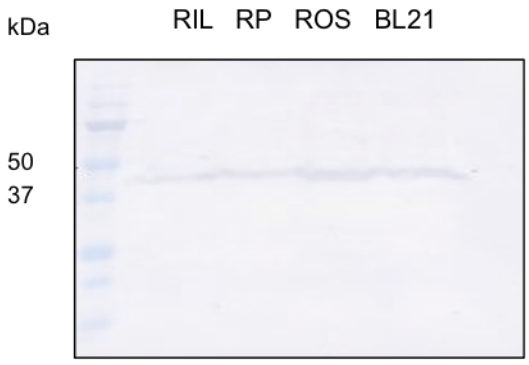

Figure 48: Expression of murine TSAd (42 kDa) in *E. Coli via* autoinduction
Murine TSAd was cloned into pET 15b-vector and expressed in different *E.Coli* strains (indicated) via autoinduction. Expression of TSAd was monitored on immunoblots using an antibody against the His-tag.

A

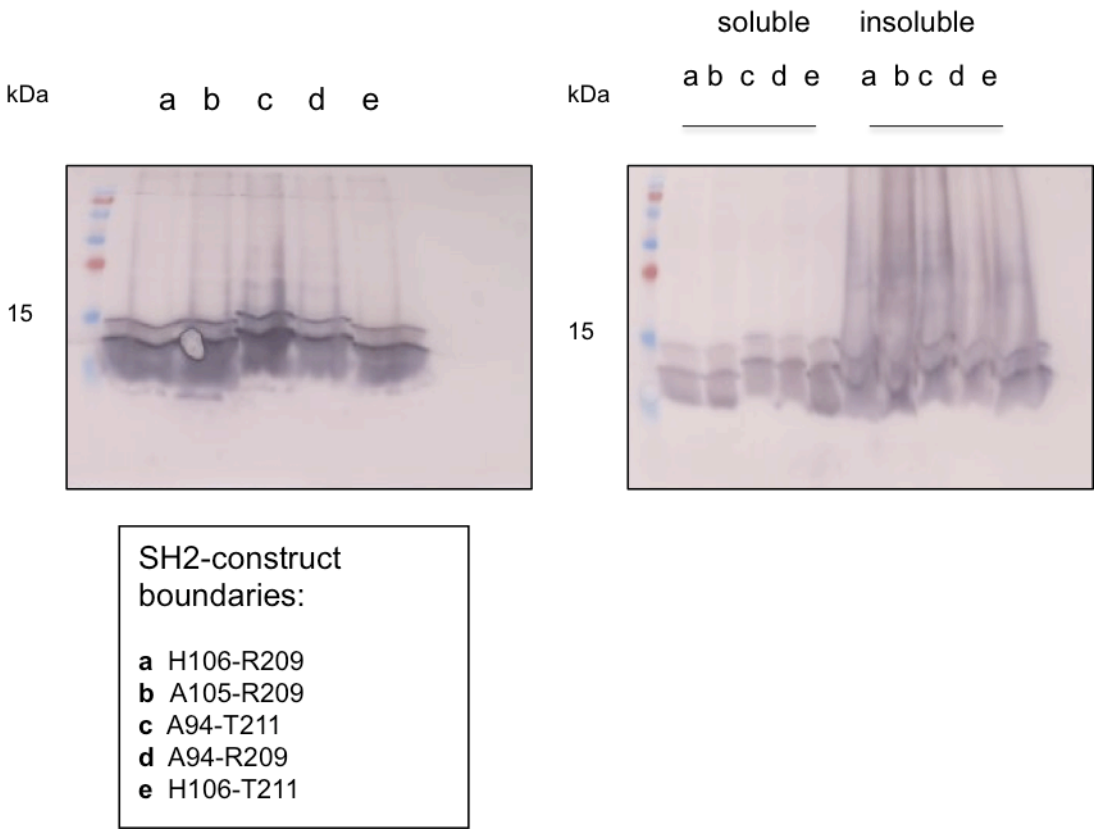

B

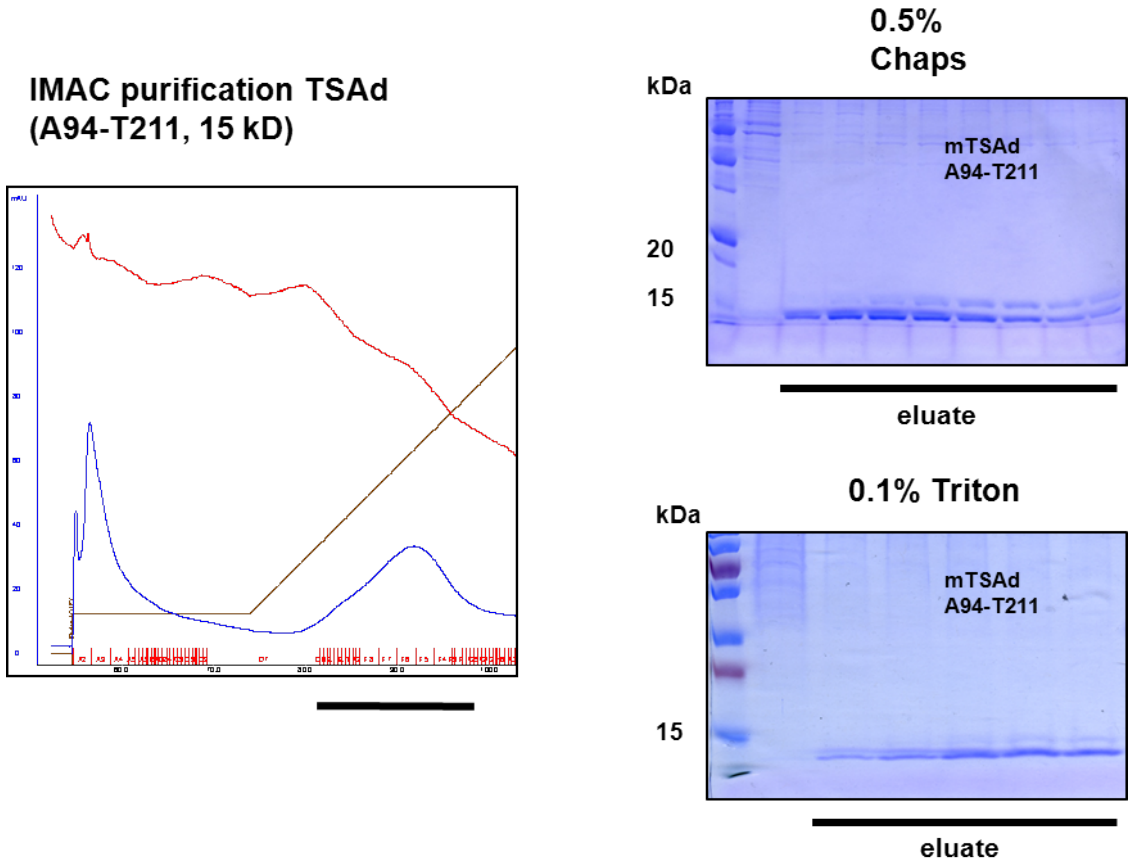

Figure 49: Expression and purification of SH2-domain of murine TSAd in Sf21 insect cells
(A) The soluble and insoluble fraction of baculovirus infected cells were analyzed for their recombinant proteins on immunoblots using an antibody against the His-tag (construct boundaries are indicated). (B) IMAC purification of SH2-domain construct A94-T211 in presence of either 0.5% Chaps or 0.1% Triton.

Construct	Tag	Cleavage Site	Expression (Sf21)	Pattern	*In vitro* phos	*In vitro* dephos	Tag Removal
VEGFR-2 KD	+	TEV	+	1 band	+	-	-
VEGFR-2 K868M KD	+	TEV	+	1 band	+	-	-
VEGFR-2 ΔKID KD	+	TEV	+	1 band	+	-	-
VEGFR-2 ΔC KD (Y1175)	+	TEV	+	2 bands	+	-	-
VEGFR-2 ΔJMD KD	+	TEV	+	1 band	+	-	-
VEGFR-2 ΔJMDΔC (1214) KD	+	TEV	+	2 bands	+	-	-
VEGFR-2 +JMD (GELK) ΔKIDΔC KD (Y1175)	+	TEV	+	1 band	+	-	-
VEGFR-2 +JMD (TGYL) ΔKIDΔC KD (Y1175)	+	TEV	+	1 band	+	-	-

Table 15: VEGFR-2 KD constructs used for crystallization trials
All VEGFR-2 constructs were screened at several concentrations ranging from 5 mg/mL-15 mg/mL. All proteins (except of VEGFR-2 K868M KD) were initially *in vitro* phosphorylated to fully activate the kinase. The His-tag was not removed for crystallization. Screens used for the assessment of crystal growth: pHClear I and II (determination of optimal concentration), JCSG core suite, Classics, PEG suite and $AmSO_4$ suite.

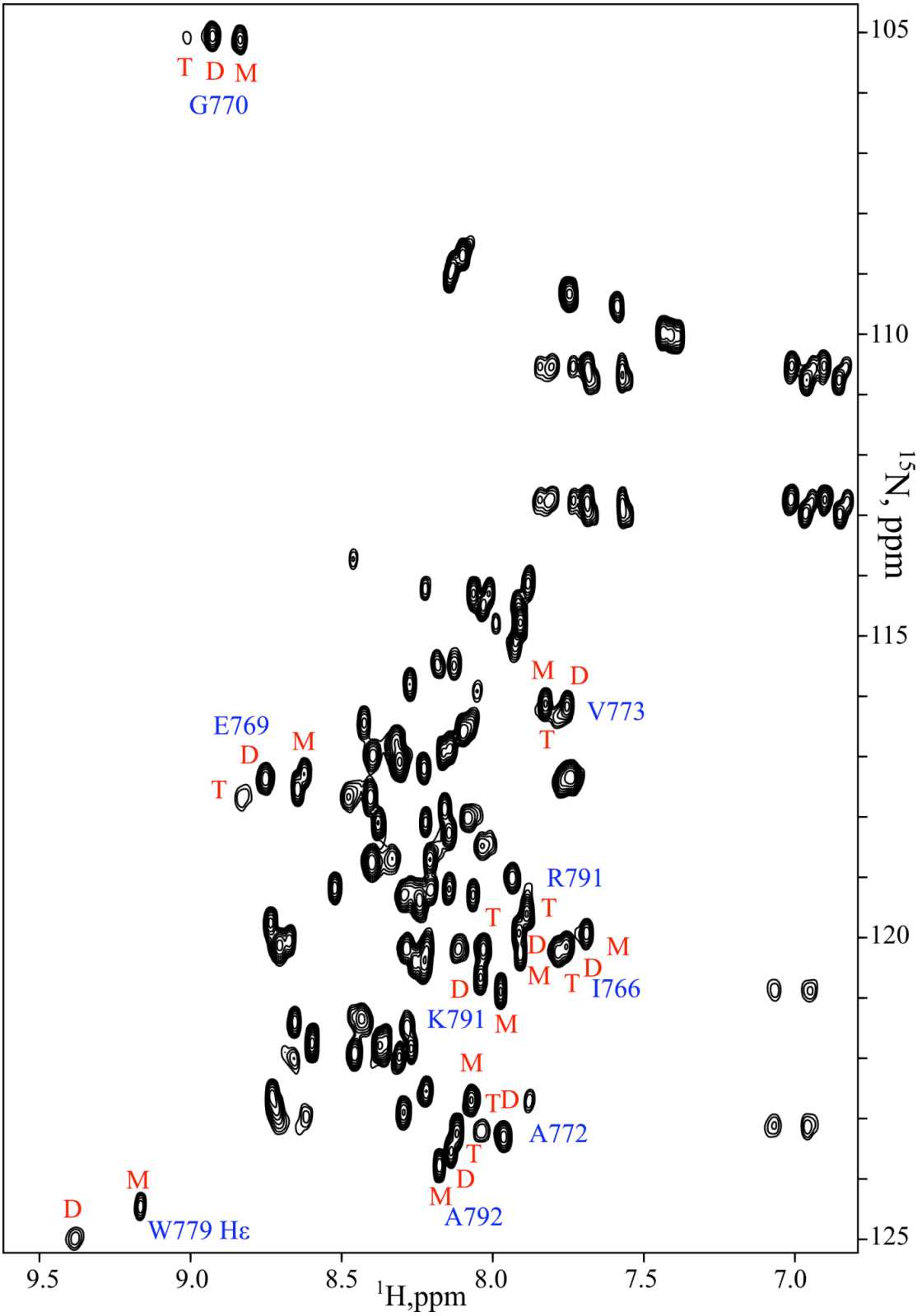

Figure 50: ^{1}H, ^{15}N-TROESY-HSQC spectrum of V769E-TMD
Conditions: Lipid / protein ratio was 800:1, pH 4.5, 318K. The Assignment of signals to amino acid residues and the oligomeric state is indicated.

NMR Distance & Dihedral Restraints		
TMD domain	wt	mutant
Total unambiguous NOE restraints	418	606
intra-residue	98	150
inter-residue	302	435
sequential (|i-j|=1)	138	150
medium-range (1<|i-j|≤4)	164	285
long-range (|i-j|>4)	0	0
inter-monomeric	18	21
Hydrogen bond restraints (upper / lower)	162/162	243/243
Total torsion angle restraints	136	204
backbone φ	62	93
backbone ψ	62	93
side chain χ^1	12	18
side chain χ^2	0	0
Structure calculation statistics		
CYANA target function (Å^2)	1.2 ± 0.2	0.5 ± 0.1
Restraint violations		
distance (>0.2 Å)	2	3
distance (>0.3 Å)	0	0
dihedral (>5)^o)	0	0
Average pairwise r.m.s.d. (Å)		
α-helical region $(761\text{-}794)_2/(761\text{-}794)_3$		
backbone atoms	0.24 ± 0.08	1.5 ± 0.5
all heavy atoms	0.74 ± 0.12	2.0 ± 0.4
Ramachandran analysis [a]		
% residues in most favored regions	100.0	87.9
% residues in additional allowed regions	0	12.1
% residues in generously allowed regions	0	0
% residues in disallowed regions	0	0
Helix-helix packing		
Contact surface area per monomer in pair of interacting helices (Å^2)	613 ± 20	340 ± 10
Angle *θ* between the helix axes (deg.)	25 ± 1	-50 ± 5
Distance *d* between the helix axes (Å)	9.2 ± 0.2	9.5 ± 0.5

Table 16: Statistics of ensemble of 10 best NMR structures of wt-TMD and V769E-TMD of VEGFR-2

11. Publications

11.1. Manuscripts in preparation

I. An analysis of specific VEGFR-2 kinase subdomains required for activation and downstream signaling of the receptor.

II. Receptor kinase activation by dimerization-promoting transmembrane domains of VEGF receptor 2; a functional and structural study.

12. Acknowledgment

My special thanks go to Prof. Dr. Kurt Ballmer-Hofer for giving me the opportunity to conclude a PhD in his research group. His insatiable fascination for scientific questions always motivated and pushed me to address new scientific challenges throughout the entire thesis. I enjoyed this collaboration very much.

My thanks go to my PhD thesis committee: Prof. Dr. Britta Engelhardt and Dr. Guido Capitani for their precious inputs during our meetings. It was a great pleasure to learn and profit from their big knowledge and experience.

I thank Kaisa Kisko for introducing me to Small Angle X-ray Scattering. Thanks go to Dimitry Veprintsev for introducing me to Analytical Ultracentrifugation. I would like to thank Rolf Jaussi for his valuable advices in molecular biology.

My thanks go to all present and former members of BMR and especially the MCB group for always providing an inspiring atmosphere: Alexandra Giese, Katharina Gegenschatz, Edward Stuttfeld, Thomas Schleier, Sandra Markovich-Müller Andrijana Kriz, Carolyne Hyde, Debora Dosch, Andreas Gsell, Aline Borer, Mayanka Asthana, Maysam Mansouri, Dragana Avramovic, Aurélien Risk, Philipp Berger, Ulla Suter and Antonietta Gasperina.

Last I thank my family and Evelyne Brun for their great support during the years.

13. Curriculum Vitae

PERSONAL DETAILS

Name: Sandro Manni

Address: Bümplizstrasse 28, 3027 Bern

Tel: +41 79 687 85 69

Email: s.manni@gmx.ch

Date of birth: 06.11.1978

Nationality: Italy, permit C

EDUCATION AND EXPERIENCE

2008 - 2013 ***PhD in Biochemistry***
Paul Scherrer Institute, Villigen
Swiss Federal Institute of Technology (ETH)

Thesis: "*Structural and functional characterization of the intracellular kinase domain of VEGFR-2"*

2006 - 2008 ***MSc in Molecular Life Science***
University of Berne, Theodor Kocher Institut (TKI)

Thesis: "*Characterization of protein-protein interaction of ICAM-1 with putative cytoplasmic interaction partner"*

2006 ***Lab Co-Worker***
F. Hoffman-La Roche AG Basel
Division Pharma, PRBD-E, Molecular Structure Research

2003 - 2006 ***BSc in Biochemistry and Molecular Biology***
University of Berne, Department of Chemistry and Biochemistry (DCB)

Thesis: *"Stereoselective synthesis of Furo[3,4-c]pyranons via a intramolecular hetero-Diels Alder reaction for the development of a QSAR-study in human cancer cells"*

2001 ***Federal University Entrance Qualification, Type C***
Focus: mathematics and physics

14. References

Aase,K. *et al.* (2001). Vascular endothelial growth factor-B-deficient mice display an atrial conduction defect. Circulation *104*, 358-364.

Abedi,H. and Zachary,I. (1997). Vascular endothelial growth factor stimulates tyrosine phosphorylation and recruitment to new focal adhesions of focal adhesion kinase and paxillin in endothelial cells. J. Biol. Chem. *272*, 15442-15451.

Albuquerque,R.J. *et al.* (2009). Alternatively spliced vascular endothelial growth factor receptor-2 is an essential endogenous inhibitor of lymphatic vessel growth. Nat Med *15*, 1023-1030.

Autiero,M., Luttun,A., Tjwa,M., and Carmeliet,P. (2003). Placental growth factor and its receptor, vascular endothelial growth factor receptor-1: novel targets for stimulation of ischemic tissue revascularization and inhibition of angiogenic and inflammatory disorders. J. Thromb. Haemost. *1*, 1356-1370.

Bae,J.H., Boggon,T.J., Tome,F., Mandiyan,V., Lax,I., and Schlessinger,J. (2010). Asymmetric receptor contact is required for tyrosine autophosphorylation of fibroblast growth factor receptor in living cells. Proc. Natl. Acad. Sci. U. S. A *107*, 2866-2871.

Bae,J.H. and Schlessinger,J. (2010). Asymmetric tyrosine kinase arrangements in activation or autophosphorylation of receptor tyrosine kinases. Mol. Cells *29*, 443-448.

Baldwin,M.E., Halford,M.M., Roufail,S., Williams,R.A., Hibbs,M.L., Grail,D., Kubo,H., Stacker,S.A., and Achen,M.G. (2005). Vascular endothelial growth factor D is dispensable for development of the lymphatic system. Mol. Cell Biol. *25*, 2441-2449.

Bardelli,A., Longati,P., Williams,T.A., Benvenuti,S., and Comoglio,P.M. (1999). A peptide representing the carboxyl-terminal tail of the met receptor inhibits kinase activity and invasive growth. J. Biol. Chem. *274*, 29274-29281.

Bargmann,C.I., Hung,M.C., and Weinberg,R.A. (1986). Multiple independent activations of the neu oncogene by a point mutation altering the transmembrane domain of p185. Cell *45*, 649-657.

Bargmann,C.I. and Weinberg,R.A. (1988). Increased tyrosine kinase activity associated with the protein encoded by the activated neu oncogene. Proc. Natl. Acad. Sci. USA *85*, 5394-5398.

Barleon,B., Sozzani,S., Zhou,D., Weich,H.A., Mantovani,A., and Marmé,D. (1996). Migration of human monocytes in response to vascular endothelial growth factor (VEGF) is mediated via the VEGF receptor flt-1. Blood *87*, 3336-3343.

Bates,D.O., Cui,T.G., Doughty,J.M., Winkler,M., Sugiono,M., Shields,J.D., Peat,D., Gillatt,D., and Harper,S.J. (2002). VEGF165b, an Inhibitory Splice Variant of Vascular Endothelial Growth Factor, Is Down-Regulated in Renal Cell Carcinoma. Cancer Res. *62*, 4123-4131.

Bell,C.A., Tynan,J.A., Hart,K.C., Meyer,A.N., Robertson,S.C., and Donoghue,D.J. (2000). Rotational coupling of the transmembrane and kinase domains of the neu receptor tyrosine kinase. Mol. Biol. Cell *11*, 3589-3599.

Berger,I., Fitzgerald,D.J., and Richmond,T.J. (2004). Baculovirus expression system for heterologous multiprotein complexes. Nat. Biotechnol. *22*, 1583-1587.

Bocharov,E.V., Mineev,K.S., Volynsky,P.E., Ermolyuk,Y.S., Tkach,E.N., Sobol,A.G., Chupin,V.V., Kirpichnikov,M.P., Efremov,R.G., and Arseniev,A.S. (2008). Spatial structure of the dimeric transmembrane domain of the growth factor receptor ErbB2 presumably corresponding to the receptor active state. J. Biol. Chem. *283*, 6950-6956.

Brozzo,M.S., Bjelic,S., Kisko,K., Schleier,T., Leppanen,V.M., Alitalo,K., Winkler,F.K., and Ballmer-Hofer,K. (2012a). Thermodynamic and structural description of allosterically regulated VEGF receptor 2 dimerization. Blood *119*, 1781-1788.

Brozzo,M.S., Bjelic,S., Kisko,K., Schleier,T., Leppanen,V.M., Alitalo,K., Winkler,F.K., and Ballmer-Hofer,K. (2012b). Thermodynamic and structural description of allosterically regulated VEGF receptor 2 dimerization. Blood *119*, 1781-1788.

Carmeliet,P. *et al.* (1998). Role of HIF-1alpha in hypoxia-mediated apoptosis, cell proliferation and tumour angiogenesis. Nature *394*, 485-490.

Carmeliet,P. *et al.* (1996). Abnormal blood vessel development and lethality in embryos lacking a single VEGF allele. Nature *380*, 435-439.

Carmeliet,P. and Jain,R.K. (2000). Angiogenesis in cancer and other diseases. Nature *407*, 249-257.

Carmeliet,P. *et al.* (2001). Synergism between vascular endothelial growth factor and placental growth factor contributes to angiogenesis and plasma extravasation in pathological conditions. Nat Med *7*, 575-583.

Carmeliet,P. *et al.* (1999). Impaired myocardial angiogenesis and ischemic cardiomyopathy in mice lacking the vascular endothelial growth factor isoforms VEGF164 and VEGF188. Nat Med *5*, 495-502.

Cébe-Suarez,S., Pieren,M., Cariolato,L., Arn,S., Hoffmann,U., Bogucki,A., Manlius,C., Wood,J., and Ballmer-Hofer,K. (2006). A VEGF-A splice variant defective for heparan sulfate and neuropilin-1 binding shows attenuated signaling through VEGFR-2. Cell Mol. Life Sci. *63*, 2067-2077.

Chen,H., Ma,J., Li,W., Eliseenkova,A.V., Xu,C., Neubert,T.A., Miller,W.T., and Mohammadi,M. (2007). A molecular brake in the kinase hinge region regulates the activity of receptor tyrosine kinases. Mol. Cell *27*, 717-730.

Chen,H., Xu,C.F., Ma,J., Eliseenkova,A.V., Li,W., Pollock,P.M., Pitteloud,N., Miller,W.T., Neubert,T.A., and Mohammadi,M. (2008). A crystallographic snapshot of tyrosine trans-phosphorylation in action. Proc. Natl. Acad. Sci. USA *105*, 19660-19665.

Chen,L., Placone,J., Novicky,L., and Hristova,K. (2010). The extracellular domain of fibroblast growth factor receptor 3 inhibits ligand-independent dimerization. Sci. Signal. *3*, ra86.

Choma,C., Gratkowski,H., Lear,J.D., and DeGrado,W.F. (2000). Asparagine-mediated self-association of a model transmembrane helix. Nat. Struct. Mol. Biol. *7*, 161-166.

Cunningham,S.A., Arrate,M.P., Brock,T.A., and Waxham,M.N. (1997). Interactions of FLT-1 and KDR with phospholipase C ã: identification of the phosphotyrosine binding sites. Biochem. Biophys. Res. Commun. *240*, 635-639.

Cunningham,S.A., Waxham,M.N., Arrate,P.M., and Brock,T.A. (1995). Interaction of the Flt-1 tyrosine kinase receptor with the p85 subunit of phosphatidylinositol 3-kinase. Mapping of a novel site involved in binding. J. Biol. Chem. *270*, 20254-20257.

Dayanir,V., Meyer,R.D., Lashkari,K., and Rahimi,N. (2001). Identification of tyrosine residues in vascular endothelial growth factor receptor-2/FLK-1 involved in activation of phosphatidylinositol-3 kinase and cell proliferation. J. Biol. Chem. *276*, 17686-17692.

Dell'Era Dosch,D. and Ballmer-Hofer,K. (2009a). Transmembrane domain-mediated orientation of receptor monomers in active VEGFR-2 dimers. FASEB J. *24*, 32-38.

Dell'Era Dosch,D. and Ballmer-Hofer,K. (2009b). Transmembrane domain-mediated orientation of receptor monomers in active VEGFR-2 dimers. FASEB J. *24*, 32-38.

Dixelius,J., Makinen,T., Wirzenius,M., Karkkainen,M., Wernstedt,C., Alitalo,K., and Claesson-Welsh,L. (2003). Ligand-induced vascular endothelial growth factor receptor-3 (VEGFR-3) heterodimerization with VEGFR-2 in primary lymphatic endothelial cells regulates tyrosine phosphorylation sites. J. Biol. Chem. *278*, 40973-40979.

Dougher Vermazen,M., Hulmes,J.D., Bohlen,P., and Terman,B.I. (1994). Biological activity and phosphorylation sites of the bacterially expressed cytosolic domain of the KDR VEGF-receptor. Biochem. Biophys. Res. Commun. *205*, 728-738.

Dumont,D.J., Jussila,L., Taipale,J., Lymboussaki,A., Mustonen,T., Pajusola,K., Breitman,M., and Alitalo,K. (1998). Cardiovascular failure in mouse embryos deficient in VEGF receptor-3. Science *282*, 946-949.

Ebos,J.M., Bocci,G., Man,S., Thorpe,P.E., Hicklin,D.J., Zhou,D., Jia,X., and Kerbel,R.S. (2004). A naturally occurring soluble form of vascular endothelial growth factor receptor 2 detected in mouse and human plasma. Mol. Cancer Res. *2*, 315-326.

Endres,N.F. *et al.* (2013). Conformational Coupling across the Plasma Membrane in Activation of the EGF Receptor. Cell *152*, 543-556.

Ferrara,N., Carver Moore,K., Chen,H., Dowd,M., Lu,L., O Shea,K.S., Powell,B.L., Hillan,K.J., and Moore,M.W. (1996). Heterozygous embryonic lethality induced by targeted inactivation of the VEGF gene. Nature *380*, 439-442.

Ferrara,N. and Davis-Smyth,T. (1997). The biology of vascular endothelial growth factor. Endocr. Rev. *18*, 4-25.

Ferrara,N. and Kerbel,R.S. (2005). Angiogenesis as a therapeutic target. Nature *438*, 967-974.

Finger,C., Escher,C., and Schneider,D. (2009a). The single transmembrane domains of human receptor tyrosine kinases encode self-interactions. Sci Signal. *2*, ra56.

Finger,C., Escher,C., and Schneider,D. (2009b). The single transmembrane domains of human receptor tyrosine kinases encode self-interactions. Sci Signal. *2*, ra56.

Fitzgerald,D.J., Berger,P., Schaffitzel,C., Yamada,K., Richmond,T.J., and Berger,I. (2006). Protein complex expression by using multigene baculoviral vectors. Nat. Methods *3*, 1021-1032.

Folkman,J. (1971). Tumor angiogenesis: therapeutic implications. N. Engl. J. Med. *285*, 1182-1186.

Fong,G.H., Rossant,J., Gertsenstein,M., and Breitman,M.L. (1995). Role of the Flt-1 receptor tyrosine kinase in regulating the assembly of vascular endothelium. Nature *376*, 66-70.

Fong,G.H., Zhang,L., Bryce,D.M., and Peng,J. (1999). Increased hemangioblast commitment, not vascular disorganization, is the primary defect in flt-1 knock-out mice. Development *126*, 3015-3025.

Fuh,G., Li,B., Crowley,C., Cunningham,B., and Wells,J.A. (1998). Requirements for binding and signaling of the kinase domain receptor for vascular endothelial growth factor. J. Biol. Chem. *273*, 11197-11204.

Fujio,Y. and Walsh,K. (1999). Akt mediates cytoprotection of endothelial cells by vascular endothelial growth factor in an anchorage-dependent manner. J. Biol. Chem. *274*, 16349-16354.

Fukumura,D. *et al.* (1998). Tumor induction of VEGF promoter activity in stromal cells. Cell *94*, 715-725.

Furdui,C.M., Lew,E.D., Schlessinger,J., and Anderson,K.S. (2006). Autophosphorylation of FGFR1 kinase is mediated by a sequential and precisely ordered reaction. Mol. Cell *21*, 711-717.

Gerber,D., Sal-Man,N., and Shai,Y. (2004). Two motifs within a transmembrane domain, one for homodimerization and the other for heterodimerization. J. Biol. Chem. *279*, 21177-21182.

Gratkowski,H., Lear,J.D., and DeGrado,W.F. (2001). Polar side chains drive the association of model transmembrane peptides. Proc. Natl. Acad. Sci. USA *98*, 880-885.

Griffith,J., Black,J., Faerman,C., Swenson,L., Wynn,M., Lu,F., Lippke,J., and Saxena,K. (2004). The structural basis for autoinhibition of FLT3 by the juxtamembrane domain. Mol. Cell *13*, 169-178.

Grünewald,F.S., Prota,A.E., Giese,A., and Ballmer-Hofer,K. (2010). Structure-function analysis of VEGF receptor activation and the role of coreceptors in angiogenic signaling. Biochim. Biophys. Acta *1804*, 567-580.

Guentert,P. Automated NMR protein structure calculation. Progress in Nuclear Magnetic Resonance Spectroscopy 43, 105-125. 2003.
Ref Type: Journal (Full)

Gullick,W.J., Bottomley,A.C., Lofts,F.J., Doak,D.G., Mulvey,D., Newman,R., Crumpton,M.J., Sternberg,M.J., and Campbell,I.D. (1992). Three dimensional structure of the transmembrane region of the proto-oncogenic and oncogenic forms of the neu protein. EMBO J. *11*, 43-48.

Hanahan,D. and Folkman,J. (1996). Patterns and Emerging Mechanisms of the Angiogenic Switch during Tumorigenesis. Cell *86*, 353-364.

Hattori,K. *et al.* (2002). Placental growth factor reconstitutes hematopoiesis by recruiting VEGFR1(+) stem cells from bone-marrow microenvironment. Nat Med *8*, 841-849.

Heidaran,M.A., Pierce,J.H., Lombardi,D., Ruggiero,M., Gutkind,J.S., Matsui,T., and Aaronson,S.A. (1991). Deletion or substitution within the alpha platelet-derived growth factor receptor kinase insert domain: effects on functional coupling with intracellular signaling pathways. Mol. Cell Biol *11*, 134-142.

Hellstrom,M., Gerhardt,H., Kalen,M., Li,X., Eriksson,U., Wolburg,H., and Betsholtz,C. (2001). Lack of pericytes leads to endothelial hyperplasia and abnormal vascular morphogenesis. J. Cell Biol. *153*, 543-554.

Helmlinger,G., Endo,M., Ferrara,N., Hlatky,L., and Jain,R.K. (2000). Formation of endothelial cell networks. Nature *405*, 139-141.

Hiratsuka,S., Maru,Y., Okada,A., Seiki,M., Noda,T., and Shibuya,M. (2001). Involvement of Flt-1 tyrosine kinase (vascular endothelial growth factor receptor-1) in pathological angiogenesis. Cancer Res. *61*, 1207-1213.

Hiratsuka,S., Minowa,O., Kuno,J., Noda,T., and Shibuya,M. (1998). Flt-1 lacking the tyrosine kinase domain is sufficient for normal development and angiogenesis in mice. Proc. Natl. Acad. Sci. USA *95*, 9349-9354.

Hiratsuka,S., Nakao,K., Nakamura,K., Katsuki,M., Maru,Y., and Shibuya,M. (2005). Membrane fixation of vascular endothelial growth factor receptor 1 ligand-binding domain is important for vasculogenesis and angiogenesis in mice. Mol. Cell Biol. *25*, 346-354.

Holash,J., Maisonpierre,P.C., Compton,D., Boland,P., Alexander,C.R., Zagzag,D., Yancopoulos,G.D., and Wiegand,S.J. (1999a). Vessel cooption, regression, and growth in tumors mediated by angiopoietins and VEGF. Science *284*, 1994-1998.

Holash,J., Wiegand,S.J., and Yancopoulos,G.D. (1999b). New model of tumor angiogenesis: dynamic balance between vessel regression and growth mediated by angiopoietins and VEGF. Oncogene *18*, 5356-5362.

Holmqvist,K., Cross,M.J., Rolny,C., Hägerkvist,R., Rahimi,N., Matsumoto,T., Claesson-Welsh,L., and Welsh,M. (2004). The adaptor protein Shb binds to tyrosine 1175 in the Vascular Endothelial Growth Factor (VEGF) Receptor-2 and regulates VEGF-dependent cellular migration. J. Biol. Chem. *279*, 22267-22275.

Huang,T.C., Blanton,T.N., and Wu,Y. (1993). X-ray-powder diffraction analysis of silver behenate, a possible low-angle diffraction standard. J. Appl. Crystallogr. *26*, 180-184.

Hubbard,S.R. (1997). Crystal structure of the activated insulin receptor tyrosine kinase in complex with peptide substrate and ATP analog. EMBO J. *16*, 5572-5581.

Hubbard,S.R. (2004). Juxtamembrane autoinhibition in receptor tyrosine kinases. Nat. Rev. Mol. Cell Biol. *5*, 464-471.

Huse,M. and Kuriyan,J. (2002). The conformational plasticity of protein kinases. Cell *109*, 275-282.

Hyder,S.M. and Stancel,G.M. (1999). Regulation of angiogenic growth factors in the female reproductive tract by estrogens and progestins. Mol. Endocrinol. *13*, 806-811.

Jain,R.K. and Munn,L.L. (2000). Leaky vessels? Call Ang1! Nat Med *6*, 131-132.

Johnson,L.N., Noble,M.E.M., and Owen,D.J. (1996). Active and Inactive Protein Kinases: Structural Basis for Regulation. Cell *85*, 149-158.

Joukov,V., Pajusola,K., Kaipainen,A., Chilov,D., Lahtinen,I., Kukk,E., Saksela,O., Kalkkinen,N., and Alitalo,K. (1996). A novel vascular endothelial growth factor, VEGF-C, is a ligand for the Flt4 (VEGFR-3) and KDR (VEGFR-2) receptor tyrosine kinases. EMBO J. *15*, 290-298.

Jura,N., Endres,N.F., Engel,K., Deindl,S., Das,R., Lamers,M.H., Wemmer,D.E., Zhang,X., and Kuriyan,J. (2009). Mechanism for activation of the EGF receptor catalytic domain by the juxtamembrane segment. Cell *137*, 1293-1307.

Kabrun,N., Buhring,H.J., Choi,K., Ullrich,A., Risau,W., and Keller,G. (1997). Flk-1 expression defines a population of early embryonic hematopoietic precursors. Development *124*, 2039-2048.

Kaipainen,A., Korhonen,J., Mustonen,T., van,H., V, Fang,G.H., Dumont,D., Breitman,M., and Alitalo,K. (1995). Expression of the fms-like tyrosine kinase 4 gene becomes restricted to lymphatic endothelium during development. Proc. Natl. Acad. Sci. USA *92*, 3566-3570.

Karkkainen,M.J. *et al.* (2003). Vascular endothelial growth factor C is required for sprouting of the first lymphatic vessels from embryonic veins. Nat Immunol *5*, 74-80.

Kazlauskas,A. and Cooper,J.A. (1989). Autophosphorylation of the PDGF receptor in the kinase insert region regulates interactions with cell proteins. Cell *58*, 1121-1133.

Kendall,R.L., Rutledge,R.Z., Mao,X., Tebben,A.J., Hungate,R.W., and Thomas,K. (1999). Vascular endothelial growth factor receptor KDR tyrosine kinase activity is

increased by autophosphorylation of two activation loop tyrosine residues. J. Biol. Chem. *274*, 6453-6460.

Keyt,B.A., Berleau,L.T., Nguyen,H.V., Chen,H., Heinsohn,H., Vandlen,R., and Ferrara,N. (1996). The carboxyl-terminal domain (111-165) of vascular endothelial growth factor is critical for its mitogenic potency. J. Biol. Chem. *271*, 7788-7795.

Koch,S. and Claesson-Welsh,L. (2012). Signal transduction by vascular endothelial growth factor receptors. Cold Spring Harb. Perspect. Med. *2*, a006502.

Kornev,A.P., Haste,N.M., Taylor,S.S., and Eyck,L.F. (2006). Surface comparison of active and inactive protein kinases identifies a conserved activation mechanism. Proc. Natl. Acad. Sci. USA *103*, 17783-17788.

Kubatzky,K.F., Ruan,W., Gurezka,R., Cohen,J., Ketteler,R., Watowich,S.S., Neumann,D., Langosch,D., and Klingmuller,U. (2001). Self assembly of the transmembrane domain promotes signal transduction through the erythropoietin receptor. Curr. Biol. *11*, 110-115.

Kukk,E., Lymboussaki,A., Taira,S., Kaipainen,A., Jeltsch,M., Joukov,V., and Alitalo,K. (1996). VEGF-C receptor binding and pattern of expression with VEGFR-3 suggests a role in lymphatic vascular development. Development *122*, 3829-3837.

Lamalice,L., Houle,F., and Huot,J. (2006). Phosphorylation of Tyr1214 within VEGFR-2 triggers the recruitment of Nck and activation of Fyn leading to SAPK2/p38 activation and endothelial cell migration in response to VEGF. J. Biol. Chem.

Lamalice,L., Houle,F., Jourdan,G., and Huot,J. (2004). Phosphorylation of tyrosine 1214 on VEGFR2 is required for VEGF-induced activation of Cdc42 upstream of SAPK2/p38. Oncogene *23*, 434-445.

Lawson,N.D. and Weinstein,B.M. (2002). Arteries and veins: making a difference with zebrafish. Nat Rev Genet *3*, 674-682.

Lemmon,M.A., Flanagan,J.M., Hunt,J.F., Adair,B.D., Bormann,B.J., Dempsey,C.E., and Engelman,D.M. (1992). Glycophorin A dimerization is driven by specific interactions between transmembrane alpha-helices. J Biol Chem. *267*, 7683-7689.

Leppänen,V.M., Prota,A.E., Jeltsch,M., Anisimov,A., Kalkkinen,N., Strandin,T., Lankinen,H., Goldman,A., Ballmer-Hofer,K., and Alitalo,K. (2010). Structural determinants of growth factor binding and specificity by VEGF receptor 2. Proc. Natl. Acad. Sci. USA *107*, 2425-2430.

Lev,S., Givol,D., and Yarden,Y. (1992). Interkinase domain of kit contains the binding site for phosphatidylinositol 3' kinase. Proc. Natl. Acad. Sci. USA *89*, 678-682.

Li,E., You,M., and Hristova,K. (2006). FGFR3 dimer stabilization due to a single amino acid pathogenic mutation. J. Mol. Biol. *356*, 600-612.

Li,J., Zhang,Y.P., and Kirsner,R.S. (2003a). Angiogenesis in wound repair: angiogenic growth factors and the extracellular matrix. Microsc. Res. Tech. *60*, 107-114.

Li,R., Mitra,N., Gratkowski,H., Vilaire,G., Litvinov,R., Nagasami,C., Weisel,J.W., Lear,J.D., DeGrado,W.F., and Bennett,J.S. (2003b). Activation of integrin alphaIIbbeta3 by modulation of transmembrane helix associations. Science *300*, 795-798.

Li,Y., Mangasarian,K., Mansukhani,A., and Basilico,C. (1997). Activation of FGF receptors by mutations in the transmembrane domain. Oncogene *14*, 1397-1406.

Lofts,F.J., Hurst,H.C., Sternberg,M.J., and Gullick,W.J. (1993). Specific short transmembrane sequences can inhibit transformation by the mutant neu growth factor receptor in vitro and in vivo. Oncogene *8*, 2813-2820.

Ma,Y *et al.* (1999). Inhibition of spontaneous receptor phosphorylation by residues in a putative alpha-helix in the KIT intracellular juxtamembrane region. J. Biol. Chem. 274, 13399-13402.

MacKenzie,K.R., Prestegard,J.H., and Engelman,D.M. (1997). A transmembrane helix dimer: structure and implications. Science *276*, 131-133.

Maes,C., Carmeliet,P., Moermans,K., Stockmans,I., Smets,N., Collen,D., Bouillon,R., and Carmeliet,G. (2002). Impaired angiogenesis and endochondral bone formation in mice lacking the vascular endothelial growth factor isoforms VEGF(164) and VEGF(188). Mech. Dev. *111*, 61-73.

Maglione,D., Guerriero,V., Viglietto,G., Delli-Bovi,P., and Persico,M.G. (1991). Isolation of a human placenta cDNA coding for a protein related to the vascular permeability factor. Proc. Natl. Acad. Sci. USA *88*, 9267-9271.

Maglione,D., Guerriero,V., Viglietto,G., Ferraro,M.G., Aprelikova,O., Alitalo,K., Del Vecchio,S., Lei,K.J., Chou,J.Y., and Persico,M.G. (1993). Two alternative mRNAs coding for the angiogenic factor, placenta growth factor (PlGF), are transcribed from a single gene of chromosome 14. Oncogene *8*, 925-931.

Maisonpierre,P.C. *et al.* (1997). Angiopoietin-2, a natural antagonist for Tie2 that disrupts in vivo angiogenesis. Science *277*, 55-60.

Makinen,T., Olofsson,B., Karpanen,T., Hellman,U., Soker,S., Klagsbrun,M., Eriksson,U., and Alitalo,K. (1999). Differential binding of vascular endothelial growth factor B splice and proteolytic isoforms to neuropilin-1. J. Biol. Chem. *274*, 21217-21222.

Matsumoto,T. *et al.* (2005). VEGF receptor-2 Y951 signaling and a role for the adapter molecule TSAd in tumor angiogenesis. EMBO J. *24*, 2342-2353.

Matsumoto,T. and Claesson-Welsh,L. (2001). VEGF Receptor Signal Transduction. Sci. STKE *2001*, RE21.

McTigue,M.A. *et al.* (1999a). Crystal structure of the kinase domain of human vascular endothelial growth factor receptor 2: a key enzyme in angiogenesis. Structure *7*, 319-330.

McTigue,M.A. *et al.* (1999b). Crystal structure of the kinase domain of human vascular endothelial growth factor receptor 2: a key enzyme in angiogenesis. Structure *7*, 319-330.

Mendrola,J.M., Berger,M.B., King,M.C., and Lemmon,M.A. (2002). The single transmembrane domains of ErbB receptors self-associate in cell membranes. J. Biol. Chem. *277*, 4704-4712.

Meyer,R.D., Dayanir,V., Majnoun,F., and Rahimi,N. (2002). The presence of a single tyrosine residue at the carboxyl domain of vascular endothelial growth factor receptor-2/FLK-1 regulates its autophosphorylation and activation of signaling molecules. J. Biol. Chem. *277*, 27081-27087.

Meyer,R.D., Mohammadi,M., and Rahimi,N. (2006). A single amino acid substitution in the activation loop defines the decoy characteristic of VEGFR-1/FLT-1. J. Biol. Chem. *281*, 867-875.

Meyer,R.D., Singh,A.J., and Rahimi,N. (2003). The carboxyl terminus controls ligand-dependent activation of VEGFR-2 and its signaling. J. Biol. Chem. *279*, 735-742.

Mineev,K.S., Bocharov,E.V., Pustovalova,Y.E., Bocharova,O.V., Chupin,V.V., and Arseniev,A.S. (2010). Spatial structure of the transmembrane domain heterodimer of ErbB1 and ErbB2 receptor tyrosine kinases. J. Mol. Biol. *400*, 231-243.

Mohammadi,M., McMahon,G., Sun,L., Tang,C., Hirth,P., Yeh,B.K., Hubbard,S.R., and Schlessinger,J. (1997). Structures of the tyrosine kinase domain of fibroblast growth factor receptor in complex with inhibitors. Science *276*, 955-960.

Mol,C.D., Dougan,D.R., Schneider,T.R., Skene,R.J., Kraus,M.L., Scheibe,D.N., Snell,G.P., Zou,H., Sang,B.C., and Wilson,K.P. (2004). Structural basis for the autoinhibition and STI-571 inhibition of c-Kit tyrosine kinase. J. Biol. Chem. *279*, 31655-31663.

Mol,C.D., Lim,K.B., Sridhar,V., Zou,H., Chien,E.Y., Sang,B.C., Nowakowski,J., Kassel,D.B., Cronin,C.N., and McRee,D.E. (2003). Structure of a c-kit product complex reveals the basis for kinase transactivation. J. Biol. Chem. *278*, 31461-31464.

Mould,A.W., Tonks,I.D., Cahill,M.M., Pettit,A.R., Thomas,R., Hayward,N.K., and Kay,G.F. (2003). Vegfb gene knockout mice display reduced pathology and synovial angiogenesis in both antigen-induced and collagen-induced models of arthritis. Arthritis Rheum. *48*, 2660-2669.

Nilsson,I. *et al.* (2010). VEGF receptor 2/-3 heterodimers detected in situ by proximity ligation on angiogenic sprouts. EMBO J. *29*, 1377-1388.

Niu,X.L., Peters,K.G., and Kontos,C.D. (2002). Deletion of the carboxy-terminus of Tie2 enhances kinase activity, signaling, and function: Evidence for an autoinhibitory mechanism. J. Biol. Chem. *277*, 31768-31773.

Nowak,D.G., Woolard,J., Amin,E.M., Konopatskaya,O., Saleem,M.A., Churchill,A.J., Ladomery,M.R., Harper,S.J., and Bates,D.O. (2008). Expression of pro- and anti-

angiogenic isoforms of VEGF is differentially regulated by splicing and growth factors. J. Cell Sci. *121*, 3487-3495.

Oliver,G. and Detmar,M. (2002). The rediscovery of the lymphatic system: old and new insights into the development and biological function of the lymphatic vasculature. Genes Dev. *16*, 773-783.

Olofsson,B., Pajusola,K., Kaipainen,A., von Euler,G., Joukov,V., Saksela,O., Orpana,A., Pettersson,R.F., Alitalo,K., and Eriksson,U. (1996a). Vascular endothelial growth factor B, a novel growth factor for endothelial cells. Proc. Natl. Acad. Sci. USA *93*, 2576-2581.

Olofsson,B., Pajusola,K., von Euler,G., Chilov,D., Alitalo,K., and Eriksson,U. (1996b). Genomic organization of the mouse and human genes for vascular endothelial growth factor B (VEGF-B) and characterization of a second splice isoform. J. Biol. Chem. *271*, 19310-19317.

Olsson,A.K., Dimberg,A., Kreuger,J., and Claesson-Welsh,L. (2006). VEGF receptor signalling - in control of vascular function. Nat. Rev. Mol. Cell Biol. *7*, 359-371.

Park,J.E., Chen,H.H., Winer,J., Houck,K.A., and Ferrara,N. (1994). Placenta growth factor. Potentiation of vascular endothelial growth factor bioactivity, in vitro and in vivo, and high affinity binding to Flt-1 but not to Flk-1/KDR. J. Biol. Chem. *269*, 25646-25654.

Pepper,M.S. (1997). Transforming growth factor-beta: vasculogenesis, angiogenesis, and vessel wall integrity. Cytokine Growth Factor Rev. *8*, 21-43.

Pepper,M.S. (2001). Lymphangiogenesis and tumor metastasis: myth or reality? Clin. Cancer Res. *7*, 462-468.

Perrin,R., Konopatskaya,O., Qiu,Y., Harper,S., Bates,D., and Churchill,A. (2005). Diabetic retinopathy is associated with a switch in splicing from anti- to pro-angiogenic isoforms of vascular endothelial growth factor. Diabetologia *48*, 2422-2427.

Persico,M.G., Vincenti,V., and DiPalma,T. (1999). Structure, expression and receptor-binding properties of placenta growth factor (PlGF). Curr. Top. Microbiol. Immunol. *237*, 31-40.

Petoukhov,M.V., Konarev,P.V., Kikhney,A.G., and Svergun,D.I. (2007a). ATSAS 2.1 - towards automated and web-supported small-angle scattering data analysis. J. Appl. Cryst. *40*, s223-s228.

Petoukhov,M.V., Konarev,P.V., Kikhney,A.G., and Svergun,D.I. (2007b). ATSAS 2.1 - towards automated and web-supported small-angle scattering data analysis. J. Appl. Cryst. *40*, s223-s228.

Poltorak,Z., Cohen,T., and Neufeld,G. (2000). The VEGF splice variants: properties, receptors, and usage for the treatment of ischemic diseases. Herz *25*, 126-129.

Poltorak,Z., Cohen,T., Sivan,R., Kandelis,Y., Spira,G., Vlodavsky,I., Keshet,E., and Neufeld,G. (1997). VEGF145, a secreted vascular endothelial growth factor isoform that binds to extracellular matrix. J. Biol. Chem. *272*, 7151-7158.

Pritchard-Jones,R.O., Dunn,D.B., Qiu,Y., Varey,A.H., Orlando,A., Rigby,H., Harper,S.J., and Bates,D.O. (2007). Expression of VEGFxxxb, the inhibitory isoforms of VEGF, in malignant melanoma. Br. J. Cancer *97*, 223-230.

Risau,W. (1997). Mechanisms of angiogenesis. Nature *386*, 671-674.

Ruan,W., Becker,V., Klingmuller,U., and Langosch,D. (2004). The interface between self-assembling erythropoietin receptor transmembrane segments corresponds to a membrane-spanning leucine zipper. J. Biol. Chem. *279*, 3273-3279.

Ruch,C., Skiniotis,G., Steinmetz,M.O., Walz,T., and Ballmer-Hofer,K. (2007). Structure of a VEGF-VEGF receptor complex determined by electron microscopy. Nat. Struct. Mol. Biol. *14*, 249-250.

Sakurai,Y., Ohgimoto,K., Kataoka,Y., Yoshida,N., and Shibuya,M. (2005). Essential role of Flk-1 (VEGF receptor 2) tyrosine residue 1173 in vasculogenesis in mice. Proc. Natl. Acad. Sci. USA *102*, 1076-1081.

Salven,P., Lymboussaki,A., Heikkila,P., Jaaskela,S.H., Enholm,B., Aase,K., von,E.G., Eriksson,U., Alitalo,K., and Joensuu,H. (1998). Vascular endothelial growth factors VEGF-B and VEGF-C are expressed in human tumors. Am. J. Pathol. *153*, 103-108.

Sato,T.N., Tozawa,Y., Deutsch,U., Wolburg Buchholz,K., Fujiwara,Y., Gendron Maguire,M., Gridley,T., Wolburg,H., Risau,W., and Qin,Y. (1995). Distinct roles of the receptor tyrosine kinases Tie-1 and Tie-2 in blood vessel formation. Nature *376*, 70-74.

Sawamiphak,S., Seidel,S., Essmann,C.L., Wilkinson,G.A., Pitulescu,M.E., Acker,T., and Acker-Palmer,A. (2010). Ephrin-B2 regulates VEGFR2 function in developmental and tumour angiogenesis. Nature *465*, 487-491.

Sawano,A., Iwai,S., Sakurai,Y., Ito,M., Shitara,K., Nakahata,T., and Shibuya,M. (2001). Flt-1, vascular endothelial growth factor receptor 1, is a novel cell surface marker for the lineage of monocyte-macrophages in humans. Blood *97*, 785-791.

Sawano,A., Takahashi,T., Yamaguchi,S., and Shibuya,M. (1997). The phosphorylated 1169-tyrosine containing region of flt-1 kinase (VEGFR-1) is a major binding site for PLCgamma. Biochem. Biophys. Res. Commun. *238*, 487-491.

Schubert,C. *et al.* (2006). Crystal structure of the tyrosine kinase domain of colony-stimulating factor-1 receptor (cFMS) in complex with two inhibitors. J. Biol. Chem. *282*, 4094-4101.

Seetharam,L., Gotoh,N., Maru,Y., Neufeld,G., Yamaguchi,S., and Shibuya,M. (1995). A unique signal transduction from FLT tyrosine kinase, a receptor for vascular endothelial growth factor VEGF. Oncogene *10*, 135-147.

Shalaby,F., Rossant,J., Yamaguchi,T.P., Gertsenstein,M., Wu,X.F., Breitman,M.L., and Schuh,A.C. (1995). Failure of blood-island formation and vasculogenesis in Flk-1- deficient mice. Nature *376*, 62-66.

Shen,Y., Delaglio,F., Cornilescu,G., and Bax,A. (2009). TALOS+: a hybrid method for predicting protein backbone torsion angles from NMR chemical shifts. J. Biomol. NMR *44*, 213-223.

Shewchuk,L.M., Hassell,A.M., Ellis,B., Holmes,W.D., Davis,R., Horne,E.L., Kadwell,S.H., McKee,D.D., and Moore,J.T. (2000a). Structure of the Tie2 RTK domain: self-inhibition by the nucleotide binding loop, activation loop, and C-terminal tail. Structure *8*, 1105-1113.

Shewchuk,L.M., Hassell,A.M., Ellis,B., Holmes,W.D., Davis,R., Horne,E.L., Kadwell,S.H., McKee,D.D., and Moore,J.T. (2000b). Structure of the Tie2 RTK domain: self-inhibition by the nucleotide binding loop, activation loop, and C-terminal tail. Structure *8*, 1105-1113.

Shibuya,M. (2003). Vascular endothelial growth factor receptor-2: Its unique signaling and specific ligand, VEGF-E. Cancer Sci. *94*, 751-756.

Shibuya,M., Yamaguchi,S., Yamane,A., Ikeda,T., Tojo,A., Matsushime,H., and Sato,M. (1990). Nucleotide sequence and expression of a novel human receptor-type tyrosine kinase gene (flt) closely related to the fms family. Oncogene *5*, 519-524.

Shiote,M., Nagano,I., Ilieva,H., Murakami,T., Narai,H., Ohta,Y., Nagata,T., Shoji,M., and Abe,K. (2005). Reduction of a vascular endothelial growth factor receptor, fetal liver kinase-1, by antisense oligonucleotides induces motor neuron death in rat spinal cord exposed to hypoxia. Neuroscience *132*, 175-182.

Siekmann,A.F., Covassin,L., and Lawson,N.D. (2008). Modulation of VEGF signalling output by the Notch pathway. BioEssays *30*, 303-313.

Smith,S.O., Smith,C.S., and Bormann,B.J. (1996). Strong hydrogen bonding interactions involving a buried glutamic acid in the transmembrane sequence of the neu/erbB-2 receptor. Nat. Struct. Mol. Biol. *3*, 252-258.

Solowiej,J., Bergqvist,S., McTigue,M.A., Marrone,T., Quenzer,T., Cobbs,M., Ryan,K., Kania,R.S., Diehl,W., and Murray,B.W. (2009). Characterizing the effects of the juxtamembrane domain on vascular endothelial growth factor receptor-2 enzymatic activity, autophosphorylation, and inhibition by axitinib. Biochemistry *48*, 7019-7031.

Songyang,Z. *et al.* (1993). SH2 Domains Recognize Specific Phosphopeptide Sequences. Cell *72*, 767-778.

Stacker,S.A., Caesar,C., Baldwin,M.E., Thornton,G.E., Williams,R.A., Prevo,R., Jackson,D.G., Nishikawa,S., Kubo,H., and Achen,M.G. (2001). VEGF-D promotes the metastatic spread of tumor cells via the lymphatics. Nat Med *7*, 186-191.

Stamos,J., Sliwkowski,M.X., and Eigenbrot,C. (2002). Structure of the epidermal growth factor receptor kinase domain alone and in complex with a 4-anilinoquinazoline inhibitor. J. Biol. Chem. *277*, 46265-46272.

Sternberg,M.J. and Gullick,W.J. (1989). Neu receptor dimerization. Nature *339*, 587.

Sternberg,M.J. and Gullick,W.J. (1990). A sequence motif in the transmembrane region of growth factor receptors with tyrosine kinase activity mediates dimerization. Protein Eng. *3*, 245-248.

Sturk,C., Kim,H., Jones,N., and Dumont,D.J. (2009). A negative regulatory role for Y1111 on the Tie-2 RTK. Cell Signal. *22*, 676-683.

Sun,Y., Jin,K., Childs,J.T., Xie,L., Mao,X.O., and Greenberg,D.A. (2006). Vascular endothelial growth factor-B (VEGFB) stimulates neurogenesis: evidence from knockout mice and growth factor administration. Dev. Biol. *289*, 329-335.

Suri,C., Jones,P.F., Patan,S., Bartunkova,S., Maisonpierre,P.C., Davis,S., Sato,T.N., and Yancopoulos,G.D. (1996). Requisite role of angiopoietin-1, a ligand for the TIE2 receptor, during embryonic angiogenesis. Cell *87*, 1171-1180.

Takahashi,H. and Shibuya,M. (2005). The vascular endothelial growth factor (VEGF)/VEGF receptor system and its role under physiological and pathological conditions. Clin. Sci. (Lond) *109*, 227-241.

Takahashi,N., Haba,A., Matsuno,F., and Seon,B.K. (2001a). Antiangiogenic Therapy of Established Tumors in Human Skin/Severe Combined Immunodeficiency Mouse Chimeras by Anti-Endoglin (CD105) Monoclonal Antibodies, and Synergy between Anti-Endoglin Antibody and Cyclophosphamide. Cancer Res. *61*, 7846-7854.

Takahashi,T., Ueno,H., and Shibuya,M. (1999). VEGF activates protein kinase C-dependent, but Ras-independent Raf-MEK-MAP kinase pathway for DNA synthesis in primary endothelial cells. Oncogene *18*, 2221-2230.

Takahashi,T., Yamaguchi,S., Chida,K., and Shibuya,M. (2001b). A single autophosphorylation site on KDR/Flk-1 is essential for VEGF-A-dependent activation of PLC-gamma and DNA synthesis in vascular endothelial cells. EMBO J. *20*, 2768-2778.

Tao,Q., Backer,M.V., Backer,J.M., and Terman,B.I. (2001). Kinase insert domain receptor (kdr) extracellular immunoglobulin-like domains 4-7 contain structural features that block receptor dimerization and vascular endothelial growth factor-induced signaling. J. Biol. Chem. *276*, 21916-21923.

Tischer,E., Mitchell,R., Hartman,T., Silva,M., Gospodarowicz,D., Fiddes,J.C., and Abraham,J.A. (1991). The human gene for vascular endothelial growth factor. Multiple protein forms are encoded through alternative exon splicing. J. Biol. Chem. *266*, 11947-11954.

Waltenberger,J., Claesson-Welsh,L., Siegbahn,A., Shibuya,M., and Heldin,C.H. (1994). Different signal transduction properties of KDR and Flt1, two receptors for vascular endothelial growth factor. J. Biol. Chem. *269*, 26988-26995.

Wang,H.U., Chen,Z.F., and Anderson,D.J. (1998). Molecular Distinction and Angiogenic Interaction berween Embryonic Arteries and Veins Revealed by ephrin-B2 and Its Receptor Eph-B4. Cell *93*, 741-753.

Wang,Y. *et al.* (2010). Ephrin-B2 controls VEGF-induced angiogenesis and lymphangiogenesis. Nature *465*, 483-486.

Wedegaertner *et al.* (1992). Effect of carboxyl terminal truncation on the tyrosine kinase activity of the epidermal growth factor receptor. Arch. Biochem. Biophys. 292, 273-280.

Wiesmann,C., Fuh,G., Christinger,H.W., Eigenbrot,C., Wells,J.A., and de Vos,A.M. (1997). Crystal structure at 1.7 Å resolution of VEGF in complex with domain 2 of the Flt-1 receptor. Cell *91*, 695-704.

Woolard,J. *et al.* (2004). VEGF165b, an inhibitory vascular endothelial growth factor splice variant: mechanism of action, in vivo effect on angiogenesis and endogenous protein expression. Cancer Res. *64*, 7822-7835.

Wriggers,W. and Chacon,P. (2001). Using Situs for the registration of protein structures with low-resolution bead models from X-ray solution scattering. Journal of Applied Crystallography *34*, 773-776.

Wu,L.W., Mayo,L.D., Dunbar,J.D., Kessler,K.M., Ozes,O.N., Warren,R.S., and Donner,D.B. (2000). VRAP is an adaptor protein that binds KDR, a receptor for vascular endothelial cell growth factor. J. Biol. Chem. *275*, 6059-6062.

Wybenga-Groot,L.E., Baskin,B., Ong,S.H., Tong,J., Pawson,T., and Sicheri,F. (2001). Structural basis for autoinhibition of the Ephb2 receptor tyrosine kinase by the unphosphorylated juxtamembrane region. Cell *106*, 745-757.

Yamazaki,Y., Matsunaga,Y., Tokunaga,Y., Obayashi,S., Saito,M., and Morita,T. (2009). Snake venom vascular endothelial growth factors (VEGF-Fs) exclusively vary their structures and functions among species. J Biol Chem. *284*, 9885-9891.

Yancopoulos,G.D., Davis,S., Gale,N.W., Rudge,J.S., Wiegand,S.J., and Holash,J. (2000). Vascular-specific growth factors and blood vessel formation. Nature *407*, 242-248.

Yang,K. and Cepko,C.L. (1996). Flk-1, a receptor for vascular endothelial growth factor (VEGF), is expressed by retinal progenitor cells. J. Neurosci. *16*, 6089-6099.

Yang,W., Ahn,H., Hinrichs,M., Torry,R.J., and Torry,D.S. (2003). Evidence of a novel isoform of placenta growth factor (PlGF-4) expressed in human trophoblast and endothelial cells. J. Reprod. Immunol. *60*, 53-60.

Zelzer,E., McLean,W., Ng,Y.S., Fukai,N., Reginato,A.M., Lovejoy,S., D'Amore,P.A., and Olsen,B.R. (2002). Skeletal defects in VEGF(120/120) mice reveal multiple roles for VEGF in skeletogenesis. Development *129*, 1893-1904.

Zeng,H., Dvorak,H.F., and Mukhopadhyay,D. (2001). VPF/VEGF receptor-1 down-modulates VPF/VEGF receptor-2 mediated endothelial cell proliferation, but not migration, through phosphatidylinositol 3-kinase dependent pathways. J. Biol. Chem.

Zhang,X., Gureasko,J., Shen,K., Cole,P.A., and Kuriyan,J. (2006). An allosteric mechanism for activation of the kinase domain of epidermal growth factor receptor. Cell *125*, 1137-1149.

Zhou,F.X., Cocco,M.J., Russ,W.P., Brunger,A.T., and Engelman,D.M. (2000). Interhelical hydrogen bonding drives strong interactions in membrane proteins. Nat. Struct. Mol. Biol. *7*, 154-160.